Schematization uncertainties in the macrostability safety assessment

Case study for primary dikes in the Alblasserwaard

MSc Thesis

Mariska Naaktgeboren

Delft University of Technology

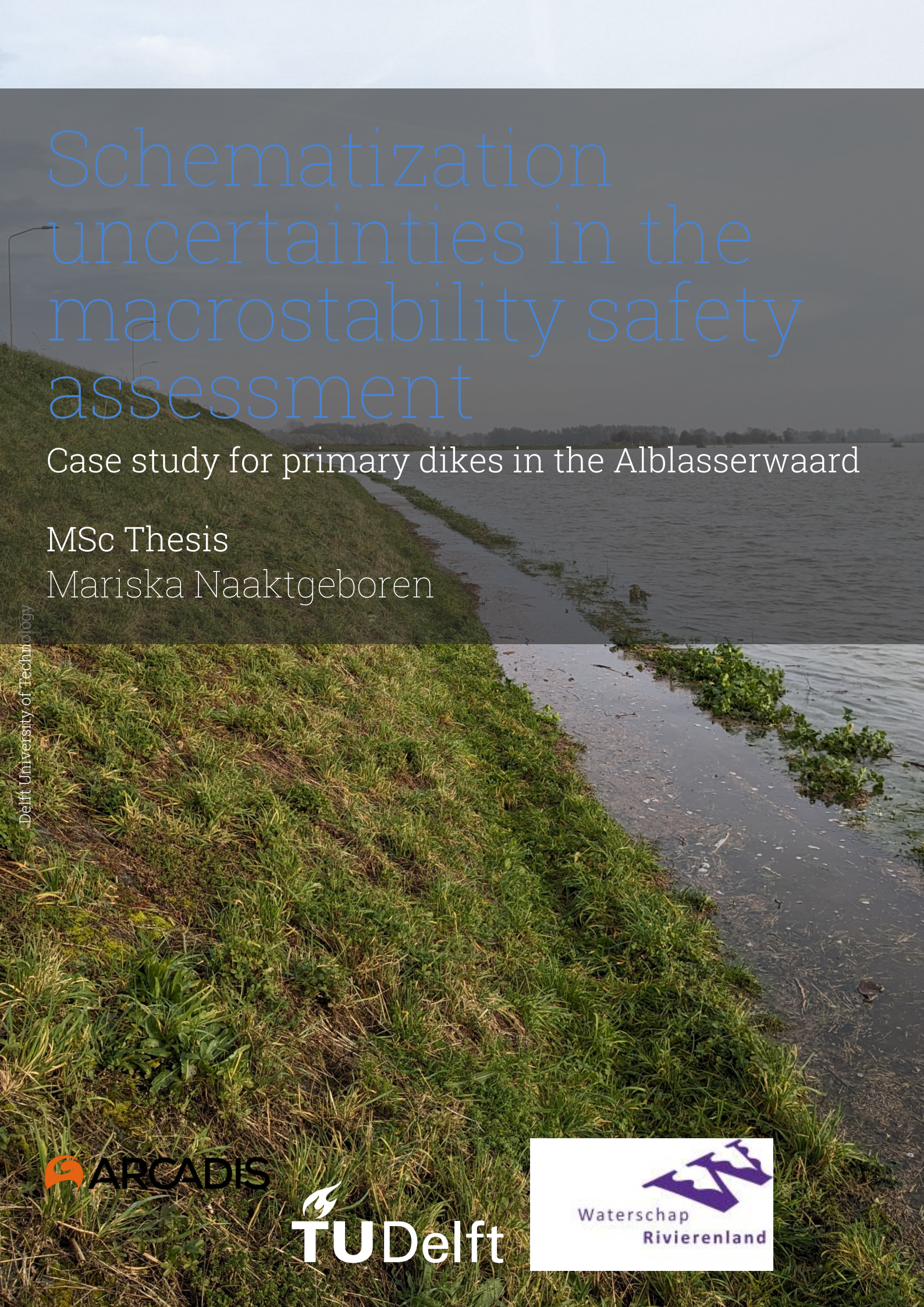

ARCADIS

TU Delft

Waterschap Rivierenland

Schematization uncertainties in the macrostability safety assessment

Case study for primary dikes in the Alblasserwaard

by

Mariska Naaktgeboren

to obtain the degree of Master of Science
at the Delft University of Technology,
to be defended publicly on Tuesday March 5, 2024 at 13:00.

Student number:	5145244	
Project duration:	May 1, 2023 – March 5, 2024	
Thesis committee:	Dr. ir. A.P. van den Eijnden,	TU Delft
	Dr. ir. R. C Lanzafame,	TU Delft
	Martin Arends,	Arcadis
	Sander Kapinga,	Waterschap Rivierenland

TU Delft

Abstract

The current macrostability safety assessment for primary river dike trajectories in the Netherlands is applied to approach the failure probability of a dike during high water events. However, in the current schematization process that is described in the *Wettelijk Beoordelings Instrumentarium* (WBI) to assess the macrostability, aleatory and epistemic uncertainties are approached 'sufficiently safe' by applying design values based on expert judgement via a semi-probabilistic assessment. Several primary river dike sections in the Alblasserwaard do not suffice the current safety standard set for the failure mechanism macrostability. The region is composed of a highly complex subsurface with large spatial variation, resulting in large schematization uncertainties for the macrostability assessment of the primary dike trajectories of the Alblasserwaard. With the recent development of full-probabilistic analysis possibilities in software such as D-Stability, it becomes possible to consider uncertainties as a stochastic variable in the macrostability safety assessment. Including schematization uncertainties within the macrostability safety assessment will improve the approximation of the failure probability of the primary dike trajectory. The largest schematization uncertainties in the macrostability safety assessment are currently considered to be the schematization of the subsurface in a vertical soil profile and the uncertainties in the schematization process of the pore water pressures in the dike during high water events. These uncertainties will be included in the calculation process to investigate the influence on the expected reliability of the primary dikes in the Alblasserwaard region.

The subsurface schematization uncertainties are investigated by using soil scenarios to investigate the influence of local subsurface schematization in the vertical soil profile. The simplification of the soil profile and position of the soil layers is considered. The pore water pressures are separated into three components: the hydraulic head in the aquifer, the intrusion length, and the phreatic line. Each component will be included as a stochastic variable in the stability analysis. Fragility curves can be applied to describe the distribution function for each pore water pressure component, where the combined fragility curve will provide the combined failure probability and reliability index that includes the schematization uncertainty of the pore water pressures considered.

The soil scenarios can be applied to include schematization uncertainties of the subsurface in the macrostability safety assessment. The analysis showed that the simplification of the subsurface schematization only has a minor influence on the reliability index and failure probability of the case study dike cross-section Kortenhoevendijk. The schematization uncertainties of the pore water pressures can be considered in the macrostability safety assessment by combining the fragility curves of each component describing the pore water pressures underneath the dike. Results of the pore water pressure analysis are that failure probability is improved significantly for case study Kortenhoevendijk by a factor 1000 and case study Bergstoep by a factor 10. The approach to consider schematization uncertainties in the macrostability safety assessment via a full-probabilistic analysis can be used for dike sections prone to the uplift mechanism. This approach provides insight into the influence of schematization uncertainties on the failure probability of a dike cross-section. Including the pore water pressure schematization uncertainties in the macrostability safety assessment can have a significant impact on the outcome of the assessment. Including these uncertainties can make the difference between deciding whether a dike trajectory needs reinforcement, or deciding that reinforcement is not necessary.

Contents

List of Figures

List of Tables

Nomenclature

Abbreviations

Abbreviation	Definition
AHN4	Actueel Hoogtebestand Nederland
CDF	Cumulative Density Function
CPT	Cone Penetration Test
CRS	Constant Rate of Strain
DSS	Direct Simple Shear
FORM	First Order Reliability Method
GWL	Ground Water Level
HLc	Holocene formation
KRz	Kreftenheye formation
LBOI	Landelijk Beoordelings- en Ontwerpinstrumentarium
MC	Mohr-Coulomb
MCIS	Monte Carlo Importance Sampling
NAP	Normaal Amsterdams Peil
OCR	Over-Consolidation Ratio
PDF	Probability Density Function
POP	Pre-Overburden Pressure
PTK	Probabilistic Toolkit
SAFE	Streefkerk, Ameide and Fort Everdingen
SHANSEP	Stress History and Normalized Soil Engineering Properties
STz	Sterksel formation
SOS	Stochastische Ondergrondschematisatie
TR	Technical Report on pore water pressures at dikes
URz	Urk formation
WBI	Wettelijk Beoordelings Instrumentarium
WBN	Waterstand Bij Norm
WSRL	Waterschap Rivierenland

List of Symbols

Symbol	Definition	Unit
α	Influence factor	$[-]$
β	Reliability index	$[-]$
γ	Volumetric weight	$[kN/m^3]$
γ_d	Model factor	$[-]$
λ	Leakage length	$[m]$
λ_w	Cyclic leakage length	$[m]$
ϕ	Friction angle	$[^\circ]$
$\phi(x)$	Potential	$[m]$
σ'_v	Vertical effective stress	$[kN/m^2]$
τ	Shear strength	$[kN/m^2]$
ω	Angle frequency of a wave	$[rad/sec]$
A	Amplitude	$[m]$
a	Correlation between instability probabilities	$[-]$

Symbol	Definition	Unit
b	Representative length of local dike trajectory	$[m]$
c	Cohesion	$[kPa]$
c_i	Resistance	$[days]$
C_v	Consolidation coefficient	$[-]$
D	Aquifer thickness	$[m]$
h	Outer water level	$[m]$
k	Hydraulic conductivity	$[m/s]$
L	Length unit	$[m]$
L'	Intrusion length	$[m]$
m	Strength exponent	$[-]$
N	Precipitation	$[m/s]$
OCR	Over-Consolidation Ratio	$[-]$
P_f	Probability of failure	$[-]$
$P_standard$	Flooding probability dike trajectory	$[-]$
POP	Pre-Overburden Pressure	$[kN/m^2]$
Q	Discharge	$[m^3/s]$
$r(x)$	Response	$[-]$
S	Shear strength ratio	$[-]$
S_u	Undrained shear strength	$[kN/m^2]$
T	Return period	$[years]$
$U*$	Design point MCIS analysis	$[-]$
W	Resistance	$[days]$
x_{entry}	Entry point	$[m]$

1 Introduction

The macrostability safety assessment on the inner slope of primary dike trajectories in the Netherlands is used to predict the probability of failure during extreme loading conditions for which the dike should not lose its retaining function. The stability of the primary dike trajectory is assessed by using the *Wettelijk Beoordelings Instrumentarium* (WBI), which describes several schematization processes to simulate the dike stability during high water events. Large schematization uncertainties within the macrostability safety assessment are usually approached by applying safe design values. This could lead to an overestimation of the failure probability. With the recent introduction of approachable full-probabilistic calculations applicable in the macrostability safety assessment, several uncertainties within the schematization can be included in the calculation of the failure probability of the dike trajectory. However, it is not yet possible to consider all schematization uncertainties during the macrostability safety assessment. Including more uncertainties in the schematization process will provide a better insight into the true strength of the primary dike trajectory.

An Additional Graduation Work project (Naaktgeboren, 2023) and Master Thesis is initiated per request of the Water Authority Rivierenland to gain insight into the influence of several uncertainties in the macrostability safety assessment for local dike sections in the Alblasserwaard. In this region, The Water Authority Rivierenland is responsible for the safety assessment of the primary dike trajectories. The Alblasserwaard is located in the deltas of the province of South Holland in the Netherlands and is enclosed by 85.6 kilometers of primary dike trajectory. The subsurface in the Alblasserwaard is highly complex and the spatial variation is large. Thick peat and clay layers are intertwined with sandy fluvial deposits, as visible from figure 1.1. Differential settlements occur due to the oxidation of peat, resulting in 1 to 2 cm per year of settlement throughout the region. For example, in 1984 a large macro-instability failure occurred near Streefkerk.

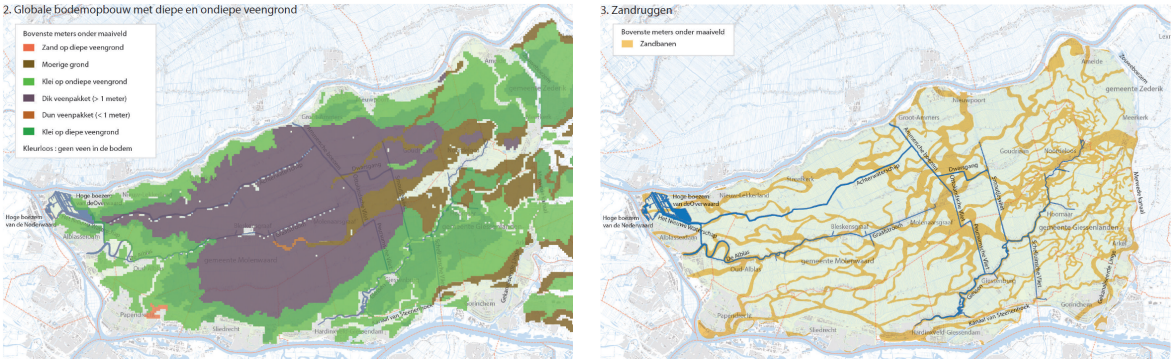

(a) General subsurface of the Alblasserwaard, composed of mostly thick peat layers (in brown) and shallow clays (in green)

(b) Locations of old sandy river deposits throughout the Alblasserwaard

Figure 1.1: Subsurface maps of the Alblasserwaard (Waterschap Rivierenland, 2017)

The Additional Graduation Work focused on the change in test collection in between safety as-

sessments (Naaktgeboren, 2023). Furthermore, the change of the shear strength calculation model from Mohr-Coulomb to SHANSEP (Stress History and Normalized Soil Engineering Properties) was also investigated. For a local dike-cross section these changes impacted the macrostability safety assessment negatively. The water authority Rivierenland is interested in gaining more insight into the sensitivity of the large uncertainties within the schematization processes of the macrostability safety assessment. The main objective of the research project is to find an approachable method to include various schematization uncertainties in the macrostability safety assessment. If the uncertainties can be included in the safety assessment, the influence of these uncertainties on the reliability of the dike can be highlighted, to gain more insight into the actual reliability of the dike.

The approach for the project is to determine the true strength of the dikes in the Alblasserwaard region by considering multiple schematization uncertainties during the macrostability safety assessment. In the current assessment process, conservative design values and lower limits of probability distributions are used to create safe assumptions that overestimate the failure probability of dike cross-sections. During the thesis project, the macrostability of the dike cross-sections will be analyzed by using full-probabilistic calculation methods. Probabilistic calculations can be used to include uncertain parameters as a stochastic variable. The uncertainties, which would be taken into consideration as deterministic parameters in compliance with the WBI, will be included as stochastic variables by using the methods developed in this project.

Several dike cross-sections that have a representative layout concerning the Alblasserwaard are investigated to determine if the reliability of the uncertainties is uniform over the region. If proven that the method can be applied to more than one cross-section, the water authority will have the ability to investigate more dike sections after the conclusion of the project. The method developed in the thesis project should be approachable and repeatable for this reason. The feasibility of the project is analyzed by using multiple case studies of dike sections in the Alblasserwaard.

The main research question is:

What is the influence of the schematization uncertainties in the macrostability safety assessment on the expected reliability of the primary dikes in the Alblasserwaard region?

The main research question is supported by the following sub-questions:

1. What is the current methodology for assessing the macrostability of a primary dike trajectory and what are the uncertainties and limitations of the schematization processes?
2. Which uncertainties within the schematization process have a large influence on the macrostability of a dike cross-section?
3. How can large uncertainties within the schematization process be included in the current macrostability safety assessment?
4. How do these uncertainties measure over different dike sections that are representative of the Alblasserwaard?

Scope

The project is focused on investigating the influence of the schematization uncertainties during the inner slope macrostability safety assessment of a local dike cross-section of a primary dike in the Alblasserwaard. Since the process of determining the location of the most critical cross-section from a section of the dike trajectory is complex, the schematization uncertainties are viewed on the scale for a local dike cross-section. This process also excludes the integration of the failure probability over the dike trajectory. Other dike failure mechanisms such as overflow or wave overtopping during high water events are not taken into consideration during the project. The dike cross-section case studies that are considered during the project should have a blanket layer in the hinterland of more than 4 meters to exclude the influence of the uplift mechanism in the stability analysis. The influence of traffic loads on the macrostability of the dike cross-section will also not be taken into consideration. The macrostability of the dike cross-sections will be assessed via the Uplift-Van limit equilibrium method since this method proved more useful for the local dike cross-sections in the Alblasserwaard during the Additional Graduation Work.

The most recent test collection of the water authority Rivierenland for the dike reinforcement project of the Lekdijk from Streefkerk, Ameide, and Fort Everdingen (SAFE) will be used in the stability analysis for each of the case studies. The SAFE reinforcement project includes a large section of the Lekdijk located in the Alblasserwaard, so will provide representative values for the local soil properties. The Additional Graduation Work is used to investigate the impact of the recent test collection, so will not be discussed during the thesis project. The modeling process of assessing the macrostability will be done in D-Stability version 2023.01 in combination with the Probabilistic ToolKit version 2023.0.3153.0 provided by Deltares. These software programs are also used by the water authority Rivierenland and will therefore be approachable for the water authority.

Report structure

The report describes the current process of the macrostability safety assessment as provided by the WBI in chapter 2. By the end of the chapter, the main uncertainties and limitations that are expected to have a large influence on the macrostability safety assessment outcome are discussed. Chapter 3 describes the main uncertainties that are considered during the project are discussed. Furthermore, the method by which these uncertainties can be considered as stochastic variables within the macrostability safety assessment is also discussed. Chapter 4 describes the schematization uncertainties of the subsurface for the case study of the Kortenhoevendijk. Chapter 5 includes the schematization uncertainties of the pore water pressure components for the case study of the Kortenhoevendijk and the case study Bergstoep in the Alblasserwaard. Chapter 6 concludes the rapport and includes the discussion and recommendations.

2

Current macrostability safety assessment

Chapter 2 describes the current assessment methodology that is applied in the macrostability safety assessment of primary dike trajectories in the Netherlands. The chapter describes the general process of performing a macrostability safety assessment including the safety standard for primary dike trajectories. The current schematization process of both relevant geotechnical and hydraulic components is described in more detail. At the end of the chapter, the uncertainties and limitations of the current macrostability safety assessment process are discussed.

2.1. Introduction

A macro-instability at the inner slope of a river dike occurs when the dike no longer resist a variation in loading conditions without losing its function. The function of a river dike can be described as the retainment of the water. During an instability, the dike material and soil fail along a circular slip plane, visible in figure 2.1.

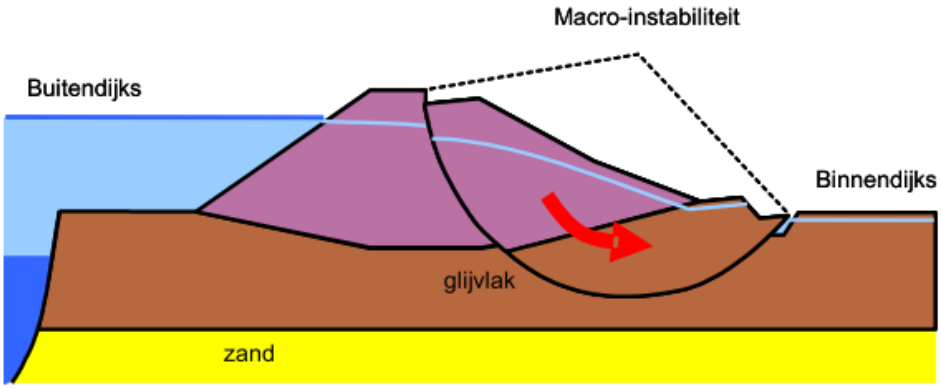

Figure 2.1: Schematization of the macrostability failure mechanism for a dike cross-section during high water conditions (van Duinen, 2014)

The current macrostability safety assessment of primary dike trajectories in the Netherlands is performed in the software D-Stability: where a dike cross-section is assessed on the overall stability to provide a failure probability. The general assessment procedure and schematization processes that are relevant to enquiring the failure probability concerning the macrostability of a dike cross-section are described by the WBI (in Dutch: Wettelijk Beoordelings Instrumentarium). This document is used before 2023 and the LBOI (in Dutch: Beoordelings- en Ontwerpinstrumentarium) is implemented from 2023 to 2035. Both programs describe the methods and processes of assessing and designing primary dike trajectories in the Netherlands (Rijksoverheid, 2019). The safety assessment as described by the WBI and LBOI for the macrostability of primary dike trajectories includes descriptions and instructions

on the schematization process of multiple relevant components to assess the inner slope and outer slope stability. The software D-Stability is used to approach realistic failure behaviour of a dike cross-section. A macro-instability failure can be simulated in D-Stability for high water conditions with a very low probability of occurrence. The schematization processes described in the WBI to approach failure behaviour often apply conservative design values to describe aleatory and epistemic uncertainties: natural uncertainties due to spatial variations and uncertainties due to a lack of knowledge.

The safety assessment of a primary dike concerning macrostability can be performed by using a simplified stability analysis or a detailed analysis. The simplified analysis is applied to determine if the stability of a certain dike section can be analyzed by using simple design rules that are based on the safe dimensions of a flood defense system. The simplified assessment is mostly used as a screening or relevance test for individual components or failure mechanisms. The simplified analysis is not often used in the Netherlands, since the analysis is generally used for dikes that are apparent safe, with languid slopes and wide crests, which is often not the case in the Netherlands. If the dike does suffice according to the simplified analysis, failure of the dike trajectory is negligibly small. If the dike does not suffice, a detailed analysis is required. However, it is not required to perform the simplified test before performing a detailed analysis (Rijkswaterstaat and Water Verkeer en Leefomgeving, 2019). In practice, the simplified assessment is mostly skipped and a detailed safety assessment is executed.

2.2. Safety standard

After the North Sea Flood in 1953 in the Netherlands, design rules and safety standards were introduced for the design of primary flood defense systems. The safety standards were based on the design values of the hydraulic loading conditions. The dike should suffice in withstanding high water levels during floods and high river discharges, protecting the areas and regions behind these defenses. The design values of the hydraulic loading conditions can be translated to an exceedance frequency of the design level. This methodology of designing flood defense systems has been the general approach in the Netherlands for years. With the introduction of the WBI in 2017, a new approach to the safety standard is applied in the safety assessment. A required failure probability is determined for a dike trajectory, which can be compared to the actual failure probability of a dike cross-section (Rijkswaterstaat and Ministerie van Infrastructuur en Waterstaat, 2021). The failure probability of a cross-section can be determined for each dike failure mechanism. The failure probability of a dike cross-section for macrostability is given by equation 2.1. The failure probability of a cross-section $P_{cross-section}$ should be lower than $P_{required,cross-section}$ to suffice to the safety standard on a dike trajectory level.

$$P_{required,cross-section} = \frac{\omega P_{standard}}{(1 + \frac{aL}{b})P_{f|inst}} \tag{2.1}$$

ω describes the failure probability sample space factor, where the value for the macrostability failure mechanism $\omega = 0.04$ (Rijkswaterstaat and Ministerie van Infrastructuur en Waterstaat, 2021). $P_{standard}$ describes the flooding probability of the dike trajectory per year. Factor $a = 0.033$ describes the correlation between instability probabilities of the separate dike sections. Factor b is equal to 50 meters, the representative length for the stability analysis of the cross-section. L describes the length of the local dike trajectory. $P_{f|inst}$ is the probability of failure given instability, which is equal to 1 for the macrostability failure. This implies that through a macro-instability, flooding will occur.

2.3. Geotechnical components

The schematization process for several relevant geotechnical components concerning the primary dike trajectory in the macrostability safety assessment is summarized in this section. The primary dike trajectory is schematized into dike sections, where each section is schematized into one (most critical) dike cross-section. The process is iterative, for which the subsurface underneath the dike and varying hydraulic loading conditions are prominent. The failure probability of a dike cross-section concerning macrostability can be determined by schematizing the dike geometry, subsurface, and pore water pressures acting on the dike and simulating the stability of the inner dike slope.

Dike geometry

The geometry of the dike should be relatively constant along the dike section to schematize the section into one cross-section. The geometry of the dike cross-section directly influences the failure probability. The least favorable cross-section and dike geometry are considered in the stability calculations. This geometry will have the largest contribution to the failure probability of the entire dike trajectory. The geometry of the dike cross-section is based on AHN4 satellite data, which can be directly implemented into the stability assessment model. This data is measured with 5-centimeter accuracy ("AHN Actueel Hoogtebestand Nederland", 2023).

Subsurface schematization

Local site investigations via Cone Penetration Test (CPT) tests and mechanical borings provide insight into the local subsurface underneath primary dike trajectories. This data is applied to schematize the subsurface: the subsurface is schematized into a vertical soil profile that can be used for input of the macrostability calculation model. The WBI provides a starting point for the schematization process of the subsurface underneath primary dike trajectories in the Netherlands. Stochastic subsurface schematization Scenarios SOS (in Dutch: Stochastische Ondergrondschematisatie) can be used as an initial schematization of the general subsurface underneath a primary dike trajectory. For each dike trajectory in the Netherlands, several scenarios are set up that describe the local subsurface underneath the dike trajectories that can be applied in the macrostability safety assessment. For each soil scenario, a probability of occurrence is assigned that describes the possibility that the specified soil scenario can be found at a given section of the dike trajectory. This probability of occurrence is based on the relative frequency of the occurrence of the soil, based on local CPT data and mechanical borings (Kruse and Hijma, 2015). The SOS scenarios are available through D-Soil Model, a software program provided by Deltares (Deltares, 2017). The SOS scenarios are, however, applicable for dike trajectories: it is difficult to apply these generalized subsurface schematizations to a complex region such as the Alblasserwaard. Due to the high spatial variation in this region, the SOS scenarios can vary from local subsurface data found by CPTs and mechanical borings. The use of SOS scenarios is considered conservative and limits the accuracy of the subsurface schematization on a local scale. In the current process of the macrostability safety assessment, local site investigation data is used in complex regions to provide a schematization of the subsurface. This schematization is often based on expert judgement and simplified compared to the site investigation data. Uncertainties in the schematization process of the subsurface are often approached with conservative values for deterministic input. The deterministic input of uncertain parameters is a large limitation in the subsurface schematization process. Parameters such as the position of a soil layer is a deterministic input, but has spatial variation and is a aleatory uncertainty. The schematization of the subsurface is considered to be a simplification of reality, and the impact on the reliability of the dike cross-section due to this simplification is unknown.

Soil parameters

Once the schematization of the subsurface is known, the parameters for each of the soil layers located underneath the dike are required to be determined. An indication for each soil parameter required in the macrostability safety assessment can be found in the WBI. Water Authorities that are situated in the Netherlands will set up a test collection, for example for large dike reinforcement projects, that contains soil parameters derived from laboratory tests on local soil layers. Local soil parameters are extracted from soil laboratory tests on local soil samples, taken from in and around the dike trajectory. The strength parameters and soil properties that are required to determine the strength of the soil can be determined for each soil type. The test collection includes relevant soil parameters that describe the soil strength such as the unit weight γ and friction angle ϕ. In the macrostability modelling in D-Stability, the unit weight γ is applied as a deterministic input. This is considered a limitation since the unit weight of soil is considered as an aleatory uncertainty. Strength parameters such as the shear strength ratio S, friction angle ϕ, and cohesion c are implemented as stochastic variables. These parameters can be described with continuous distributions and have a large influence on the reliability of the dike cross-section. The test collection includes the mean and standard deviation of these parameters, which can be determined from soil laboratory tests accurately.

Soil behaviour

The WBI separates the soil behaviour into drained behaviour or undrained behaviour. For each soil type, the type of behaviour is assigned where the soft soils in general behave undrained and sandy

soils display drained behaviour. The WBI provides a table for where each soil type most common in the Netherlands is assigned to behave as drained or undrained. Realistically, whether the soil behaviour is drained or undrained mainly depends on the loading characteristics. If the drainage length of a soil layer is relatively small, clay soil can still behave drained during a macrostability failure. This is also valid the other way around, if the drainage length is relatively large, sandy soil can behave undrained (Tigchelaar, 2023). The assigned soil behavior influences the soil parameters that are required to be determined from the laboratory tests on the local soil samples. Drained soil behaviour is simulated in D-Stability via the Mohr-Coulomb criterion (MC), described by equation 2.2 (Verruijt, 2010).

$$\tau_f = c + \sigma \tan \phi \tag{2.2}$$

With c describing the cohesion of the soil, σ' the normal stress, and ϕ the friction angle. The criterion describes the failure of shearing soil due to the exceedance of the shear strength around the failure surface. This formula is applied if the dilatancy angle is equal to the friction angle. The shear strength of the soil is linear to the stress state. Undrained soil behaviour is approached via the SHANSEP formulation (Stress History and Normalized Soil Engineering Properties) in the macrostability safety assessment in D-Stability. The SHANSEP formulation is given by equation 2.3.

$$S_u = \sigma'_v * S * OCR^m \tag{2.3}$$

The SHANSEP formulation requires two material properties, S the shear strength ratio and m the strength increase exponent, and one state parameter, σ'_y the effective vertical stress (Deltares, 2020). The Over-Consolidation Ratio (OCR) is the ratio between the initial effective stress and the effective vertical stress. This ratio can also be expressed via the Pre-Overburden Pressure (POP) where $POP = |\sigma'_y - \sigma_{vi}|$ (Backhausen and van der Stoel, 2013). For transitional soils or embankment material above the phreatic line, the behaviour can not always be described via the SHANSEP formulation. In the macrostability safety assessment, the undrained shear strength table, or (S_u) table, can be used to manually enter the relationship between effective stress and the undrained shear strength of a transitional soil. This table can be extracted from laboratory soil testing (Deltares, 2020).

2.4. Hydraulic boundary conditions

Two hydraulic boundary conditions are relevant during the macrostability safety assessment on primary river dikes in the Netherlands via D-Stability: the (design) outer water level h, and the pore water pressure distribution at this design load $h(t)$. The fluctuations in water levels influence the pore water pressure distribution in the local soil layers underneath the dike. These loading conditions have a large contribution to the overall stability of the dike. The design outer water level that is applied in the macrostability safety assessment is the WBN (in Dutch: Waterstand Bij Norm), based on the safety standard. Multiple design hydraulic loading conditions are considered in the macrostability safety assessment: the unsaturated conditions without infiltration due to overtopping and the saturated conditions with infiltration due to overtopping. For fully saturated conditions, only two water levels are considered: the water level with the highest probability of overtopping $q > 1l/s/m$ and the WBN level. When the combined fragility curve includes the saturated and unsaturated conditions with the distribution function of the water level, the failure probability for the cross-section concerning the inner slope macrostability is given. The pore water pressure distribution at design load $h(t)$ can be described by the level of the phreatic line, the hydraulic head in the aquifer, the leakage length, and the intrusion length in the blanket layer. Each of these components is described in more detail.

Phreatic level

The phreatic level in the dike describes the pore water pressures acting in the dike body provided a hydraulic boundary condition (Kanning and van der Krogt, 2016). The height of the phreatic line depends on several uncertainties: the dike geometry, hydraulic conductivity of the dike material, the daily loading conditions and degree of saturation, the duration of high water levels, and the state of the groundwater flow (stationary or non-stationary) (Technische Adviescommissie voor de Waterkeringen, 2004). Figure 2.2 displays the time-dependent effect of high water levels on the phreatic line over time. At the inner dike toe, the phreatic level requires more time to adjust to the new loading conditions.

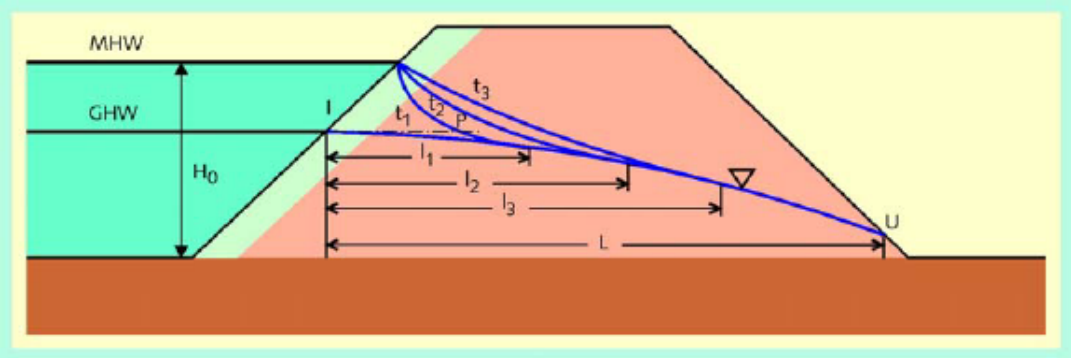

Figure 2.2: Development of the phreatic line during high water conditions (Technische Adviescommissie voor de Waterkeringen, 2004)

Since the height of the phreatic line is dependent on the aleatory uncertainties such as the hydraulic conductivity of the dike material and epistemic uncertainties such as the (initial) degree of saturation, it is difficult to determine the position of the phreatic line in the macrostability safety assessment. The schematization process of the height and location of the phreatic line as described by the WBI is displayed in figure 2.3. Figure (a) displays the schematization of the phreatic line in a clay dike body during high water loading conditions. Figure (b) displays the schematization of the phreatic line for a sandy dike body, where the line is situated significantly lower than the schematization of the clay dike body.

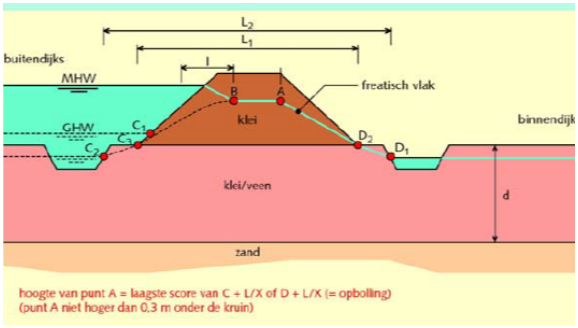

(a) Schematization of the phreatic line for clay dike body

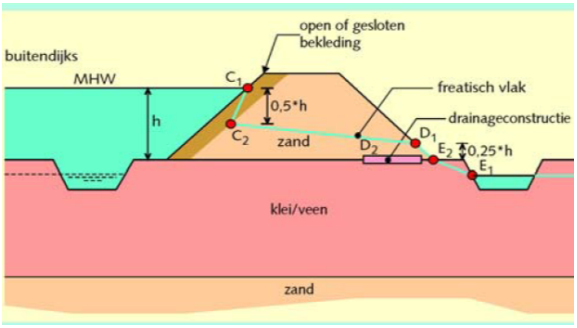

(b) Schematization of the phreatic line for sandy dike body

Figure 2.3: Schematization of the phreatic line (Technische Adviescommissie voor de Waterkeringen, 2004)

Leakage length

The leakage length λ is a measurement of distance that describes the hydraulic head over the length of the aquifer. It describes how far excess water pressures propagate in the sand layer (Kanning and van der Krogt, 2016). A longer leakage length correlates to the lower stability of the dike (Jonkman et al., 2021). The leakage length for stationary groundwater flow is dependent on the hydraulic resistance of the blanket layer and the transmissivity of the aquifer, which can be determined with equation 2.4.

$$\lambda = \sqrt{kDW} \tag{2.4}$$

Where k is the hydraulic conductivity of the aquifer, D is the thickness of the aquifer, and W is the resistance. The subsurface in the foreshore influences the leakage length and subsequently the level of the hydraulic head in the aquifer. In the Netherlands, the leakage length under stationary conditions can vary from 100 to 1000 meters (Kruse and Hijma, 2015). (Kanning and van der Krogt, 2016) describes that for higher leakage lengths, the outer dike leakage length has a higher influence than the inner dike leakage length. In case there is an uplift of the blanket layer in the hinterland, the leakage length has a very limited influence on the safety factor. The value for the leakage length is included in the macrostability safety assessment as an average deterministic value due to spatial variability and the epistemic uncertainties of the leakage length.

Intrusion length

The intrusion length can be described as the length over which the pore water pressure changes in the aquifer influence the pore water pressures inside the blanket layer, as shown in figure 2.4. With the increase in hydraulic head in the aquifer below the dike, the pore water pressures in the blanket layer will adjust over time. At the bottom of the blanket layer, the pore water pressure will adjust faster than at the top of the blanket layer. The red line in figure 2.4 is the schematization of the intrusion length in the blanket layer. The intrusion length is mostly influenced by the composition of the local subsurface, the thickness of the blanket layer, and the duration of the high water conditions (Technische Adviescommissie voor de Waterkeringen, 2004).

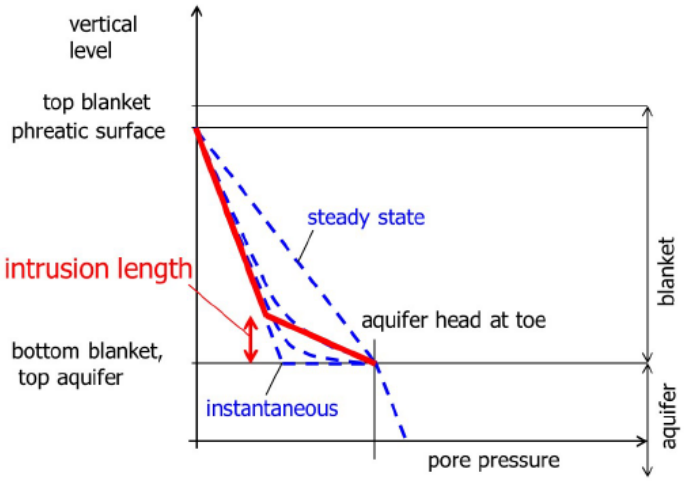

Figure 2.4: Schematization of the intrusion of the pore water pressures in a low permeable blanket layer (Jonkman et al., 2021)

The adjustment of the pore water pressures at the bottom of the blanket layer can be described via one-dimensional consolidation described in equation 2.5 (Technische Adviescommissie voor de Waterkeringen, 2004).

$$\frac{\partial u}{\partial t} = C_v \frac{\partial^2 u}{\partial z^2} \tag{2.5}$$

The consolidation coefficient C_v is dependent on the permeability of the soil, compressibility of the soil, and water. The intrusion length L' can be approached via the simplified equation 2.6.

$$L' \approx 4\sqrt{C_v(t - t_0)} \tag{2.6}$$

A limitation to equation 2.6 is that the intrusion length in the blanket layer is described with the consolidation coefficient for one soil type. In a complex region such as the Alblasserwaard, the blanket layer is composed of multiple soil layers with a different consolidation coefficient. The value for the intrusion length in the blanket layer is taken into consideration in the macrostability safety assessment by applying the default values as described in the WBI, or via expert judgement. The WBI indicates the intrusion length for blanket layers composed of different soil types, as shown in table 2.1. The intrusion length is assumed to be only dependent on the duration of the high water conditions and the soil type of the blanket layer (Rijkswaterstaat and Ministerie van Infrastructuur en Waterstaat, 2021). The blanket layer is assumed to fully adapt to the high water conditions if the layer is composed of silty clay or clay that is interlayered with sand.

Soil type	Intrusion length at high water duration of 5 days	Intrusion length at high water duration of 20 days
Peat layers or clay	1 m	2 m
Organic clays, clay with peat or clayey peat	1 m	2 m
Hollandsveen (peat)	1 m	>6 m
Silty clay or clay interlayered with sand	>6 m	>6 m

Table 2.1: Intrusion length indication as described by the WBI (Rijkswaterstaat and Ministerie van Infrastructuur en Waterstaat, 2021)

The exact value for the intrusion into the blanket layer during high water events is difficult to determine and measure in situ due to the time dependency and aleatory uncertainty of the consolidation coefficient. The intrusion length applied in the safety assessment is assigned to be sufficiently safe.

Hydraulic head in the aquifer

The hydraulic head in the aquifer describes the groundwater flow underneath the dike through the aquifer. The hydraulic head in the aquifer can be measured in situ over a period of weeks or months from which the properties of the geohydrological systems can be determined. The level of the hydraulic head is unknown at high water conditions with a very low probability of occurrence. The in-situ measurement data requires to be extrapolated to the low probability occurrences, which results in uncertainties in the level of the hydraulic head. In the macrostability safety assessment, the hydraulic head at WBN is calculated via analytical models as described by the *Technische rapport Waterspanningen bij dijken* (TR). Deterministic input parameters for the analytical model are used to provide a sufficiently safe value for the hydraulic head in the aquifer that is applied in a D-Stability model. The analytical models that are used in the macrostability safety assessment are separated by the time dependency of the hydraulic head. Stationary groundwater flow can be assumed for the schematization of the hydraulic head level in the aquifer in the upper river area since the period of the high water conditions is relatively long (Technische Adviescommissie voor de Waterkeringen, 2004). Groundwater flow in the lower river area of the Netherlands cannot be assumed to be stationary, since the high water level period is relatively short in comparison to the upper river area, and is influenced by time-dependent phenomena.

Stationary approach of the groundwater flow

High water levels in the upper river area of the Netherlands are the result from high river discharges lasting for multiple weeks. Time-dependent effects can therefore be neglected in the upper river area. The hydraulic head level is calculated via analytical formulas as described by the *Technische rapport Waterspanningen bij dijken* (Technische Adviescommissie voor de Waterkeringen, 2004). The primary dike trajectories in the Alblasserwaard can be schematized as clay dikes on a sand aquifer, as shown in figure 2.5.

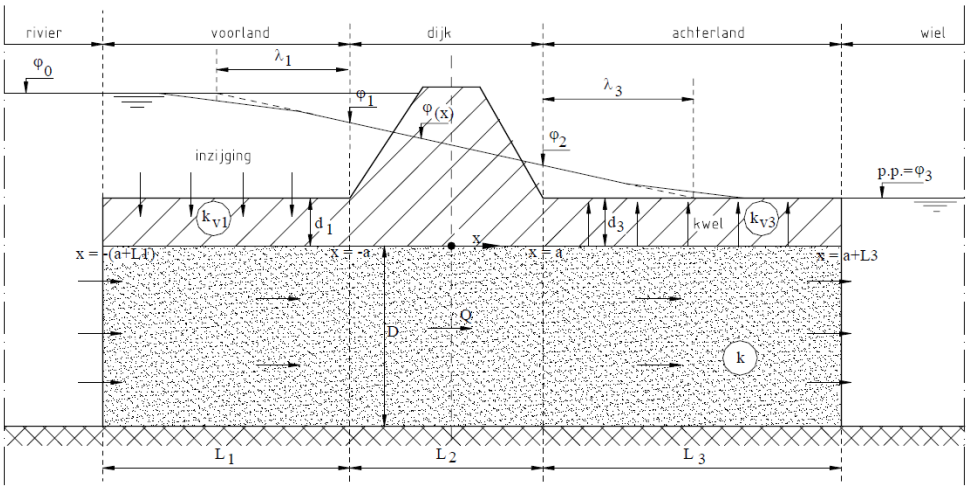

Figure 2.5: Schematization of stationary groundwater flow underneath a clay dike (Technische Adviescommissie voor de Waterkeringen, 2004)

The hydraulic head resulting in the aquifer can be calculated for any location along the dike cross-section via equation 2.7.

$$\phi(x) = \phi_{polder} + r(x)(\phi_0 - \phi_{polder}) \tag{2.7}$$

Where $\phi(x)$ describes the potential that can be determined for each location on the dike cross-section. The response $r(x)$ describes the influence of the hydraulic head due to the presence of the blanket layer concerning the foreshore or hinterland, and the resistance of the hinterland can be described with equation 2.8.

$$r(x) = \frac{W_3}{W_1 + L_2 + W_3} \frac{\sinh\left(\frac{L_3 - x}{\lambda_3}\right)}{\sinh\left(\frac{L_3}{\lambda_3}\right)} \tag{2.8}$$

Where W_1 describes the resistance of the foreshore and W_3 describes the resistance of the hinterland. The resistance is dependent on the transmissivity of the aquifer and the leakage length λ. Since the response is considered to be stationary, it is only dependent on the transmissivity of the aquifer kD, and the resistance of the blanket layer. The uncertainties in the calculation process of the hydraulic head for dikes in the upper river area are the aleatory uncertainties of the hydraulic conductivity of the aquifer k and the variable aquifer thickness D. These components will influence the flow of the groundwater through the aquifer, and therefore the steepness of the hydraulic head line in the D-Stability schematization. The resistance of the foreshore influences the initial height of the hydraulic head at the river side of the dike. In the current macrostability safety assessment, the input parameters are deterministic input, approached sufficiently safe. To determine the distribution of the stationary hydraulic head, the uncertainties taken into consideration as stochastic input and the distribution will result from the calculations.

Time dependent approach groundwater flow

The response of the groundwater flow in dikes of the lower river area of the Netherlands is dependent on three time-dependent components: river discharges, tidal influences, and storm set-up. The schematization of the time-dependent groundwater flow by the *Technische rapport Waterspanningen bij dijken* is displayed in figure 2.6. The time and location-dependent potential underneath the dike can be described by equation 2.9. This equation is valid under the assumption that no foreshore is present at the dike (Technische Adviescommissie voor de Waterkeringen, 2004).

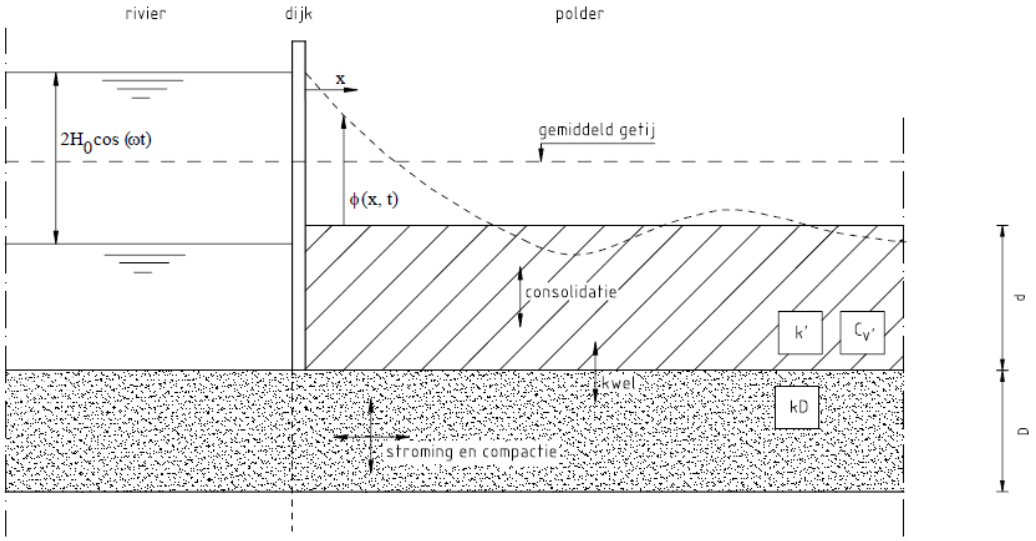

Figure 2.6: Schematization of time-dependent groundwater flow underneath a clay dike (Technische Adviescommissie voor de Waterkeringen, 2004)

$$\phi(x,t) = H_0 \exp(\frac{-0,924x}{\lambda_\omega}) \cos \omega t - \frac{0.383x}{\lambda_\omega} \tag{2.9}$$

Where $\phi(x,t)$ describes the potential at location x and time t. H_0 is the amplitude of the tidal wave. λ_ω is the cyclic leakage length, which is now dependent on the duration of the hydraulic loading conditions. The cyclic leakage length describes the measure of intrusion of the cyclic response in the aquifer The formulation for the cyclic leakage length is given by formula 2.10.

$$\lambda_\omega = \sqrt{\frac{kD}{k'}\sqrt{\frac{C_v}{\omega}}} \tag{2.10}$$

With the transmissivity kD of the aquifer, the consolidation coefficient C_v, and the hydraulic conductivity k' of the soft soil in the hinterland. The uncertainties in the calculation of the cyclic leakage length are aleatory uncertainties. The subsurface is highly complex, and therefore the cyclic leakage length is often determined from piezometer measurements of tidal influences on the hydraulic head. In the macrostability safety assessment, the maximum response of the high water conditions is relevant, and therefore equation 2.9 can be simplified to equation 2.11.

$$\phi(x) = H_0 \exp(\frac{-0.924(x + x_{entry})}{\lambda_\omega}) \tag{2.11}$$

x_{entry} is the entry point from which the high water conditions are present in the aquifer underneath the dike. This parameter represents a measure of resistance of the foreshore.

In the calculation process of extrapolating the cyclic leakage length of the tidal influence to the cyclic leakage length of a high water wave, equation 2.12 is used.

$$\lambda_\omega = \lambda_{cyclic_1}(\frac{T_2}{T_1})^{0.25} \tag{2.12}$$

With the principle of superposition, the total potential along the dike cross-section is the sum of the individual components of the stationary potential and the time-dependent components with equation 2.13.

$$\phi(x,t) = \phi_{stationary} + \phi(A_{river}) + \phi(A_{tide}) + \phi(A_{storm}) \tag{2.13}$$

The stationary response is calculated via equation 2.7. The individual amplitudes of the river discharge, tidal influence, and storm set-up are dependent on the local loading conditions. The amplitudes can be based on analyzing local measurements of the pore water pressures to determine the expected value of the local hydraulic head. This process is described in detail for the case study of the local primary dike in chapter 5. This formulation to describe the time-dependent hydraulic head is used because each amplitude can be determined at WBN conditions extrapolated from measurement data.

2.5. Macrostability modelling software

The macrostability safety assessment is performed in D-Stability and the post-processing in the Probabilistic ToolKit, both provided by Deltares. These software programs are applied in the current macrostability safety assessment, therefore will also be used to investigate the influence of including the schematization uncertainties in the macrostability analysis during the project.

2.5.1. D-Stability

The macrostability safety assessment in D-Stability can include a design analysis or a probabilistic approach to assess the macrostability of a dike cross-section.

Uplift-Van

The macrostability of the dike cross-sections is calculated by applying the Uplift-Van method that calculates the slip plane separated in an active circle, passive circle, and a horizontal section connecting the two (Deltares, 2020). The schematization of the Uplift-Van slip surface is displayed in figure 2.7. Other limit equilibrium methods that can be used in D-Stability to determine the failure plane are the Bishop method of slices and the Spencer method.

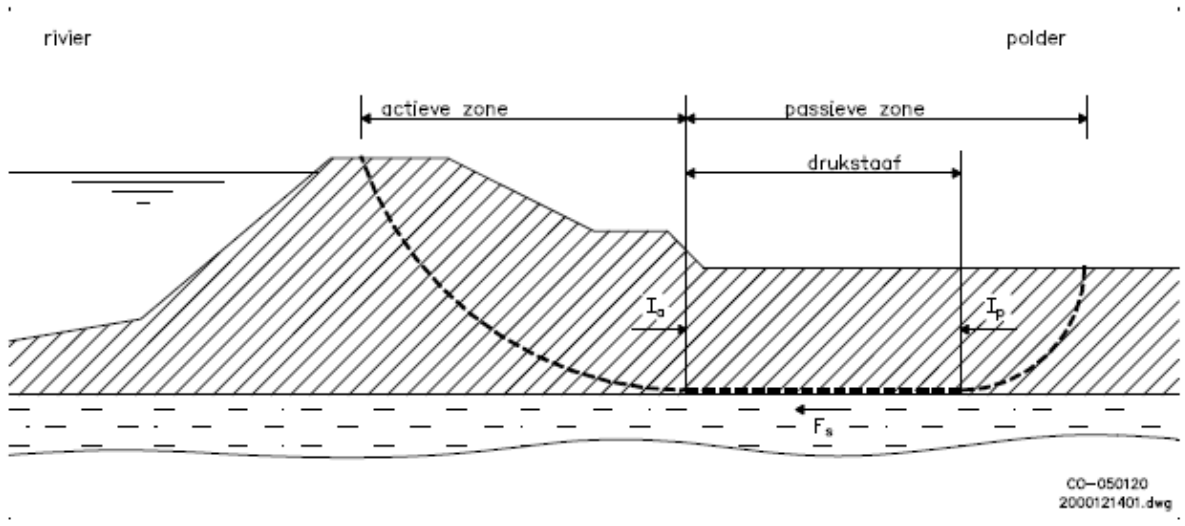

Figure 2.7: Schematization of the Uplift failure surface (Technische adviescommissie voor de waterkeringen, 1989)

During the project, only the Uplift-Van limit equilibrium method is used to provide a consistent result from each analysis and to be able to compare the failure surfaces to generate a representative fragility curve. This limit equilibrium method is used as the standard during the macrostability safety assessment. The Uplift-Van method is confirmed to provide more stable results during the Additional Graduation Work for dike cross-sections with the soft soil blanket layer situated on Pleistocene sand Naaktgeboren, 2023. The search area for the Uplift-Van method is optimized during the calculation process by using the thorough search grid that applies a population and performs several random steps to improve this population.

Semi-probabilistic assessment

The detailed semi-probabilistic assessment is an indirect, approximate approach to assessing the probabilities of failure for a dike section (Kanning et al., 2017). A semi-probabilistic approach considers the

probabilistic density functions for multiple stochastic variables to determine the failure probability for one failure surface. In practice, parameters are uncertain due to spatial variability, limited access to data and measurements, and also measurement uncertainties due to time dependencies. Several parameters in the stability assessment are assigned as a stochastic variable, usually via a lognormal distribution function. The probability density function (PDF) of the lognormal distribution is defined by equation 2.14. The advantage to using this distribution concerning the normal distribution is that the PDF only returns positive values for the soil parameters (Kroese et al., 2011).

$$f(x;\lambda,\sigma) = \frac{1}{x\sigma\sqrt{2\pi}}\exp(-\frac{(\ln(x)-\mu)^2}{2\sigma^2}) \tag{2.14}$$

The semi-probabilistic assessment in D-Stability applies design values of the loads and resistance or uses the 0.05 percentile for the probabilistic distribution of a stochastic variable. The design analysis applies combinations of unfavourable values of input parameters by calculating the 5% or 95% confidence limit from the stochastic distribution functions of the stochastic variables, depending on which value is the most unfavorable (Deltares, 2020). Uncertainties within the calculation process and methods are taken into consideration via several partial factors. The required safety factor in the safety assessment is the product of the four partial safety factors mentioned in table 2.2.

Partial factor	**Notation**	**Description**
Schematization factor	γ_b	Accounting for uncertainties in the soil profile.
Model factor	γ_d	Accounting for uncertainties in each slip surface calculation model. The model factor for LiftVan is equal to 1.05 as the 95% percentile value as described by the WBI for primary dike assessments.
Material factor	γ_m	Accounting for the uncertainties in material properties.
Damage factor	γ_n	Accounts for the failure of the dike due to high water levels. The damage factor can be determined from the target reliability and the length of the dike trajectory.

Table 2.2: Partial safety factors applied in the semi-probabilistic macrostability safety assessment (Rijkswaterstaat and Ministerie van Infrastructuur en Waterstaat, 2021)

The assessment of a dike cross-section with the design analysis will provide the factor of safety.

Full-probabilistic assessment

A full-probabilistic analysis describes the uncertain parameters with a distribution function, usually characterized by an expectation value and standard deviation (Kanning et al., 2017). In version 2023.01 of D-Stability, a First Order Reliability Method (FORM) or Monte Carlo Importance Sampling (MCIS) analysis can be performed for a dike cross-section that includes several stochastic variables for a fixed outer water level.

First Order Reliability Method

The First Order Reliability Method (FORM) is an approximation method, used in D-Stability to provide a reliability index for the dike stability. The method uses a first-order approximation, where the stochastic parameters are described by only their mean and standard deviation (Manoj, 2016). FORM applies a gradient-based search algorithm to locate the most likely location of the failure, which is the design point $U*$ in figure 2.8. This linearization is used to define the boundary between the 'safe' and 'failure' domains, to provide a failure probability (Donders et al., 2003).

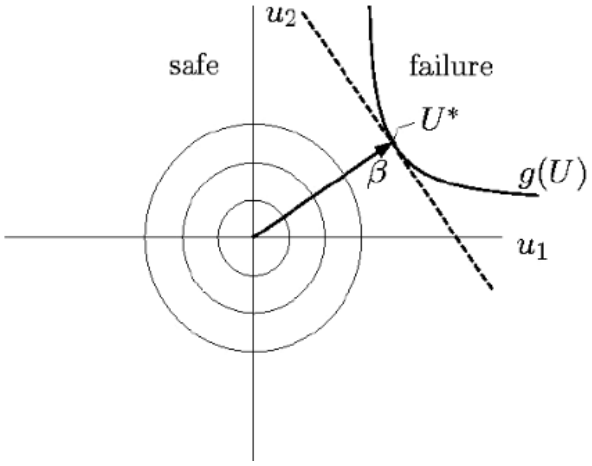

Figure 2.8: Visualization of the FORM sampling method (Donders et al., 2003)

The limit state function of the FORM analysis that is used to locate the design point is described by $Z = R - S$, where the parameters R and S are assumed to be random variables. From this point, the probability of failure can be described with equation 2.15.

$$P_f = P(Z < 0) = \phi(-\beta) = 1 - \phi(\beta) \tag{2.15}$$

The analysis in D-Stability will provide the reliability index and the failure probability that will most likely lead to failure for the slope stability analysis with a set slip surface. The precision of the FORM analysis decreases with an increasing number of stochastic parameters.

Monte Carlo Importance Sampling

The Monte Carlo Importance Sampling (MCIS) is a variance reduction method that is useful for estimating rare event probabilities (Kroese et al., 2011). The MCIS method takes the standard MC sample set and moves the origin to the design point $U*$, which is determined with the FORM analysis. The MCIS then concentrates on the sample points in the interval that are of the most 'importance' resulting in an unbiased estimator (Reiher, 1966). Since the Monte Carlo analysis produces a low sampling density in the failure domain, a high number of samples is required for a reliable failure probability estimate (Donders et al., 2003). The MCIS method repeatedly takes samples of the variables from the multivariate probability distribution functions of the stochastic parameters and computes the limit state function for each sample (Deltares, 2020).

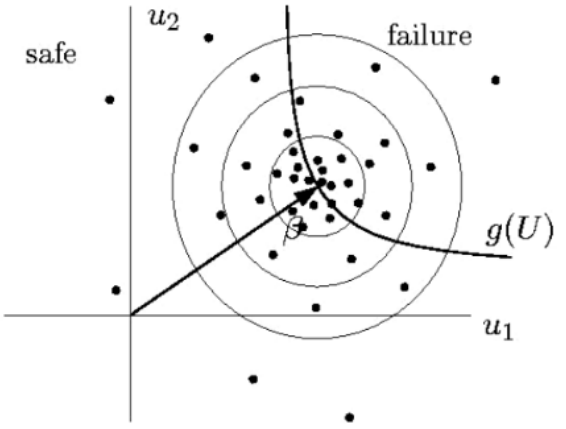

Figure 2.9: Visualization of the MCIS sampling method (Donders et al., 2003)

The importance sampling method reduces the number of stability calculations when compared to only using a Monte Carlo simulation from 10^8 to 10^9 computations to around 10^2 to 10^3, having a positive influence on the computational time (Kwakman, 2020). The MCIS analysis in D-Stability is limited to 3 variance loops, with the number of realizations in one loop limited to 2000. The MCIS analysis provides the probability of failure, the reliability index, and the design point contributions. The design point $U*$ consists of a contribution value alpha (α) for each stochastic variable. α denotes the contribution of the stochastic variable to the reliability index.

Limitations D-Stability

Several limitations to the D-Stability software should be noted before the stability analysis.

- The number of stochastic variables in the full-probabilistic analysis is limited, or the calculation will not converge to a solution. The number of stochastic variables is advised to be limited to 10.
- Only material properties can be used as a stochastic variable in D-Stability analysis, for example, the strength parameters of each soil type and the pre-overburden pressure. The unit weight of the soil or the hydraulic boundary conditions can not be included as a stochastic variable.
- The MCIS analysis realizations are limited by 3 loops each including a maximum of 2000 realizations (Deltares, 2020).
- If the reliability index is larger than 8, the MCIS analysis will experience convergence issues.

2.5.2. Integration of fragility curves

The Probabilistic ToolKit (PTK) can be used additionally to D-Stability to analyze the uncertainties of the macrostability calculation. The toolkit can perform various analyses, for example a sensitivity analysis to analyse the effects of changes to input variables (Deltares, 2022). The PTK is not required to be applied in the safety assessment, however, can provide more insight into the stability model and is widely implemented during design assessments. The PTK is used in the uncertainty analysis to perform a reliability analysis. The fragility curves exported from D-Stability can be imported in the PTK where they can be combined and provide the failure probability of the combined fragility curve. The combined failure probability is calculated via equation 2.16. The PTK applies numerical integration to compute the combined failure probability, where the failure probabilities (P_f) assigned to the imported fragility curves are multiplied by the contributions f_c provided in the PTK. These values are integrated over the distribution of the outer water level Δh (Timo and Kanning, 2017).

$$P_f = \int P_f(F|h) f_c(h) dh \tag{2.16}$$

The integral can be approached by using numerical integration via equation 2.17.

$$P_f = \sum P_f(F|h) f_c(h) \Delta h \tag{2.17}$$

The benefit of using the PTK in the macrostability safety assessment is that a CDF curve is used to describe the distribution of the outer water level. The return periods of the extreme outer water levels provided by Hydra-NL can be used as a direct input in the PTK. The exceedance frequency is used as a direct input instead of using the Gumbel approach. Additionally, the PTK can import fragility curves from D-Stability via JSON files. A limitation to the use of the PTK is that the contributions of the imported fragility curves are applied with a discrete distribution function.

2.6. Uncertainties in the macrostability safety assessment

With the transition from the WBI to the LBOI, the current standard is to apply a semi-probabilistic calculation in the macrostability safety assessment of a dike trajectory. The full-probabilistic calculations only recently became available to be applied within the macrostability safety assessment, however are not widely implemented yet. In the current methodology of schematization of components relevant to the macrostability safety assessment, several large uncertainties can be highlighted. These components are expected to have a large influence on the expected reliability and are included in the project to investigate the impact of considering the uncertainties within the macrostability safety assessment.

1. Schematization of the subsurface
   The methodology described by the WBI to schematize the subsurface underneath the dike section applies to all dike trajectories located in the Netherlands. The subsurface in the Alblasserwaard is highly complex, with large spatial variation in the subsoil, and an abundance of peat soils with high organic content. It is difficult to apply a general schematization process suited to the entire Netherlands to a local region with many exceptions and difficulties in the subsurface.
2. Schematization of the pore water pressures
   A large uncertainty in the current macrostability calculation is the schematization of the pore water pressure components that describe the groundwater flow underneath the dike cross-section at high water conditions. The three components are the hydraulic head in the aquifer, the intrusion length in the blanket layer, and the height of the phreatic line. The three components in the macrostability safety assessment are currently schematized as deterministic input.

   (a) The intrusion length in the blanket layer
   The value for the intrusion length is currently based on expert judgement and is a deterministic input in the macrostability safety assessment. The intrusion length is an epistemic and aleatory uncertainty since the parameter is dependent on the duration of the high water conditions and the consolidation coefficient of the blanket layer, which are difficult to determine and vary locally. The values that can be applied to simulate the intrusion length that are currently applied in the schematization process are a safe approximation. However, the length of the intrusion during a high water event significantly impacts the macrostability of a dike cross-section.

   (b) The hydraulic head in the aquifer
   The calculation process to determine the hydraulic head in the aquifer during high water conditions is currently dependent on local measurements or a sufficiently safe engineering judgement is considered. The uncertainties in the schematization of the hydraulic head are therefore dependent on the measurements or the extrapolation of measurements from a different, comparable location. The hydraulic head is also an epistemic uncertainty since in-situ measurements are usually representative of daily loading conditions, that require to be extrapolated to extreme loading conditions that only occur once every 10000 years that are required to be assessed in the safety assessment.

   (c) Phreatic line
   The current schematization of the phreatic line follows the process as described by the TR, which is assumed to be considerably safe. The uncertainty of the height of the phreatic line during high water events is another epistemic uncertainty. The phreatic line depends highly on the initial conditions before the high water event. The height of the phreatic line in the dike is unknown and is recommended to be measured in situ. This poses more difficulties since the relevant water levels important for the macrostability safety assessment are less likely to occur. An aleatory uncertainty concerning the phreatic level is the variability of the hydraulic conductivity of the dike material.

3

Including schematization uncertainties in the safety assessment

After describing the current methodology that is applied to assess the macrostability of a dike cross-section in chapter 2, the largest uncertainties in the current methodology are described by the end of the chapter: the schematization uncertainties in the subsurface and the pore water pressure schematization. Chapter 3 describes the process and method applied to consider these uncertainties during the current process of assessing the macrostability of a dike cross-section. The general research approach is described in this chapter, which is applied to case studies in the Alblasserwaard in chapters 4 and 5.

3.1. Process description: including uncertainties of the local subsurface

The first uncertainty that is investigated in the project is the influence of including schematization uncertainties in the local subsurface. The subsurface modelled in D-Stability has a large influence on the reliability of the dike cross-section. Including schematization uncertainties of the subsurface from site investigation data will improve insight into the actual stability of a local dike cross-section. The influence of including schematization uncertainties of the subsurface in the macrostability assessment will be determined by analyzing several different soil scenarios for one local dike cross-section. This methodology is used to compose a fragility curve that describes the reliability of each soil scenario. The scenarios can be combined by applying discrete scenario probabilities to provide the combined failure probability that includes the schematization uncertainties in the local subsurface. A flow chart shows the general process of analyzing the contribution of the schematization uncertainties to the macrostability safety assessment in figure 3.1.

Figure 3.1: Flow chart process subsurface schematization uncertainties

The schematization process of a local representative subsurface starts with the investigation of the local geology and geohydrology of the region. Local site investigation is used to set up multiple possible subsurface configurations since the layering of the soil can be highly variable over short distances. The general depth and width of certain soil layers can be documented from local CPT data and mechanical borings. The scope of the project limits the subsurface schematization to a one-dimensional vertical soil profile. Since only the macrostability of the dike cross-section is considered, the vertical layering of the soil is of the most importance.

Several different soil scenarios are set up by using the local soil investigation data. Each of the soil scenarios is assigned a probability of occurrence, which is based on the expectancy of each soil layer and the occurrence of each soil layer assigned in each of the soil scenarios. Once the soil scenarios are set up, each of the soil scenarios is modeled in D-Stability to determine the reliability index and failure probability via a full-probabilistic MCIS calculation. The calculation is performed for multiple outer water levels, which will provide the fragility curve for each soil scenario. The fragility curves are exported from D-Stability and are analyzed in the Probabilistic Toolkit (PTK). The probability of occurrence for each local soil scenario is assigned to each fragility curve in the PTK, which is similar to the current methodology concerning the SOS scenarios as described by the WBI (discussed in chapter 2. The fragility curves are integrated into the PTK by numerical integration, providing a combined fragility curve and combined failure probability. This results describes the reliability of the local dike cross-section including the schematization uncertainties of the subsurface. Note that other schematization uncertainties are considered to be constant throughout the analysis, and are a deterministic input determined according to the previously described processes concerning the WBI.

3.2. Process description: including uncertainties in the pore water pressures

The uncertainties in the schematization process of the pore water pressures can be investigated by analyzing the components that have a significant influence on the pore water pressures resulting under high loading conditions. The pore water pressure schematization as described by the WBI is considered conservative and sufficiently safe. The pore water pressures have a significant influence on the dike reliability, so will benefit from a transition to expected values for the pore water pressure including a range of uncertainty when compared to the conservative design values. The results of the macrostability safety assessment will provide more insight into the actual dike stability and the influence of the pore water pressure components on the stability can be investigated, which is beneficial for the macrostability safety assessment. The schematization process of the pore water pressure components that are included in the project are the hydraulic head level in the aquifer, the intrusion length in the blanket layer, and the phreatic level. The uncertainty of the leakage length is included directly in the analysis of the uncertainty of the hydraulic head in the aquifer. These components are considered during the project since the current processes, as described in chapter 2, are considered conservative and can be improved by using the full-probabilistic assessment. The flow chart that describes the general process is shown in figure 3.2.

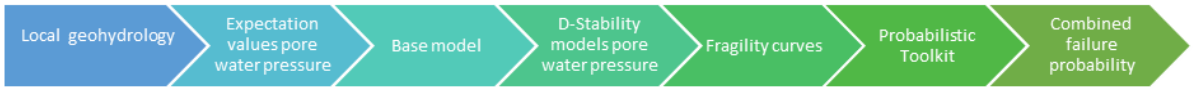

Figure 3.2: Flow chart process schematization uncertainties of the pore water pressures

The local geohydrology of the Alblasserwaard is investigated to highlight the local loading conditions on the dike cross-sections. Local measurement data is available for the outer water levels and river discharges. Additionally, piezometer measurement data will be used to accurately calculate the hydraulic head in the aquifer. The local geohydrology of the Alblasserwaard can be separated into two categories: upper river and lower river area, or the transitional area. The boundary between the upper river area and the lower river area of the Netherlands is located in the middle of the Alblasserwaard region, as displayed by figure 3.3. The transition between areas is an arbitrary border, where the transition is dominated by the duration of the high water event which determines the geohydrological response. Since the research methodology of the uncertainties in the pore water pressure components should be representative of the Alblasserwaard region, one case study should be located in the upper river area (R) and one in the transitional area / lower river area (O).

Figure 3.3: Separation of the river areas of the Netherlands: Z: sea area, O: transition area / lower river area, R: upper river area (Rijksinstituut voor Integraal Zoetwaterbeheer en Afvalwaterbehandeling., 2007)

The calculation process to determine a realistic range for the intrusion length, hydraulic head, and the phreatic level can be calculated for each case study. These results are additionally used to set up a base model, which is used to display the influence of implementing the schematization uncertainties in the macrostability safety assessment. The general process of determining the expectation values of the pore water pressure components is shown in figure 3.4.

3.2.1. Calculation process pore water pressure components

The process of each component describing the pore water pressures is discussed below. The full-probabilistic base model is set up by implementing all the 95% expectation values for each of the pore water pressure components. The base model is used to compare the results with the analysis including the schematization uncertainties of the pore water pressures. The failure probability of the base model can be compared to the combined failure probability including the schematization uncertainties. For each case study, a base model is set up. Other components in the analysis will remain constant in compliance with the WBI.

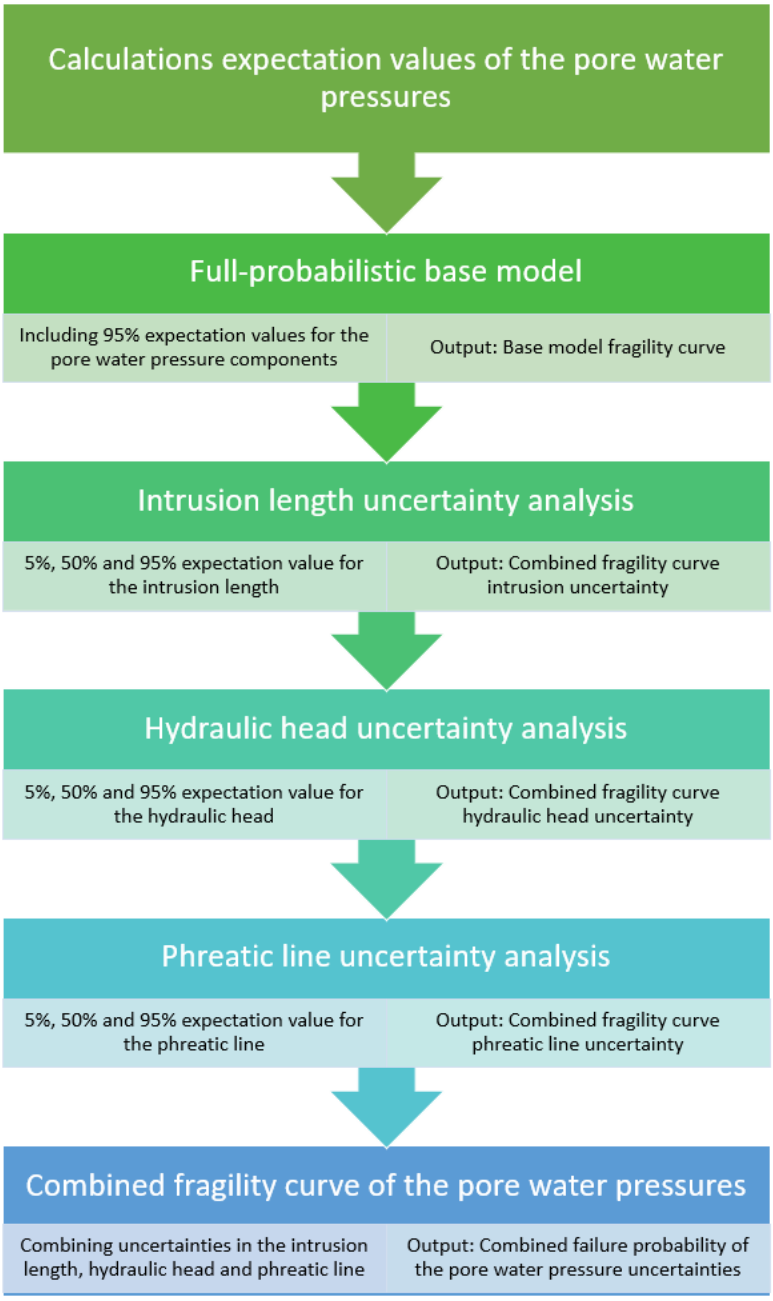

Figure 3.4: Detailed flow chart of the process of the pore water pressure analysis

Calculation process intrusion length analysis

The influence of the schematization of the intrusion length is analyzed by using a distribution function that describes the value for the intrusion length over the blanket layer. The distribution function will be based on expert judgement since the value of the intrusion length depends on the mostly duration of the high water conditions and the soil type of the blanket layer. These variables are aleatory uncertainties and are difficult to quantify. The distribution function for the intrusion length, however, will cover the thickness of the blanket layer. The distribution function for the intrusion length will be case-dependent.

Calculation process hydraulic head analysis

The hydraulic head can be calculated by applying realistic input values including the uncertainty of these parameters for each case study. The stationary groundwater flow approach will be applied to the case study located in the upper river area, and the time-dependent approach will be applied to the

case study in the lower river area. The same analytical models are used to calculate the hydraulic head as a stochastic variable that is described by the *Technische rapport Waterspanningen bij dijken* and are currently applied in the macrostability safety assessment. The calculation method should be approachable and reproducible for the Water Authority Rivierenland (WSRL) for other case studies in the future. The input for these calculations are expected values for deterministic input, and stochastic variables for uncertain parameters.

Approach stationary groundwater flow

The stochastic variables that are considered in the calculation of the stationary groundwater flow are the transmissivity of the aquifer and the resistance of the foreshore and hinterland. Other deterministic parameters remain constant throughout the analysis and are determined in compliance with the WBI. The hydraulic head is calculated with the stochastic variables taken into consideration in equation 3.1.

$$\phi(x) = \phi_{polder} + r(x)(\phi_0 - \phi_{polder}) \tag{3.1}$$

The distribution function is applied on the response r_i. The resulting hydraulic head for dike sections located in the upper river area is calculated via equation 3.1.

Approach time dependent groundwater flow

The stochastic variables that are considered during the analysis of the time-dependent hydraulic head are the entry point and the resistance of the blanket layer. The stochastic variables are input for equation 3.2.

$$\phi(x,t) = H_0 \,\mathsf{exp}(-0,924\frac{x + x_{entry}}{\lambda_\omega}) \tag{3.2}$$

Via a Monte Carlo simulation, the distribution of the time-dependent hydraulic head follows from equation 3.2 as a normal distribution function.

Calculation process phreatic level analysis

The phreatic level can be described as the gradient of the head from the water level in the river concerning the water level behind the dike. If the dike body is composed of sandy soil, the phreatic level coincides with the river water levels. Due to the lower permeable soil layers in the Holocene deposits in river dikes, this can result in a deviation in the phreatic line. The current methodology of determining the height of the phreatic level is based on (conservative) design values. The uncertainties in the height of the phreatic level during high water events are not well included in the macrostability safety assessment yet. The position of the phreatic line is difficult to calculate accurately, it requires to be measured. An initial schematization of the phreatic line on an impermeable dike body can be based on in-situ measurements. However, pore water pressure measurements will mostly cover daily loading conditions, since extreme storm conditions have an extremely low probability of occurrence. The actual height of the phreatic line during high water events is difficult to determine due to aleatory and epistemic uncertainties:

- The initial loading conditions concerning the degree of saturation of the dike body. If the dike body is saturated before the high water conditions, the resulting phreatic line during high water conditions will be higher than for unsaturated initial conditions.
- Seasonal influences can also cause the phreatic line to fluctuate by 0,5m in clay dikes (Rozing, 2015).
- The position of the phreatic line is dependent on the hydraulic conductivity of the dike body. Since river dikes are usually composed of a clay cover and core material, it is difficult to assign a value to the hydraulic conductivity of the dike body. Cracks in the clay cover that occur due to wetting and drying of the clay can also impact the hydraulic conductivity of the dike body significantly.

Due to these major uncertainties in the height of the phreatic line, the approach to analyzing the uncertainties in the schematization process of the phreatic line is based on the methodology used in the safety assessment, as described by the *Technische rapport Waterspanningen bij dijken* (TR) (Technische Adviescommissie voor de Waterkeringen, 2004) and described in chapter 2.

Appendix E includes the Dupuit formulation to describe the height of the phreatic line, as described in a memo on the uncertainties of the pore water pressures of the WBI (Rozing, 2015). Since this method is unsuccessful, the TR is used to simulate the uncertainty in the design value for the phreatic line. The TR describes the schematization process of the phreatic line for a dike with a clay core and a sandy core, shown in figure 2.3. The dikes in the Alblasserwaard have been reinforced multiple times in the past by adding dike material, usually to the crest and inner and outer slope of the dike body. The material used in the reinforcement can be composed of clay or sandy material. However, the behaviour of the dike material is difficult to predict. This behaviour depends on several factors such as the soil permeability, drainage length of the soil layer, and the degree of over-consolidation (van Duinen, 2014). The schematization of the phreatic line for the clay dike body can be applied as the 95% upper limit since this schematization is considered conservative. This schematization is based on fully saturated initial conditions and low permeable dike material to simulate the most critical conditions. The schematization of the phreatic line for the sandy dike body can be considered as the 5% lower limit. This schematization is based on unsaturated initial conditions and porous dike material.

3.2.2. Modelling process

The input of the pore water pressures in D-Stability is deterministic, therefore these components require a deterministic input. Each component that describes the pore water pressures that follow from the calculation process is a stochastic variable, described by a distribution function. From each distribution function, the 5%, 50%, and 95% percentile are modeled individually in three different scenarios in D-Stability for multiple outer water levels. Fragility curves are constructed for each percentile for multiple outer water levels. The fragility curves describe the range of the reliability for each component of the pore water pressures. The full-probabilistic analysis is used in D-Stability to include all stochastic variables and keep the failure surface free, so the most critical slip surface can be found considering all uncertainties.

The fragility curves can be combined in the Probabilistic ToolKit by assigning a contribution to each imported fragility curve. The distribution of the fragility curves in the PTK is limited to a discrete distribution. Since the process should be accessible for the WSRL, the Toolkit is used to combine the fragility curves. The limitation is the discrete distribution of the 5%, 50%, and 95% percentile fragility curves. Each combined fragility curve that describes the uncertainties of each pore water pressure component, hydraulic head in the aquifer, intrusion length, and phreatic line, can be combined again in the ToolKit that eventually provides the failure probability of a dike cross-section taken the pore water pressure uncertainties into account.

4

Schematization uncertainties of the subsurface

This chapter describes the process of including the schematization uncertainties of the subsurface in the macrostability safety assessment for the first case study of the Kortenhoevendijk. The process of investigating the schematization uncertainties is additionally performed for a dike cross-section of the Lekdijk near Kinderdijk, on the west side of the Alblasserwaard. However, this local dike section proved to be considerably stable due to the settlement of previous dike reinforcement material into the local peat layer. The overall stability of this cross-section posed issues during the full-probabilistic analysis. Since the process is very similar to the first case study, the description of the analysis of the Lekdijk near Kinderdijk is added in Appendix E. This chapter first will introduce the case study of the Kortenhoevendijk, after which the process of the soil investigation is discussed by analyzing the SOS scenarios and setting up the soil profiles through local soil investigation. After this, the D-Stability and PTK analysis are discussed.

4.1. Introduction case study: Kortenhoevendijk

The Kortenhoevendijk is a section of the primary dike trajectory in the north-east the Alblasserwaard near Vianen next to the river Lek, shown in figure 4.1. The Kortenhoevendijk is included in the most recent dike reinforcement project 'SAFE' by the WSRL. The dike reinforcement project SAFE includes the reinforcement of the Lekdijk from Streefkerk to Ameide and Fort Everdingen in the Alblasserwaard. The project was initiated in 2017 with local soil investigation using mechanical pulse borings, CPT testing, and laboratory testing on local soil samples to gain insight into local soil layers and strength parameters. The Kortenhoevendijk is a representative dike section for the Alblasserwaard region since the dike is locally subjected to the uplift of the blanket layer during high water conditions, a failure mechanism that is known to occur around the region. The location of the Kortenhoevendijk section is displayed in figure 4.1 (a).

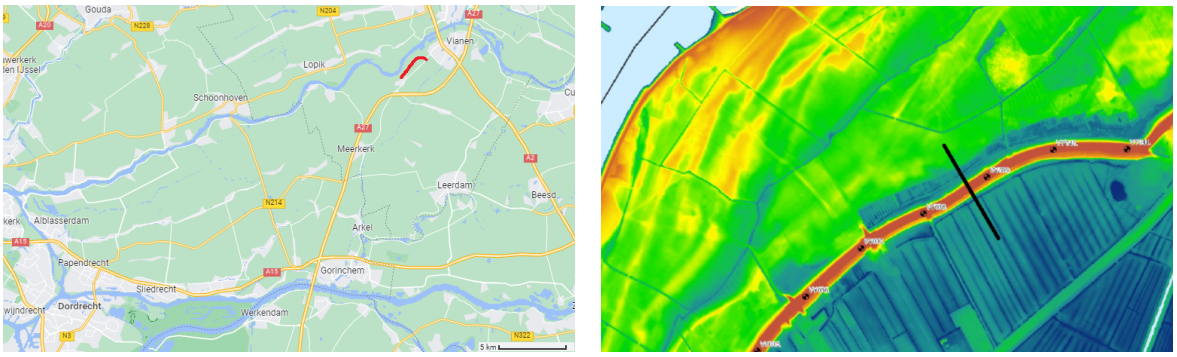

(a) Location of the Kortenhoevendijk with respect to the Alblasserwaard

(b) Height map of the Kortenhoevendijk, scale 1:6000 meters

Figure 4.1: Location of primary dike section Kortenhoevendijk in the Alblasserwaard

The research into the schematization uncertainties of the subsurface will focus on a local section of the Kortenhoevendijk. Figure 4.1 (b) displays the location of the local dike-cross section on the height map of the region. This location is assigned by the most recent macrostability safety assessment to be the location of the most critical subsurface of the entire dike section. The crest of the dike is situated at 7.25 m NAP, and the foreshore and hinterland are situated at 1.8 m NAP and 1.3 m NAP respectively. The local foreshore at this location has a length of around 600 to 700 meters. To gain insight into the subsurface underneath the dike section of the Kortenhoevendijk, the SOS scenarios are investigated.

4.1.1. WBI SOS Scenarios

The first step in the macrostability safety assessment as described by the WBI is to investigate the SOS scenarios for the relevant dike section. Four SOS scenarios can be extracted from D-Soil Model that describes the subsurface underneath the entire length of the Kortenhoevendijk and are displayed in figure 4.2. D-Soil Model is used throughout the assessment of primary dike trajectories in the Netherlands. The soil layers of the D-Soil Model scenarios are based on the notation as described by the WBI. The macrostability safety assessment uses the soil classifications provided by the WSRL in the test collection and vertical soil profiles. The table added in figure 4.2 displays the comparison between the two notations for each soil layer and a short description of the soil type.

WTI SOS Notation	WSRL Notation	Soil description
$H\_Ro\_z\&k$	Z_k	Clayey sand
$P\_Rk\_k\&s$	K_z	Sandy clay
P_Ova_sd	K_z	Humus clay
H_Vhv_v	V	Peat
H_Rk_ko	K_o	Organic clay
H_Vbv_v	V	Peat
H_Rk_vk	V_k	Clayey peat
H_Rk_k	K_s	Silty clay
P_Rg_zm	Zh	Sand
P_Wrd_zm	Zh	Sand
P_Rg_zg	Zp_K	Pleistocene sand Kreftenheye

Figure 4.2: WBI Soil scenarios for Kortenhoevendijk dike trajectory, extracted from D-Soil Model (Deltares, 2017)

Due to the large spatial variability of the subsurface locally, the four scenarios display a large variation in soil layers. The first two scenarios (D1 & D2) display a subsurface mostly composed of soft soil layers such as peat and organic clays. The 3rd and 4th scenarios (D3 & D4) display a mostly sandy subsurface underneath the Kortenhoevendijk. These scenarios describe a Holocene sand layer

on top of the Pleistocene sand due to local river deposits. The SOS scenarios display the importance of a local schematization of the subsurface since these soil scenarios show a large spatial variation in the subsurface. In the selection of a representative subsurface schematization, the outcome of the macrostability safety assessment is impacted greatly. The sandy subsurface schematizations are likely to create more resistance during high water events concerning the macrostability when compared to the soft soil scenarios.

For each SOS scenario that is provided by D-Soil Model, a probability of occurrence is assigned which describes the likelihood of the soil profile at the specified location. These probabilities are based on background information from local soil investigation data (Deltares, 2017). The probability of occurrence for each soil scenario is displayed in table 4.1. Soil scenario 1 has the largest probability of occurrence with 80% in this particular dike section.

Soil scenario	Probability of occurrence %
Segment_16027_1D1	80
Segment_16027_1D2	15
Segment_16027_1D3	2.5
Segment_16027_1D4	2.5

Table 4.1: Probability of occurrence for each WBI soil scenario (Deltares, 2017)

The soft soil scenario has acquired the largest probability of occurrence and is also expected to be the most critical subsurface schematization in the macrostability safety assessment.

4.2. Local subsurface schematization

The macrostability of the dike cross-section is mostly dependent on the shear strength of the soil layers located underneath the inner dike slope. The process of setting up a local, representative subsurface at the inner dike slope is initiated via the borings and CPT data which is used to identify the precise boundaries between different soil layers. To visualize the local subsurface during the dike reinforcement project, a vertical profile of the subsurface configuration was set up by geotechnical experts from Arcadis. The local subsurface layout at the local section of the Kortenhoevendijk at the inner dike slope is displayed in figure 4.3. The vertical profile set up by Arcadis is used for the identification of the specific soil layers in combination with the borings and CPTs for the local subsurface profiles.

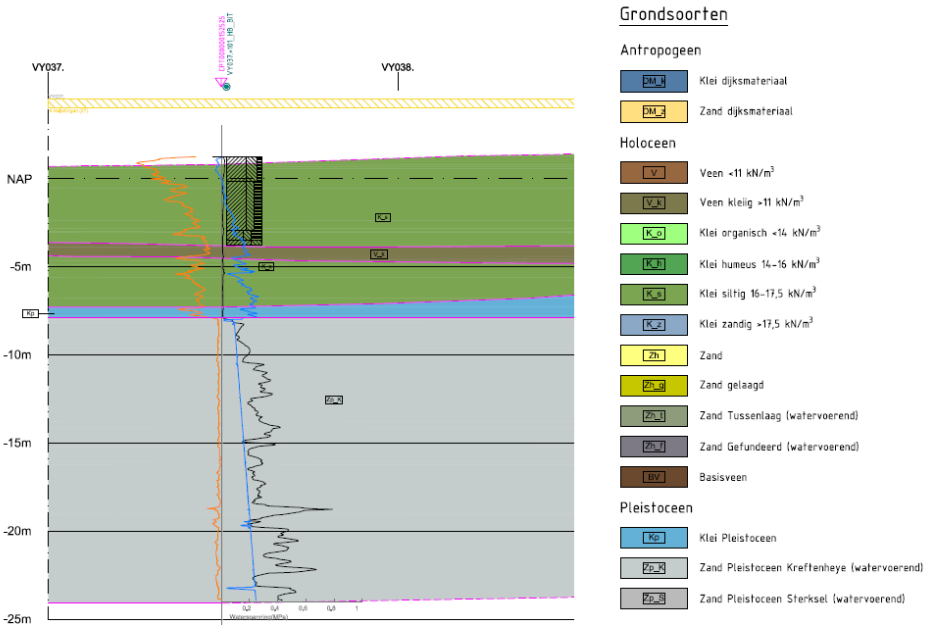

Figure 4.3: Local subsurface soil profile for the Kortenhoevendijk local dike section below the inner dike slope

The local subsurface in the soil profile displays a soft soil blanket layer, composed of silty clay and clayey peat. The local spatial variation in the subsurface underneath the Kortenhoevendijk is large due to old river deposits. As previously mentioned, this is not uncommon in the Alblasserwaard. This can result in a completely different subsurface layout at the next dike pole.

4.2.1. Local soil investigation

The location of the soil investigation that is present at the chosen dike location of the Kortenhoevendijk is displayed in figure 4.4. The measurements are situated at around 25 meters from the initial specified location. All of the CPTs and mechanical borings performed during the investigation set up for the dike reinforcement project SAFE are equally spaced at 100 meters apart. If the spatial variation in the soil is known to be larger than 100 meters at a specific location, additional site investigation was performed. The CPTs and borings are equally placed at the outer slope of the dike, the crest, the inner slope, and one in the hinterland.

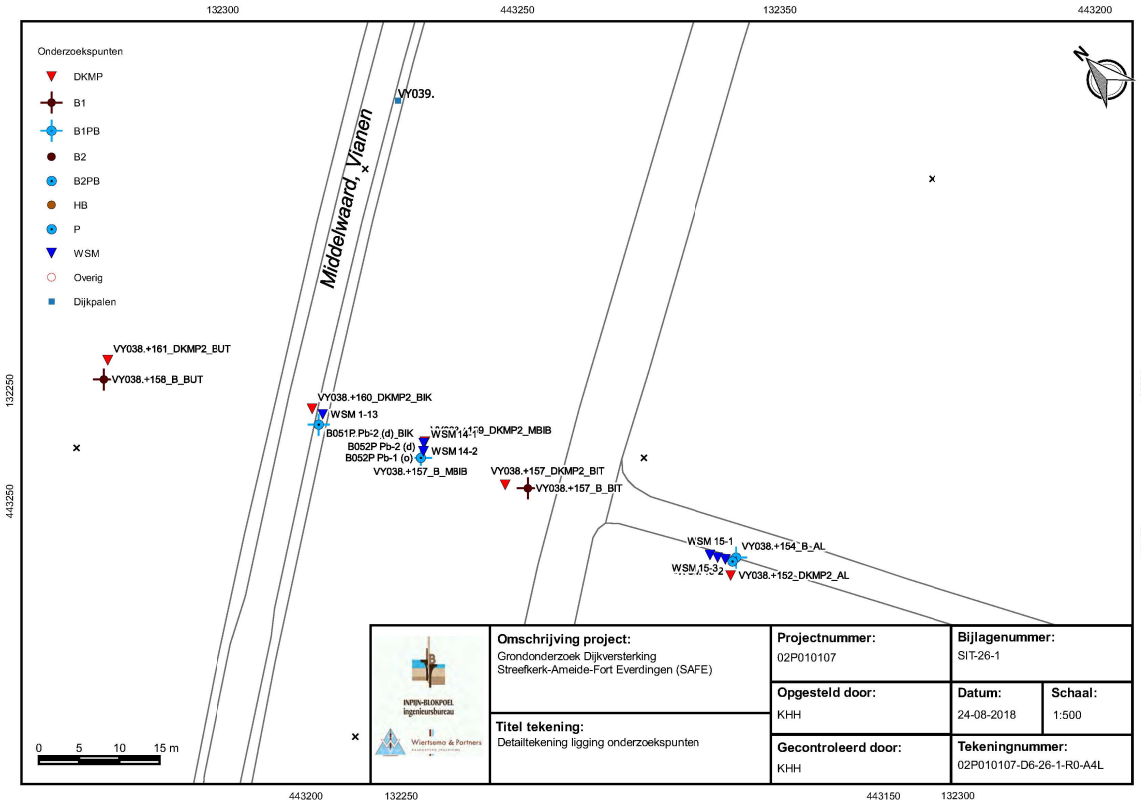

Figure 4.4: Locations of the local soil investigations at the local dike cross-section of the Kortenhoevendijk

The results of analyzing the mechanical borings and CPT's displayed in figure 4.4 and provide insight into the local subsurface near the critical cross-section. The CPT data and visuals of the mechanical borings are included in Appendix A and are analyzed with pen and paper. A total number of 5 borings and 5 CPTs are taken at this location. The borings in combination with the CPTs are used to create a cross-section of the dike from this local soil data, shown in figure 4.5. The soil classification applied in this figure is based on the notation provided by the WSRL. This will simplify the process of setting up the scenarios in D-Stability since the soil parameters that will be assigned to each layer can be used directly from the SAFE test collection, which is discussed later in this chapter.

Figure 4.5 is set up to follow the vertical layout of the dike cross-section, on the left the outer dike slope is in contact with the river (only at high water events), and on the right side the hinterland. Figure 4.5 displays a foreshore mostly composed of sand (Zh) with a silty clay interlayer (K_s). At the inner

dike slope and in the hinterland, the subsurface consists of mostly clay layers with relatively thin peat layers. The separation in these clay layers is based on the test collection from the WSRL, where the soil type is mainly identified by the unit weight of the soil. Since the subsurface at the inner dike slope is of most importance concerning the macrostability of this dike cross-section, the analysis will focus on the most right borings of figure 4.5. The blanket layer at this location appears to be around 7 to 10 meters thick.

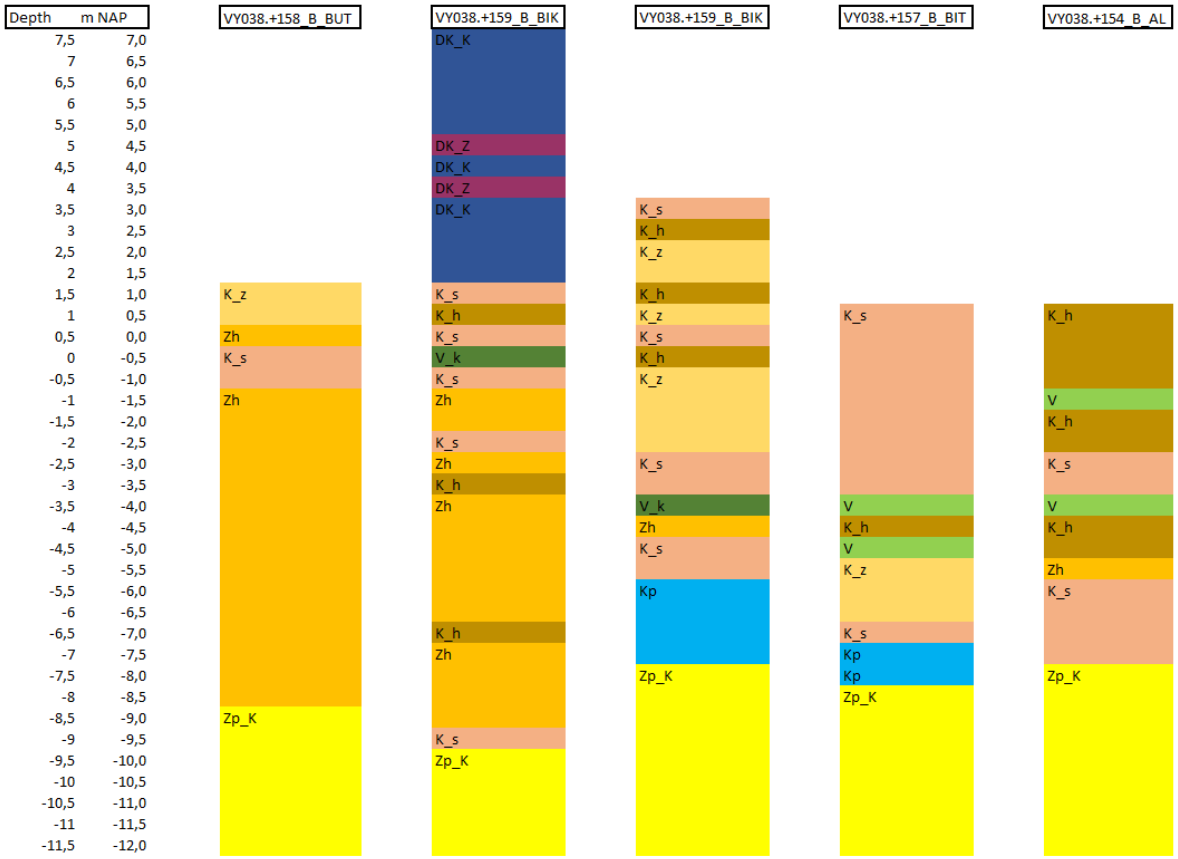

Figure 4.5: Soil profiles extracted from the site investigation data at the locations displayed in figure 4.4

Uncertainties concerning the soil type, layer thickness, and soil layer position are taken into consideration by using multiple local soil scenarios which are each assigned a probability of occurrence. This method is based on the methodology as described by the WBI, only on a local scale. During the analysis, all scenarios will be taken into consideration, where the WBI only takes one. Based on the soil investigation data from the inner slope of the dike, four detailed soil scenarios can be set up that will be analyzed in D-Stability on the macrostability of the local dike cross-section.

4.2.2. Soil scenarios for the inner dike slope

The local soil scenarios that can be set up for the Kortenhoevendijk are variations of the mechanical boring data and CPTs extracted from the inner dike toe. The four local soil scenarios that are set up for the Kortenhoevendijk are displayed in figure 4.6. The soil layers in each scenario are considered to 2 decimals precise, based on the mechanical borings, and checked with the CPT data. Two thicknesses of the blanket layer are included to investigate the influence of this important variable. The different depths of the dike material are used to indicate the influence of the schematization assumptions in the layer positions. The same can be done for the silty clay layer (K_s) at the bottom of the blanket layer. The scenarios are set up far more detailed than the schematizations that would be used in safety assessments for macrostability. The four scenarios are purposefully set up as more complex and include more of the thin soil layers (< 0.5 meters) that can be used to indicate the influence of including or excluding these thin soil layers, and the uncertainties that the schematization of these thin

soil layers bring in the macrostability safety assessment. Scenarios 1 and 4 show a more complex soil layering, whereas scenarios 2 and 3 are more simplified cases. The influence of simplifying a complex soil layering into one soil type can be investigated by comparing the results of scenarios 1 & 4 with scenarios 2 & 3. The dike material in the crest is simplified by removing the interlayered soil since the general influence of the strength of the dike material on the macrostability is expected to be negligible.

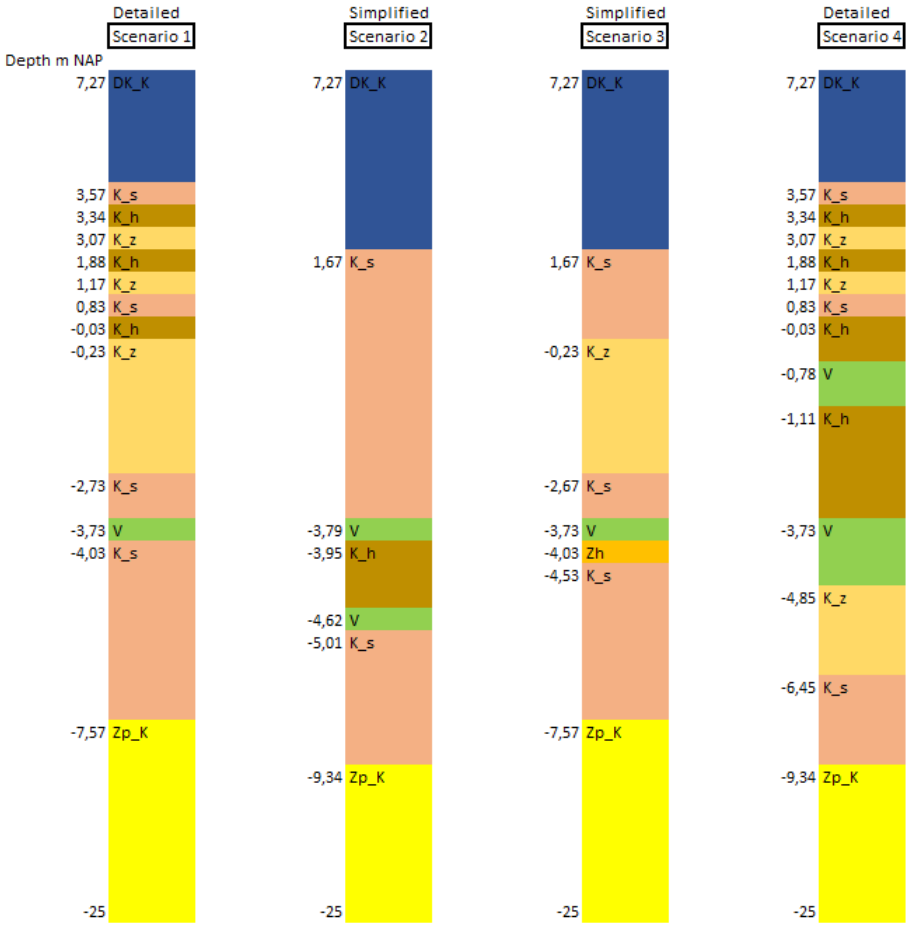

Figure 4.6: Local soil scenarios set up for Kortenhoevendijk based on local soil investigation data in the inner dike slope

Scenario 3 is the simplified profile for soil scenario 1, and scenario 2 is the simplified profile for scenario 4. For each scenario, a probability of occurrence can be assigned. The probability of a soil layer occurring in the SOS scenario as described by the WBI depends on the number of observations of the soil layer in soil investigations and the frequency of the unit in local observations and soil investigations (Kruse and Hijma, 2015). Since the scenarios that are set up for the local schematization of the subsurface are very similar and based on local soil investigations, the probability of occurrence for each scenario is assumed to be 25%.

4.2.3. D-Stability modelling

The standard in the safety assessment of the macrostability of primary dikes in the Netherlands is to use D-Stability to assess the overall stability of the most critical cross-section. The D-Stability model that is used in the most recent macrostability safety assessment is displayed in figure 4.7. The dike is modeled in D-Stability to determine the macrostability by using a clay dike cover by assigning a value for the cohesion of the soil. This provides representative strength for the cover material in the D-Stability model. The safety assessment separates the dike material into a saturated and unsaturated zone, where the behaviour of the saturated clay is described by using laboratory soil test data. The unsaturated zone behaviour is described with the Mohr-Coulomb criterion. The soil underneath the dike body is silty clay with one thin peat layer on the inner slope.

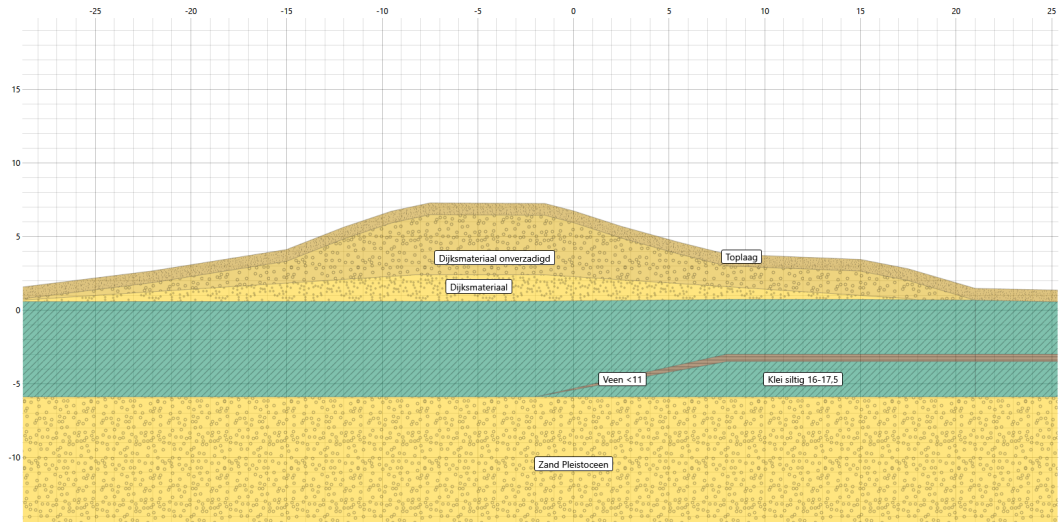

Figure 4.7: Most recent macrostability assessment model for the dike section Kortenhoevendijk

Similar D-Stability models are set up for each soil scenario from figure 4.6 in D-Stability version 2023.01. The macrostability is analyzed for each soil scenario for three different outer water levels: the daily water level, the water level determined by the safety standard, and an extra intermediate water level to compose the fragility curve. The D-Stability models are set up by using the following process:

1. Geometry and subsurface schematization.
   The dike geometry is copied directly from the macrostability safety assessment since this is not included in the scope of the project. For each soil scenario, one D-Stability model can be set up. The soil layers are assumed to be constant in the horizontal direction, this is also the case in the D-Stability models. Each soil scenario is analysed for three different water levels to construct the fragility curve, resulting in a total of 3 x 4 = 12 fully-probabilistic calculations. Each calculation can last from 1 to 2 hours, resulting in a total computational time of at least 12 hours.
2. Material input.
   The soil strength parameters that are used in the D-Stability model are taken directly from the test collection of the WSRL. The test collection of the WSRL is based on laboratory tests on soil samples in the region taken from multiple mechanical borings that were executed from 2017 to 2022. The soil samples are taken from the dike crests, inner and outer dike toes, and in the hinterland. From these mechanical borings, a number of soil samples are taken and tested in different laboratory tests. The current test collection of the WSRL is composed of 128 Constant Rate of Strain (CRS) tests, 170 triaxial tests, and 94 Direct Simple Shear (DSS) tests. The clay soil samples are tested in the triaxial test apparatus, the DSS tests are used on both clay and peat soils. Table 4.2 displays the values that are applied for each soil layer included in all four soil scenarios in the D-Stability model.

Soil notation	**Unit weight** $[kN/m^3]$	$\phi_{Char}[^\circ]$	$\phi_{Mean}[^\circ]$	$\phi_{SD}[^\circ]$	**m [-]**	S_{Char} **[-]**	S_{Mean} **[-]**	S_{SD} **[-]**
DK_k	18.56	33.6	36.2	1.6				
DK_z	18.56	32.4	34	0.986				
K_s	16.86				0.5	0.26	0.28	0.013
K_h	15.11				0.5	0.28	0.31	0.019
K_z	18.56	33.6	36.2	1.6				
Z_h	20	33.6	36.2	1.6				
V	10.55				0.5	0.35	0.4	0.032
Z_p	20	32.4	34	0.986				

Table 4.2: Test collection parameters used in the D-Stability modelling of the soil scenarios (Kwakman, 2023)

The soil types mentioned in table 4.2 that are assigned a value for the friction angle ϕ, are assigned the shear strength model of Mohr-Coulomb (drained behaviour). The soil types that are assigned values of the shear strength ratio S and strength increase exponent m are assigned the SHANSEP formulation (undrained behaviour). The cohesion is only assigned to the dike cover in the D-Stability model to simulate the variable strength of the layer by a conservative estimation of the strength of the clay material. Since the dike cover does contain a level of shear strength that should not be neglected, however, can contain rips and tears decreasing the level of shear strength significantly, only the cohesion is provided with a mean and standard deviation.

Full probabilistic calculations are prone to convergence issues if the number of stochastic variables is too large. To avoid convergence issues in D-Stability, it is recommended to limit the number of stochastic variables to 10, although the model might still converge with 20 stochastic variables (Deltares, 2020). The parameters that are assigned as stochastic variables in the full probabilistic calculations are therefore limited. In the most recent macrostability safety assessment, the number of stochastic variables describing the soil strength parameters is limited to the POP, S, c and ϕ. The distribution of these parameters is assumed to be a lognormal distribution, and the test collection includes the characteristic value, average, and standard deviation. The strength increase component m is not considered a stochastic variable in the safety assessment, since the characteristic value for m is assumed to be equal to the average value, so the standard deviation is equal to zero.

3. Assigning the state.
   The pre-overburden pressure (POP) can be assigned to each soil layer in D-Stability by assigning the state. The POP is assigned to the clay and peat layers, except for sandy clay. The POP is assumed to be fully correlated with the soil underneath the dike, this additionally greatly reduces the number of stochastic parameters, but will still consider the values for the POP as a stochastic variable. The values for the POP that are used in the D-Stability model are displayed in table 4.3. Since the separation is made in the test collection in the soil properties assigned to soil layers located underneath the dike, or next to the dike, these are both added in the table. This is not taken into consideration during this analysis, however is used in the most recent macrostability safety assessment. This separation is also considered in the analysis of the schematization uncertainties of the pore water pressures.

Soil type	POP Characteristic	POP Mean	POP SD
Next to the dike	16	26	7
Underneath the dike	29	43	10

Table 4.3: Assigned pre-overburden pressures in the D-Stability model (Kwakman, 2023)

4. Checking the water lines.
   The water lines are directly copied from the safety assessment. The lines are kept constant throughout the calculations for all scenarios, to create constancy and only adjust the soil profile for each scenario. The pore water pressures are assumed to adapt to the high water conditions.
5. Checking the calculation.
   Three calculations are performed for each scenario: a design, FORM, and MCIS analysis. In the design calculation, an initial semi-probabilistic analysis indicates the location of the most critical slip surface. The results of the design analysis are a safety factor (SF) for the given failure surface. Since the calculation method of the slip surface is limited to the Uplift Van method within the scope of the project, the particle swarm is simulated with a large initial calculation grid. The search grid can be narrowed down when the initial calculation finds a solution for the most critical slip surface. By moving the grid to the center of the slip circle and re-analyzing the model again the most critical slip surface can be found. The slip surface in the design analysis is imported into the FORM analysis, where a fully-probabilistic calculation is performed to provide a reliability index and failure probability for a given failure surface. The MCIS calculation should provide a similar result to the FORM analysis, and the search grid that is used in the MCIS calculation is based on the center of the slip surface found in the design analysis. The model factor that is used for the Uplift Van calculation has a mean expectation value of 1.005 and the standard deviation

is equal to 0.033 (Kanning et al., 2017).

Figure 4.8 displays the D-Stability models for the four different soil scenarios. The lines in the models between soil layers indicate the correlation between the soft soil layers. Initially, a separation was made in the model between the soil underneath and the soil located next to the dike. The strength parameters are assigned to be higher for the soil layers located underneath the dike body. The soil layers next to the dike body are known to have lower strength. However, this drastically increases the number of stochastic parameters in the probabilistic calculation. The number of variables exceeded 10, which resulted in convergence issues during the MCIS analysis. By removing the separation and assigning the least favorable strength parameters to the soil layers as a conservative assumption, the number of stochastic parameters is decreased (< 10) and the MCIS analysis does converge.

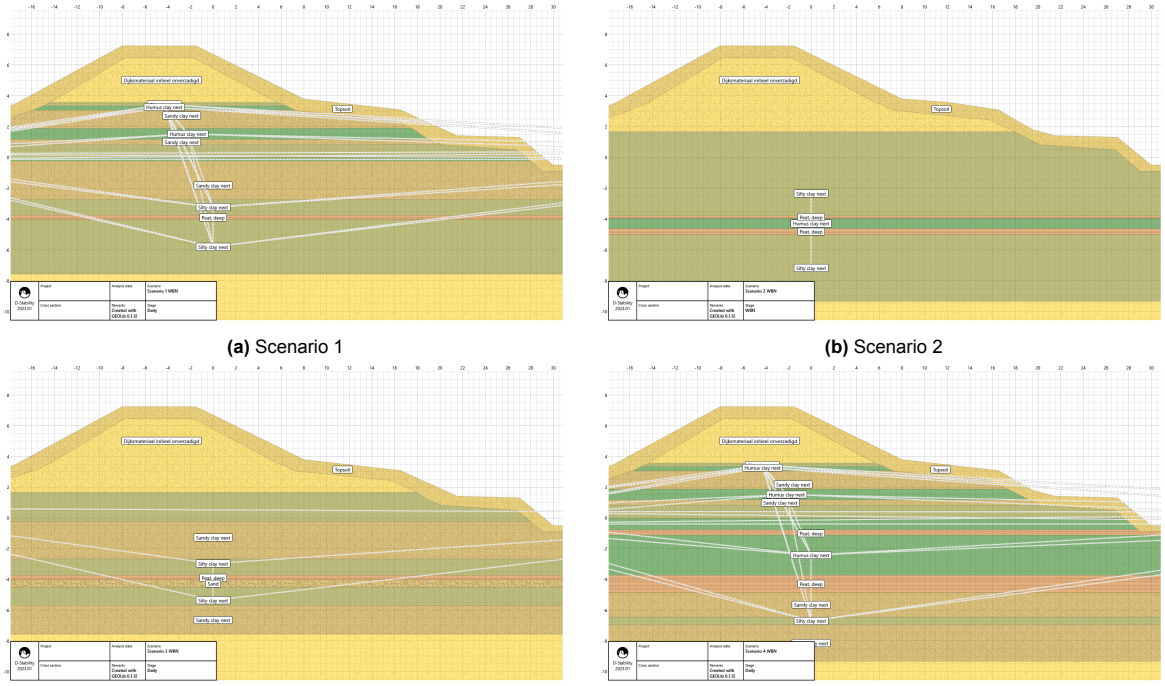

(a) Scenario 1 **(b)** Scenario 2

(c) Scenario 3 **(d)** Scenario 4

Figure 4.8: D-Stability models for the local soil scenarios for the Kortenhoevendijk

Another issue during the modeling process is that this dike section is prone to experience the uplift failure mechanism under WBN loading conditions near the ditch at the inner dike slope. This mechanism results in negative effective stresses at the location of uplift of the blanket layer. However, in D-Stability, the effective stress cannot become negative so is set to the default value of zero. The failure surface will follow the soil layers without any resistance assigned, however this is not representative. Negative effective stresses cannot be simulated in D-Stability, so a drop in the hydraulic head of the aquifer is modeled to avoid unrealistic results and convergence issues in the calculations.

Additional soil scenario models

Soil scenario 2 is investigated in more detail since this scenario is most comparable to the soil profile used in the macrostability safety assessment and is most representative of the subsurface on the specified location on the Kortenhoevendijk. The additional models extending soil scenario 2 are displayed in figure 4.9.

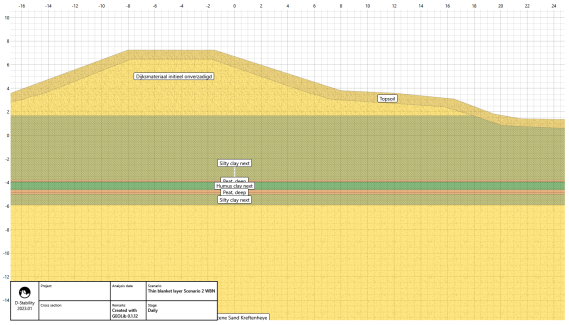

(a) Scenario 2 with thin blanket layer

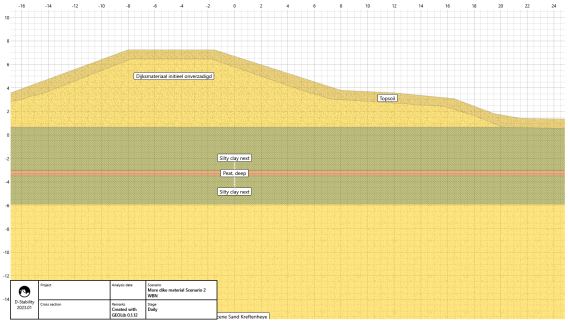

(b) Scenario 2 with more dike material and profile simplification

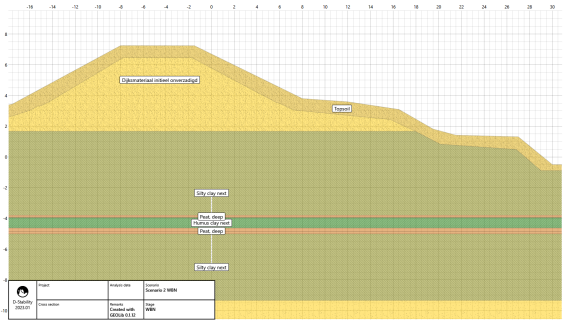

(c) Scenario 2 for reference

Figure 4.9: Additional soil scenarios of the Kortenhoevendijk

Figure 4.9 (c) displays soil scenario 2, the same subsurface schematization as mentioned before. Two additional scenarios are set up to analyze the influence of changes in the soil profile. The first scenario takes soil scenario 2 is modeled with a thin blanket layer, taken from the macrostability safety assessment (figure 4.9 (a)). This will provide more insight into the influence of the thickness of the blanket layer. A direct comparison can be made on the influence of the variation of blanket layer thickness on the reliability index and the failure probability. Figure 4.9 (b) is modeled with more dike material than scenario 2. The influence of the thickness of the dike material on the failure probability can be investigated directly. In the last model, the humus clay layer in between the peat soil is removed as well. With all the models set up, the full-probabilistic calculations can be performed, and the results can be analyzed.

4.3. Results local subsurface uncertainties analysis

The fragility curves are exported from D-Stability and are composed of the results from the MCIS analysis for three water levels for each soil scenario. The Probabilistic Toolkit (PTK) is used to combine the fragility curves exported from D-Stability. The fragility curves of each soil scenario and the combined fragility curve are displayed in figure 4.10. During the analysis of the macrostability of the dike cross-section, it is apparent that if the dike is considerably stable, with a large value for β (> 8), the MCIS analysis has difficulties with converging to a solution. The dike cross-section under the daily loading conditions is considerably stable, resulting in non-convergence in the MCIS calculation. Or, if the dike material is prone to a sliding failure (micro-instability) the MCIS calculation will provide the sliding of the dike material since this is the most critical failure surface with the lowest reliability index. However, this failure surface is not representative of a macro-instability. In case of non-convergence of the MCIS analysis or a shallow slip surface, the FORM analysis is used to provide the fragility point. The design analysis is forced to determine the safety factor of a deep sliding surface, which can be imported into the FORM analysis. The fragility points that are used to compose the fragility curve are added in Appendix B.

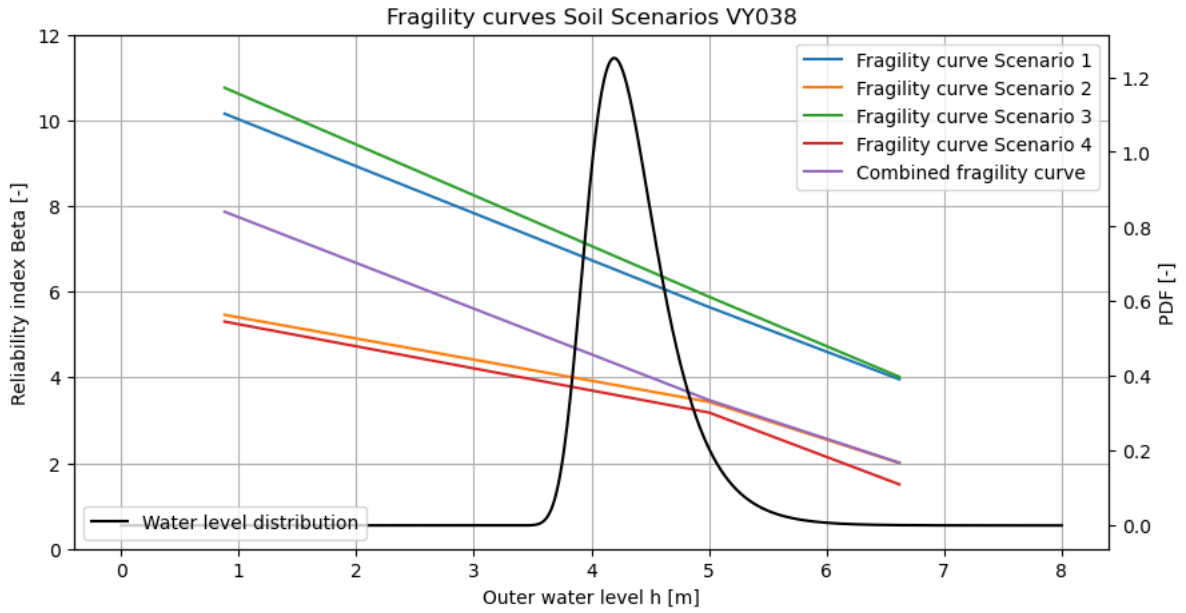

Figure 4.10: Resulting fragility curves for the local soil scenarios of the Kortenhoevendijk

Another component that results in non-convergence for the MCIS analysis is the presence of relatively thin soil layers (< 0.5 meters). Especially if the failure surface is located near these thin soil layers, the MCIS calculation can loop continuously between two similar failure surfaces alternating between the bottom and the top of these thin layers. The failure surface can slide along the top or bottom of the thin layer and will provide a similar reliability index and failure probability. The MCIS calculation will alternate between the two failure surfaces and will fail to converge to a solution. D-Stability will still provide a failure probability and value for the reliability, however, in the fragility curves, these points will be excluded. The FORM analysis results will be used instead to provide a representative fragility curve.

The combined reliability index that includes all four soil scenarios is 3.52 and the combined failure probability is equal to 2.15E-04. Figure 4.10 displays that the fragility curves of scenarios 3 and 1 are very similar, where the value for the reliability index β deviates the most at the daily water conditions by 0.6. However, the results of the daily loading conditions are not 100% reliable but still provide a representative value since the reliability index is high. The fragility curves for the two soil scenarios are similar where scenario 1 is more detailed compared to scenario 3. The same pattern is visible for scenarios 2 and 4, where the fragility curves are very similar. The difference in the reliability index β for the two scenarios ranges from 0.15 to 0.5. It appears from figure 4.10 that the simplified scenarios 2 & 3 overestimate the reliability index. From this figure, it can be concluded that the simplification of the thin soil layers or interlayered soil layers has a small impact on the reliability index during the macrostability analysis, and can be considered as a conservative assumption.

Figure 4.11 displays the failure surface found in the MCIS analysis for each soil scenario at WBN conditions. The failure surfaces found a similar entry and exit point of the slip surface. The thickness of the blanket layer or this specific location does not seem to influence the resulting failure surface in the MCIS analysis, since none of the resulting failure surfaces in figure 4.11 reach the bottom of the blanket layer.

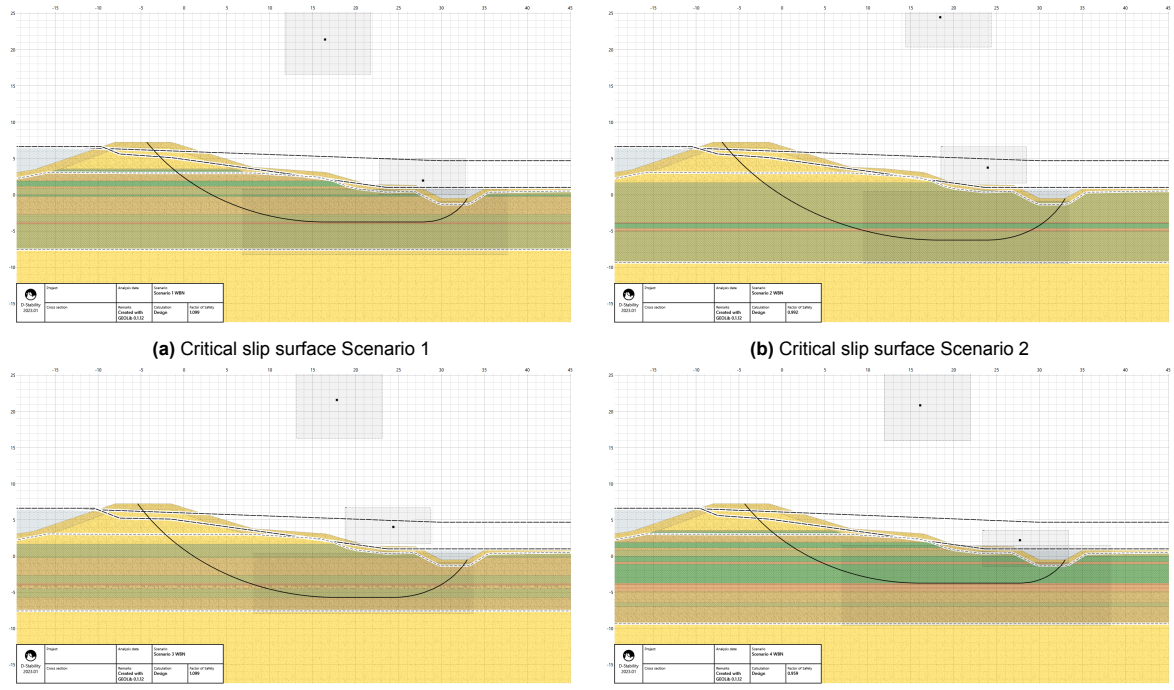

(a) Critical slip surface Scenario 1

(b) Critical slip surface Scenario 2

(c) Critical slip surface Scenario 3

(d) Critical slip surface Scenario 4

Figure 4.11: Resulting failure surfaces for the soil scenarios of the Kortenhoevendijk at WBN conditions

The alpha contributions to the failure probability of the dike cross-section are given in table 4.4. The POP, S, and γ_d are the largest contributions, where the model factor contributes negatively to the overall result provided in the MCIS analysis during WBN conditions.

Variables	Scenario 1		Scenario 2		Scenario 3		Scenario 4	
	α	Physical value	α	Physical value	α	Physical value	α	Physical value
S Peat	-0.0383	0.404	-0.0558	0.402	0.193	0.375	0.131	0.393
S Humus clay	0.621	0.266	0.667	0.285	0.661	0.247	0.583	0.293
S Silty clay	0.621	0.250	0.667	0.233	0.140	35.268	0.583	0.269
ϕ Dike material	0.282	34.423	-0.00827	36.191	0.122	35.382	0.119	35.881
ϕ Pleistocene sand	-0.0266	34.090	0.0135	33.959	-0.00657	34.0119	0.0780	33.870
c Cohesion	0.128	6.239	0.0909	6.6383	0.0133	6.803	0.190	6.508
POP	0.352	-	0.427	-	0.315	-	0.490	-
γ_d Model factor	-0.621	1.0888	-0.601	1.0449	-0.626	1.0918	-0.588	1.034

Table 4.4: Alpha contributions of the soil scenarios for case study Kortenhoevendijk at WBN conditions

It is difficult to conclude on the influence of the thickness of the dike material since it does not seem to influence the resulting slip surface. Also, the alpha contributions of the friction angle of the dike material are almost equal for scenario 3, where more dike material is simulated, and scenario 4 where less dike material is analyzed.

Results additional analysis

The resulting slip surfaces for the additional analysis of scenario 2 at WBN conditions are displayed in figure 4.12. The slip surfaces are comparable to the results of the soil scenario analysis.

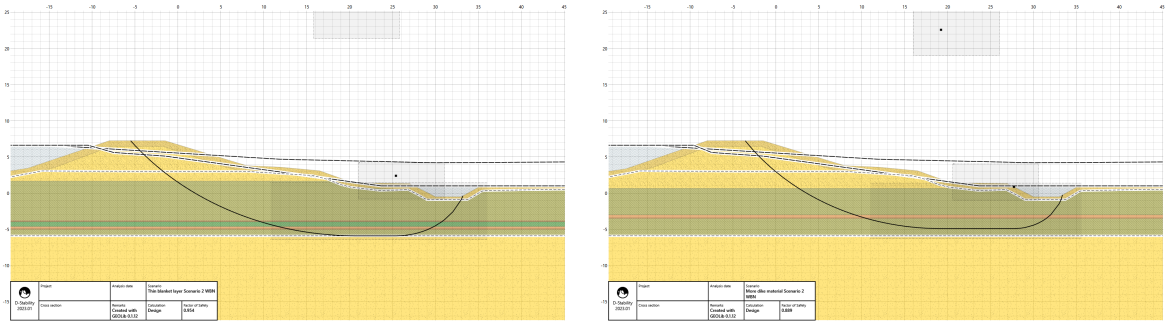

(a) Results additional scenario 2a with thin blanket layer

(b) Results additional scenario 2b with more dike material and profile simplification

Figure 4.12: Resulting failure surfaces for the additional soil scenarios of the Kortenhoevendijk at WBN conditions

From figure 4.12 (a) the slip surface is situated on the bottom of the blanket layer. The reliability index is decreased by 0.7 and failure probability is increased by 0.1 when scenario 2 and scenario 2 (a) are compared. Figure 4.13 displays the vertical effective stresses resulting in the blanket layer at WBN conditions of the additional scenarios in the MCIS calculation. Figure 4.13 (a) displays the vertical effective stresses underneath the crest of the dike and figure 4.13 (b) displays the vertical effective stresses in the blanket layer at the inner slope. The thickness of the blanket layer impacts the vertical effective stress at the inner dike slope the most. The vertical effective stress decreases in the blanket layer for the additional scenarios.

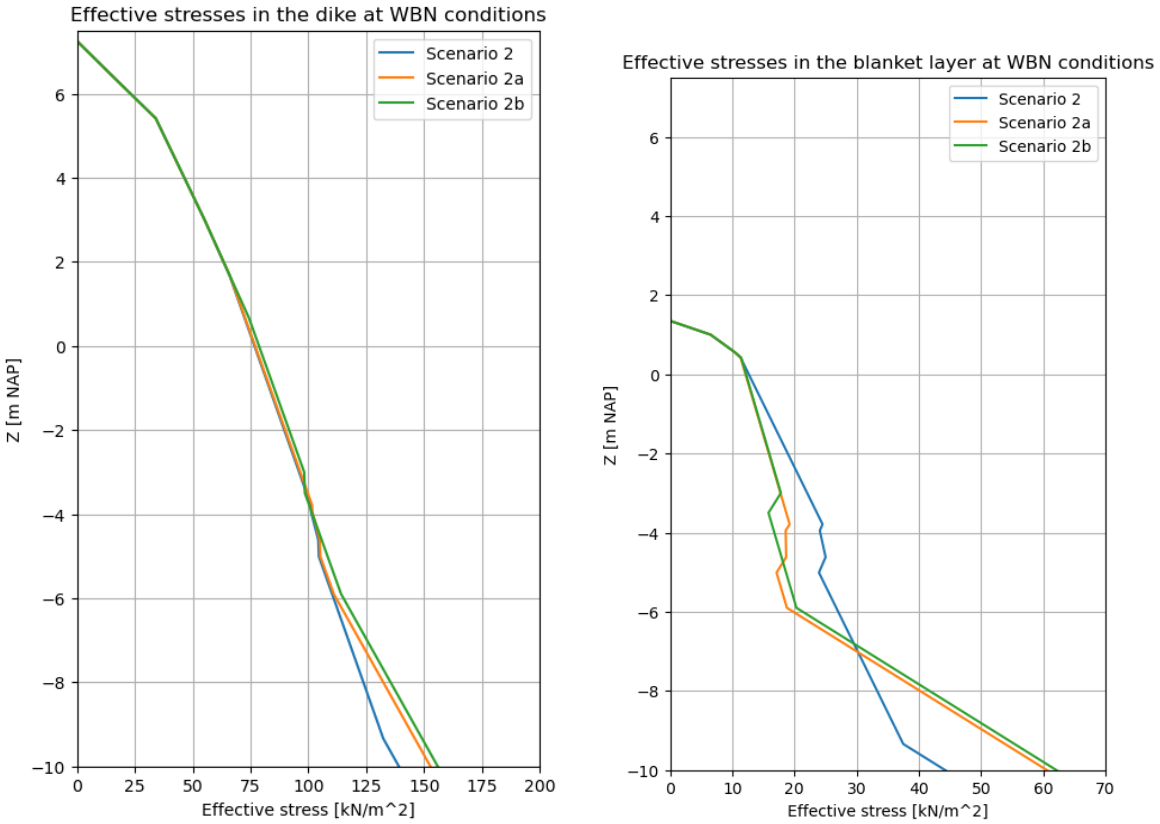

(a) Effective stresses underneath the dike crest

(b) Effective stresses in the blanket layer

Figure 4.13: Resulting effective stresses at WBN conditions of the MCIS analysis

The decrease in blanket layer thickness results in less vertical effective stress in the blanket layer. The vertical effective stresses in the dike are not affected as much. The addition of more dike material does not seem to affect the vertical effective stresses occurring in the MCIS analysis. The difference between scenario 2a and scenario 2b is the removal of the humus clay layer and replacement by one peat layer. This also results in less effective stresses in the blanket layer. The alpha contributions for each additional scenario are given in table 4.5.

Stochastic variables	**Scenario 2**		**Scenario 2 (a)**		**Scenario 2 (b)**	
	α	**Physical value**	**α**	**Physical value**	**α**	**Physical value**
S Peat	-0.056	0.402	0.060	0.396	0.116	0.4
S Humus clay	0.667	0.285	0.590	0.296	-	-
S Silty clay	0.667	0.263	0.590	0.270	0.706	0.284
ϕ Dike material	-0.008	36.191	-0.058	36.282	0.026	36.184
ϕ Pleistocene sand	0.014	33.959	0.033	33.944	0.048	34.008
c Cohesion	0.091	6.638	0.144	6.638	0.137	6.957
POP	0.427	-	0.498	-	0.358	-
γ_d Model factor	-0.601	1.045	-0.612	1.03	-0.582	0.996

Table 4.5: Alpha contributions for the stochastic variables for extended D-Stability models of scenario 2

Note that the shear strength ratio of the clay layers has the same contribution to the failure probability, in the unity check these components should be combined as one parameter. Since the physical values for the POP vary for each soil layer, these individual values are not included in the table. The alpha contribution of the POP, however, does influence the MCIS analysis significantly. The strength parameter S however is the largest alpha contribution, together with the POP and the model factor.

The strength parameter remains relatively constant throughout the scenarios. The influence of the additional dike material simulated in Scenario 2 (b) is minor. The contribution of the alpha value becomes positive, however the physical value remains constant.

Conclusion

Table 4.6 displays the influence of each component investigated in the soil scenarios for the Kortenhoevendijk.

Component	**Influence on β**	**Influence on the failure probability**
Alternating blanket layer thickness	0.74	factor 10
Simplification subsurface	0.16 to 0.61	factor 10 to 100
Thickness soil layer	1.73	factor 10

Table 4.6: Resulting influence on the reliability of the soil scenario schematization uncertainties of the Kortenhoevendijk

Several conclusions can be drawn from the analysis of the soil scenarios of the Kortenhoevendijk.

- Different soil scenarios that are representative of a dike section or trajectory assigned with a probability of occurrence can be used to highlight schematization uncertainties in the macrostability safety assessment. Via the full-probabilistic calculation method MCIS, for each soil scenario, the fragility point can be extracted. The combining of the fragility curves of each soil scenario can be used to describe the combined reliability index and failure probability including schematization uncertainties in the subsurface, such as a variation in layer thickness or locations of soil layers.
- Additional analysis should be done to conclude with more certainty on the influences on the reliability index and the failure probability of the components that are uncertain in the schematization process of the subsurface.
- The methodology of including the uncertainties by combining fragility curves is more effective for smaller effects in the schematization uncertainties. For variations in layer thickness or location, the combined fragility curve will be more representative than for the soil scenarios that are set up for the case study of the Kortenhoevendijk. The sandy soil scenarios vs the soft soil scenarios create a large range for the reliability index and the failure probability, for which the combined fragility curve will be less representative.

5

Schematization uncertainties of pore water pressures

This chapter describes the analysis of the uncertainties in the schematization process of the pore water pressures in the macrostability safety assessment. The chapter first introduces the base model that is set up by using expectation values of the pore water pressures which can be used to analyze the influence of the schematization uncertainties. Two case studies are performed to analyze the influence of the schematization of the pore water pressures that are both representative dike cross-sections for the Alblasserwaard. After the case studies, the findings are discussed.

5.1. Introduction

The influence of the schematization process of the pore water pressures in the macrostability safety assessment is analyzed via D-Stability models. A base model is set up that includes the local subsurface schematization as previously described in chapter 4 to compare the results of the pore water pressure analysis. The base model includes the 95 % upper limit expectation values for each of the pore water pressure components. The expectation values for the pore water pressure components are calculated by using the methodologies described in chapter 2. For each component that describes the overall pore water pressures occurring underneath the dike, a D-Stability model can be set up, where the component is analyzed by varying the expectation value. Table 5.1 displays each analysis that is included in D-Stability models which are used to calculate the uncertainties in the schematization of the components of the pore water pressures.

Pore water pressure component	**Base assessment**	**Hydraulic head analysis**	**Intrusion length analysis**	**Phreatic line analysis**
Hydraulic head	95% upper limit	Variation in scenario	50% expectation value	50% expectation value
Phreatic line	95% upper limit	50% expectation value	50% expectation value	Variation in scenario
Intrusion length	95% upper limit	50% expectation value	Variation in scenario	50% expectation value

Table 5.1: Assessment models of the pore water pressure uncertainties

Each component of the pore water pressure that is included in the analysis is treated as a stochastic variable. The components that are included in the analysis of the schematization uncertainties in the pore water pressures are the components that are expected to have a significant influence on the failure probability of the primary dike in the macrostability analysis: the hydraulic head in the aquifer, the intrusion length, and the phreatic line. The base models for the two case studies are discussed in more detail.

5.1.1. Introduction case study: Kortenhoevendijk

The D-Stability model for the base model for the case study of the Kortenhoevendijk is displayed in figure 5.1. Soil scenario 2, as mentioned in chapter 4, is used which describes the local subsurface most accurately and does not require extensive computational time in the MCIS calculations due to reduced complexity in the subsurface schematization. Figure 5.1 displays that in the base model, the intrusion of the pore water pressure is fully saturated. The height of the phreatic line and the hydraulic head in the aquifer is analyzed at the 95% upper limit of the expectation values. The calculation process for these values is discussed later in this chapter.

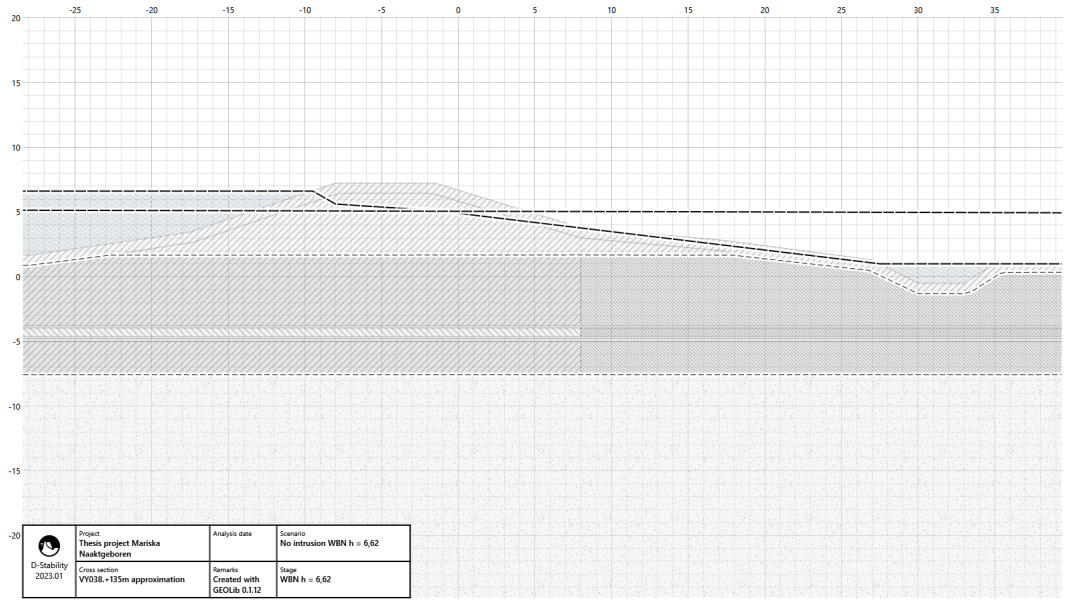

Figure 5.1: D-Stability model of the base assessment of the pore water pressure analysis for the case study of the Kortenhoevendijk

Components in the D-Stability model such as the dike geometry and material properties remain constant throughout the analysis. Table 5.2 displays the summary of the components that are analyzed in the pore water pressure analysis.

Pore water pressure component	**Base assessment**	**Hydraulic head analysis**	**Intrusion length analysis**	**Phreatic line analysis**
Hydraulic head	95% upper limit	50% expectation value	50% expectation value	Variation in scenario
Intrusion	Fully saturated	Variation in scenario	Combined intrusion	Combined intrusion
Phreatic line	95% upper limit	95% upper limit	Variation in scenario	95% upper limit

Table 5.2: Summary components D-Stability models for the case study Kortenhoevendijk

During the pore water pressure analysis, the combined fragility curve for the intrusion length was situated around 4m intrusion length. This process is described later in this chapter, however, this value for the intrusion length is applied throughout this case study. The level of the phreatic line is simulated at the design value since using the 50% percentile created non-convergence issues in the MCIS analysis due to the large reliability index (> 8).

The resulting fragility curve of the base assessment for the Kortenhoevendijk is displayed in figure 5.2. This fragility curve is set up with different hydraulic loading conditions as used in chapter 4 and is therefore different from the fragility curves shown in the soil scenario analysis.

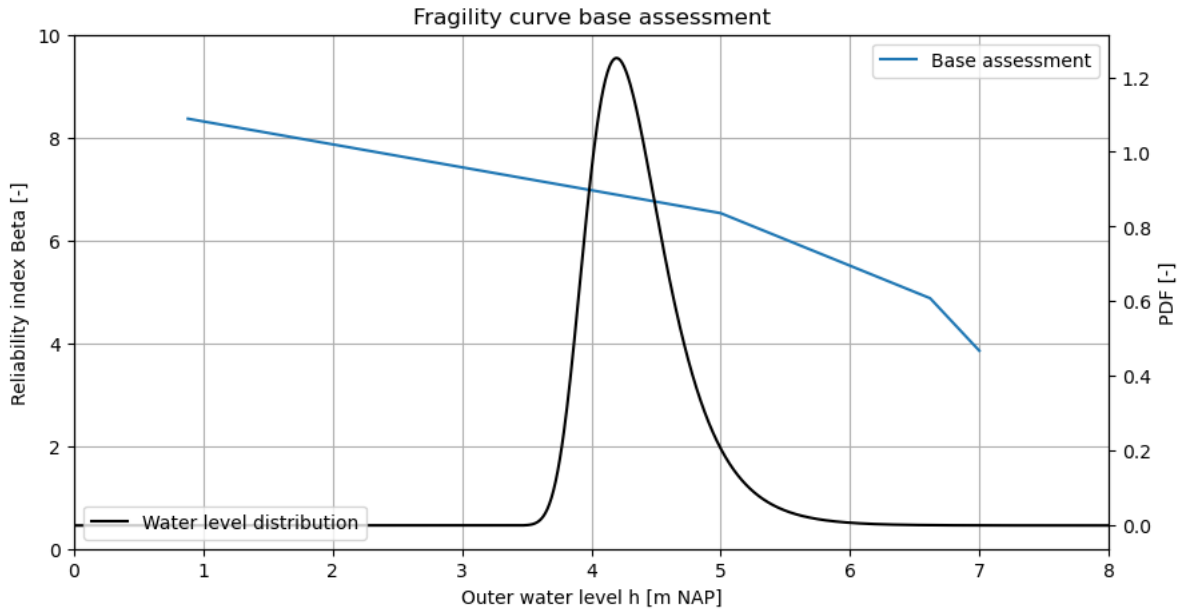

Figure 5.2: Fragility curve of the base assessment for the case study of the Kortenhoevendijk

The results of the most recent safety assessment for the local dike cross-section of the Kortenhoevendijk cannot be compared directly to the results of this analysis due to the local dike cross-section approach, as to where the safety assessment represents the entire dike section. Additionally, the macrostability safety assessment includes design values for the schematization of the pore water pressures, where this analysis includes the expectation values for different components describing the resulting pore water pressures.

Distribution function of the outer water level

Figure 5.2 displays the fragility curve and additionally the distribution of the outer water level for the Kortenhoevendijk. The combining of fragility curves for each component describing the pore water pressure is possible if the distribution function of the outer water level is known. In the current macrostability safety assessment, a Gumbel distribution is used to describe the distribution of the outer water level. This specific distribution function is used since this distribution considers the extreme values. However, this methodology is still an approximation of reality. Data from Hydra-NL (version 2.8) provides the required return periods of high water levels for the primary dike trajectories (Duits, 2020). This software is applied by water authorities in the assessment of primary dike trajectories throughout the Netherlands. Table 5.3 displays the data extracted from Hydra-NL from the dike trajectory including the Kortenhoevendijk. Since the expectation values for the pore water pressures are used in the analysis, the return periods for the outer water levels are determined for the current conditions in 2023, excluding external factors such as the influence of climate change.

Return period (years)	**Probability of occurrence (-)**	**Outer water level h (m)**
30	0.033	5.55
100	0.010	5.96
300	0.003	6.19
1000	0.001	6.37
3000	0.00033	6.50
10000	0.00010	6.62
30000	0.00003	6.72

Table 5.3: Return periods high outer water levels extracted from Hydra-NL for the Kortenhoevendijk

The data from table 5.3 can be fitted to the Gumbel distribution to describe the distribution of the outer water level for this primary dike location according to the macrostability safety assessment

methodology. Figure 5.3 displays the fit of the extreme water levels with the Gumbel distribution. A Python script is used to execute the fit and is added to appendix D.

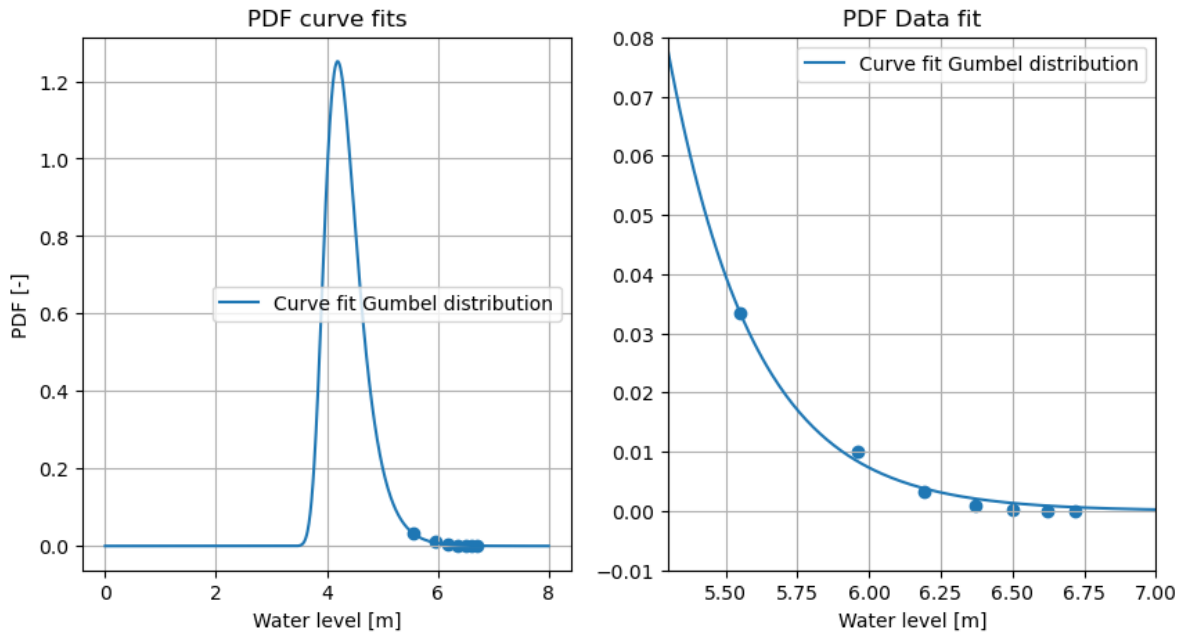

Figure 5.3: Fitting the Gumbel distribution to the exceedance frequency of the water levels

From the Gumbel distribution, the average outer water level h is 4.364 and the standard deviation is 0.377.

However, in version 2023.0.3153.0 of the Probabilistic Toolkit, the option to fill in the return periods of high water levels as described by table 5.3 is possible. This removes another assumption in the analysis resulting in a more accurate result of the combined failure probability. The Gumbel distribution of the outer water level can still be used to plot the fragility curves. In the pore water pressure analysis, the return periods are entered directly in the PTK to remove the approximation of the water levels by the Gumbel distribution.

5.1.2. Introduction case study: Bergstoep

The second case study included to investigate the influence of including the uncertainties in the pore water pressure schematization in the macrostability safety assessment is the primary dike section Bergstoep, located in between Streefkerk and Groot-Ammers in the Alblasserwaard. This location is selected for an additional study into the schematization uncertainties of the pore water pressures since this dike section is located in the lower river area of the Netherlands, where a different approach is required to analyze the now time-dependent pore water pressures. Figure 5.4 displays the dike section investigated with this case study and the height map of the dike. The primary dike section includes a foreshore on the side of the river Lek, visible in the height map. The hinterland is situated lower than the foreshore, and the local blanket layer is known to be relatively thin at this location. The most recent macrostability safety assessment displays a low-reliability index for this dike location due to the uplift of the blanket layer.

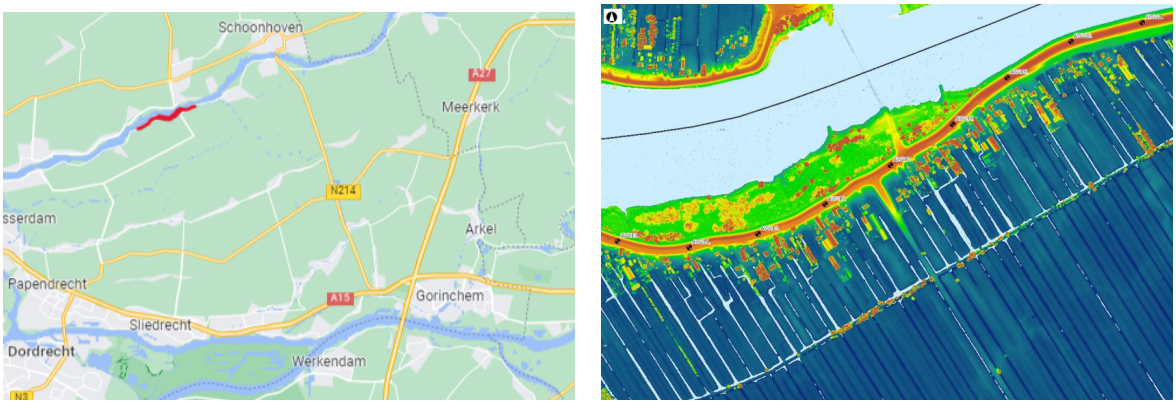

(a) Dike location Bergstoep with respect to the Alblasserwaard

(b) Height map of case Bergstoep, scale 1:5000 meters

Figure 5.4: Location of primary dike section Bergstoep in the Alblasserwaard

The pore water pressure analysis performed for the local dike section Bergstoep follows the procedure mentioned in table 5.1. The base assessment consists of the 95% upper limit values of the expectation value for each of the pore water pressure components. Since this dike cross-section is analyzed and the reliability index calculated during the D-Stability analysis is situated at 6 to 2, the calculations should experience fewer convergence issues. Therefore, each analysis of a component of the pore water pressure uses the 50% expectation value and the component as the stochastic variable.

The base assessment is set up by using the subsurface schematization of the most recent macrostability safety assessment. The D-Stability model for the Bergstoep case study is displayed in figure 5.5. The model is set up by using parameters taken from the most recent test collection used in the SAFE dike reinforcement project. The model distinguishes the soil layers into the soil underneath and next to the dike.

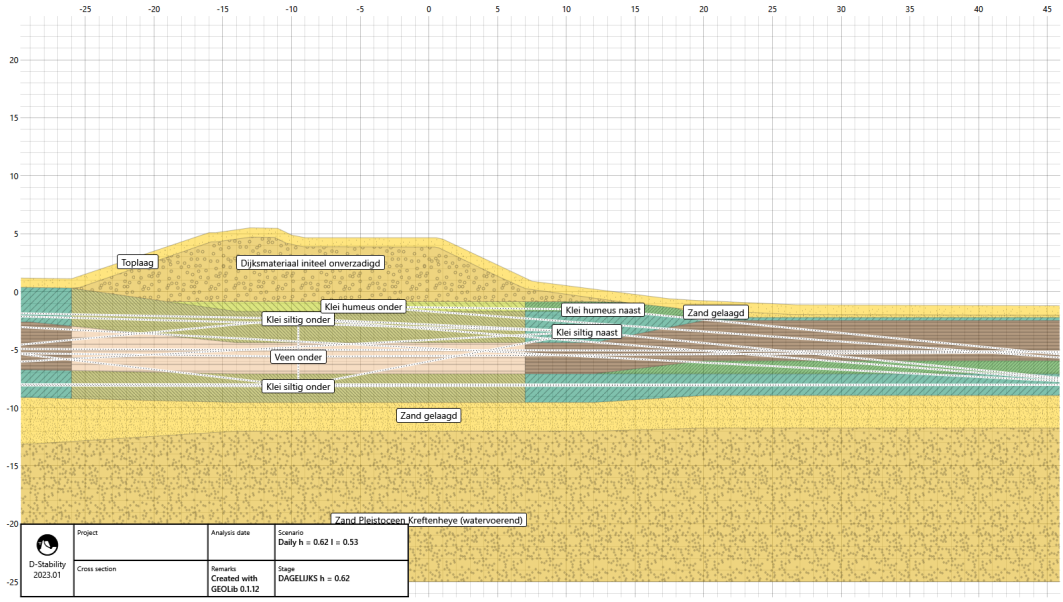

Figure 5.5: D-Stability model for case Bergstoep

The base model in D-Stability is used to calculate the stability for the local cross-section with the 95% upper limit values calculated for the expected pore water pressures during high water events. The fragility curve can be constructed which is used to compare the results of each component of the pore water pressures. The fragility curve is shown in figure 5.6 concerning the distribution of the outer water level.

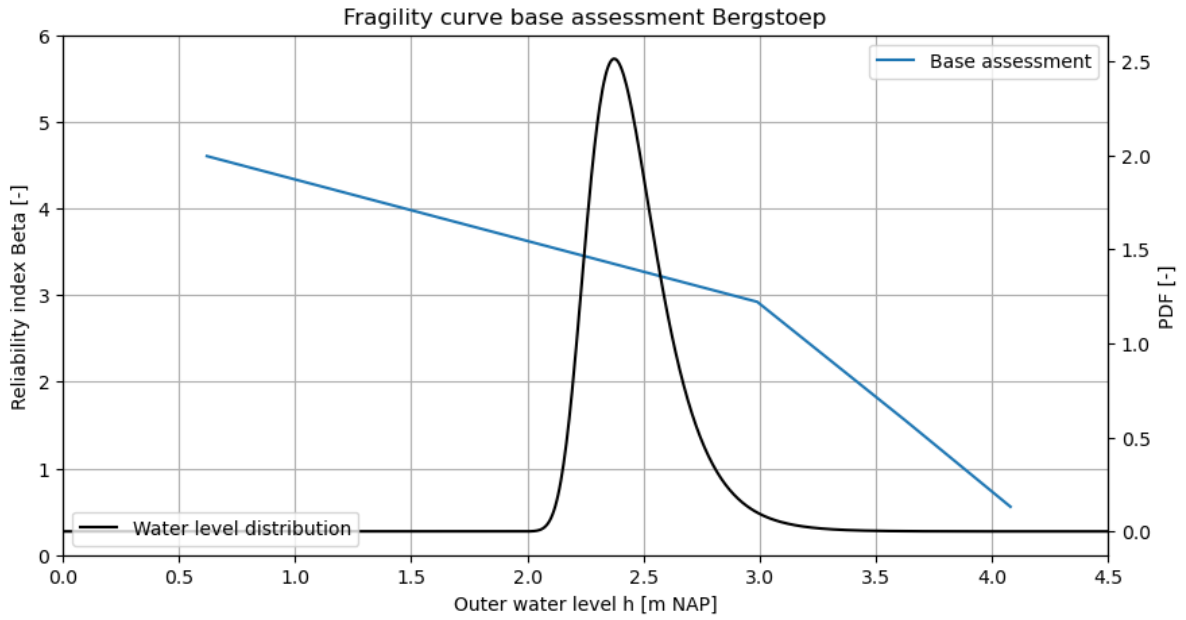

Figure 5.6: Fragility curve of the base assessment for case Bergstoep

The local cross-section is more prone to the uplift mechanism of the blanket layer compared to the Kortenhoevendijk case study. The resulting reliability index in the base analysis is lower, which will result in fewer convergence issues since $\beta < 8$.

Return periods outer water levels

The return periods of the outer water levels are taken from Hydra-NL for the location Bergstoep and are displayed in table 5.4. The numbers are considered for current climate conditions.

Return period (years)	Probability of occurrence (-)	Outer water level h (m)
10	0.100	2.99
100	0.010	3.33
1000	0.001	3.63
10000	0.00010	3.92
30000	0.00003	4.08

Table 5.4: Return periods high outer water levels extracted from Hydra-NL for the Bergstoep case study

5.2. Pore water pressure analysis Kortenhoevendijk

This section includes the analysis of the pore water pressure components of the hydraulic head in the aquifer, the intrusion length, and the phreatic line for the Kortenhoevendijk.

5.2.1. Hydraulic head

The hydraulic head level in the aquifer below the Kortenhoevendijk can be calculated with equation 2.7 given in chapter 3, which provides the stationary hydraulic head in the aquifer given an outer water level. The case study is situated in the upper river area of the Netherlands, so the assumption of a stationary hydraulic head is valid. The stationary hydraulic head formulation depends on the hydraulic conductivity and thickness of the aquifer below the dike cross-section (the transmissivity of the aquifer), the resistance of the blanket layer, the length of the foreshore and the hinterland, and the location of the inner and outer dike toe. The deterministic parameters in this equation are therefore the dimensions that describe the dike cross-section, foreshore, and hinterland. The stochastic variables in the formulation are considered to be the hydraulic conductivity, the thickness of the aquifer, and the resistance of the blanket layer. These are the parameters that will be included as stochastic variables throughout the analysis.

Stochastic variable: Aquifer thickness

The thickness of the aquifer below the dike cross-section is included as a stochastic variable in the analysis since the exact value is unknown. However, with data on the local subsurface, an average value for the thickness with a standard deviation can be extracted. The local subsurface is investigated in DINOloket since this will provide more insight into deep subsurface layers. The vertical profile of the local subsurface is shown in figure 5.7. The top layer (HLc in green) represents the Holocene deposits. Underneath these deposits, the Kreftenheye (KRz in fuchsia), Urk (URz in light green), and Sterksel (STz in pink) formations make up the sandy aquifer underneath the dike cross-section. With data extracted from DINOloket, the aquifer thickness can be determined as a stochastic variable. The thickness of the aquifer (D) is on average 50 meters, on which a standard deviation of 2.5 meters can be applied.

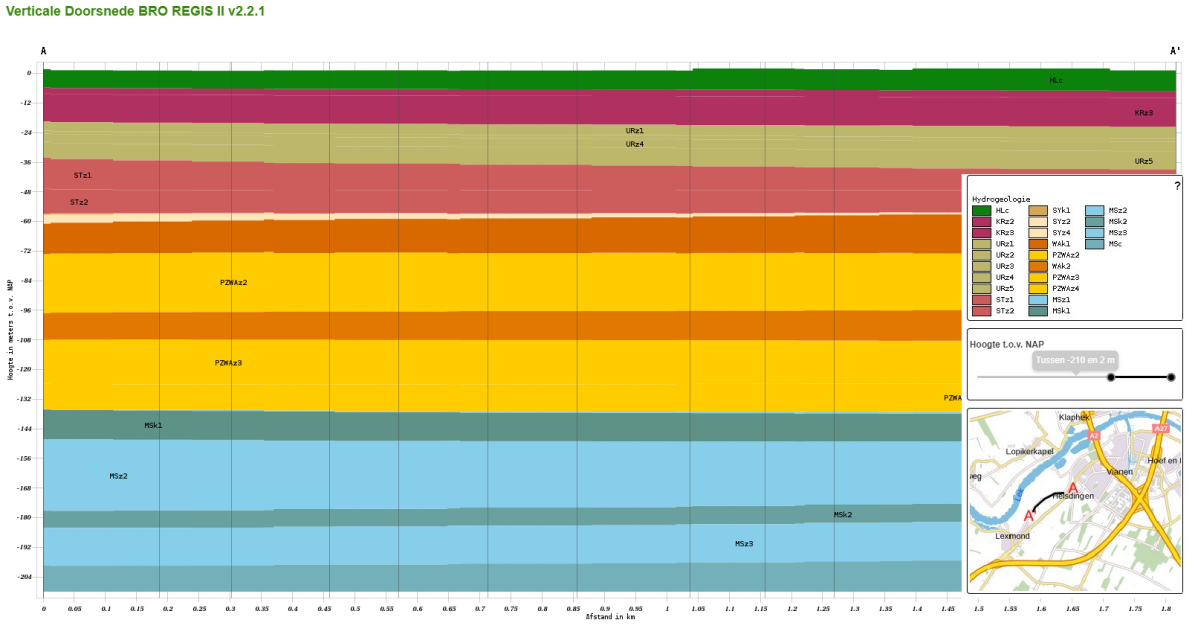

Figure 5.7: Vertical cross-section of the subsurface underneath the Kortenhoevendijk dike trajectory ("Ondergrondmodellen | DINOloket", 2023)

Stochastic variable: Hydraulic conductivity of the aquifer

The hydraulic conductivity k of the aquifer is given by DINOloket for each of the relevant formations. This data is also used in the macrostability safety assessment to indicate the conductivity of the aquifer.

The value of the hydraulic conductivity of the aquifer is determined to be 54 meters per day, with a coefficient of variation of 0.5.

Stochastic variable: Resistance of the foreshore and hinterland

The resistance c_i of the foreshore and hinterland are used to determine the leakage length of the dike cross-section with $\lambda = \sqrt{kDc_i}$ with kD describing the transmissivity of the aquifer. The resistance c_i of the foreshore and hinterland is based on a digital map provided by the WSRL that includes data on the subsurface that can be applied during the safety assessment of primary dike trajectories. The map includes local data on the depth of sand layers and locations of old river deposits throughout the subsurface. The local expectation value for c_i can be determined from this map. The resistance at the foreshore for this particular location is expected to be 150 to 500 days, whereas the resistance in the hinterland is expected to be around 700 to 1400 days. The average resistance is taken for the stochastic variable, with a fitting standard deviation.

Deterministic parameters

Several parameters are included as deterministic in the determination of the expectation value of the hydraulic head. A summary of all the deterministic input parameters is given in table 5.5.

Parameter	Notation	Value	Unit
Hydraulic conductivity blanket layer	k	0.032	m/day
Leakage length foreshore	λ1	936.75	m
Leakage length hinterland	λ2	1683.75	m
Resistance foreshore	c1	325	day
Resistance hinterland	c3	1050	day
Length foreshore	L1	700	m
Length hinterland	L3	5000	m
x-coordinate outer dike toe	x_but	-28	m
x-coordinate inner dike toe	x_bit	27	m

Table 5.5: Deterministic parameters included in the calculation of the hydraulic head for the Kortenhoevendijk case study

The hydraulic conductivity of the blanket layer is a deterministic value provided by the test collection for the SAFE reinforcement project. Laboratory soil tests on locally taken soil samples provide insight into the value of hydraulic conductivity of the blanket layer. The length of the foreshore is validated to be 700 meters distance from the river Lek to the Kortenhoevendijk. The zone of influence in the hinterland is determined to be 5000 meters via the digital map provided by the WSRL. The x-coordinates that are provided in the table correspond with the D-Stability model that will be used to analyze the influence of the hydraulic head level in the aquifer. The uncertainty in the expectation value for the hydraulic head of the aquifer is considered in three parameters as previously mentioned. The parameters k_i, D, and c_i are included in the calculation as stochastic parameters and are given in table 5.6.

Description	Variable	μ	Coefficient of variation
Hydraulic conductivity aquifer	k	54	0.5
Thickness aquifer	D	50	0.05
Resistance foreshore	c1	325	0.3
Resistance hinterland	c3	1050	0.3

Table 5.6: Stochastic variables described with a lognormal distribution in the calculation of the hydraulic head for the Kortenhoevendijk case study

Distribution function of the potential

Appendix D displays the Python script that is used to calculate the potential at the specified locations along the dike cross-sections, from where the expectation value of the hydraulic head line can be interpolated. The code applies a Monte Carlo simulation via the Python package OpenTurns to determine the response of the system, including the previously described stochastic variables. These values are fitted with a lognormal distribution. The results of the code provide the lognormal distribution of values

for the hydraulic head in the aquifer, provided the previously mentioned deterministic parameters and stochastic variables. Figure 5.8 displays the output of one realization of the Python code: a lognormal distribution of the dike response at the inner dike toe.

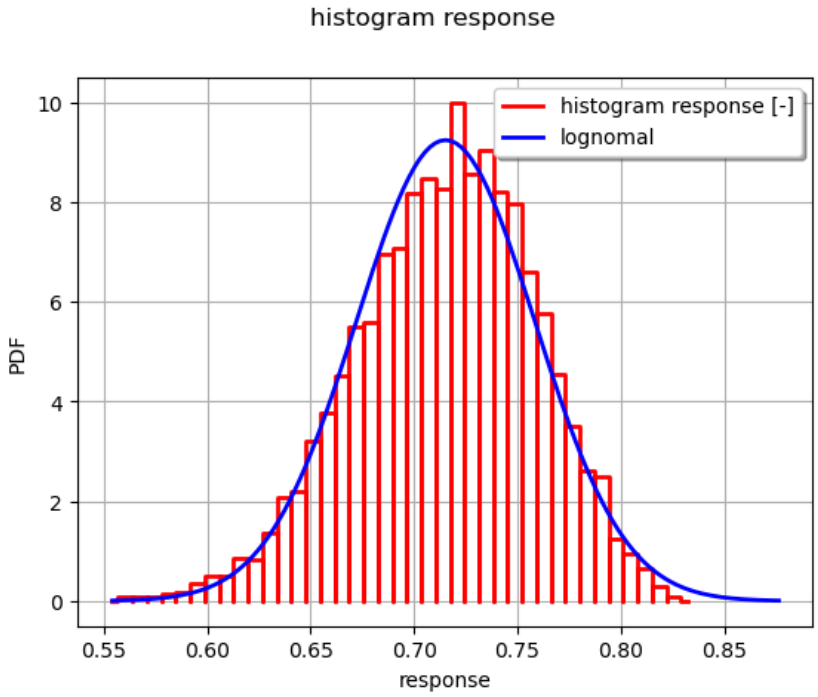

Figure 5.8: Histogram of the uncertainties in the response at the inner dike toe ($i = 17.5m$)

From the lognormal distribution, the average response and the confidence interval are extracted that describe the uncertainty in the expectation value for the hydraulic head level. The confidence interval is set at the 5% and 95% percentile of the response. The total hydraulic head can be calculated at each location of the dike cross-section by using equation 2.7. The expectation value for the hydraulic head concerning the schematization of the head in the macrostability safety assessment is shown in figure 5.9.

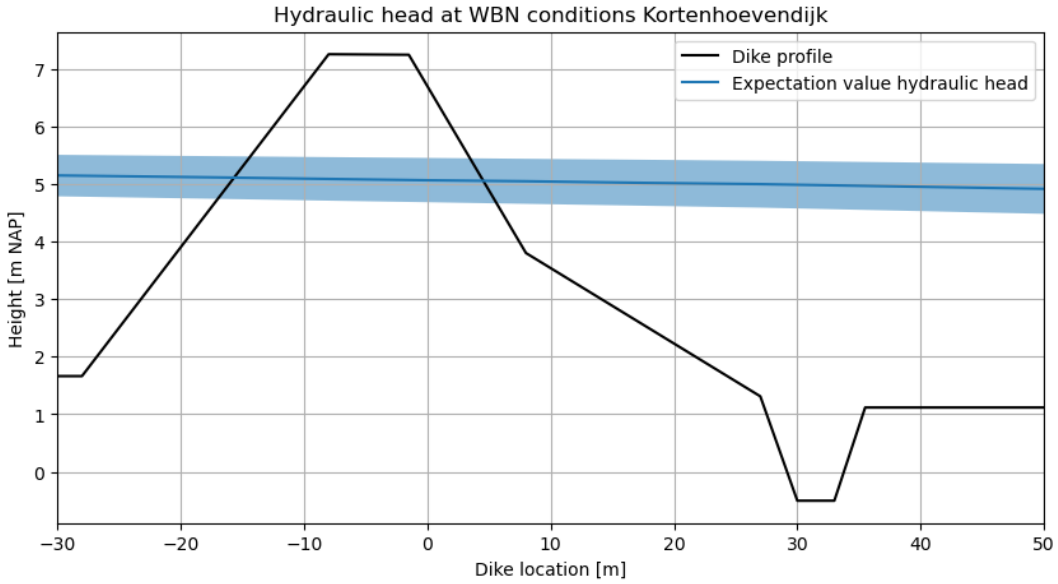

Figure 5.9: Confidence interval of the hydraulic head for the Kortenhoevendijk at WBN conditions

Figure 5.9 displays the confidence interval of the calculated expectation value for the hydraulic head in the aquifer during WBN conditions (the water level as described by the safety standard). This process is performed for multiple outer water levels to provide fragility points.

The influence of the uncertainty in the level of the hydraulic head in the aquifer is investigated by setting up a D-Stability model to investigate the macrostability. For several outer water levels, the average expectation value and the confidence interval of the hydraulic head are calculated and included in appendix B. Each scenario in D-Stability will include the 5%, 50%, or 95% percentiles for the expectation value of the hydraulic head, from which an MCIS, full probabilistic analysis will provide the fragility points. The points can be used to create fragility curves that describe the 5%, 50%, or 95% expectation value. These fragility curves can be used to determine the combined failure probability, which includes the uncertainties in the expectation value of the hydraulic head.

Each MCIS analysis in D-Stability provides a reliability index and failure probability for a given water level. The fragility points are composed of the water level and the reliability index. A minimum of three fragility points is required to compose the fragility curve. For the lower 5% limit, the average 50 %, and the 95 % expectation value of the hydraulic head the fragility curves are composed from the D-Stability analysis in the PTK. Table 5.7 displays the values that are used to combine the three fragility curves in the PTK.

Composing fragility curves contributions	5% percentile	50% percentile	95% percentile
Contribution	0.05	0.90	0.05

Table 5.7: Fragility curves contributions for the hydraulic head analyses in the Probabilistic ToolKit

Results

The results of the full-probabilistic macrostability analysis are displayed in figure 5.10. The three fragility curves for each limit are included and represent the influence of the uncertainty of the hydraulic head on the reliability.

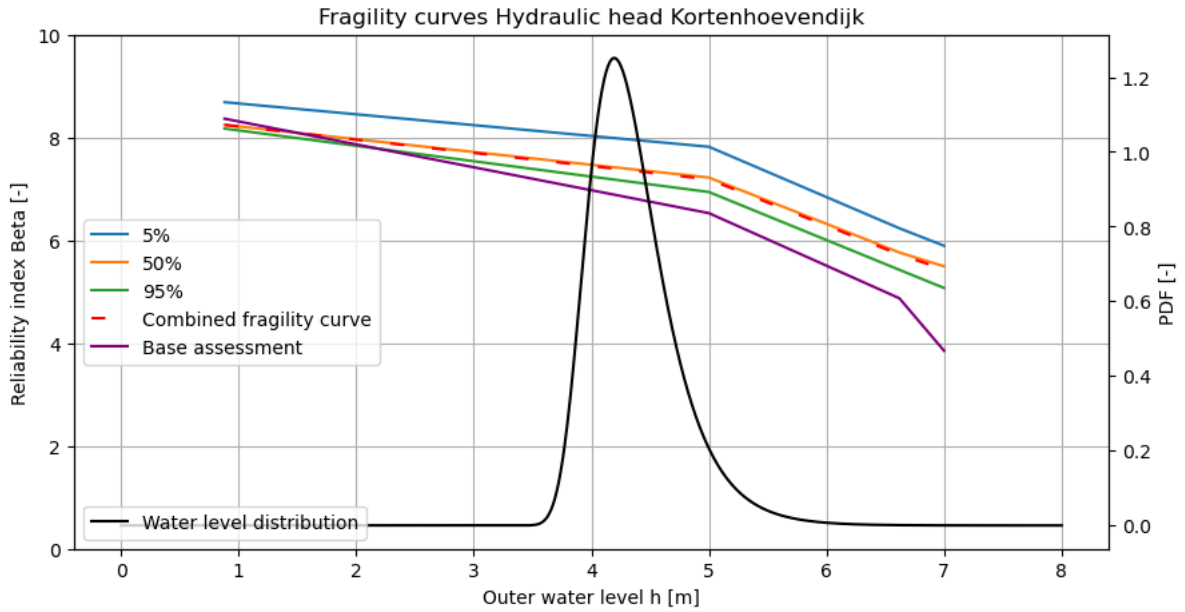

Figure 5.10: Resulting fragility curves of the hydraulic head uncertainties for the Kortenhoevendijk case study

The stability of the dike cross-section during the daily conditions is sufficient, so no large slip surfaces are deemed to be most critical by the software. The most critical slip surfaces are shallow sliding of the dike material or dike cover near the ditch at the inner dike toe. The MCIS analysis searches for the failure surface with the lowest reliability index, so will find these micro-stability failures, not macrosta-

bility failures. The MCIS analysis results in non-convergence when the search grid of the center of the slip circles is based on a deep sliding failure, reaching the bottom of the blanket layer. The reliability index becomes too large to reach convergence for the limit on the samples in the MCIS analysis. Therefore, the FORM analysis will be used to determine the stability during the daily loading conditions for a macrostability sliding failure with a deep slip surface. The sliding surface is analyzed in the design analysis, so a semi-probabilistic analysis. This surface is imported to the FORM full-probabilistic analysis, to provide a representative reliability index and failure probability for a macro-instability.

The range of the reliability index for the uncertainty in the expectation value for the hydraulic head is about 1. The combined reliability index is 6.75 and the combined failure probability is 7.5E-12. The reliability index has increased when comparing the combined fragility curve to the base assessment fragility curve. The value for β has increased by 1.5 at the highest water level. Combining the range of the expectation value other than the 95% expectation value explains this significant impact on the reliability index.

The contributions to the failure probability are included in figure 5.11. The alpha values and physical values of each stochastic variable in the MCIS analysis are included in table 5.8.

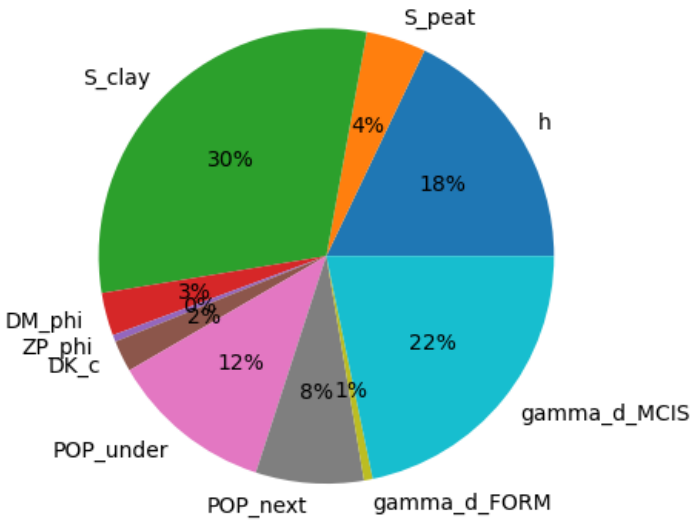

Figure 5.11: Contributions to the failure probability of the hydraulic head analysis

Variable	Alpha	Influence factor	Correlated alpha	Physical value
h	-0.402	0.165	-0.402	6.190
S Peat layer	0.0956	0.00931	0.0956	0.379
S Clay layers	0.684	0.477	0.684	0.258
Dike material ϕ	0.0683	0.00474	0.0683	35.436
Pleistocene sand ϕ	-0.011	0.000123	-0.011	34.059
Cohesion dike cover	0.0501	0.00256	0.0501	6.443
POP under	0.261	0.0694	0.261	27.952
POP next	0.172	0.0301	0.172	18.467
FORM.γ_d	-0.014	0.000198	-0.014	1.0076
MCIS.γ_d	-0.488	0.242	-0.488	1.119

Table 5.8: Alpha contributions of the hydraulic head analysis

Large contributions to the failure probability are the outer water level h and the shear strength ratio S for the (fully) correlated clay layers. A lognormal distribution is used to describe the ratio as a stochastic variable in the MCIS analysis. The value for S for the clay layers is determined in the test collection with

normally consolidated triaxial tests. The test collection that is applied in the stability analysis describes that the average expectation value for the shear strength ratio of the humus clay layer is $S = 0.347$ with a standard deviation of 0.022. The standard deviation is relatively low since the fit of the shear strength ratio on the test data is reasonable. Only the fit on lower stresses (<30 kPa) is considered conservative. However, in the high water level conditions, the resulting stresses in this clay layer range from 75 kPa to 150 kPa, so this conservative assumption does not influence this analysis. In the daily loading conditions, the failure surfaces do not reach the humus clay layer. The silty clay layer also fits well with the test data as described in the test collection. Here, the fit to the lower stresses is relatively better when compared to the fit of the humus clay test results. The average expectation value for the shear strength ratio of the silty clay layer is $S = 0.308$ with a standard deviation of 0.023.

5.2.2. Intrusion length

The intrusion length in the blanket layer is considered in the macrostability safety assessment if the blanket layer thickness exceeds 4 meters and is composed of low permeable clay and/or peat soil layers. In any other situations, the pore water pressures during the high water event are assumed to be fully adapted to the new loading conditions. Since the D-Stability model for the safety assessment is mainly composed of silty clay, the WBI describes applying an intrusion length of larger than 6 meters in this situation. Therefore, it is assumed that the pore water pressures in the dike profile simultaneously adapt to the new loading conditions during the macrostability safety assessment for the local cross-section of the Kortenhoevendijk.

Stochastic variable: Intrusion length

To analyze the influence of the uncertainty of the schematization of the intrusion length, the intrusion length will be considered as a stochastic variable. This can be compared with the model using the base assessment, where the intrusion length is assumed to be fully adapted to the high water conditions. According to (Kanning and van der Krogt, 2016), the intrusion length can be described via a normal distribution. With a blanket thickness of 10 meters, the average is equal to 3 meters with a standard deviation of 0.9. The distribution function for the intrusion length is shown in figure 5.12.

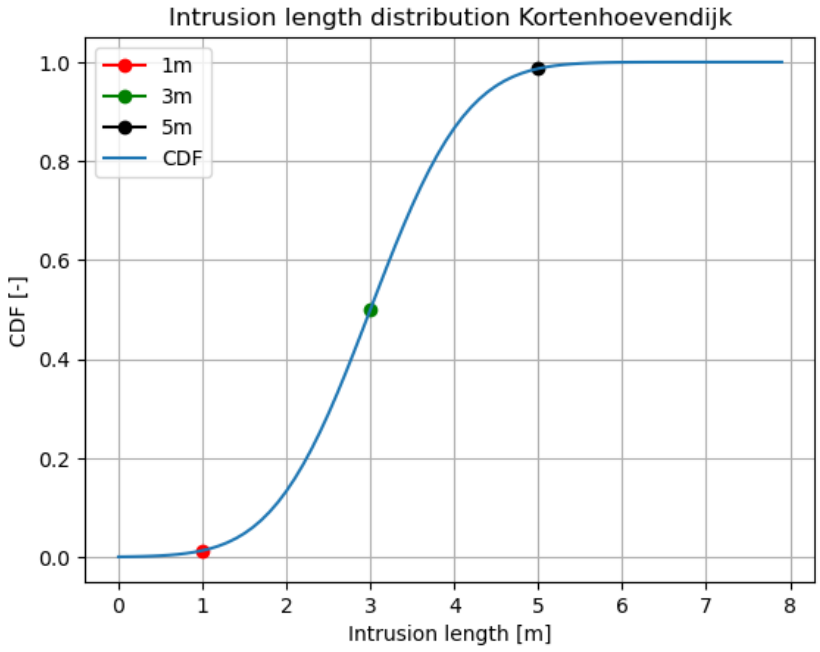

Figure 5.12: Normal distribution of the intrusion length

The resulting intrusion length is a large uncertainty and is highly dependent on the duration of the high water loading conditions. The distribution function can be used to describe the uncertainty of the value of the intrusion length. The values of 1, 3, and 5 meters of intrusion length concerning the bottom of the blanket layer will be used in the initial analysis, which are values based on expert judgement.

D-Stability modeling

The D-Stability model used to investigate the influence of the intrusion length on the macrostability is set up by using soil scenario 2 as described in chapter 4. For each scenario, multiple deterministic values for the intrusion length will be simulated for several outer water levels. The pore water pressure distribution over the dike cross-section for different intrusion length values is displayed in figure 5.13. Note that the blue section in the profile displays the stresses resulting from pore water pressures, these show the influence of the intrusion length on the total pore water pressures. The dark green section in the profile displays the total effective stress, and the light green the pre-overburden pressure POP.

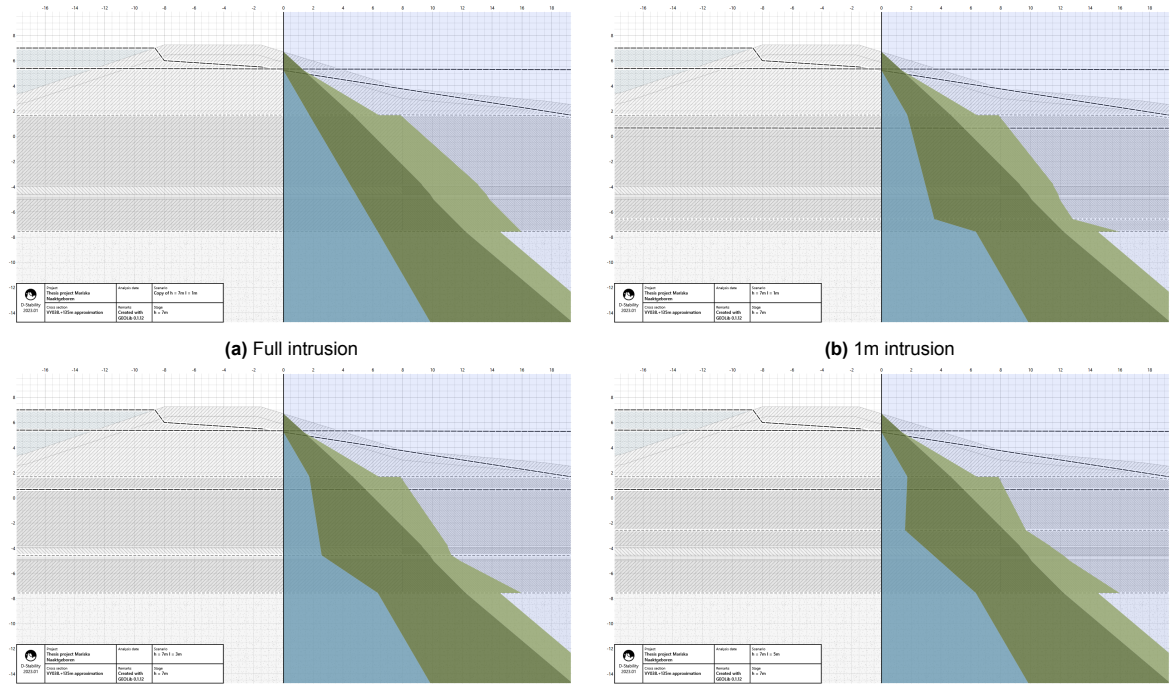

(a) Full intrusion

(b) 1m intrusion

(c) 3m intrusion

(d) 5m intrusion

Figure 5.13: Simulation of the influence of the intrusion length on the pore water pressure in the dike profile

For multiple water levels, the different intrusion lengths can be simulated in D-Stability. The material properties that are used remain constant throughout the analysis and do not vary over the entire pore water pressure analysis.

Results intrusion length

The fragility curves resulting from the D-Stability modeling are separated by the value for the intrusion length. The fragility curves for each value of the intrusion length are displayed in figure 5.14.

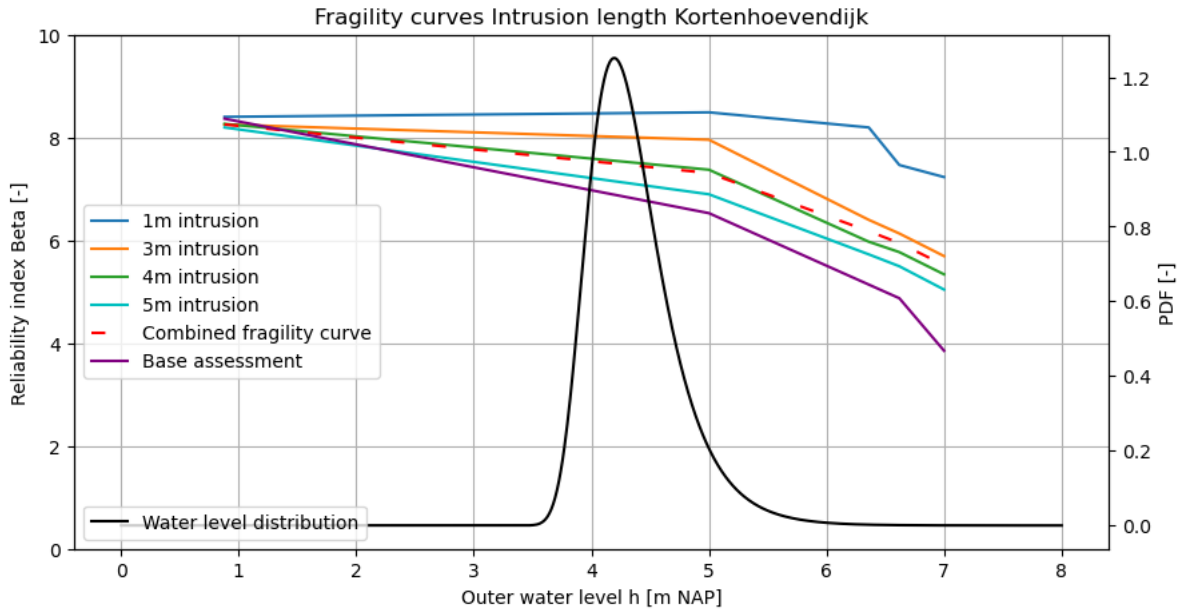

Figure 5.14: Resulting fragility curves intrusion length analysis Kortenhoevendijk

The dike cross-section is considerably stable at the daily loading conditions $(h = 0.88m)$. The MCIS analysis posed convergence issues for all the daily loading conditions and all the 1m intrusion length analyses. The MCIS analysis of the daily loading conditions all resulted in micro-instabilities of the dike material. To provide a representative fragility curve, a deep sliding surface is forced in the design analysis, and imported to perform a FORM analysis to provide a reliability index. The deep slip surface during the design analysis is forced by activating a circle constraint zone at the dike crest, so the entry point of the slip surface is situated at the crest. Using these constraints in the MCIS will result in non-convergence if the reliability index is still significantly large (>8). This method does converge in the MCIS for the intermediate water level at 5 m NAP, where the reliability index is lower than about 7.

The fragility curves displayed in figure 5.14 for each value of the intrusion length are taken from the D-Stability model. The fragility curves are displayed for the analysis with 1, 3, 4, and 5 meters of intrusion. The PTK is used to combine the fragility curves for 1, 3, and 5 meters to determine the combined failure probability. The contributions are displayed in table 5.9.

Composing fragility curves contributions	1m	3m	5m
Contribution	0.05	0.90	0.05

Table 5.9: Composing fragility curves contributions for the intrusion length analyses in the Probabilistic ToolKit

During the initial analysis of the intrusion length, the combined fragility curve appeared to be situated around the value of 4m intrusion. This is also visible in figure 5.14, where the combined fragility curve matches the 4m intrusion fragility curve. The reliability index is significantly lower in the base analysis when compared with the resulting fragility curves for all the values of the intrusion. The results at the lower outer water levels are less reliable due to the fragility points being taken from the FORM analysis. At higher outer water levels, the influence on the reliability index is large, where the reliability index is increased by 1.5 in the combined fragility curve.

The Probabilistic ToolKit additionally provides the combined failure probability. This value includes the uncertainties in the schematization of the intrusion length. The reliability index resulting from the fragility curve integration is 6.93. The value for β can be considered to be relatively high since this analysis is considerably stable. The combined failure probability is low, $2.09E-12$.

The resulting contributions of each stochastic variable in the D-Stability analysis are displayed in figure 5.15.

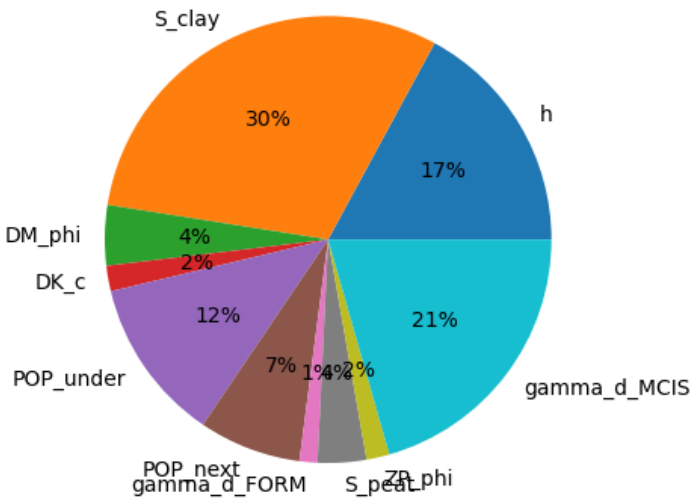

Figure 5.15: Contributions to the failure probability of the intrusion length analysis

Interesting to note is that the contributions in the intrusion length analysis are very similar to the hydraulic head analysis. The largest contribution to the failure probability is the shear strength ratio S for the clay layers. Other large contributions are the outer water level h and the model factor γ_d that is used in the MCIS analysis.

Variable	Alpha	Influence factor	Correlated alpha	Physical value
h	-0.392	0.155	-0.392	6.190
S Clay layers	0.698	0.494	0.698	0.255
Dike material ϕ	0.1	0.0101	0.1	35.076
Cohesion dike cover	0.0423	0.00182	0.0423	6.499
POP under	0.271	0.0744	0.271	27.221
POP next	0.17	0.0295	0.17	18.368
FORM γ_d	-0.0298	0.000904	-0.0298	1.0113
S Peat layer	0.0807	0.0066	0.0807	0.381
Pleistocene sand ϕ	-0.0381	0.00147	-0.0381	34.247
MCIS γ_d	-0.472	0.225	-0.472	1.118

Table 5.10: Alpha contributions of the intrusion length analysis

Table 5.10 displays the alpha values resulting from the fragility curve integration analysis in the PTK. The negative contributions to the failure probability are the outer water level h, the model factor γ_d for both the MCIS and FORM analysis, and the friction angle ϕ of the Pleistocene sand layer (the aquifer below the blanket layer). These results are very similar to the analysis of the hydraulic head since the stochastic variables used remain constant.

5.2.3. Phreatic line

The expectation value of the phreatic line is difficult to predict since this variable requires in-situ measurements during high water events loading the dike body. However, it is still difficult to measure the height of the phreatic line in clay dike bodies, since the spatial variation in the clay is large. It is difficult to calculate and estimate the actual level of the phreatic line during high water events, the time dependency, pre-overburden pressure, and dependency on the initial loading conditions create more assumptions resulting in larger uncertainties. To still investigate the influence of the schematization

of the phreatic line, the *Technische rapport Waterspanningen bij dijken* (Technische Adviescommissie voor de Waterkeringen, 2004) will be used. This document describes the methodology to calculate the design values for the height of the phreatic line in a clay dike body.

Stochastic variable: Phreatic line

The phreatic line as schematized as previously mentioned in chapter 3 for a clay dike body is considered conservative. This line can be considered as an upper limit value since this line is composed of conservative design values, which conditions are only reached when the initial condition of the clay dike is fully saturated. If the dike body in initial conditions is unsaturated and the clay cover is cracked and/or damaged, the phreatic line can follow the schematization as described by the TR for sand core dike bodies. This can be considered as a (conservative) lower limit for the phreatic line. Both limits can be considered as the 5% and 95% boundary as described by a normal distribution. The schematization of the phreatic line for the case study of the Kortenhoevendijk is displayed in figure 5.16 for the daily loading conditions and WBN loading conditions in figure 5.17.

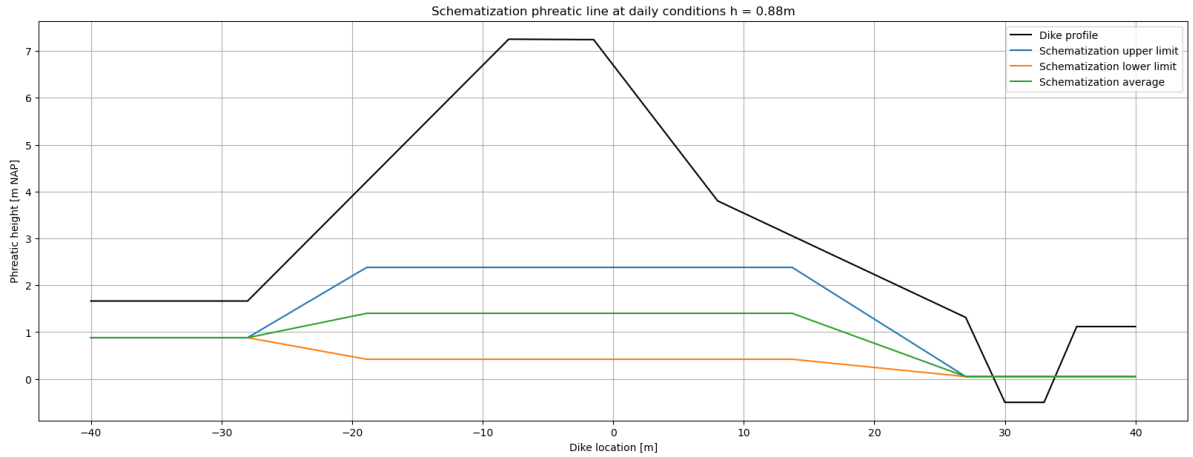

Figure 5.16: Phreatic line schematization at daily loading conditions for the Kortenhoevendijk

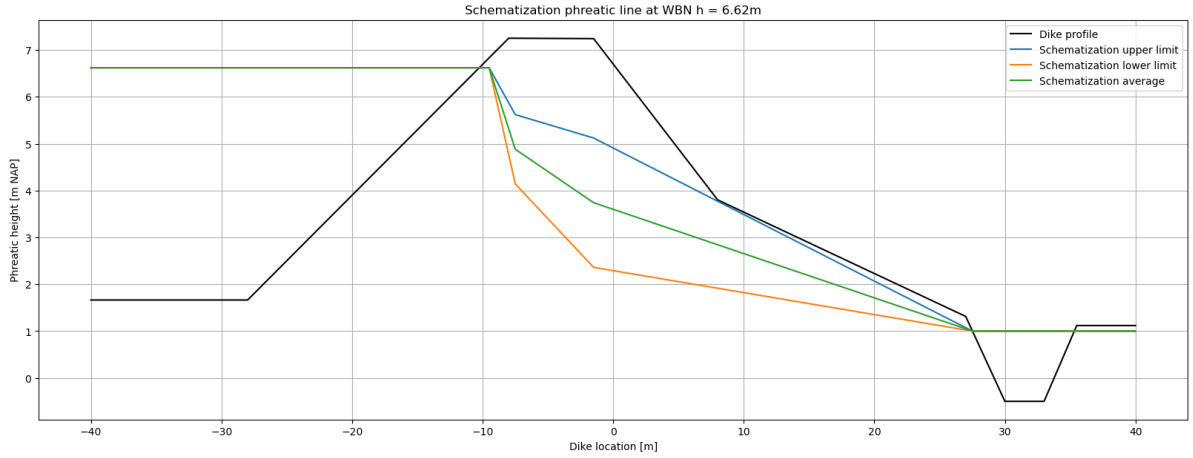

Figure 5.17: Phreatic line schematization at WBN loading conditions for the Kortenhoevendijk

The same approach as previously described for the analysis of the uncertainties in the hydraulic head and intrusion length is used to simulate the upper and lower limit for all other outer water levels that are used to construct the fragility curves. The same D-Stability model is used for the other pore water pressure analysis. The PTK is used to combine the fragility curves that are exported from the D-Stability model, for which the contributions are described in table 5.11.

Composing fragility curves	5% design value	50% design value	95% design value
Contribution	0.05	0.90	0.05

Table 5.11: Composing fragility curves contributions for the phreatic line analyses in the Probabilistic ToolKit

Results

The resulting combined fragility curve for the phreatic line analysis for the Kortenhoevendijk case study is displayed in figure 5.18. The fragility curve for the base assessment is included as well.

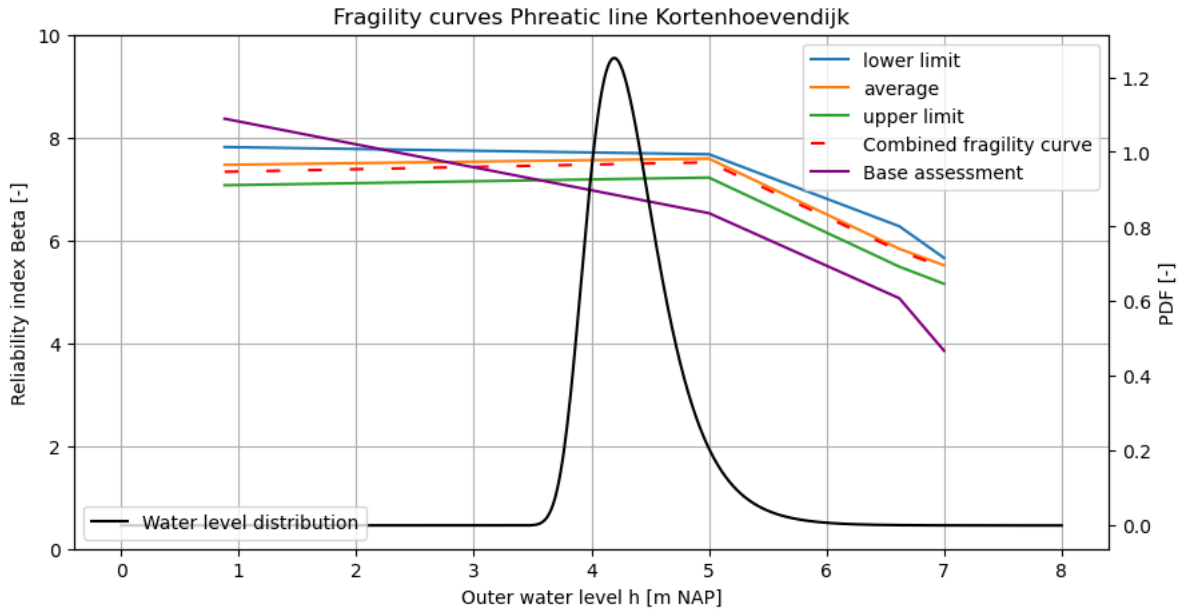

Figure 5.18: Resulting fragility curves for the phreatic line analysis for the Kortenhoevendijk

The influence of the uncertainty in the phreatic line schematization on the reliability of the dike cross-section is visible in the fragility curve by comparing the upper and lower limit fragility curves. The dike cross-section is significantly stable, resulting in a flat fragility curve up to an outer water level of 5 meters. For this water level and the daily loading conditions, the FORM analysis is used to provide a fragility point with a reliability index. The WBN water level and extra water level of 7 meters are analyzed with the MCIS analysis and provide more reliable results. The combined fragility curve of the phreatic line is situated at the 50% average value. The combined reliability index is 6.86 and the combined failure probability is 3.52E-12. The range of the phreatic line uncertainty on the reliability index is around 0.5 at all of the water levels. The values for the reliability index are improved for the consideration of the uncertainties in the design value of the phreatic line when compared to the base assessment fragility curve.

The contributions of each stochastic variable in the MCIS analysis of the combined fragility curve are displayed in figure 5.19 with the accompanying values in the table 5.12.

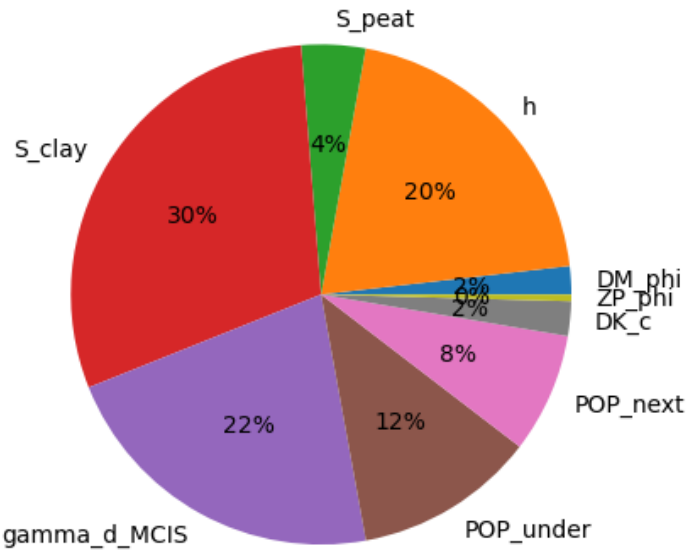

Figure 5.19: Contributions to the failure probability of the phreatic line analysis

Variable	Alpha	Influence factor	Correlated alpha	Physical value
Dike material ϕ	0.0404	0.00166	0.0404	35.724
h	-0.451	0.206	-0.451	6.370
S Peat layer	0.0918	0.00855	0.0918	0.379
S Clay layers	0.661	0.444	0.661	0.260
MCIS γ_d	-0.484	0.238	-0.484	1.12
POP under	0.26	0.0686	0.26	27.822
POP next	0.172	0.0302	0.172	18.367
Cohesion dike cover	0.0495	0.00249	0.0495	6.442
Pleistocene sand ϕ	0.00961	9.38E-05	0.00961	33.921

Table 5.12: Contributions to the combined failure probability of the MCIS analysis for the phreatic line analysis

The contributions to the failure probability are again very similar to the other pie charts of the hydraulic head and the intrusion length. The largest negative contributions are also the outer water level h and the model factor used in the MCIS analysis. The physical value for γ_d is similar to the other analysis and is relatively high compared to the average value of 1.005.

5.2.4. Results case study Kortenhoevendijk

The uncertainties in the schematization of the pore water pressures in the macrostability safety assessment for the case study of the Kortenhoevendijk are separated in the hydraulic head in the aquifer analysis, intrusion length, and phreatic line analysis. From the three analyses, the resulting (combined) fragility curves are taken and used as input in the PTK to create one fragility curve that includes the results of the pore water pressure components. Fragility curve integration can be used again to provide one failure probability and the reliability index that includes the uncertainties in these components of the pore water pressures. The contributions of each fragility curve are not correlated, therefore the contribution for each component is equal to 1/3. The combined fragility curve that describes the uncertainties in the pore water pressure schematization is displayed in figure 5.20 together with the base assessment. The combined reliability index and failure probabilities are provided in table 5.13.

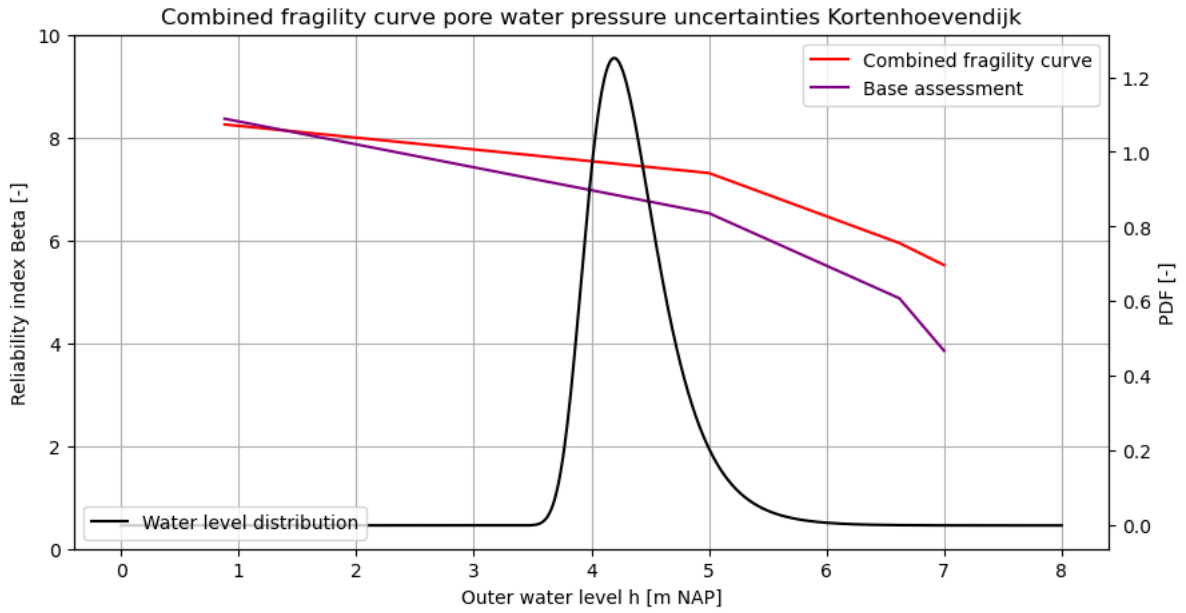

Figure 5.20: Combined fragility curve including the uncertainties in the pore water pressures for case study Kortenhoevendijk

Component	**Combined Reliability index β [-]**	**Combined Failure probability P_f [-]**
Base assessment	5.96	1.24E-09
Hydraulic head analysis	6.75	7.5E-12
Intrusion length analysis	6.93	2.09E-12
Phreatic line analysis	6.86	3.52E-12
Combined pore water pressures	6.83	4.37E-12

Table 5.13: Resulting reliability of the pore water pressure uncertainty analysis for case study Kortenhoevendijk

The combined fragility curve in figure 5.20 in red displays an increased reliability when compared to the base assessment. By integrating the pore water pressures in the macrostability safety assessment the overall stability of this local dike section has increased significantly. The reliability index has improved by 0.87 and the failure probability has improved by a factor of 1000.

Discussion

Several points for discussion can be mentioned after the analysis of the uncertainties of the pore water pressures for the case study of the local dike cross-section for the Kortenhoevendijk.

- The FORM analysis results of this dike cross-section are not 100% reliable. The design calculation should be used to find the most critical failure surface, however, during the analysis of the daily loading conditions the dike is considerably stable. This results in the most critical slip surface a micro-instability near the ditch of the dike. This failure surface also occurs in some of the cases where the outer water level is below WBN, however still at $h = 5m$. The slip surface that is used in the FORM analysis and applied in the fragility curves is based on the slip surface constraint that forces a deep failure surface, however, it is difficult to find the most critical deep failure surface. If the search grid is too large, the micro-instability will be found. This can result in higher reliability indexes, creating a skewed fragility curve at the more stable loading conditions.
- The largest influence on the improvement of the reliability of the dike cross-section is the intrusion length.
- It is recommended to perform more measurements with piezometers near and in the dike during high water conditions. The conditions simulated in the macrostability analysis have a low return period (once every 100 to 10000 years). It is recommended to perform measurements under

different loading conditions and during different periods and/or seasons to create more insight into the expected values of the pore water pressures.

5.3. Pore water pressure analysis Bergstoep

This section includes the analysis of the pore water pressure components that are known to have a significant impact on the macrostability safety assessment. This dike-cross section is situated in the lower river area, whereas the case study of the Kortenhoevendijk is located in the upper river area of the Netherlands. This influences the expected value for the intrusion length and creates a time dependency in the hydraulic head in the aquifer. The hydraulic head, intrusion length in the blanket layer, and the position of the phreatic line are all discussed separately.

5.3.1. Hydraulic head

The methodology used to calculate the expectation value for the hydraulic head in the aquifer for the macrostability safety assessment is described in chapter 2. Equation 2.13 is used to calculate the time-dependent hydraulic head resulting during high water events at the local dike cross-section Bergstoep. The method as described by the *Technische rapport Waterspanningen bij dijken* applies a sinusoidal high water wave that is used to simulate the potential in the aquifer. Equation 2.13 shows that the non-stationary value for the hydraulic head is composed of the value of the stationary response and the peak value for the amplitude of three components: the river discharge Q, the storm set-up and tidal influence. The time-dependent components will be determined via local piezometer measurements near dike location Bergstoep that are representative of the local cross-section since no measurement data is available for location Bergstoep. Since the subsurface in the area contains old river deposits, it is important to apply measurements of the response in the dike where the subsurface is comparable to the local situation. The mechanical borings of location Bergstoep and the piezometer measurement locations are added in Appendix A. The mechanical borings display a similar configuration and composition of the local blanket layer at the location of the piezometers, therefore the measurement data can be extrapolated to the local dike location Bergstoep.

The local piezometer measurements are performed over multiple months to measure the reoccurring tidal effects and variations in the river discharge and storm set-up. From the local measurements, the stationary leakage factor at daily loading conditions can be determined via equation 5.1 and the cyclic leakage factor that includes the influence of the time-dependent components can be determined with equation 5.2.

$$\lambda_{stationary} = \lambda \tanh(\frac{L}{\lambda}) \tag{5.1}$$

$$\lambda_{cyclic} = \lambda_{T_{tide}} \sqrt[4]{\frac{T_{storm}}{T_{tide}}} \tag{5.2}$$

Equation 5.2 is described by *Getijde-respons in grondwater onder Nederlandse dijken*. This formula can be assumed to describe the cyclic leakage factor for clay river dikes on a sand aquifer in the Netherlands. The equation assumes vertical consolidation and deformation for horizontal groundwater flow (Bauduin and Barends, 1987). The equation describes that the cyclic leakage factor is dependent on the period of the storm set up and the tides and the leakage factor assigned to the tide. This data is extracted from the measurement data that is available from piezometer measurements B81, B82, and B83. The locations of each piezometer are displayed in figure 5.21 by the black box and are located in the dike crest, inner dike slope, and hinterland.

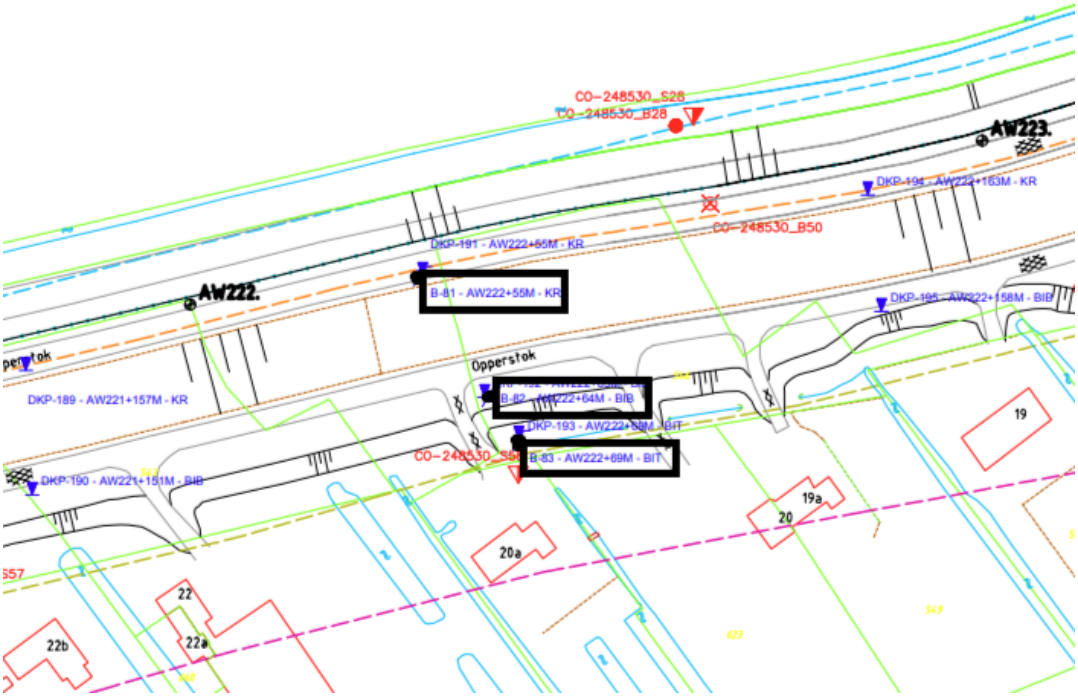

Figure 5.21: Overview of the piezometer measurements locations

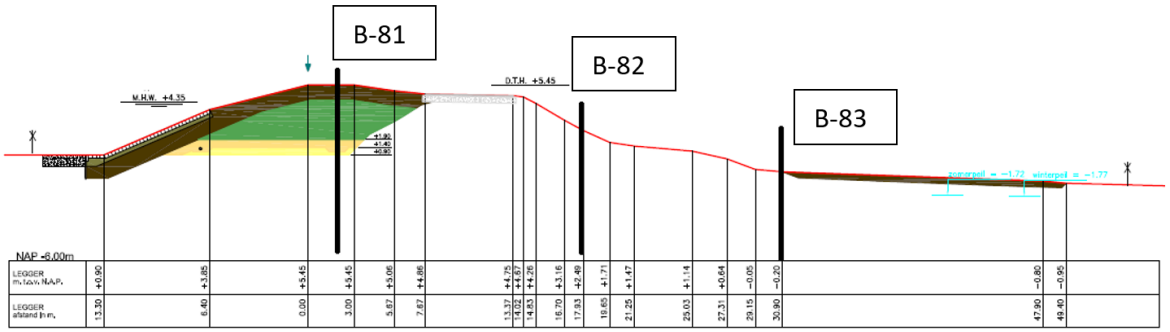

Figure 5.22: Location of the piezometer measurements over the dike cross-sections

The measurements of the piezometers display a peak in data around April and May of 2010, for which the results are plotted in figure 5.23. The water level of the river is displayed in blue. The three piezometers provide a similar water level during the measured period and overlap in the graph.

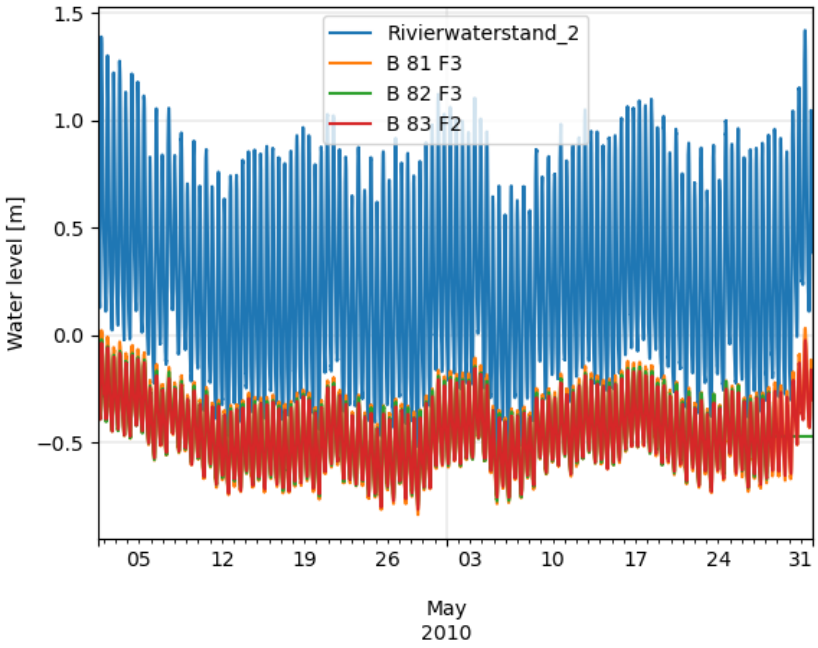

Figure 5.23: Local piezometer measurements in the month of April and May 2010 at location Bergstoep

Figure 5.24 displays the hysteresis of the piezometer measurements. The water level in the river is plotted to the response measured in the piezometer which describes the response of the water level at the piezometer location concerning the fluctuating outer water level. The piezometer in the crest of the dike (B81) displays a large influence concerning the fluctuating outer water level in the river when compared to the piezometer in the inner dike slope (B82) and the piezometer in the hinterland (B83). The hysteresis plot is used to determine the cyclic resistance leakage factor of the hinterland and the period of the tide.

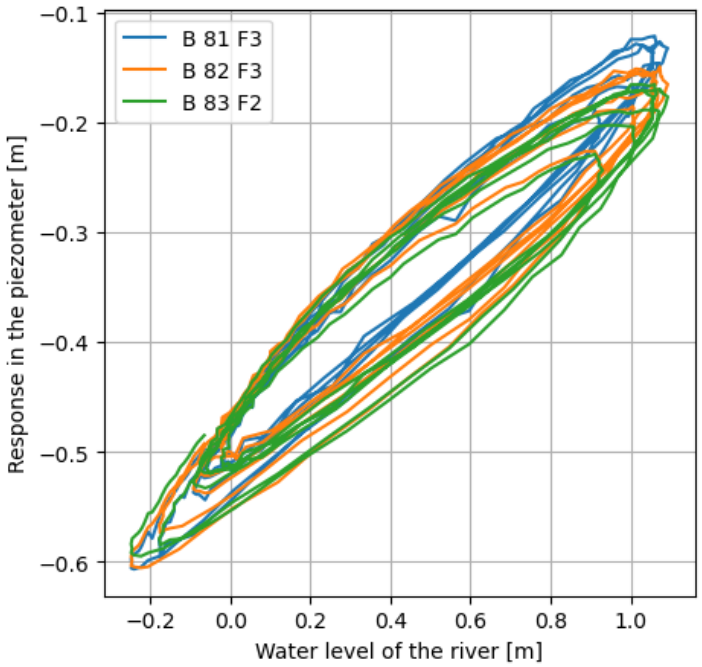

Figure 5.24: Hysteresis plot result from piezometer measurements for case Bergstoep

The probabilistic Toolkit is used to generate a dataset of possible outcomes providing deterministic input, several stochastic variables, and a calculation model. For each sample in the PTK, the distribution of the potential in the aquifer is calculated at any given position along the dike cross-section.

Deterministic parameters

The discharge Q can be extracted from Hydra-NL as a deterministic input for the PTK sample dataset. A component that should be considered in the lower river area of the Netherlands is the influence of the *Europoortkering* (flood defense barrier of the Europoort) on the resulting peak river discharges. The closing or opening of the Europoortkering influences the river discharge Q. Table 5.14 displays the percentage of contribution of opening or closing of the Europoort barrier. This percentile can be applied to calculate the combined discharge that includes the uncertainty in the position of the Europoort barrier for multiple return periods.

Situation	**T = 10 years**	**T = 1000 years**	**T = 30000 years**
Opened Europoort barrier	82.7 %	83.7 %	58.3 %
Closed Europoort barrier	17.3 %	16.3 %	41.7 %

Table 5.14: Contributions to the river discharge Q for the opening or closing for the Europoort barrier

Table 5.14 is used to determine the combined discharge when taking the influence of an opened and closed situation of the Europoort barrier into consideration. The combined discharge is provided in table 5.15 for multiple return periods. The discharge at each percentile is the sum of the Europoort contributions provided in table 5.14. The combined discharge is used to simulate the river discharge in the PTK sampling, where the uncertainty in the contribution of the Europoort barrier is taken into consideration.

Percentile	**Q(T = 10)** $[m^3/s]$	**Q(T = 1000)** $[m^3/s]$	**Q(T = 30000)** $[m^3/s]$
5 %	1309	2255	1369
10 %	1632	3487	1795
25 %	2469	9539	3263
50 %	4233	12815	12299
75 %	8054	14462	14924
90 %	11770	15656	17758
95 %	12943	16340	19222

Table 5.15: Percentile discharges for the combined contribution of the Europoort barrier

Each percentile mentioned in table 5.15 is applied as the probability of exceedance of the corresponding river discharge. This data is used as a direct input in the PTK via a CDF curve. The benefit of using the PTK here is that the CDF curve is provided as deterministic input, and a distribution for the amplitudes will be provided during the analysis.

The duration of the three amplitudes (the period) is a deterministic input in the calculation process since the duration of each amplitude has limited influence on the hydraulic head. The period of the tides is equal to 12 hours and 25 minutes. The duration of the storm set up usually lasts somewhere from 12 to 36 hours, however as a conservative assumption the period for the storm set up is assumed to last 45 hours. The duration of a high river discharge can last from 8 to 20 days. The period of river discharge is assigned to be 400 hours (about 17 days) which is correlated to local measurement data and chosen more conservatively.

In conclusion, the deterministic input for the calculation of the time-dependent hydraulic head is summarized in table 5.16.

Parameter	Notation	Value	Unit
River discharge	Q	CDF curve	$[m^3/s]$
Period tides	T_{tide}	12.25	hours
Period storm set up	T_{storm}	45	hours
Period river discharge	$T_{discharge}$	400	hours

Table 5.16: Deterministic input for the time-dependent hydraulic head analysis for case study Bergstoep

Stochastic variables

The stochastic variables that are assigned in the PTK to generate the dataset for the input of the time-dependent hydraulic head are provided in table 5.17. The entry point is used to simulate the resistance of the foreshore at the local dike cross-section.

Variable	Distribution	Mean	Coefficient of variation
x_entry	Lognormal	400	0.15
W3_cycle	Lognormal	331	0.10

Table 5.17: Stochastic variables used in the hydraulic head analysis for case study Bergstoep

The cyclic resistance of the hinterland ($W3_{cycle}$) is determined by applying the Python code added in appendix D. The fit and extrapolation code provides the cyclic resistance based on the average hydraulic head taken from the piezometer measurements. The stationary resistance is fitted from the response data, based on the width of the river and the initial water levels. The coefficient of variation is based on expert judgement.

Model

The amplitudes of the river discharge, tidal influence, and storm setup, can be calculated via equations 5.3, 5.4, and 5.5 respectively. The amplitudes are all described as a function of the river discharge. The equation describing the amplitude for the river component is a curve fit performed on data of the water level measured by the piezometer locally and the river discharge at Lobith (the first point of entry for the river Rhine into the Netherlands) with the expected river level per kilometer of the river, which is displayed in figure 5.25. The contribution of the river amplitude increases exponentially for an increasing discharge.

$$A_{river} = \min(9E-9*Q^2 + 7E-5*Q - 0.2282, (T_{ws} - gwl - 0.1)) \tag{5.3}$$

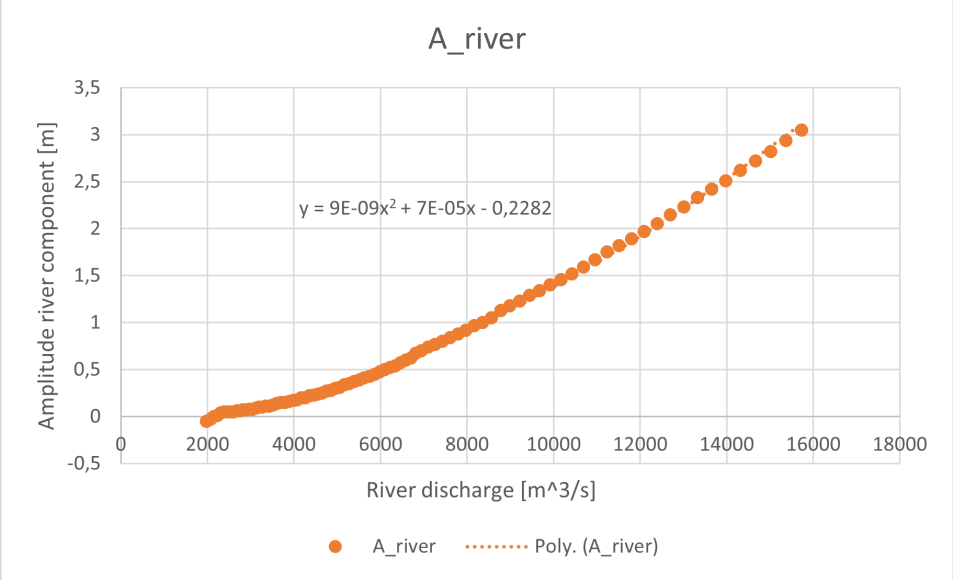

Figure 5.25: Data fit of Hydra-NL data to set up equation 5.3 to describe the contribution of the amplitude of the river

Table 5.18 describes the input data used to provide a formulation for the amplitude of the tidal influences. The data is taken from Hydra-NL, where the levels of the river discharge are extracted at Lobith to provide the amplitude of the tide directly.

$Q_{Lobith}[m^3/s]$	Amplitude of the tide [m]
2200	0.65
10000	0.05
14000	0.01

Table 5.18: Data set taken from Hydra-NL used to formulate equation 5.4 that describes the tidal amplitude

When the data provided in table 5.18 is fitted with an exponential formulation, equation 5.4 can be used to describe the amplitude of the tidal influences. Figure 5.26 displays the amplitude of the tide over the river discharge. The influence of the tidal amplitude decreases when the discharge of the river increases.

$$A_{tide} = \min(1.4658 \exp((-4.0 \times 10^{-4} Q), 0.65)) \tag{5.4}$$

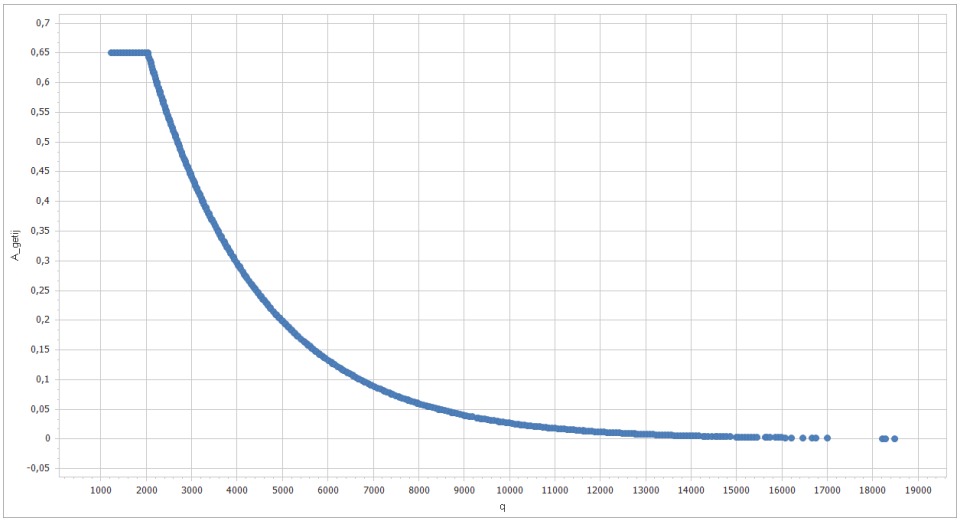

Figure 5.26: Data fit of Hydra-NL data to set up equation 5.4 to describe the contribution of the amplitude of the tide

The amplitude of the storm can be calculated by subtracting the daily water level and the amplitude as a result of the river discharge and the tidal influences from the water level determined by the safety standard (WBN). The equation that is used to calculate the storm amplitude is given by equation 5.5. The contribution of the storm setup decreases when the discharge increases.

$$A_{storm} = T_{ws} - A_{river} - A_{tide} - gwl \tag{5.5}$$

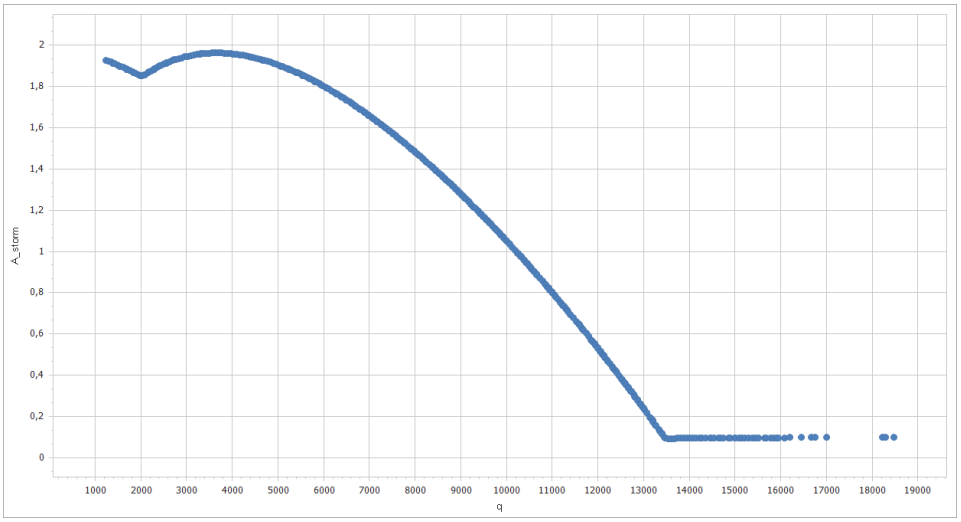

Figure 5.27: Data fit of Hydra-NL data to set up equation 5.5 to describe the contribution of the amplitude of the storm set up

With the deterministic values, stochastic variables, and model code defined, the PTK is used to generate the data set for each value for the outer water levels. The Monte Carlo sampling in the PTK results in a dataset with 10000 realizations taking into consideration all the previously mentioned stochastic variables. Table 5.19 displays a section of the 10000 samples dataset for the outer water level at T = 30000 years.

Beta	q	X_entry	W1_cycle	W3_cycle	A_river	A_storm	A_tide
1.0383	14640	387.03	523.06	324.53	2.7255	0.81027	0.0041963
1.55	17900	432.72	502.23	332.06	3.44	0.098861	0.0011392
3.4038	13618	523.27	393.31	254.1	2.3941	1.1396	0.0063153
3.2324	14089	339.33	323.33	395.85	2.5444	0.99037	0.0052316
1.5752	14339	367.74	454.77	378.63	2.6261	0.9092	0.0047326
2.5712	2745.4	281.74	438.25	306.66	0.03181	3.0194	0.48883

Table 5.19: Sample of the 10000 Monte Carlo dataset generated by the PTK for T = 30000 years, input to generate the expectation value for the time-dependent hydraulic head

The dataset from the PTK also provides the values for the cyclic resistance and the entry point. This data can be used to determine the non-stationary expectation value of the hydraulic head in the aquifer.

Stochastic variable: Hydraulic head

A Python script/notebook is provided by the WSRL to determine the time-dependent hydraulic head distribution function. The code is added in appendix D. For each position along the dike cross-section, a normal distribution can describe the uncertainties within the calculation of the local potential. The approximation of the data via a normal distribution for the potential at the inner dike toe is displayed in figure 5.28. The data appears to be separated by two peaks, skewing the distribution function. However, the fit is sufficient to currently apply during the analysis.

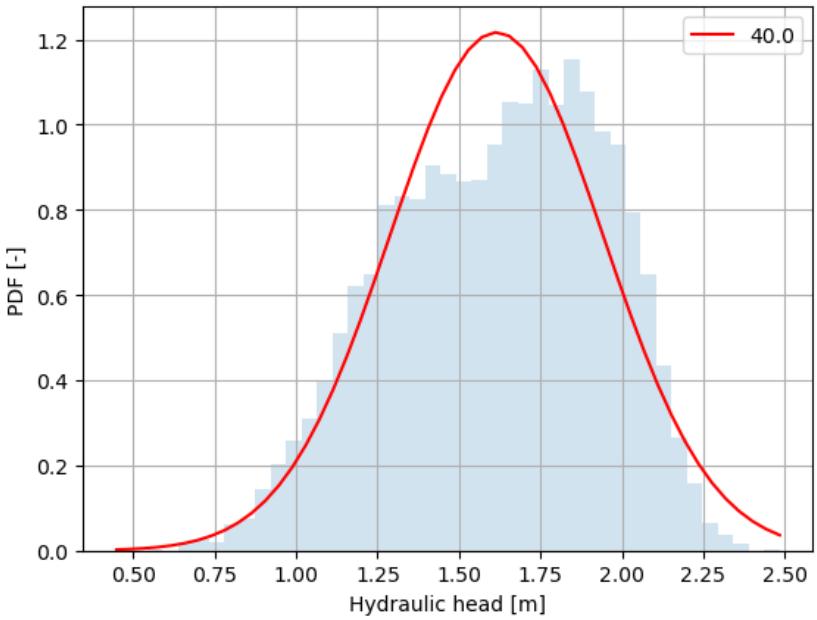

Figure 5.28: Distribution of the time-dependent hydraulic head at the inner dike toe for case Bergstoep

time-dependent hydraulic head	**T = 10 years, h = 2.99 m**	**T = 1000 years, h = 3.63 m**	**T = 30000 years, h = 4.08 m**
Mean	0.986 - 0.754	1.563 - 1.301	1.740 - 1.439
SD	0.212 - 0.213	0.248 - 0.254	0.212 - 0.333

Table 5.20: Range of the resulting distribution of the time-dependent hydraulic head for the relevant return periods

Table 5.20 displays the mean and the standard deviation of the time-dependent hydraulic head resulting from the Python script. The distribution of the time-dependent hydraulic head is used to plot figure 5.29, which displays the range of the expected value for the time-dependent hydraulic head during high water conditions at T = 30000.

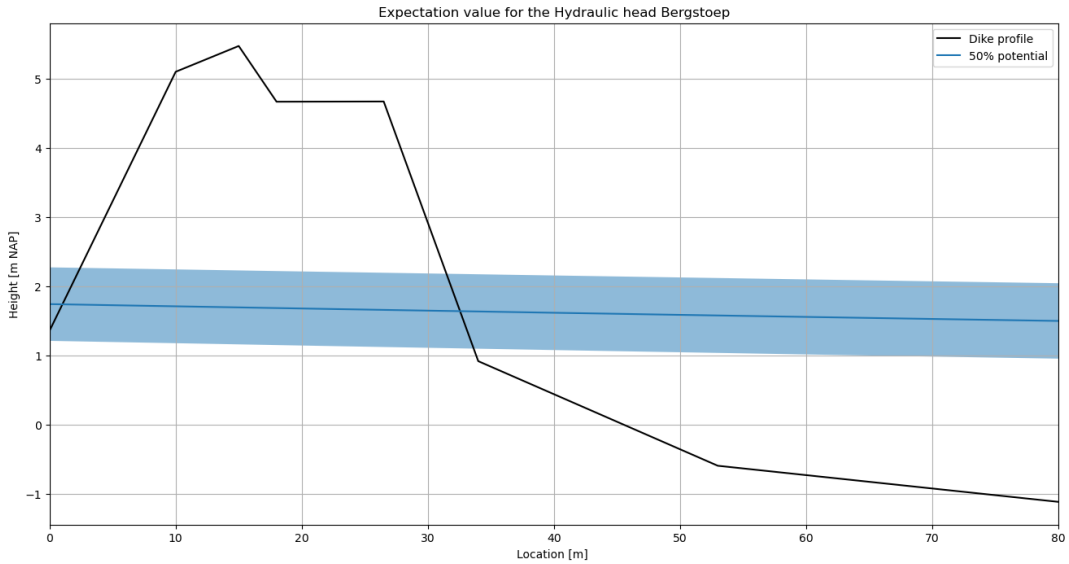

Figure 5.29: Resulting distribution for the hydraulic head for case Bergstoep at high water conditions ($h = 4.08m$)

From the normal distribution on the hydraulic head displayed in figure 5.28, the 5%, 50%, and 95% percentiles of the hydraulic head can be extracted. The 5%, 50%, and 95% hydraulic head lines are implemented in the full-probabilistic D-Stability analysis. The fragility curves for each percentage are used as input in the PTK and assigned the contributions described in table 5.21. The fragility curves are combined in the PTK and the results are described below.

Composing fragility curves	5% percentile	50% percentile	95% percentile
Contribution	0.05	0.90	0.05

Table 5.21: Composing fragility curves contributions for the hydraulic head analyses in the Probabilistic ToolKit

Results

Figure 5.30 displays the fragility curves resulting from the uncertainty analysis for the expectation value of the hydraulic head for the case study Bergstoep. The combined fragility curve is situated at the 50% percentile for the hydraulic head. The reliability index is improved significantly when the combined fragility curve is compared to the base assessment. The base assessment shows the point of uplift of the blanket layer at an outer water level of $h = 2.99m$, with a return period of 10 years due to the steepness of the curve after this outer water level is reached. It appears that this point has shifted in the combined fragility curve to the outer water level $h = 3.63m$ with a return period of 1000 years, since after this point the fragility curve increases in steepness.

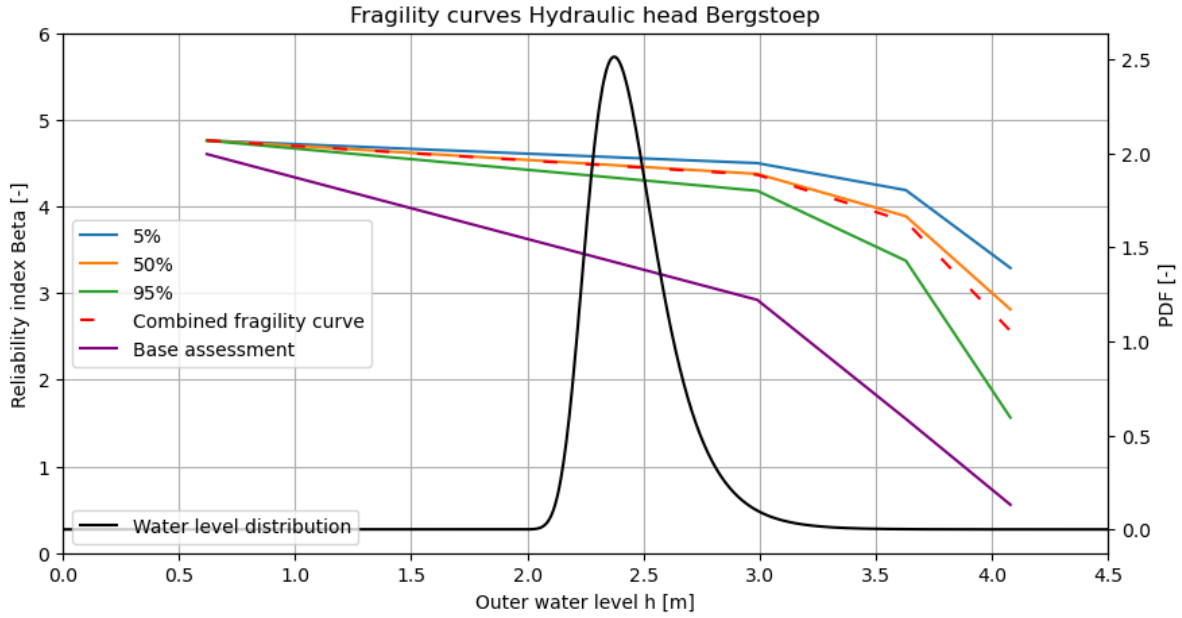

Figure 5.30: Resulting fragility curve hydraulic head analysis Bergstoep

The combined reliability index is equal to 4.39 and the combined failure probability is 5.70E-06. The contributions to the combined failure probability are displayed in figure 5.31.

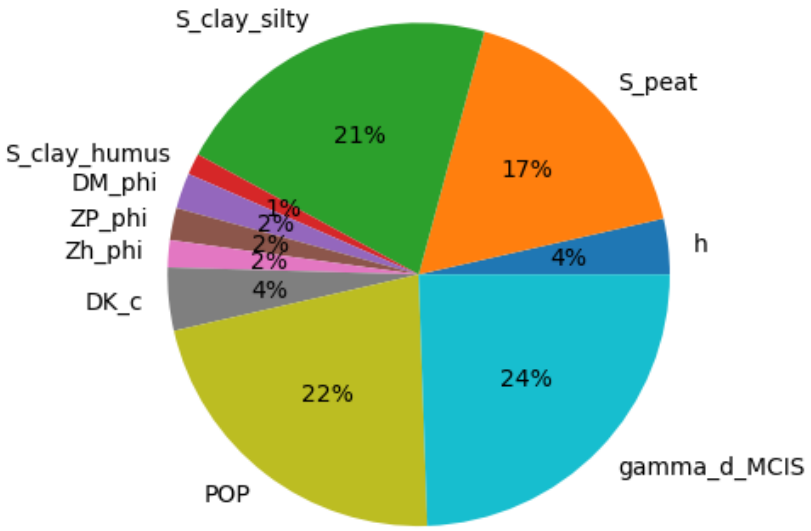

Figure 5.31: Contributions of the hydraulic head analysis Bergstoep

The contribution of the outer water level on the failure probability of the dike cross-section is low with only 4%. The largest contributions are the assigned soil parameters for the shear strength the pre-overburden pressure and the assigned model factor. The model factor used in the analysis is already improved over the model factors used in the macrostability safety assessment assigned by the WBI. The WBI describes applying the 95% percentile of the model factor for the UpliftVan limit equilibrium method. The uncertainties in the model factor applied in the macrostability safety assessment are already discussed in *Derivation of the semi-probabilistic safety assessment rule for inner slope stability* (Kanning et al., 2017), where the model uncertainty is recommended to be approached with a lognormal distribution with a mean value of 1.005 and a standard deviation of 0.033.

5.3.2. Intrusion length

The local thickness of the blanket layer at Bergstoep is 6.5 meters. The blanket layer is composed of soft soils, with mostly peat soil and humus and silty clay soil. In the lower river area of the Netherlands, the WBI describes that for the macrostability safety assessment, an intrusion length in the blanket layer should be applied of 1 meter. The intrusion length in the blanket layer can be considered as a stochastic variable during the macrostability assessment of a dike cross-section in the following way.

Stochastic variable: Intrusion length

In the most recent safety assessment of the dike section that includes the local cross-section Bergstoep, the intrusion length in the blanket layer that is applied is 2 meters. This value is based on engineering judgement and experience with previous safety assessments of similar dike cross-sections. An approximation for the intrusion length can be calculated via equation 5.6. The intrusion length is only dependent on the consolidation coefficient of the blanket layer and the duration of the high water event.

$$L' \approx 4\sqrt{C_v(t - t_0)} \tag{5.6}$$

The consolidation coefficient C_v is dependent on the soil type of the blanket layer. The values for the C_v are determined for the relevant soil types in the Alblasserwaard region during a dike reinforcement project by the water authority Rivierenland (Kwakman, 2023). The local blanket layer is composed of clay and peat material, for which the values of the consolidation coefficient are in the range of 2E-7 to 5E-8. The duration of the high water event will last anywhere between 2 to 17 days based on local piezometer measurements. The duration effects of the storm setup will last 2 days, and the elevated river discharge can last up to 17 days. With this data, the extreme values for the intrusion length can

be determined, from which a distribution function for the intrusion length can be set up. The distribution of the intrusion length for case Bergstoep is displayed in figure 5.32.

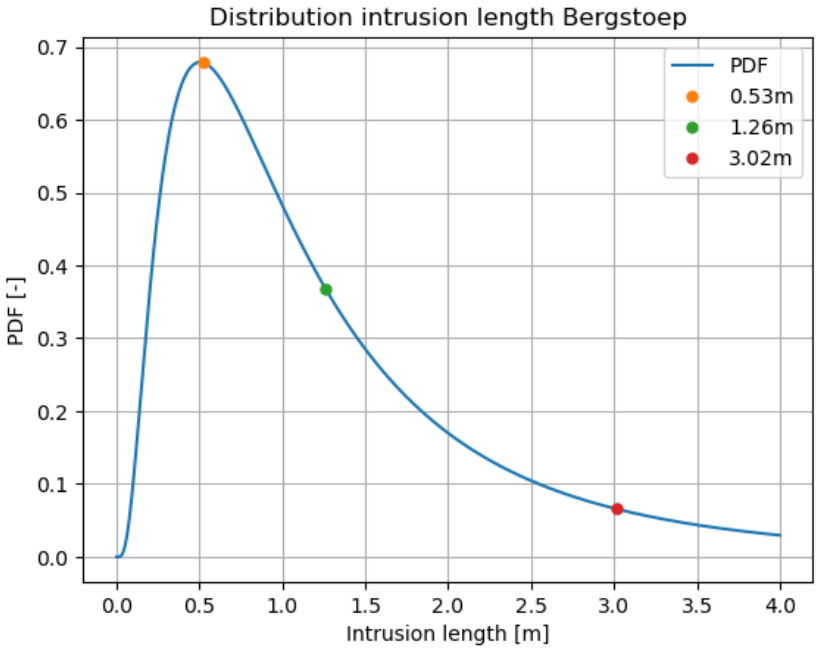

Figure 5.32: Distribution of the intrusion length for case Bergstoep

The thickness of the local blanket layer for the case study Bergstoep is less when compared to the Kortenhoevendijk case study. Due to the smaller blanket layer thickness, the lognormal distribution is better suitable to represent the intrusion length for the Bergstoep case study to avoid a negative value for the intrusion length. Figure 5.32 displays the 5%, 50%, and 95% percentiles for the intrusion length. This provides the input for D-Stability as displayed by figure 5.33.

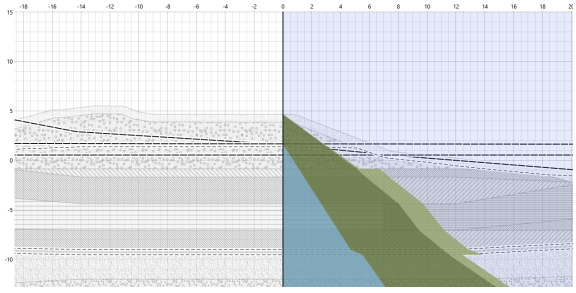

(a) 5% percentile: 0.53m intrusion length

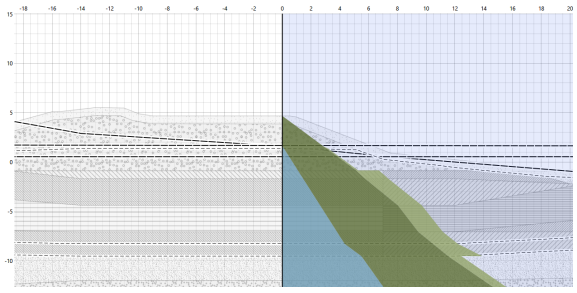

(b) 50% percentile: 1.26m intrusion length

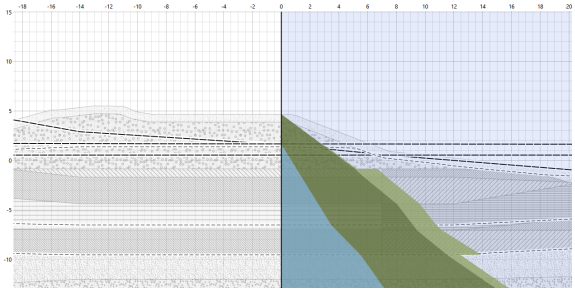

(c) 95% percentile: 3.02m intrusion length

Figure 5.33: Simulation of the intrusion length percentiles in D-Stability for case Bergstoep

Results

The fragility curves extracted from D-Stability for each percentile of the intrusion length are displayed in figure 5.34.

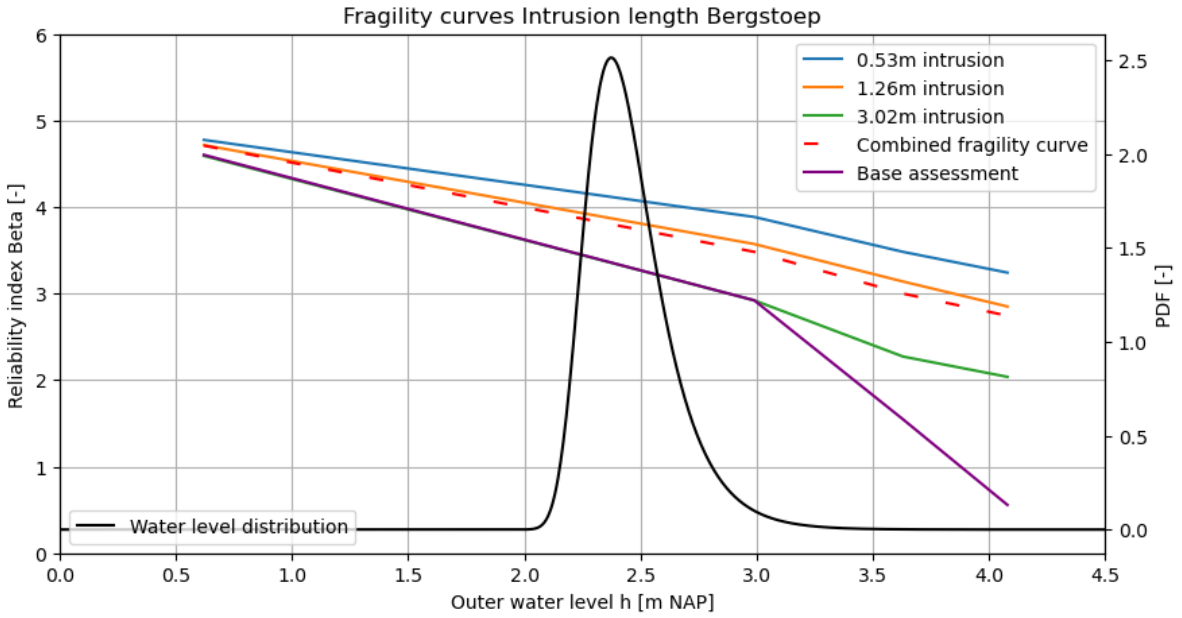

Figure 5.34: Resulting fragility curves intrusion length analysis for case Bergstoep

During the initial analysis, the combined fragility curve for the intrusion length analysis displayed a deviation at the daily outer water levels. The fragility curves of the 5%, 50%, and 95% percentile displayed a consistent starting point at the daily loading conditions with a similar value of the reliability index found during the MCIS analysis in D-Stability. However, the combined fragility curve displayed an overestimation of the reliability index. This issue can be related to the D-Stability modeling. The design points describing the reliability index at a given outer water level that are exported from D-Stability are assigned to the highest water level provided in the model. This importing issue was directly visible in the analysis of the uncertainties of the schematization of the phreatic line. During the daily loading conditions, the phreatic line inside the dike is modeled higher (1.37 meters) than the outer water level (0.62 meters). The exported design point will contain the highest assigned water level, instead of the outer water level. This modeling issue has also been the case during the analysis of the Kortenhoevendijk. However, the reliability index has been significantly higher for higher values of the outer water level, so the impact of combining the fragility curves is less. To account for this issue, the JSON file that is extracted from D-Stability is altered to the right outer water level, and so the fragility curve can be combined correctly. This step is also described in Appendix C where the entire process of D-Stability modelling is mentioned.

Figure 5.35 displays the conditional failure probability for the Bergstoep case study. The figure displays the water levels that contribute to the failure probability of the dike cross-section. When the outer water level reaches 2 meters or higher, the outer water level starts to play a role in the failure probability of the dike cross-section. Therefore, the wrongful combining of the fragility curves at the daily outer water levels do not have a large influence on the failure probability. The relevant outer water levels for the Bergstoep case start at 2 meters. Additionally, in the macrostability safety assessment, the safety standard for the dike cross-sections is described to be relevant for the WBN (waterstand bij norm) water levels that are extreme water levels with a low probability of occurrence.

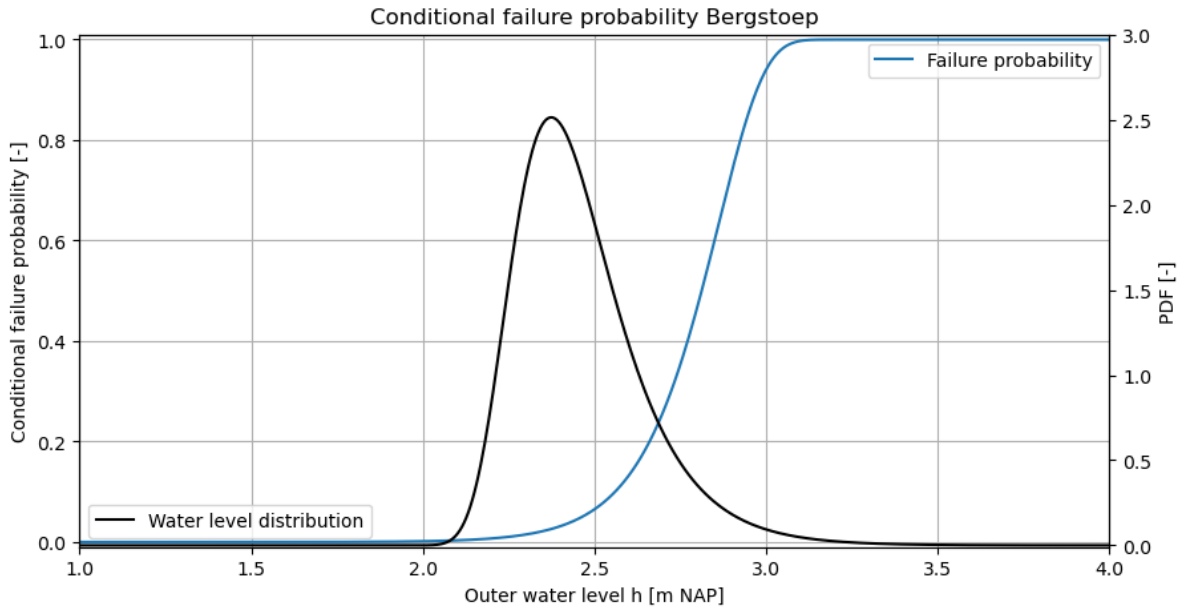

Figure 5.35: Conditional failure probability for case Bergstoep

The effect of the intrusion length analysis on the reliability index at extreme water conditions shows that the fragility curve remains more stable in comparison to the base assessment for the case Bergstoep. The base assessment shows the point of uplift of the blanket layer at an outer water level of $h = 2.99m$, with a return period of 10 years. The combined fragility curve does not display the effect of the point where the uplift of the blanket layer will occur. The combined reliability index is 3.64 and the failure probability is 1.34E-4.

The contributions to the failure probability are displayed in figure 5.36.

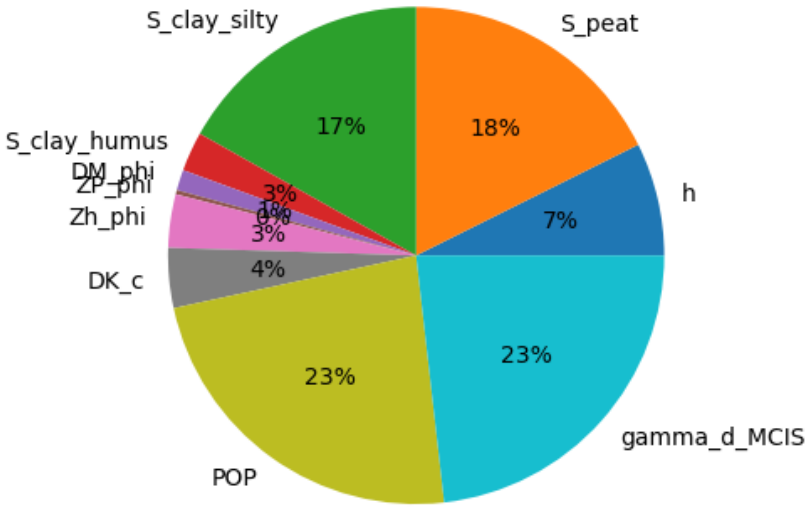

Figure 5.36: Contributions to the failure probability of the intrusion length analysis for case Bergstoep

The largest contribution to the failure probability of the intrusion length analysis is the model factor γ_d and the POP. The POP is described by the test collection with a characteristic value and a lognormal

distribution for the probabilistic analysis. The distribution of the POP is based on CRS laboratory tests on local soil samples. The fit of the POP to the test data is reasonable to good. The shear strength ratio for both the peat layer and the silty clay layer is also one of the larger contributions to the failure probability. The shear strength ratio fits well with the laboratory test data.

5.3.3. Phreatic line

The analysis of the uncertainties in the phreatic line schematization is similar to the Kortenhoevendijk case study. The schematization process as described by the *Technische rapport Waterspanningen bij dijken* is used to provide the upper and the lower limit for the phreatic line, which is used to describe the distribution function of the phreatic line.

Stochastic variable: Phreatic line

The distribution of the phreatic line is assumed to be normal where the upper limit, the 95% percentile for the phreatic line is based on the clay dike core schematization. The lower 5% limit is set up by using the sandy dike core schematization of the phreatic line. The mean of the phreatic line is situated between the two extremes. Figure 5.37 and 5.38 display the schematization of the phreatic line for the case study Bergstoep at the daily loading conditions and the high water loading conditions.

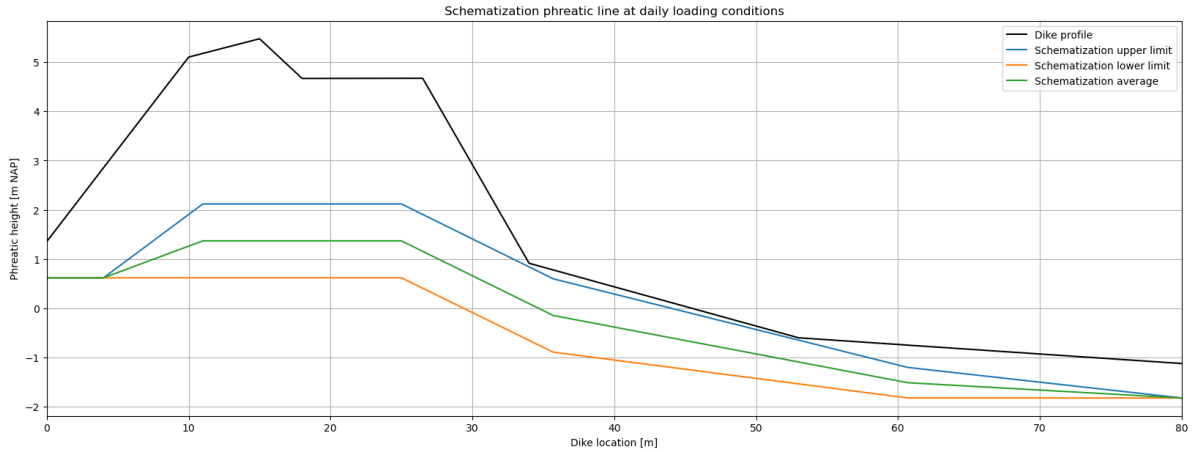

Figure 5.37: Schematization of the phreatic line during daily loading conditions for case Bergstoep

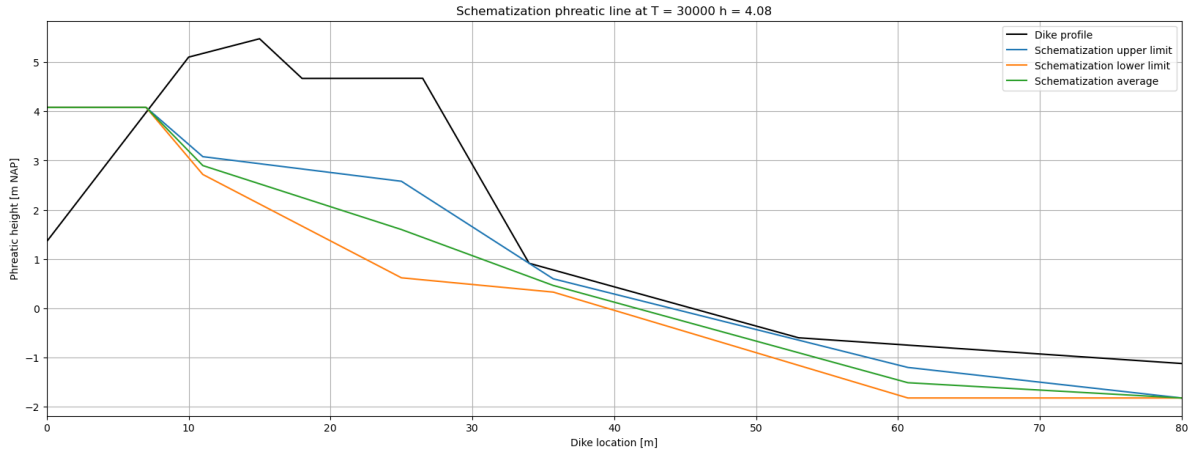

Figure 5.38: Schematization of the phreatic line during high water conditions $h = 4.08m$ for case Bergstoep

The phreatic lines displayed in figure 5.37 and 5.38 are used to set up the D-Stability model, including the 50% expectation value for the hydraulic head and the intrusion length. Other parameters and variables in the D-Stability model remain constant throughout the analysis.

Results

The fragility curve for the analysis of the phreatic line in D-Stability is displayed in figure 5.39. The PTK is used to construct the combined fragility curve.

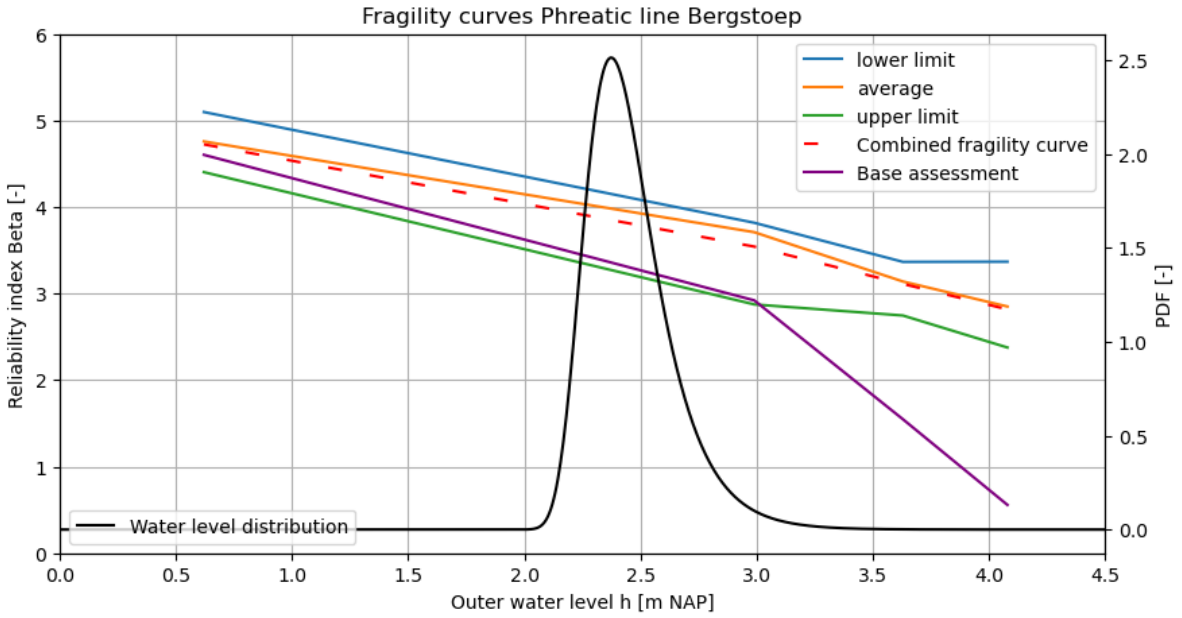

Figure 5.39: Resulting fragility curves of the phreatic line analysis for case Bergstoep

The impact of the design points at the daily conditions is visible throughout the fragility curve. The reliability index at the daily loading conditions for the fragility curve of the lower, average, and upper limit, are each assigned to the water level in the dike, instead of the outer water level of $h = 0.62m$. This results in a reliability index of the combined fragility curve at the daily outer water level that is higher than the original fragility curves, which is not a reliable outcome. However, the outer water level h contribution to the failure probability starts at 2 meters, so the lower end of the fragility curve will be neglected. The combined reliability index is 3.7 and the combined failure probability is equal to 1.06E-04. The combined fragility curve appears linear, however, the separate fragility curves describing the lower, average, and upper limits are inconsistent. The lower limit fragility curve displays a plateau between the design points of the MCIS analysis at $h = 3.63m$ and $h = 4.08m$. The design points that are taken from a D-Stability analysis via an MCIS analysis can be further investigated with figure 5.40.

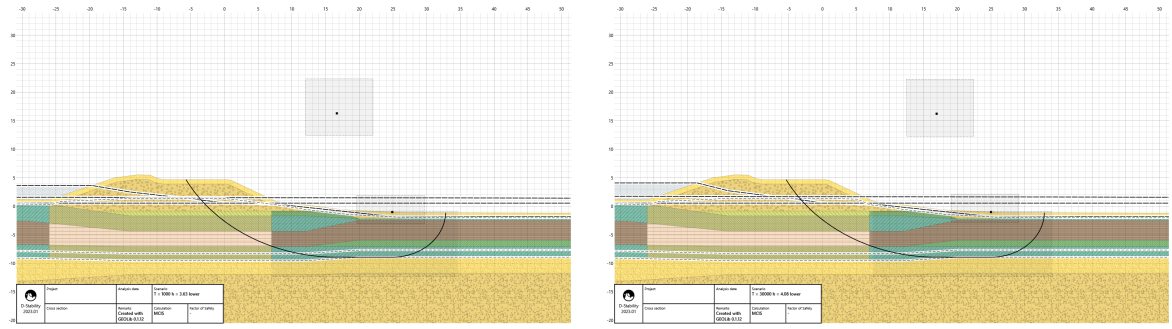

(a) D-Stability result of the lower limit of the phreatic line for $h = 3.63m$

(b) D-Stability result of the lower limit of the phreatic line for $h = 4.08m$

Figure 5.40: D-Stability MCIS results for the lower limit of the phreatic line schematization

The slip surfaces found in the MCIS analysis for both lower limit schematization of the phreatic line are almost identical for the two water levels. The reliability indexes found in the stability analysis deviate by 0.002. The increase in the outer water level appears to have a minimal effect on the stability

when the lower limit of the phreatic line is included in the stability assessment. The dike body of the case study Bergstoep is wide, and the increase of the outer water level does not affect the phreatic line in the dike body for the lower limit.

A similar pattern is visible at the upper limit schematization of the phreatic line, where a plateau is reached between $h = 2.99m$ and $h = 3.63m$. The D-Stability results for these design points are displayed in figure 5.41.

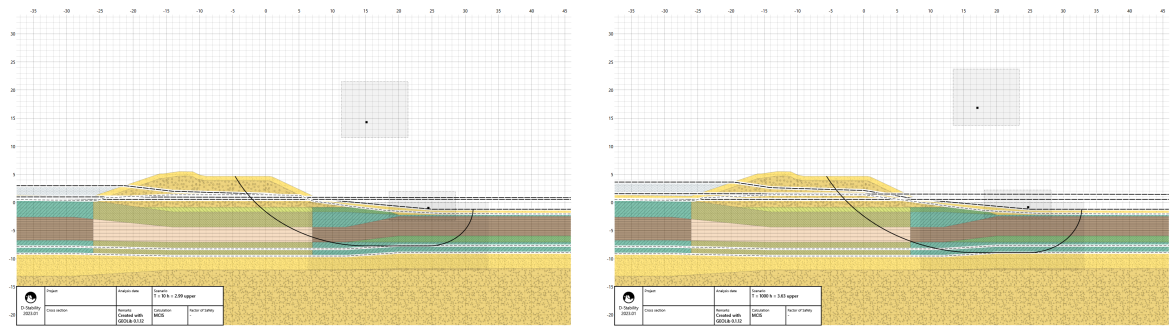

(a) D-Stability result of the upper limit of the phreatic line for $h = 2.99m$

(b) D-Stability result of the upper limit of the phreatic line for $h = 3.63m$

Figure 5.41: D-Stability MCIS results for the upper limit of the phreatic line schematization

The upper limit schematization at $h = 3.63m$ displays a more shallow slip surface, not reaching the bottom of the blanket layer. During the MCIS analysis, D-Stability searches for the slip surface where the reliability index and failure probability are the lowest, so this can result in a deviating failure surface when compared to other calculations.

The contributions to the failure probability of the phreatic line analysis are shown in figure 5.42.

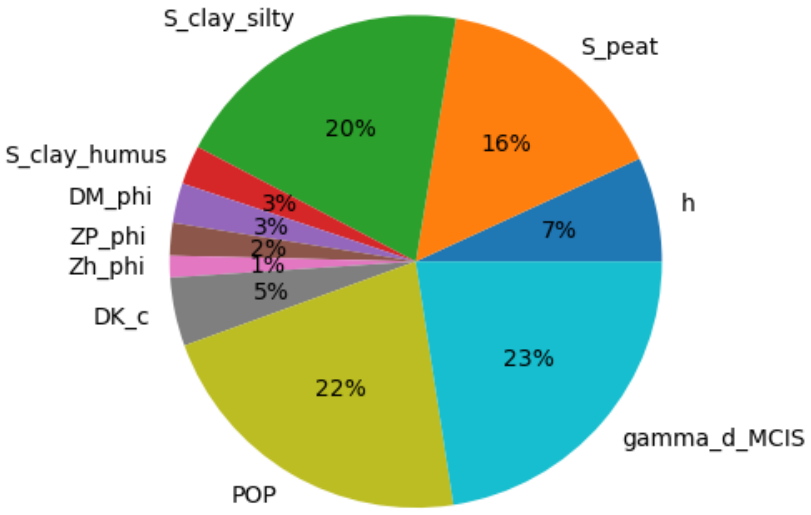

Figure 5.42: Contributions to the combined failure probability of the phreatic line analysis for case Bergstoep

The contributions to the failure probability are distributed over the shear strength ratio of the soft soils, the outer water level, the model factor, and the POP. The contributions to the failure probabilities resulting from the hydraulic head analysis and the intrusion length analysis are comparable to the contributions from the phreatic line within a few percent.

5.3.4. Results case study Bergstoep

The schematization uncertainties of the pore water pressures for the case study Bergstoep are considered by implementing the hydraulic head in the aquifer, intrusion length in the blanket layer, and the height of the phreatic line as a stochastic variable. The fragility curve describing the uncertainties in the hydraulic head, intrusion length, and phreatic line are combined in the Probabilistic ToolKit by assigning the same contribution to each imported fragility curve. The combined fragility curve that includes the schematization uncertainties of the pore water pressures for case Bergstoep is displayed in figure 5.43.

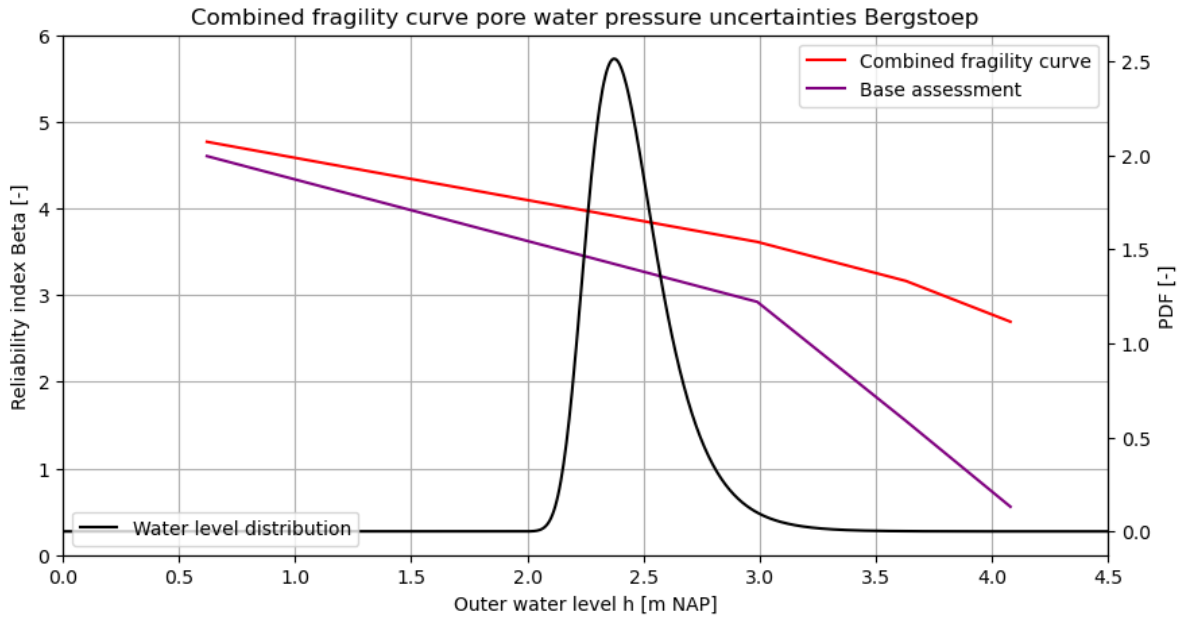

Figure 5.43: Combined fragility curve of the pore water pressure uncertainties for case Bergstoep

The combined fragility curve is shifted to a higher reliability index at all values for the outer water levels. The fragility curve displays that it is valuable to include the schematization uncertainties in the stability analysis to provide a realistic value for β that describes the actual dike stability. The point of uplift of the blanket layer in the base assessment is situated at $h = 2.99m$, as visible in the fragility curve where the slope steepness increases. In the combined fragility curve that includes the pore water pressure schematization uncertainties, this point has shifted.

Component	**Combined Reliability index β [-]**	**Combined Failure probability P_f [-]**
Base assessment	3.14	8.51E-04
Hydraulic head	4.39	5.70E-06
Intrusion length	3.64	1.34E-04
Phreatic line	3.7	1.06E-04
Combined pore water pressures	3.77	8.17E-05

Table 5.22: Results pore water pressure uncertainties analysis for case Bergstoep

The combined reliability index that includes the schematization uncertainties of the pore water pressures is improved by 0.64. The failure probability is improved by a factor of 10. The hydraulic head in the aquifer has the largest impact on the reliability index.

Discussion

Several points for discussion can be mentioned for the Bergstoep case study analysis for the consideration of the schematization uncertainties in the pore water pressures during the macrostability safety assessment.

- The process of combining the fragility curves does not work for the daily loading conditions since the design points taken at the daily conditions are assigned to the height of the phreatic line. If the phreatic line is higher than the outer water level, the design point will be assigned to a higher value for h than the outer water level. The fragility curve at lower water levels will not be consistent, and the combining of the fragility curves will result in a higher reliability index at the daily conditions than the index found during the stability analysis. Therefore, the combined fragility curve shown in figure 5.43 is not reliable for the lower outer water levels ($h < 2m$).
- The contributions of each component describing the pore water pressures are assumed to be uncorrelated. In the PTK, the contributions of each fragility curve are set to $1/3$ to simulate that the components are not correlated.
- Non-convergence issues during modeling are solved since the reliability index is significantly lower than those for the Kortenhoevendijk case study.

5.4. Summary uncertainty analysis pore water pressures

The analysis has shown that it is possible to include schematization uncertainties for components of the pore water pressures in the macrostability safety assessment. By applying a distribution function for uncertain components via three fragility curves, the combining of fragility curves is an approachable method to provide the combined reliability index and failure probability. This will include the uncertainties of the pore water pressure components provided the contributions of each fragility curve.

The case study of the local dike cross-section Kortenhoevendijk is located in the upper river area of the Netherlands. The schematization uncertainties of the phreatic line are taken into consideration by applying an uncertainty range based on schematization limits on the level of the phreatic line. The uncertainty range in the expected value for the stationary hydraulic head in the aquifer is determined by taking into consideration the transmissivity of the aquifer and the resistance of the foreshore and hinterland as stochastic variables. The coefficient of variation at the inner dike toe of the hydraulic head is equal to 1.64. The uncertainty in intrusion length over the local blanket layer is taken into account by a distribution function based on expert judgement, where the standard deviation is equal to 0.9. The analysis shows that considering the pore water pressure schematization uncertainties during the macrostability safety assessment for the case study Kortenhoevendijk improves the failure probability from 1.24E-09 to 4.37E-12. The failure probability is improved by a factor of 1000, which has a significant impact on the expected reliability of the dike cross-section. The largest impact on the reliability is the uncertainty in the intrusion length of the blanket layer.

The case study Bergstoep includes the schematization uncertainties of the phreatic line by applying a large range of uncertainty on the schematization of the height of the phreatic line. The uncertainty range in the expected value for the time-dependent hydraulic head in the aquifer is determined by taking into consideration the entry point and cyclic resistance of the hinterland as stochastic variables and considering the hydraulic head as a time and location-dependent variable. The uncertainty in intrusion length over the local blanket layer is considered by using a distribution function based on expert judgement. The analysis shows that considering the pore water pressure schematization uncertainties during the macrostability safety assessment for the case study Bergstoep improves the failure probability by a factor of 10. The largest impact on the reliability is the uncertainty in the hydraulic head.

Discussion

The method that is used during the project is still quite complex due to the amount of pre-processing. Each component requires to be calculated, stochastic variables require to be defined. The calculations then have to be implemented into a D-Stability model, for which multiple stages with multiple water levels are required to be set up. For each component of the pore water pressures, one D-Stability model is set up. For each model, one scenario describes one design point in the fragility curve. Three fragility curves are required per pore water pressure component. For each fragility curve, a minimum of 3 design points are required. This results in a minimum of 27 full-probabilistic calculations per case study. Based on experience, one successful full-probabilistic calculation can last 30 minutes to 2.5 hours. The total computational time for one case study alone will range anywhere between 14 to 67.5 hours.

There is, however, much potential for applying the described methodology to other components of the safety assessment. The soil behaviour, for example, especially the dike material behaviour is another major uncertainty in the D-Stability analysis which has a large influence on the outcome of the overall dike stability. The input in the calculation is either the drained or undrained behaviour of the dike material, however, the true behaviour will be somewhere in between drained and undrained. The soil behaviour can also be considered as a stochastic variable via the methodology used during the project. Even dike geometry can be considered as a variable by applying the suggested method used in the project.

The described methodology to take the uncertainties in the pore water pressures into consideration during the macrostability safety assessment researched in the project is not case-dependent. This method can be applied to any primary dike cross-section in the Netherlands. The calculation process of determining the expected values for the intrusion, phreatic, and hydraulic head will vary for each cross-section. The process of assigning the uncertainties as a stochastic variable, providing the fragility curves, and combining the curves in the PTK, is an approachable method.

The case study of the Kortenhoevendijk showed the largest contribution to the improvement in reliability index to be the intrusion length, whereas the Bergstoep case study's largest contribution is the hydraulic head. It is expected due to the uplift of the blanket layer for the Bergstoep case study that the lowering of the hydraulic head will impact the point of uplift. If this point is shifted in the fragility curve, the steep decline in the reliability index is shifted to the higher outer water levels. In the local cross-section for the Kortenhoevendijk, the uplift mechanism impacts the macrostability significantly less, and for this location, the intrusion length has shown to have more influence on the overall stability.

Another component of the analysis in D-Stability for both case studies is that the Bergstoep case study required much less computational time and resulted in fewer to no convergence issues during the MCIS analysis when compared to the Kortenhoevendijk study. The Bergstoep case study displayed lower values for the reliability index ($\beta < 8$), positively influencing the MCIS calculations to converge. Additionally, this significantly improved the computational time in the Bergstoep case study, where one pore water pressure component could be analyzed in one day, whereas the Kortenhoevendijk case study could take up to 3 to 4 days.

6
Conclusion

What is the current methodology for assessing the macrostability of a primary dike trajectory and what are the uncertainties and limitations of the schematization processes?
The current methodology of assessing the macrostability of a primary dike trajectory is considered by applying combinations of unfavorable values in a semi-probabilistic calculation which is a relatively quick process. However, the limitations are that the method is an approximation and can be considered conservative. It is preferred to apply the recently implemented full-probabilistic calculation methods in the macrostability safety assessment. Currently, the number of stochastic variables in the full-probabilistic calculation is limited, and only soil parameters can be assigned as a stochastic variable. Large uncertainties in the subsurface and the geohydrological response of the dike are considered via deterministic values and can not be included as a stochastic variable in the safety assessment.

Which uncertainties within the schematization process have a large influence on the macrostability of a dike cross-section?
Based on expert judgement, the uncertainties in the schematization process that have a large influence on the macrostability are the schematization of the subsurface and the schematization of the pore water pressures. The schematization of the subsurface directly influences the macrostability of the dike cross-section and is currently schematized conservatively. The influence of these schematization assumptions is unknown. The schematization process of the pore water pressures is currently based on expert judgement and conservative design values. The components describing the pore water pressures are assigned with design values, so the impact of describing these components as a stochastic variable is expected to be significant.

How can large uncertainties within the schematization process be included in the current macrostability safety assessment?
The subsurface schematization process is a large uncertainty in the macrostability safety assessment due to large spatial variation in the subsurface in the Alblasserwaard. The impact on the simplification of the subsurface and general composition is investigated via several soil scenarios. For the case study of the local dike cross-section Kortenhoevendijk, four soil scenarios are set up, where one is composed of a sandy subsurface one is composed of a clayey subsurface and the other two are simplified versions of these schematizations. For each soil scenario, one fragility curve is composed of full-probabilistic analysis design points for different outer water levels. All four fragility curves are combined in the Probabilistic ToolKit to provide a combined fragility curve and failure probability. This failure probability includes the schematization uncertainties of the local dike cross-section of the Kortenhoevendijk.

The schematization uncertainties of the pore water pressures during high water conditions are approached similarly. The pore water pressures are separated into three components that are analyzed separately: the level of the hydraulic head in the aquifer, the intrusion length in the blanket layer, and the height of the phreatic line. The fragility curves are constructed in D-Stability to represent a range of uncertainty in one component of the pore water pressure. These fragility curves can be combined to represent the failure probability of the dike cross-section including the schematization uncertainties in the pore water pressures. The hydraulic head is calculated via the methodology described by the *Technische rapport Waterspanningen bij dijken* to determine the stationary and time-dependent expectation

value for the hydraulic head. In the calculation process, the hydraulic conductivity and thickness of the aquifer, the resistance of the foreshore and hinterland, and the entry point are considered stochastic variables. The results provide the hydraulic head as a stochastic variable with a normal distribution, where the 5%, 50%, and 95% percentiles are extracted and used as D-Stability input. Three fragility curves are constructed and combined in the Probabilistic ToolKit to provide the combined fragility curve that includes the uncertainties in the expectation value for the hydraulic head. The intrusion length is applied as a stochastic variable with a normal or lognormal distribution function over the thickness of the blanket layer. The 5%, 50%, and 95% percentiles of this distribution can be extracted again, and fragility curves are composed and later combined to provide the failure probability that includes the uncertainty in the schematization of the intrusion length. The phreatic line schematization process as described by the *Technische rapport Waterspanningen bij dijken* is used to determine a distribution function for the extreme values of the phreatic line. The 5% percentile for the phreatic line is based on the sand dike core schematization and the 95% percentile on the clay dike core schematization of the phreatic line. The 50% percentile is situated in between the two extremes, where the distribution is considered normal. The same process is repeated where the three fragility curves are set up, the curves are combined in the Probabilistic ToolKit, and the combined failure probability is provided that describes the failure probability of the dike cross-section that includes the uncertainty in the schematization process of the phreatic line.

How do these uncertainties measure over different dike sections that are representative of the Alblasserwaard?
The uncertainties in the subsurface schematization are only investigated for one dike cross-section, so it is difficult to conclude on the application of this method throughout the Alblasserwaard. The analysis itself, however, displays the influence of the simplification of the soil profile having a minor influence on the reliability index for the high water levels. This could be different for different soil scenarios and/or different configurations of the subsurface schematization. The components in the pore water pressure schematization do apply over the two different dike cross-sections that are both representative of the primary dike trajectory in the Alblasserwaard. The possibilities to apply the methodology to include the uncertainties in the macrostability safety assessment is not limited to the Alblasserwaard.

What is the influence of the schematization uncertainties in the macrostability safety assessment on the expected reliability of the primary dikes in the Alblasserwaard region?
The impact of taking the schematization uncertainties in the macrostability safety assessment on the expected reliability varies for each component that is investigated. The subsurface schematization displayed an influence on the failure probability by 0.1 due to the simplification of the subsurface. The largest influence on the reliability during the pore water pressure analysis has been proven to be the intrusion length for the case study Kortenhoevendijk and the hydraulic head for the Bergstoep case study. The failure probability is improved by a factor of 1000 for the case study Kortenhoevendijk and by a factor of 10 for the case study Bergstoep when taking all three pore water pressure uncertainties into account during the macrostability assessment. The process of considering the schematization uncertainties within the macrostability safety assessment has been proven to work, where the reliability can improve depending on the local cross-section and uncertainty component. Including the pore water pressure schematization uncertainties in the macrostability safety assessment can have a significant impact on the outcome of the assessment. Including these uncertainties can make the difference between deciding whether a dike trajectory needs reinforcement, or deciding that reinforcement is not necessary.

6.1. Discussion

With the introduction to the relatively new full-probabilistic calculation methods in D-Stability, it is possible to include expectation values for strength parameters with their given uncertainty. The current methodology for the macrostability safety assessment is based on the conservative use of multiple unknown parameters or aspects. For these parameters, limit design values are assigned for each of these variables. With the new calculation approach of full-probabilistic method that can include uncertainty within the unknown parameters, it is redundant to apply limit design values and an additional uncertainty range. The macrostability safety assessment should not be executed by applying conservative

parameters with a standard deviation for each component. The true stability of a dike cross-section can be calculated by using the expectation values with a standard deviation, and software such as D-Stability will still provide the lowest reliability index.

The process of considering the schematization uncertainties in the macrostability safety assessment is much more feasible for dike sections with a reliability index under 8 to improve the full-probabilistic calculation results. If the dike section is considerably stable, higher water levels should be included in the calculation process to reduce the reliability index below 8 and provide reliable results in the MCIS analysis.

The methodology that is used throughout the project is still complex due to the amount of pre-processing. The D-Stability analysis and Probabilistic ToolKit calculations are the least complex of the entire process. There is much room left for improvement of the methodology to consider these schematization uncertainties during the macrostability safety assessment. There is also much potential for applying the described methodology to other components of the safety assessment. Using soil scenarios to include small schematization aspects in the process of setting up a representative subsurface can be included in this way, to provide a combined failure probability that includes these uncertainties. The possibility is that these do not influence the outcome of the reliability index significantly, where the process of subsurface schematization can be streamlined. Other uncertainties in the subsurface schematization such as horizontal spatial variation in the subsoil can also be taken into consideration. Van Der Burg, (2024) describes that the influence of horizontal spatial variability in the soil is more effective to be considered by the approach as described in the WBI, instead of using detailed finite element modeling (Van Der Burg, 2024). The current method as described by the WBI is sufficient to implement spatial variability. If the methodology introduced by this project could be applied to include the horizontal spatial variation in the macrostability safety assessment is actually beneficial, is to be determined.

6.2. Recommendations

The main recommendation for this project is to investigate the influence of considering the pore water pressure uncertainties for more dike cross-sections around the Alblasserwaard and throughout the Netherlands. More cross-sections should be investigated to conclude on usability of the methodology. The Alblasserwaard is selected for this project due to the high complexity of the subsurface region. If the reliability significantly improves throughout multiple case studies, if schematization uncertainties are taken into consideration as a stochastic variable, the method could help improve insight into the actual strength of the dikes throughout the Netherlands.

The methodology that is applied to include the phreatic line as a stochastic variable is based on the schematization described by the *Technische rapport Waterspanningen bij dijken*. The phreatic line schematization described by this report is a highly conservative, however arbitrary schematization of reality. There is only one way to gain insight into the level of the phreatic line during extreme water events, which is to perform measurements in situ. The level of the phreatic line does have a significant impact on the failure probability of the dike cross-section, so is an important component. More research is required to improve the schematization of the phreatic line or to create a representative distribution function for the expected value of the phreatic line. Research such as the investigation into the influence of the unsaturated zone contribution to the safety assessment by Mascini, (2022), can be used to improve the precision of the schematization of the phreatic line . However, the use is limited for high water levels, that are most relevant in the macrostability safety assessment (Mascini, 2022).

It is recommended to investigate the applicability of the method to include schematization uncertainties in the macrostability assessment while also still considering other failure mechanisms. Using multiple fragility curves and combining them in the Probabilistic ToolKit is expected to also apply to other aspects of the macrostability safety assessment, or perhaps even other failure mechanisms. Additionally, the macrostability safety assessment currently neglects the residual strength of the dike after a macro-instability occurs. For lower water levels, the residual strength after a macrostability failure that occurs can still be sufficient to suffice to the safety standard. The residual strength of the dike after

a macrostability failure should be considered in the safety assessment.

Assigning the contributions of the pore water pressure uncertainties with a discrete distribution is a large limitation of the methodology tested during the project. This should be improved by using a continuous distribution function that describes each component of the pore water pressures.

The results from the project imply that the largest impact on the reliability of the dike cross-section includes the schematization of the pore water pressure uncertainties. For dike cross-sections that are prone to the uplift failure mechanism, the uncertainties in the hydraulic head have the largest impact on the failure probability. The uncertainties in the hydraulic head can be reduced by performing more measurements via piezometers in the dike trajectory. The intrusion length uncertainty has a large influence on dike cross-sections that are less prone to the uplift mechanism, where the blanket layer thickness is larger. For the dike cross-sections with a larger blanket layer thickness, the intrusion length could be measured in situ to gain more insight into local conditions.

References

AHN Actueel Hoogtebestand Nederland. (2023).

Backhausen, U., & van der Stoel, A. (2013). *Reader Geotechniek* (tech. rep.). KIVI-NIRIA. Den Haag.

Bauduin, M. H. L. G., & Barends, F. B. J. (1987). *Getijde-respons in grondwater onder Nederlandse dijken* (tech. rep.). Grondmechanica Delft.

Deltares. (2020). *D-Geo Stability User Manual* (tech. rep.). Deltares. Delft.

Deltares. (2017). *D-Soil Model User Manual* (tech. rep.). Deltares. Delft.

Deltares. (2022). *Probabilistic Toolkit User Manual* (tech. rep.). https://www.deltares.nl

Donders, S., Van de Peer, J., & Luc Hermans. (2003). Application and Assessment of Structural Reliability Methods for the Design of Structural Components. *NAFEMS Seminar: Use of Stochastics in FEM Analyses*.

Duits, M. (2020). *Hydra-NL Gebruikershandleiding versie 2.8* (tech. rep.). HKV, Rijkswaterstaat.

Jonkman, S. N., Jorissen, R. E., Schweckendiek, T., & Van Den Bos, J. P. (2021). *Flood Defences Lecture notes CIE5314* (tech. rep.).

Kanning, W., & van der Krogt, M. G. (2016). *Memo: Pore water pressure uncertainties for slope stability* (tech. rep.).

Kanning, W., Teixeira, A., van der Krogt, M., & Rippi, K. (2017). *Derivation of the semi-probabilistic safety assessment rule for inner slope stability, Calibration STBI 2016* (tech. rep.). Deltares.

Kroese, D. P., Taimre, T., & Botev, Z. I. (2011). *Handbook of Monte Carlo Methods*. https://doi.org/10.1002/9781118014967

Kruse, G., & Hijma, M. (2015). *WTI 2017: Handleiding lokaal schematiseren met WTI-SOS* (tech. rep.). Deltares.

Kwakman, L. (2020). *Probabilistische berekeningen macrostabiliteit binnenwaarts* (tech. rep.). Arcadis.

Kwakman, L. (2023). *Proevenverzameling SAFE 2022 (OR1)* (tech. rep.). Arcadis.

Manoj, N. R. (2016). *First-order Reliability Method: Concepts and Application* (tech. rep.).

Mascini, M. (2022). *The increase of dike stability due to unsaturated soil strength A study of the spatially and temporally varying presence of matric suction* (tech. rep.). http://repository.tudelft.nl/.

Naaktgeboren, M. (2023). *Schematization of shear strength The influence of the schematization of shear strength on the macro-stability safety assessment CIE5050-09: Additional Graduation Work* (tech. rep.).

Ondergrondmodellen | DINOloket. (2023). https://www.dinoloket.nl/ondergrondmodellen/kaart

Reiher, W. (1966). Monte Carlo Methods. *Biometrische Zeitschrift*, *8*(3). https://doi.org/10.1002/bimj.19660080314

Rijksinstituut voor Integraal Zoetwaterbeheer en Afvalwaterbehandeling. (2007). *Technisch rapport ontwerpbelastingen voor het rivierengebied*. Ministerie van Verkeer en Waterstaat.

Rijksoverheid. (2019). Het programma BOI 2023.

Rijkswaterstaat & Ministerie van Infrastructuur en Waterstaat. (2021). *Schematiseringshandleiding macrostabiliteit* (tech. rep.).

Rijkswaterstaat & Water Verkeer en Leefomgeving. (2019). *Regeling veiligheid primaire waterkeringen 2017 Bijlage I: Procedure* (tech. rep.). Ministerie van Infrastructuur en Mileu. http://www.helpdeskwater.nl/onderwerpen/waterveiligheid/pri

Rozing, A. (2015). *Memo Onzekerheden Waterspanningen in WTI 2017* (tech. rep.). Deltares.

TAW. (1996). *Technisch Rapport Klei voor Dijken* (tech. rep.). Technische Adviescommissie voor de Waterkeringen. Delft.

Technische Adviescommissie voor de Waterkeringen. (2004). *Technisch rapport waterspanningen bij dijken*.

Technische adviescommissie voor de waterkeringen. (1989). *Leidraad voor het ontwerpen van rivierdijken deel 2-benedenrivierengebied* (tech. rep.). 's-Gravenhage.

Tigchelaar, J. (2023). Personal communication.

Timo, S., & Kanning, W. (2017). *Reliability updating for slope stability of dikes Approach with fragility curves (background report)* (tech. rep.).

Van Der Burg, L. (2024). *Spatial Variability in Dike Stability Assessments* (tech. rep.). http://repository.tudelft.nl/.

van Duinen, A. (2014). *Handreiking voor het bepalen van schuifsterkte parameters WTI 2017 Toetsregels Stabiliteit* (tech. rep.). Deltares. Delft.

Verruijt, A. (2010). *Grondmechanica*. Delft University Press.

Waterschap Rivierenland. (2017). *De Bosatlas van de Alblasserwaard* (Waterschap Rivierenland, Ed.; first).

A

Appendix A: Local soil investigation

A.1. Local soil investigation case study Kortenhoevendijk

Mechanical borings

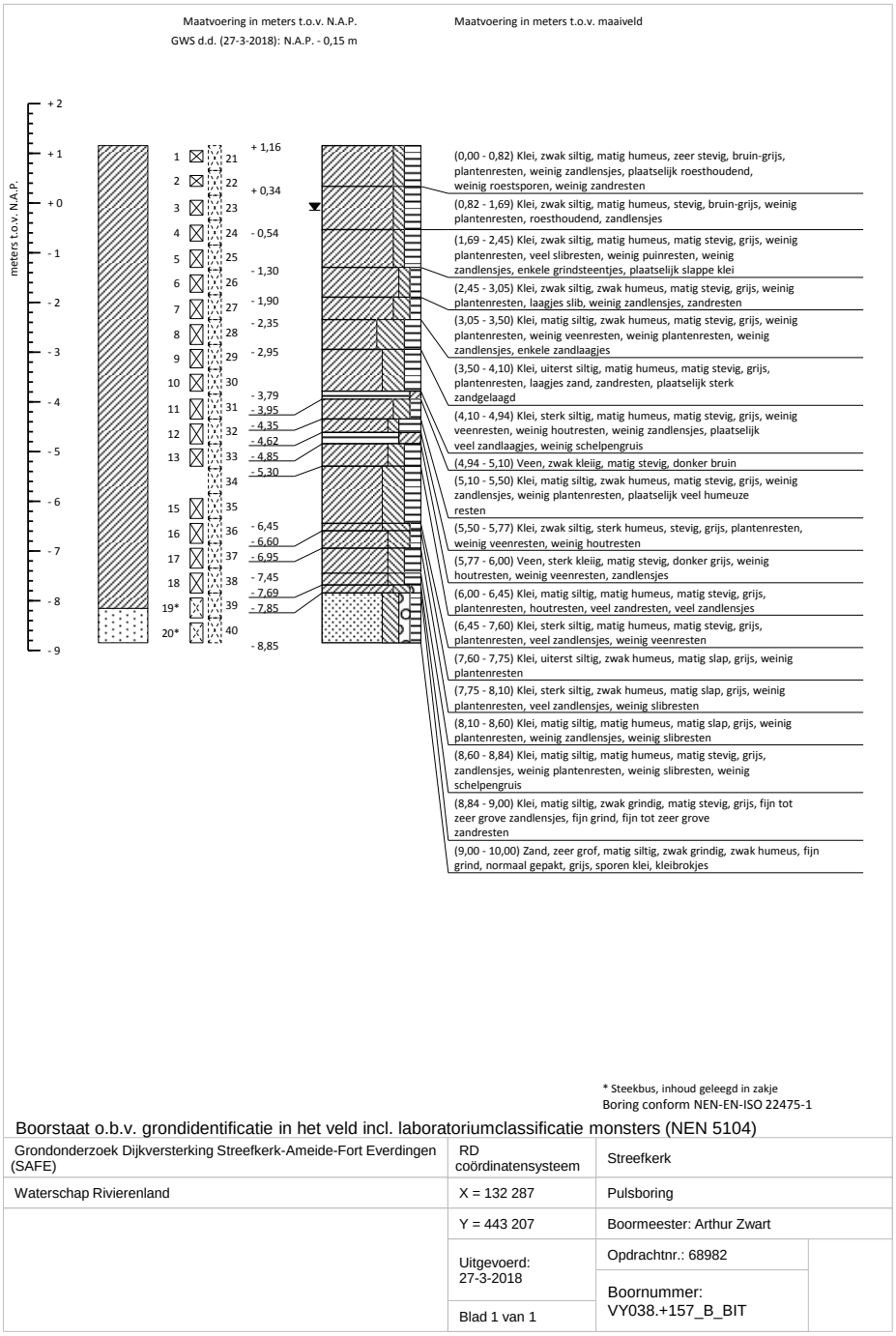

Figure A.1: Mechanical boring inner slope

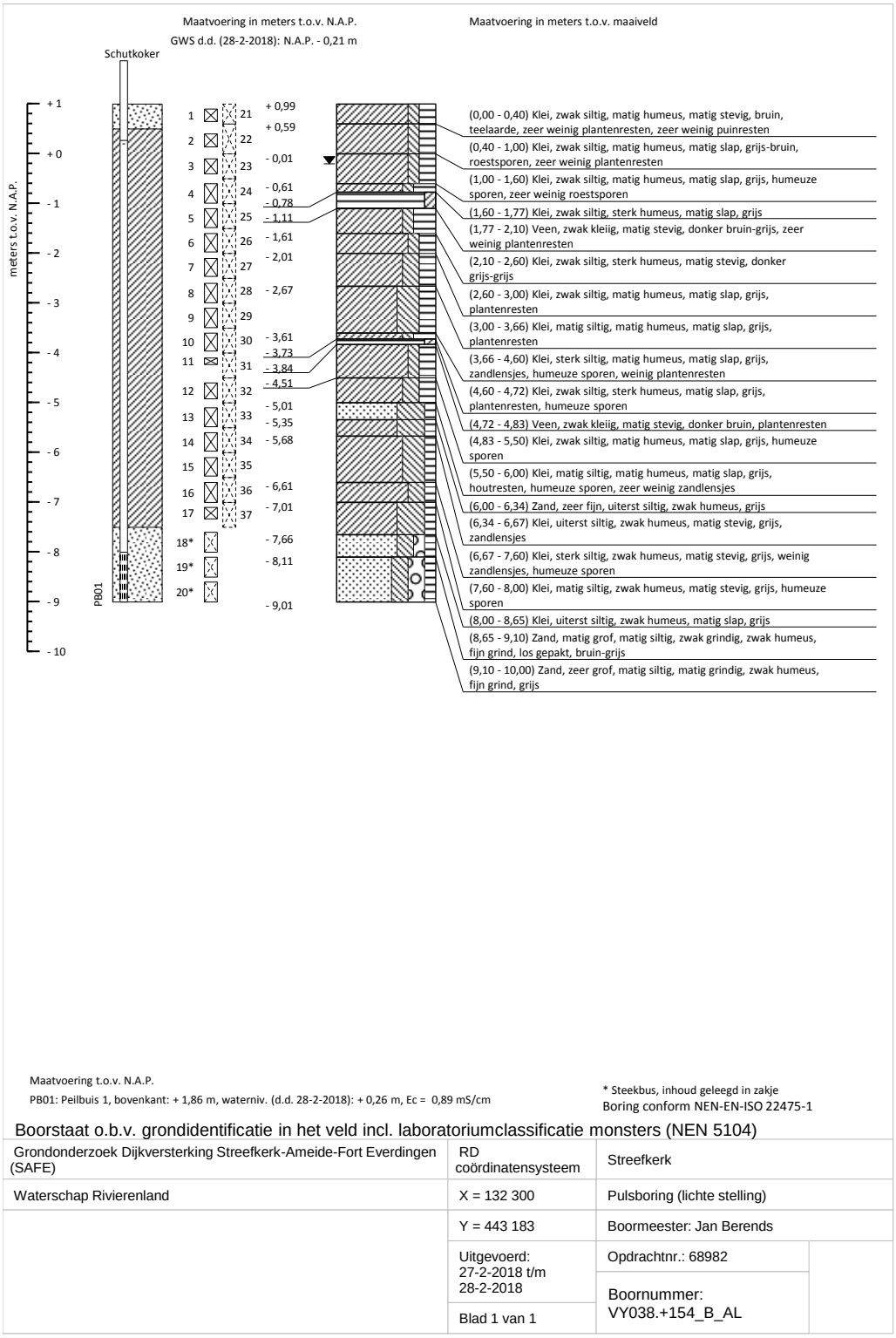

Figure A.2: Mechanical boring Hinterland

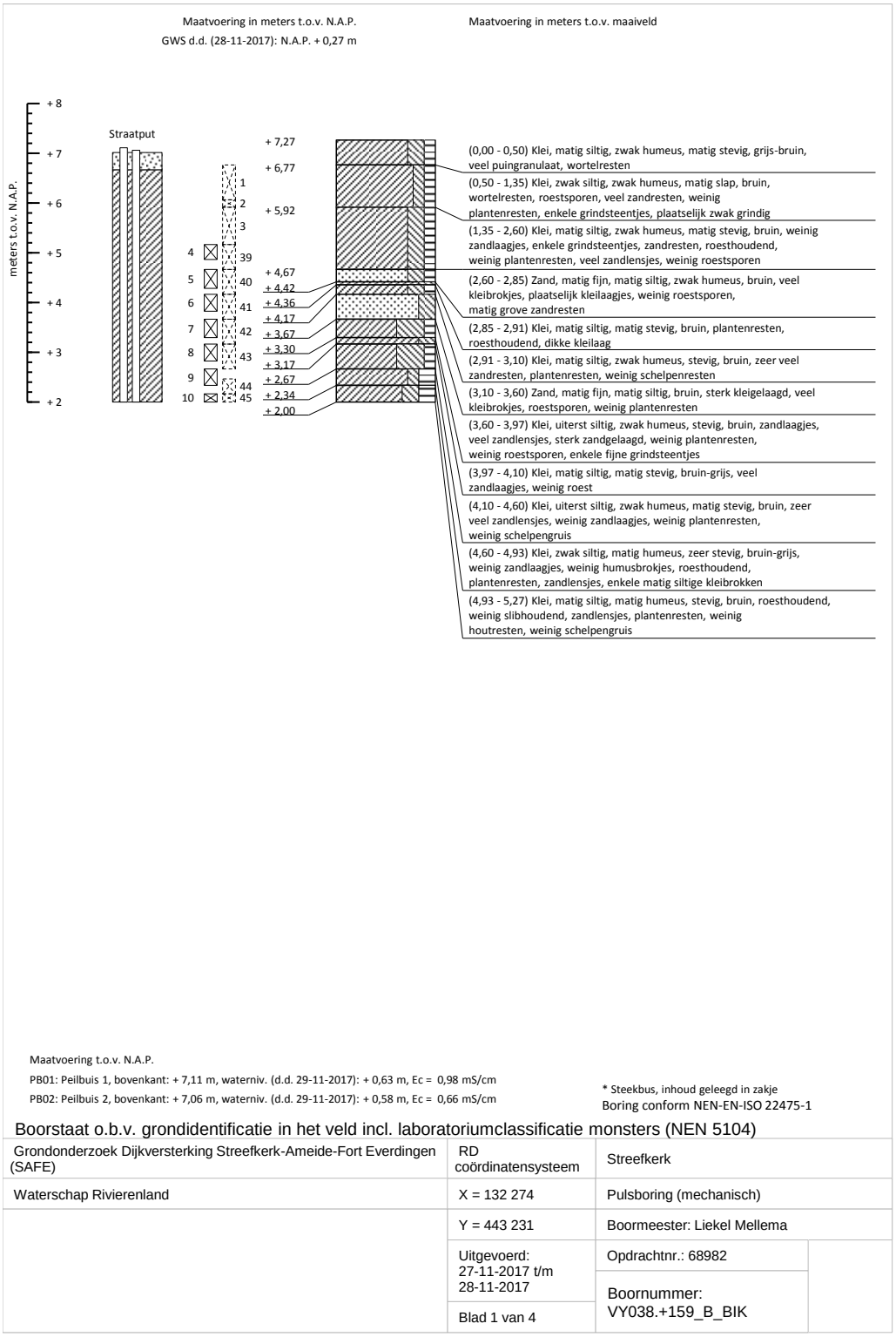

Figure A.3: Mechanical boring crest

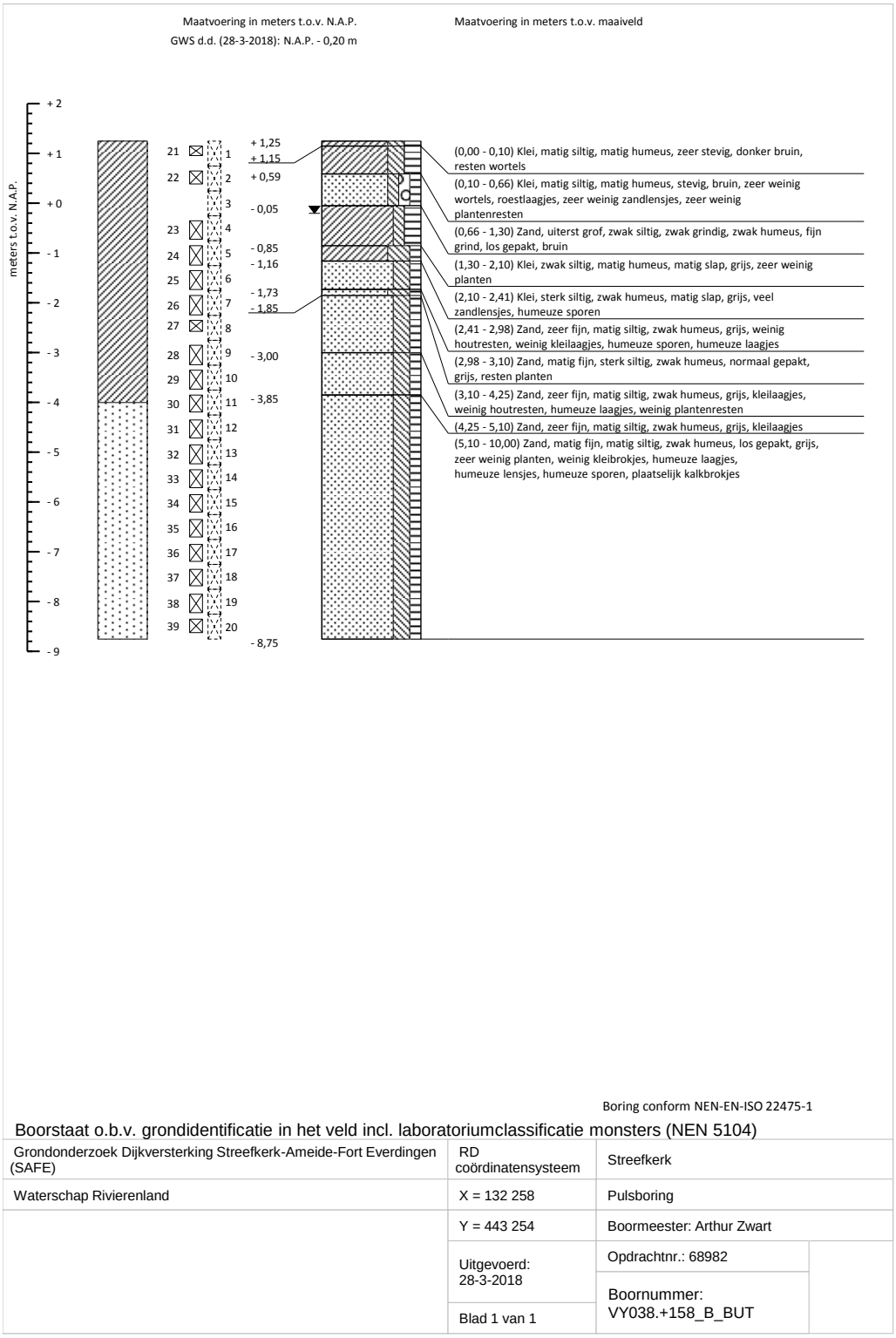

Figure A.4: Mechanical boring outer slope

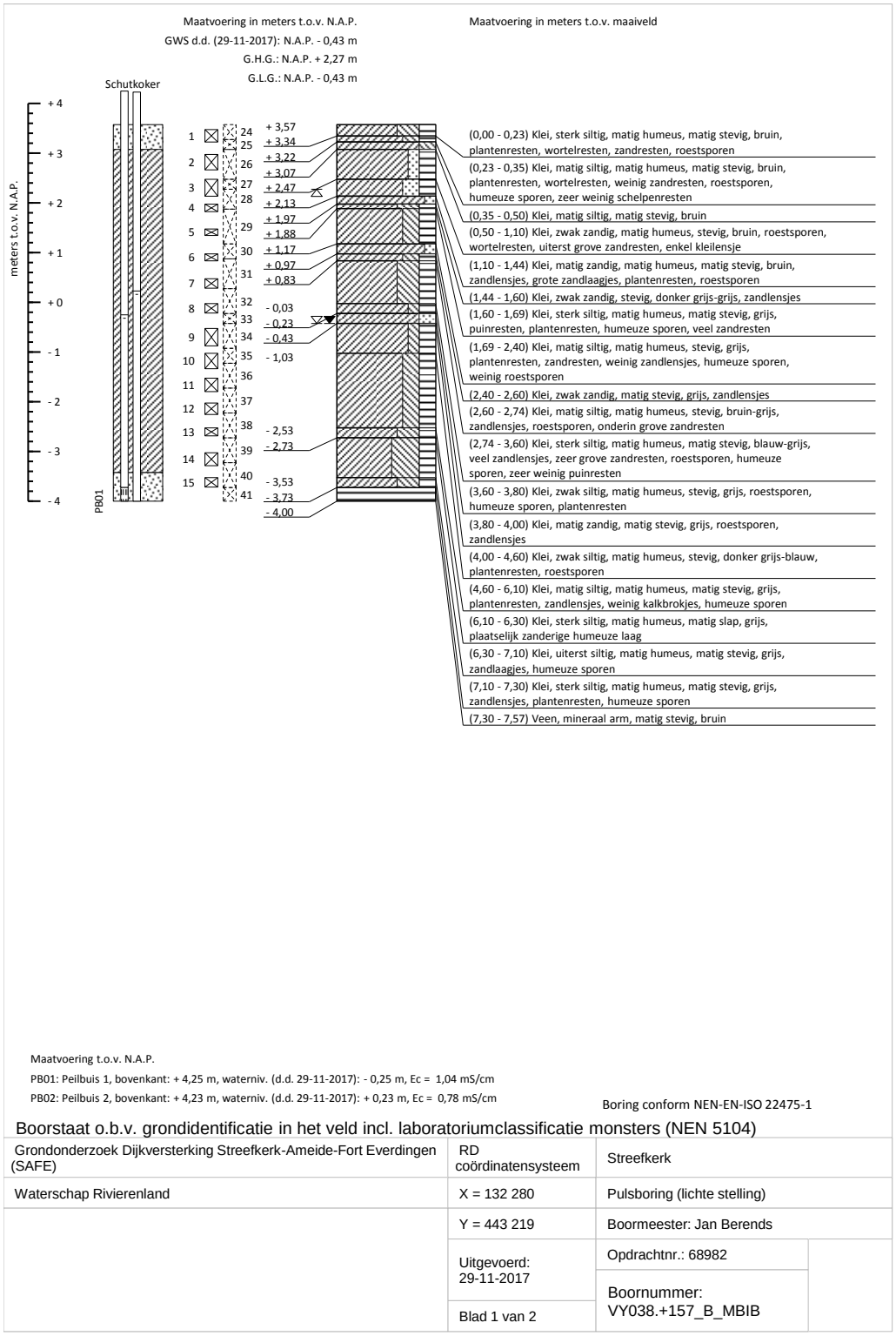

Figure A.5: Mechanical boring crest

CPT's

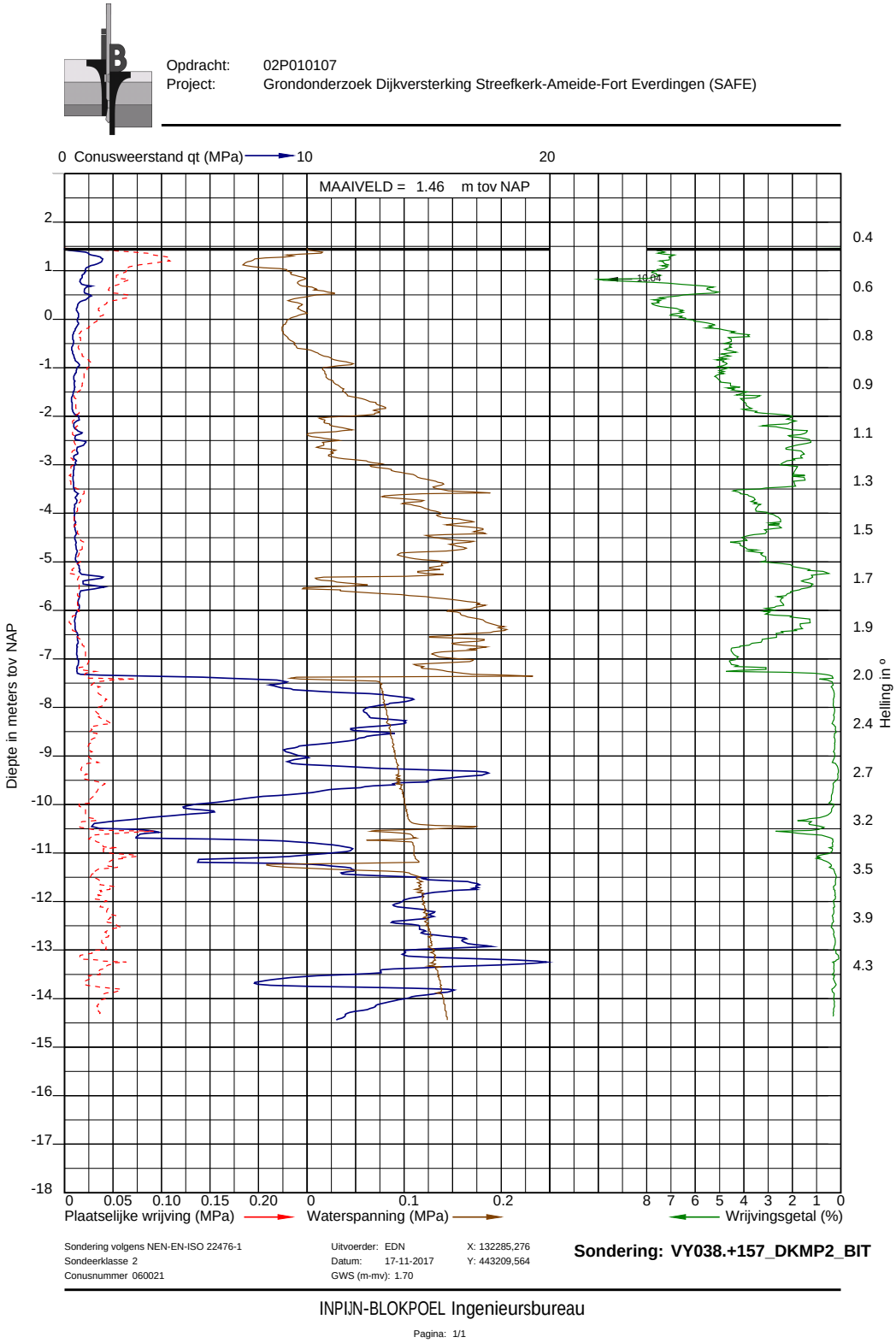

Figure A.6: CPT inner slope

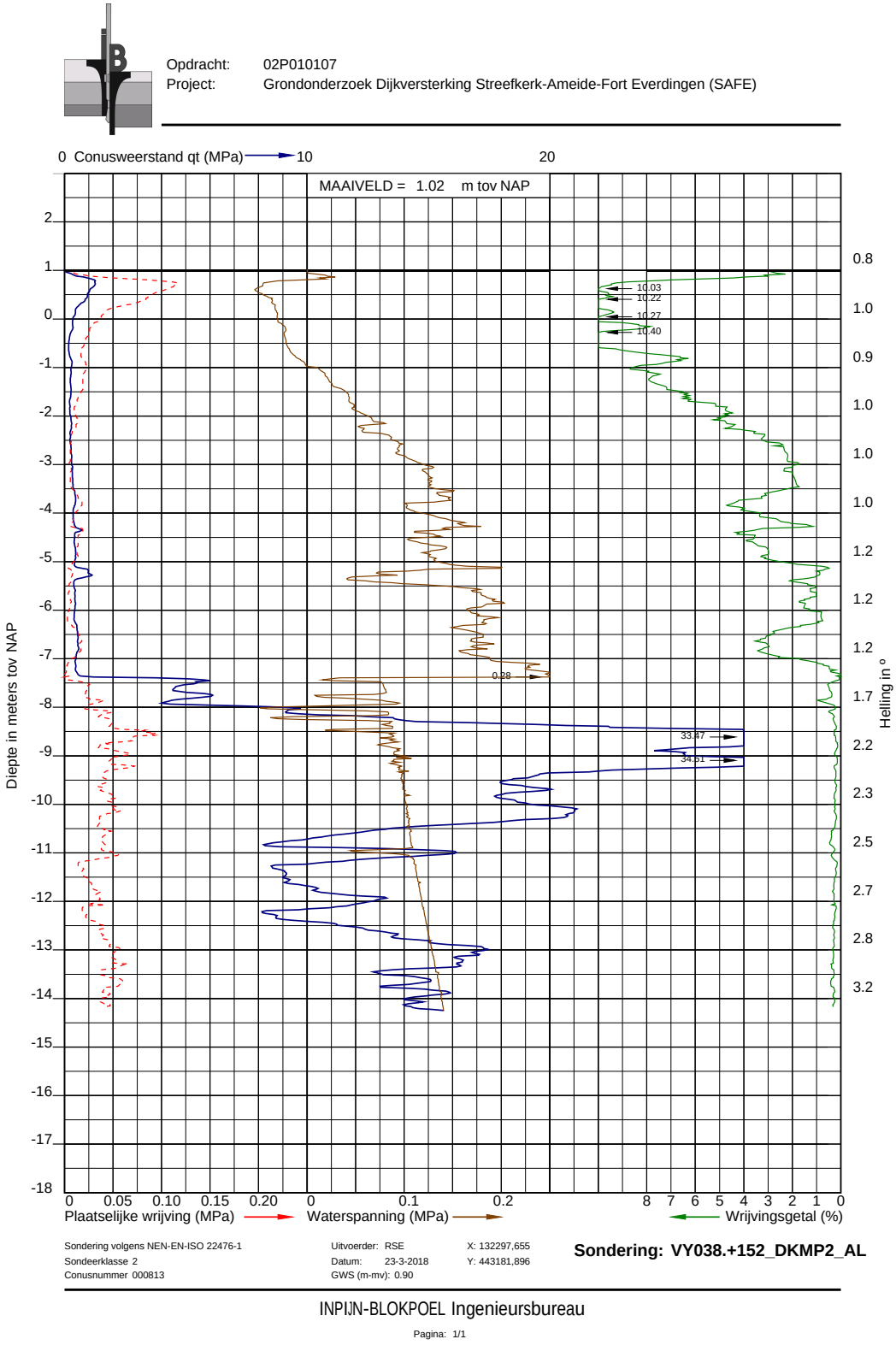

Figure A.7: CPT Hinterland

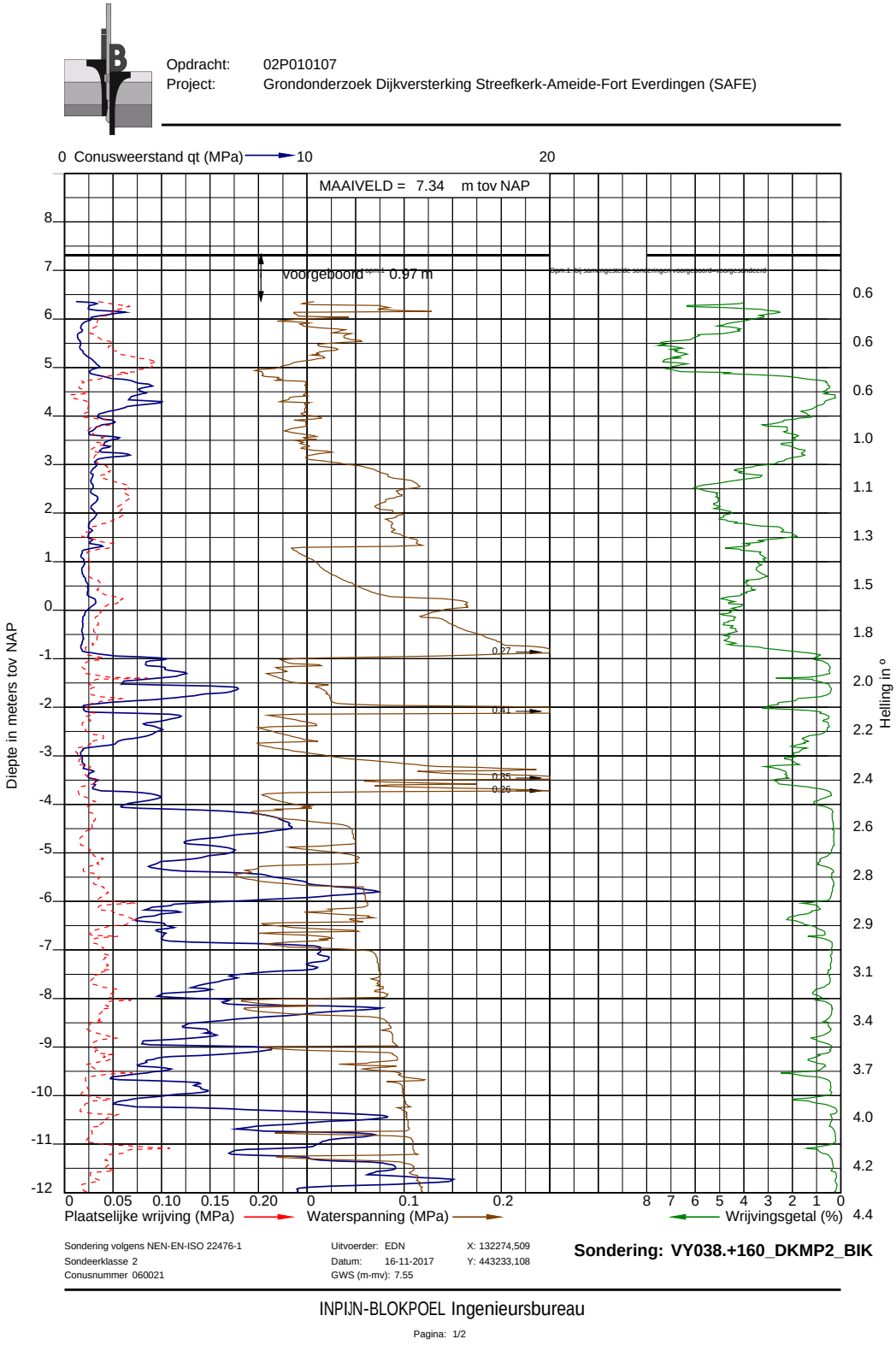

Figure A.8: CPT Crest

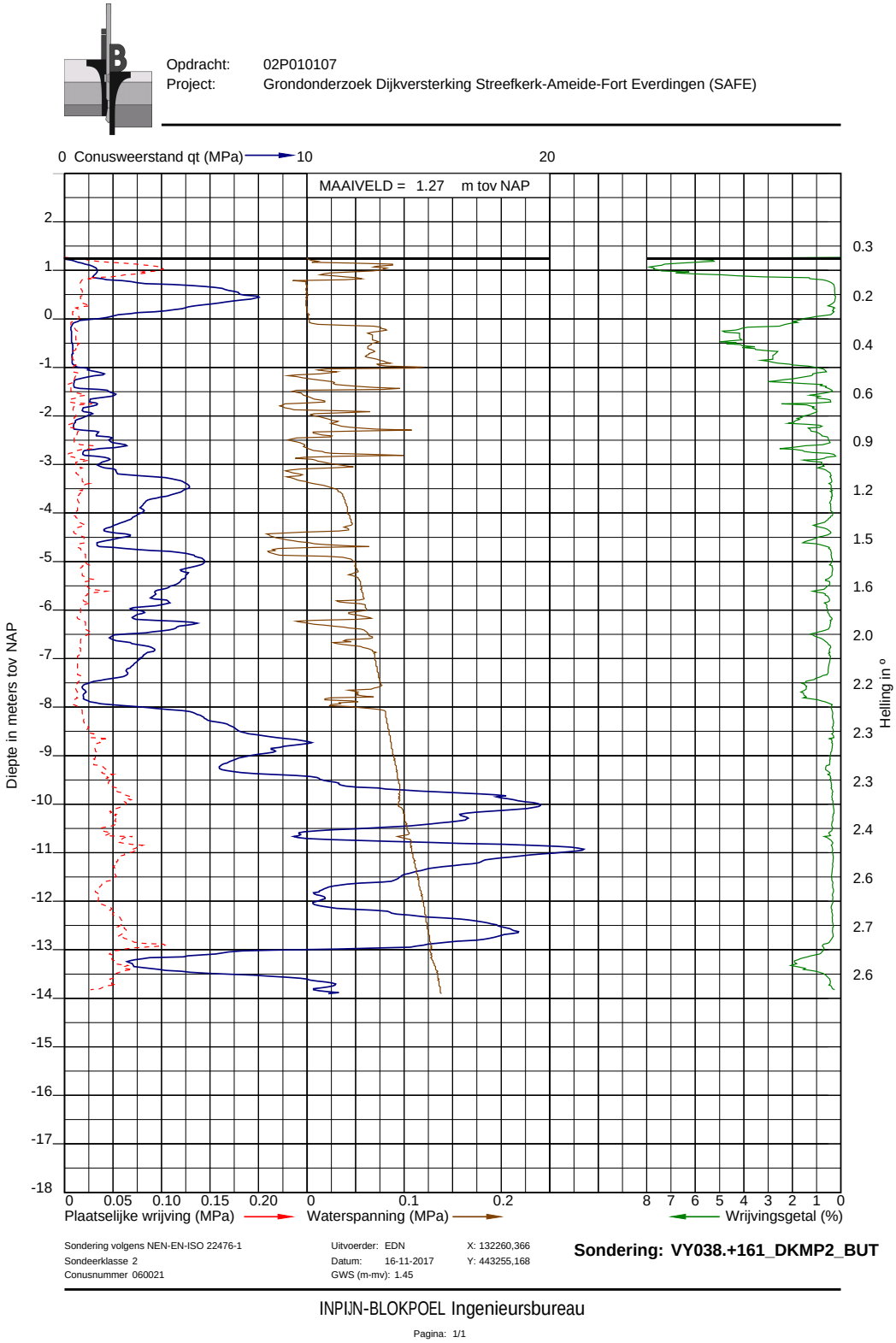

Figure A.9: CPT Outer slope

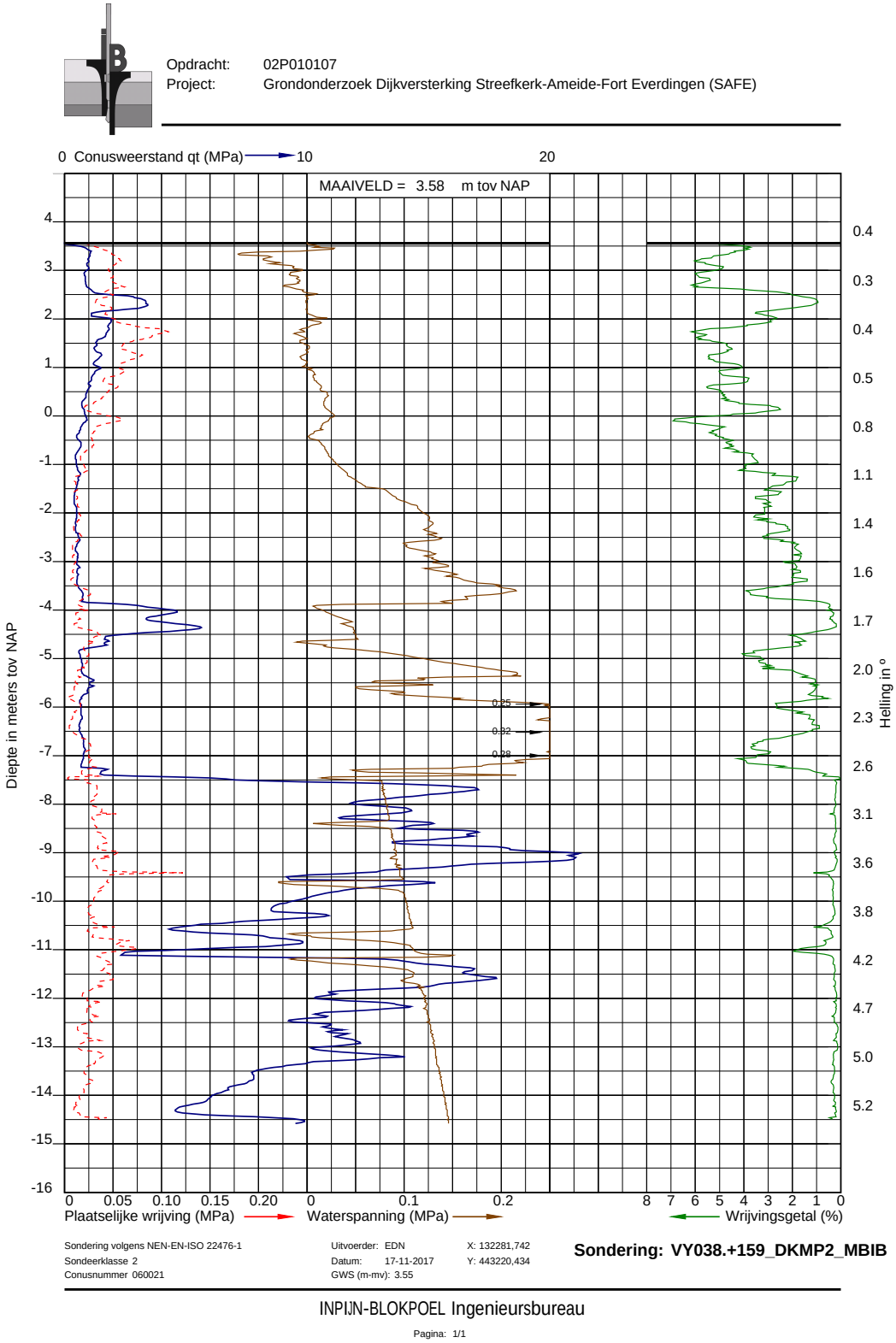

Figure A.10: CPT Crest

A.2. Local soil investigation case study Bergstoep

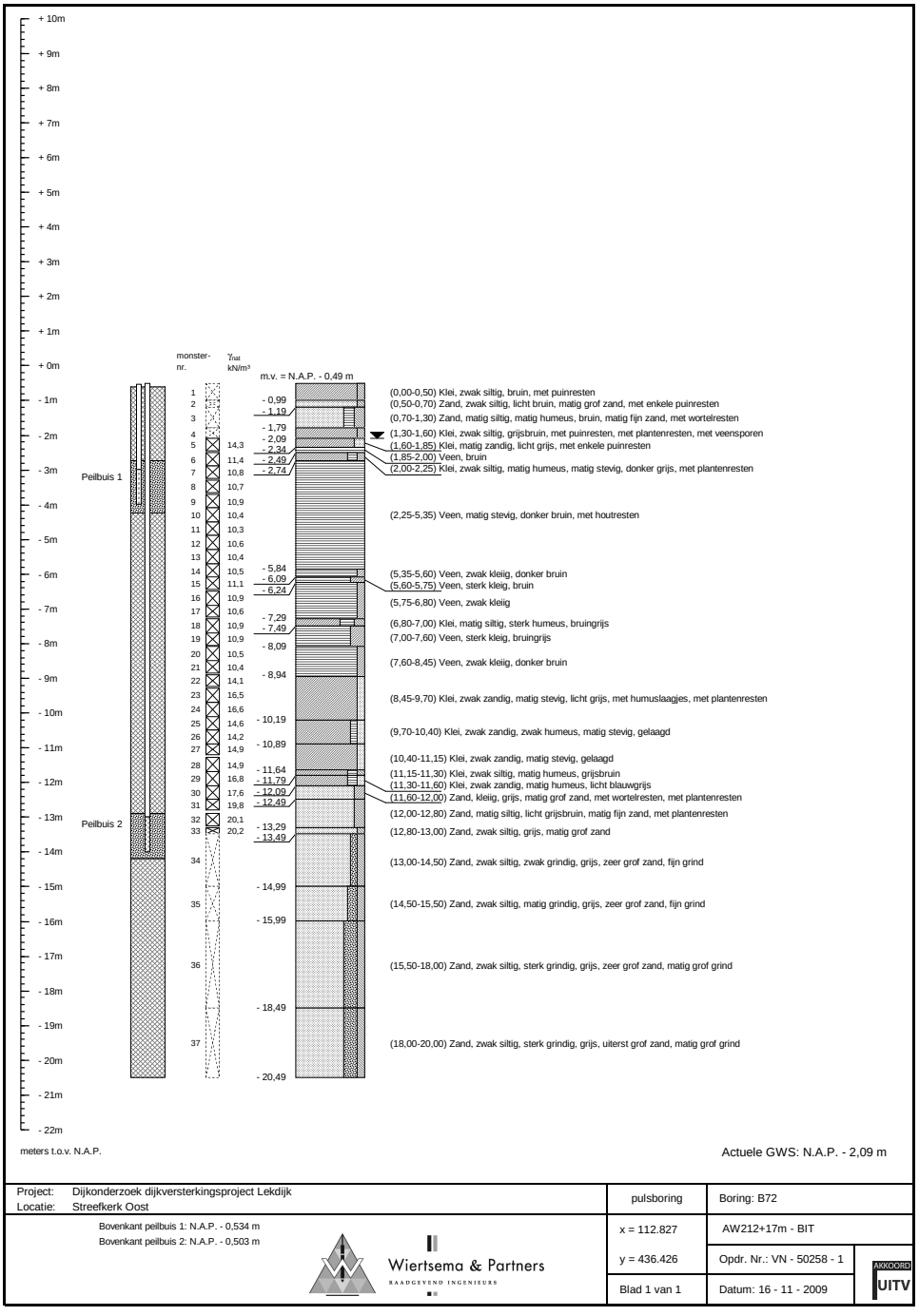

Figure A.11: Mechanical boring location Bergstoep inner dike toe

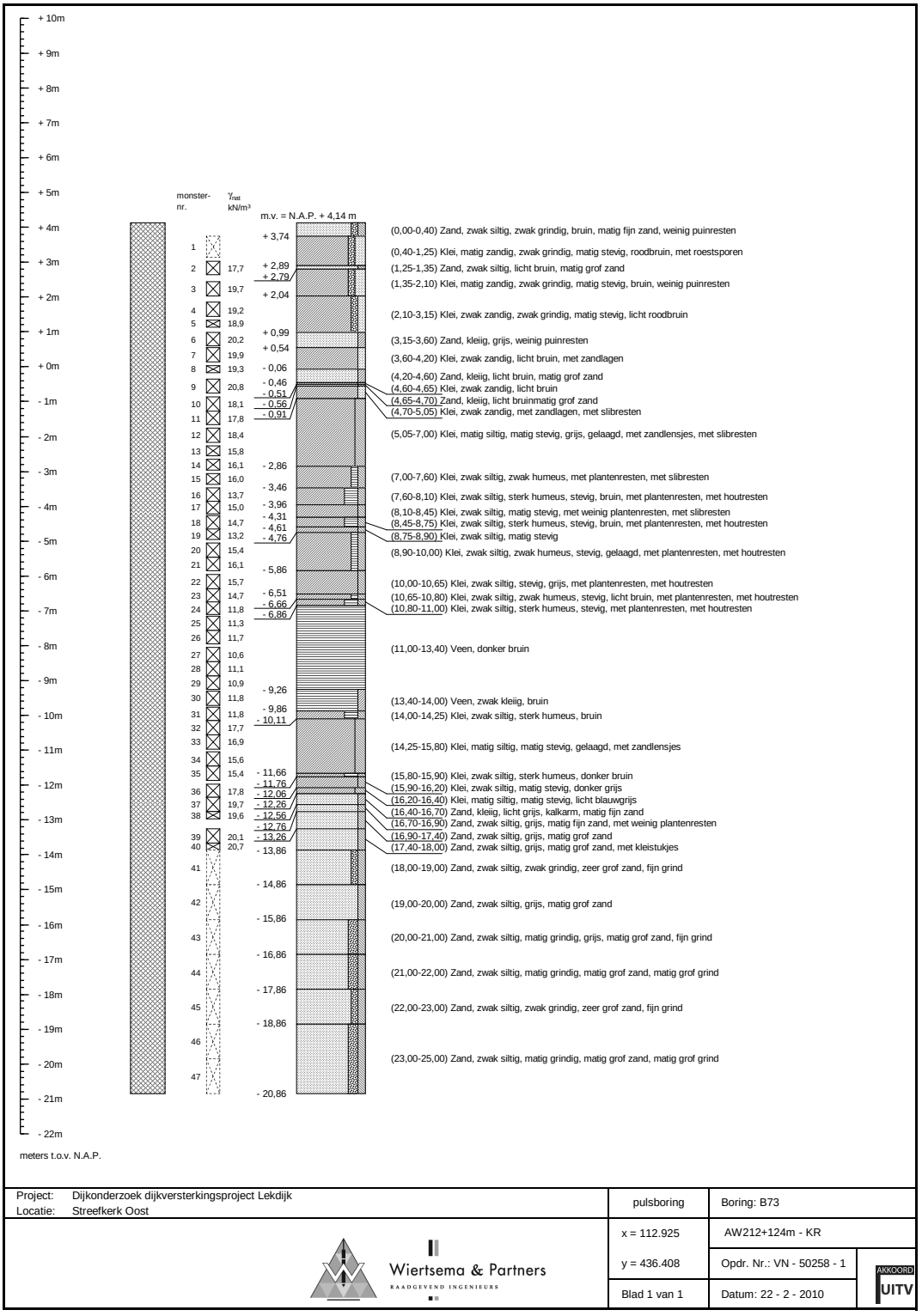

Figure A.12: Mechanical boring location Bergstoep dike crest

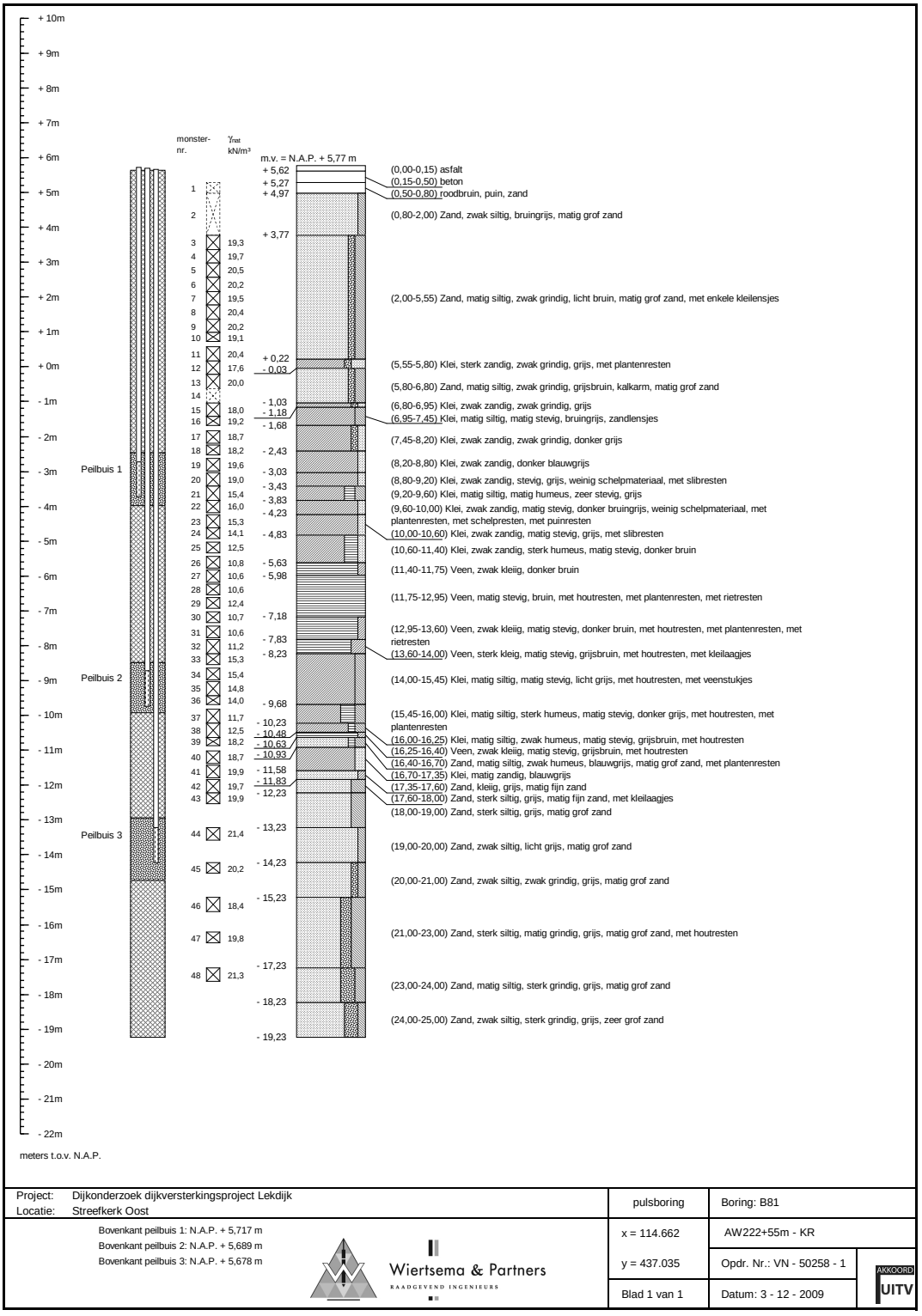

Figure A.13: Mechanical boring location piezometers crest

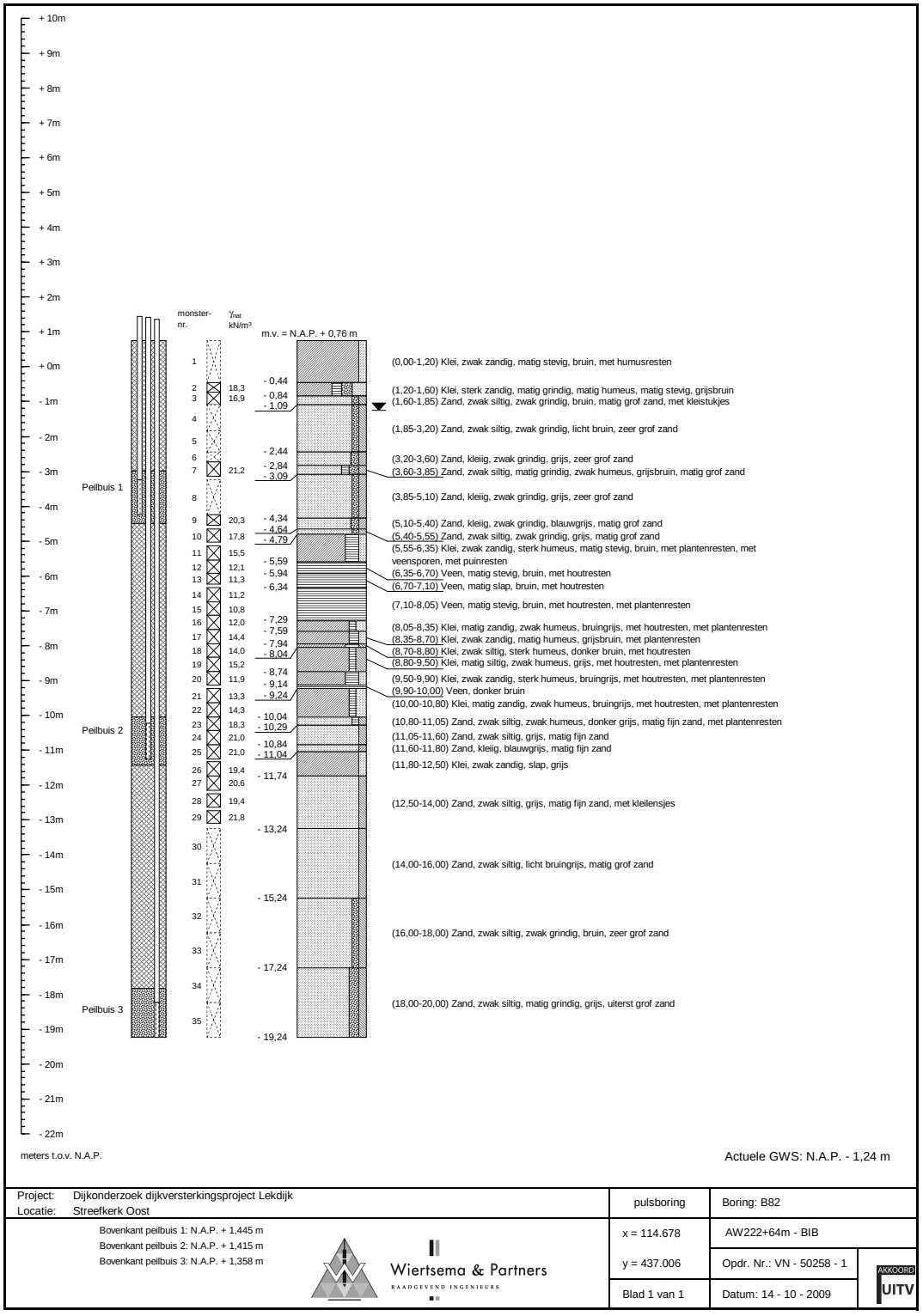

Figure A.14: Mechanical boring location piezometers inner dike berm

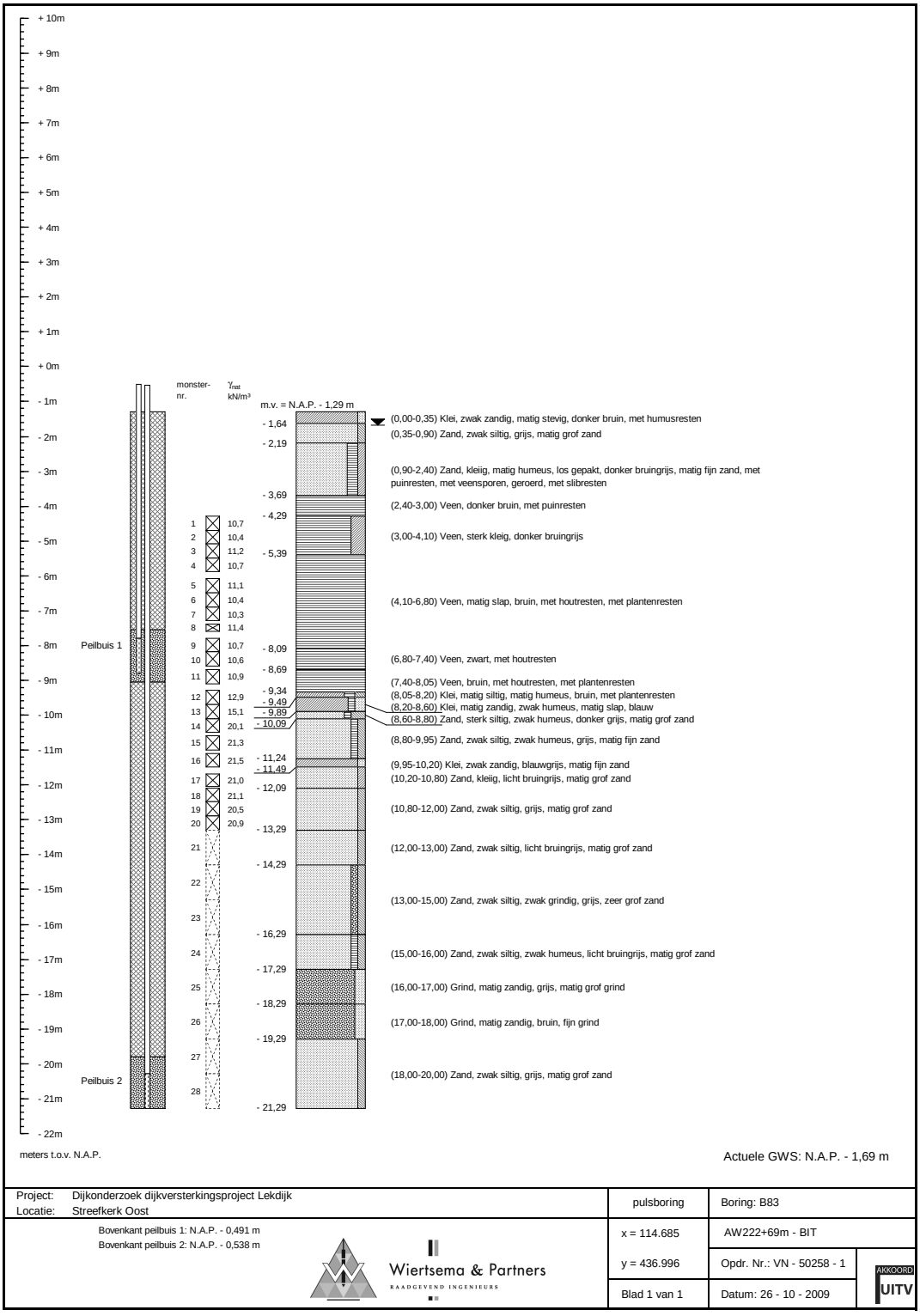

Figure A.15: Mechanical boring location piezometers inner dike toe

B

Appendix B: D-Stability results

B.1. General modelling process

Version 2023.01 of D-Stability uses scenarios and stages to define the different loading conditions for the modeling of the macrostability of a dike cross-section. One scenario is used for each separate analysis where the results of the D-Stability model are required to be used as one design point in the fragility curve. The stages are used within the scenarios to define the loading condition sequence. For example, one scenario can contain two stages to define the daily loading conditions and the conditions at WBN, where the stability is calculated by considering the previously defined daily conditions. Figure B.1 displays the build-up for the scenario and includes 2 stages.

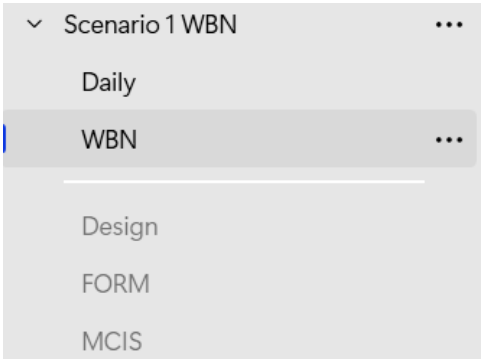

Figure B.1: Soil scenario 1: including the daily loading conditions and the conditions at WBN

The dike geometry is kept constant throughout the modeling for each case study. The materials can be assigned in D-Stability for each soil type. The majority of the soil properties are stochastic input for each soil type. Table B.1 displays the input parameters that are used in the D-Stability model for the case study Kortenhoevendijk. If the mean and standard deviation is mentioned, this parameter is a stochastic input in the calculation process. The values provided in the table are taken from the current test collection, provided by the WSRL.

Soil type	**Unit weight** $[kN/m^3]$	$\phi_{Char}[^\circ]$	$\phi_{Mean}[^\circ]$	$\phi_{SD}[^\circ]$	**m [-]**	S_{Char} **[-]**	S_{Mean} **[-]**	S_{SD} **[-]**
Clay dike material	18.56	33.6	36.2	1.6				
Sand dike material	18.56	32.4	34	0.986				
Silty clay, next	16.86				0.5	0.26	0.28	0.013
Humus clay, next	15.11				0.5	0.28	0.31	0.019
Sandy clay	18.56	33.6	36.2	1.6				
Sand	20	33.6	36.2	1.6				
Peat	10.55				0.5	0.35	0.4	0.032
Sand	20	32.4	34	0.986				

Table B.1: Test collection parameters used in the D-Stability modeling of the soil scenarios (for soils assigned next to the dike) (Kwakman, 2023)

The soft soils are assigned correlated in the D-Stability models if the soil type is both assigned next and under the dike. This correlation is used in the design macrostability safety assessment, and therefore is used during the project as well. The silty clay material and humus clay is also assumed to be correlated which is described by the test collection.

The water lines that are deterministic input in the D-Stability model are based on the most recent safety assessment for the Kortenhoevendijk. Since the soil scenario analysis was performed before the pore water pressure analysis, the design, deterministic input values are used to describe the pore water pressures. In this case, full intrusion of the blanket layer is assumed. The hydraulic head is equal to the outer water level at the outer dike slope. The phreatic line is schematized according to *Technische rapport Waterspanningen bij dijken* for a clay dike body. Each scenario is used to calculate the stability for one outer water level. The profile function in D-Stability is used to check the correctness of the implementation of the water lines.

The POP can be assigned in D-Stability by applying a state point for each soil layer. The values that are used to describe the pre-overburden pressure are provided in table B.2.

Soil type	**POP Characteristic**	**POP Mean**	**POP SD**
Next to the dike	16	26	7
Underneath the dike	29	43	10

Table B.2: Values for the POP used in the D-Stability modeling (Kwakman, 2023)

Only the soft soil materials are assigned a POP. Soils such as the dike material, dike cover, sand, and sandy clay are not assigned a POP. It is assumed that the POP is correlated with the soil layers situated underneath each other.

During the entire D-Stability analysis, no loads are assigned to the dike cross-section. The scope of the project does not include the influence of traffic load on the macrostability of the dike cross-section. No reinforcements are applied either.

Figure B.1 additionally displays the calculation stages that are used throughout each analysis. The design analysis is used to indicate the factor of safety. The design analysis provides a fast indication of the most critical failure surface for the dike cross-section. Throughout the entire D-Stability analysis during the project, the Uplift Van Particle swarm method is used to find the slip surface. During the Additional Graduation Work project, this proved to be the most reliable method to create similar failure surfaces that can be compared throughout the project. This is additionally, the most used calculation method that in the macrostability safety assessment. The swarm area is initially set to a large square

to find the location of the center of the slip circle. The search mode is selected to be thorough, which takes a little longer but will reach a better result. The tangent is assigned over the entire height of the blanket layer. After finding the most critical slip surface, the search area can be narrowed down where the circle center is situated in the middle of the search grid to provide the best result in D-Stability. Next, the FORM analysis imports the failure surface found in the design analysis and calculates the reliability index and failure probability of the cross-section. Lastly, the MCIS analysis performs a full-probabilistic calculation with the material properties as stochastic variables. The slip surface is now free, and the search grid location found in the design analysis can be used to define the Uplift Van Particle swarm area. The resulting slip surface should have the center of both slip surfaces in the middle of the search grid here as well, as confirmation that the failure surface found in the analysis is the most critical one. The MCIS should have a deep failure surface, preferably at the bottom of the blanket layer.

B.2. Results analysis subsurface schematization Kortenhoevendijk

In the D-Stability model that is used to analyze the soil scenarios set up for the Kortenhoevendijk case study, 4 different soil scenarios and 2 additional soil scenarios are analyzed in one D-Stability model. The soil layers are redefined throughout each soil scenario. The outline of the dike geometry remains constant throughout this process, with the definition of the cover layer. A total of three water levels are investigated, the daily loading conditions $(h = 0.88m)$, an extra intermediate water level $(h = 5m)$, and WBN conditions $(h = 6.62m)$. Table B.3 displays the resulting design points from the D-Stability analysis.

Scenario	**Outer water level [m NAP]**	**Calculation method**	β **Reliability index [-]**	P_f **Probability of failure [-]**
Scenario 1	0.88	FORM	10.156	1.55E-24
	5	FORM	5.644	8.32E-09
	6.62	MCIS	3.957	3.79E-05
Scenario 2	0.88	MCIS	5.461	2.37E-08
	5	MCIS	3.431	3.01E-04
	6.62	MCIS	2.003	2.26E-02
Scenario 3	0.88	FORM	10.761	2.63E-27
	5	MCIS	5.885	1.99E-09
	6.62	MCIS	4.056	2.49E-05
Scenario 4	0.88	MCIS	5.304	5.66E-08
	5	MCIS	3.182	7.31E-04
	6.62	MCIS	1.505	6.62E-02
Scenario 2 (a)	6.62	MCIS	1.265	1.03E-01
Scenario 2 (b)	6.62	MCIS	-0.46	6.77E-01

Table B.3: Results analysis soil scenarios for case study Kortenhoevendijk

Each table with the results of the D-Stability analysis displays the design point that is taken as output. These data points are used as input for the Probabilistic ToolKit. The table describes the scenario that is analyzed, for each outer water level h. The calculation method is included in the table, due to the convergence issues during the Kortenhoevendijk case study.

B.3. Results analysis pore water pressure schematization Kortenhoevendijk

Soil scenario 2, which is defined in the subsurface schematization analysis, is used in the pore water pressure analysis in D-Stability. A screenshot of the D-Stability model of the Kortenhoevendijk pore water pressure analysis is shown in figure B.2

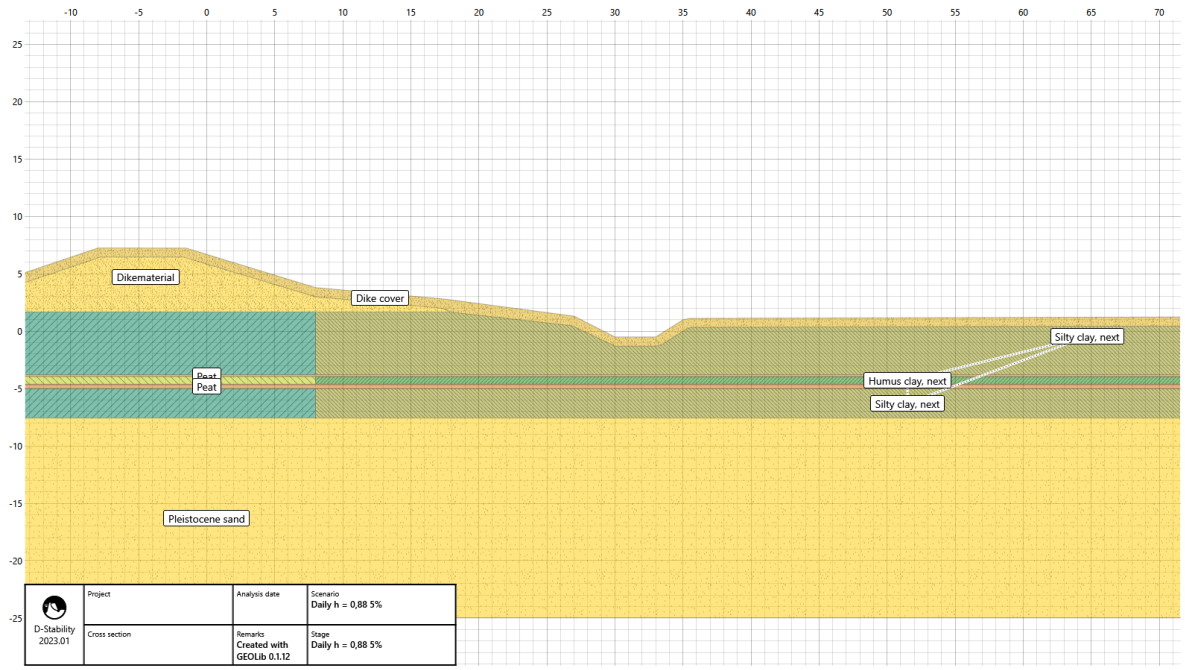

Figure B.2: Screenshot of the D-Stability model used in the pore water pressure analysis for case study Kortenhoevendijk

During this analysis, the soil layers are separated by the soil underneath the dike and next to the dike, a common practice in the macrostability safety assessment. This improves the stability of the dike cross-section significantly since the individual soil scenarios in the subsurface schematization uncertainties analysis are only calculated by using the strength parameters next to the dike. This results in a lower reliability index since the assigned strength to the soil layers next to the dike is lower than the soil strength underneath the dike. The additional soil parameters to the test collection are provided in table B.4.

Soil notation	**Unit weight** $[kN/m^3]$	**m [-]**	S_{Char} **[-]**	S_{Mean} **[-]**	S_{SD} **[-]**
K_s, under	16.86	0.9	0.272	0.308	0.023
K_h, under	15.11	0.8	0.31	0.347	0.022

Table B.4: Additional soil parameters from the test collection assigned to the soil layers underneath the dike

The general modeling process as previously described is used to gain the results from D-Stability for each pore water pressure component. The results provided in D-Stability for the base analysis of the Kortenhoevendijk case study are included in table B.5.

Outer water level [m NAP]	**Calculation method**	β **Reliability index [-]**	P_f **Probability of failure [-]**
0.88	FORM	8.366	2.982E-17
5	MCIS	6.529	3.319E-11
6.62	MCIS	4.874	5.482E-7
7	MCIS	3.854	5.815E-5

Table B.5: Results base analysis for case study Kortenhoevendijk

The D-Stability results for the hydraulic head analysis, intrusion length analysis, and phreatic line analysis are included in table B.6, B.7 and B.8 respectively.

Scenario hydraulic head analysis	Outer water level [m NAP]	Calculation method	β Reliability index [-]	P_f Probability of failure [-]
5% lower limit	0.88	FORM	8.687	1.86E-18
	5	FORM	7.820	2.649E-15
	6.62	MCIS	6.235	2.252E-10
	7	MCIS	5.895	1.874E-09
50% average	0.88	FORM	8.245	8.267E-17
	5	MCIS	7.221	2.582E-13
	6.62	MCIS	5.764	4.104E-09
	7	MCIS	5.495	1.951E-08
95% upper limit	0.88	FORM	8.174	1.494E-16
	5	MCIS	6.940	1.967E-12
	6.62	MCIS	5.427	2.873E-08
	7	MCIS	5.074	1.943E-07

Table B.6: Results hydraulic head analysis from D-Stability for case study Kortenhoevendijk

Scenario intrusion length analysis	Outer water level [m NAP]	Calculation method	β Reliability index [-]	P_f Probability of failure [-]
1m intrusion	0.88	FORM	8.402	3.74E-17
	5	FORM	8.490	1.406E-17
	6.36	MCIS	8.196	1.559E-12
	6.62	MCIS	7.465	4.175E-14
	7	MCIS	7.231	2.732E-13
3m intrusion	0.88	FORM	8.254	7.676E-17
	5	MCIS	7.957	5.969E-16
	6.36	MCIS	6.399	7.831E-11
	6.62	MCIS	6.133	4.308E-10
	7	MCIS	5.694	6.202E-09
4m intrusion	0.88	FORM	8.265	6.98E-17
	5	MCIS	7.374	8.309E-14
	6.36	MCIS	5.973	1.16E-09
	6.62	MCIS	5.771	3.94E-09
	7	MCIS	5.339	4.685E-08
5m intrusion	0.88	FORM	8.196	9.412E-17
	5	MCIS	6.896	2.668E-12
	6.36	MCIS	5.727	5.103E-09
	6.62	MCIS	5.496	1.938E-08
	7	MCIS	5.043	2.29E-07

Table B.7: Results of the intrusion length analysis from D-Stability for case study Kortenhoevendijk

Scenario phreatic line analysis	Outer water level [m NAP]	Calculation method	β Reliability index [-]	P_f Probability of failure [-]
5% lower limit	0.88	FORM	7.815	2.74E-15
	5	MCIS	7.675	8.27E-15
	6.62	MCIS	6.274	1.765E-10
	7	MCIS	5.659	7.595E-09
50% average	0.88	FORM	7.469	4.05E-14
	5	MCIS	7.59	1.61E-14
	6.62	MCIS	5.835	2.69E-09
	7	MCIS	5.515	1.74E-08
95% upper limit	0.88	FORM	7.072	7.63E-13
	5	MCIS	7.221	2.58E-13
	6.62	MCIS	5.488	2.03E-08
	7	MCIS	5.155	1.27E-07

Table B.8: Results Phreatic line analysis from D-Stability for case study Kortenhoevendijk

B.4. Results analysis pore water pressure schematization Bergstoep

The D-Stability analysis for the case study Bergstoep is set up by using the D-Stability model provided by the macrostability safety assessment. A screenshot of the D-Stability model for the case study Bergstoep is shown in figure B.3. The geometry of the dike cross-section, the soil profile, and the material input are taken directly from the safety assessment model. The material parameters are taken from the same test collection as previously mentioned in tables B.1 and B.4.

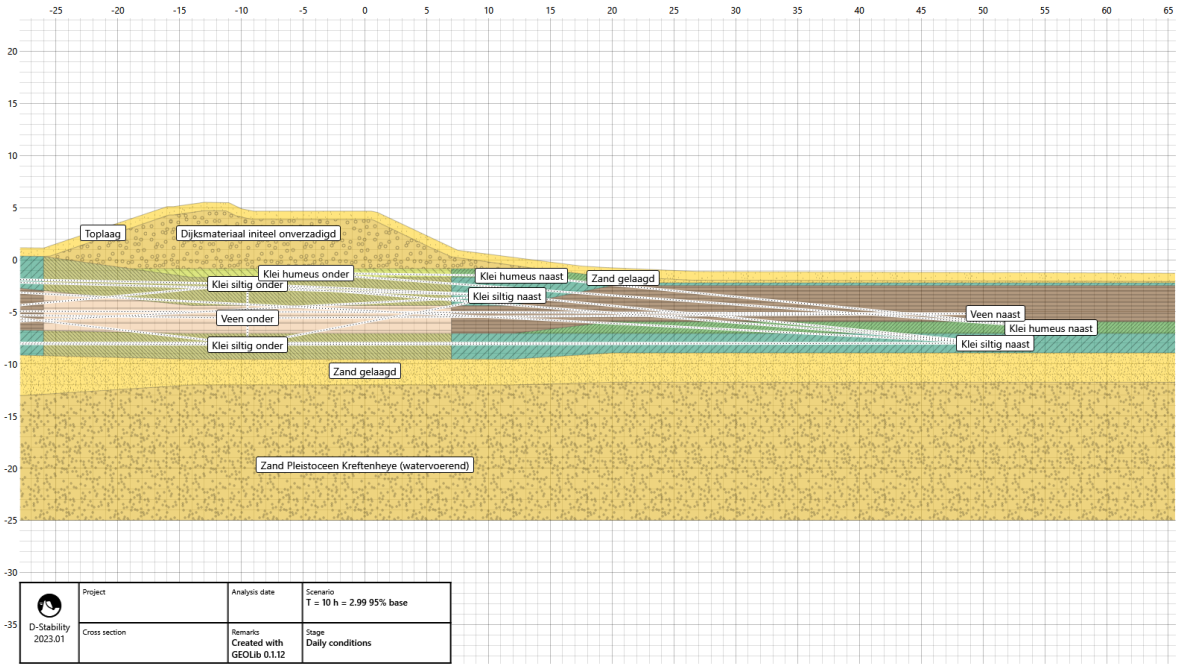

Figure B.3: Screenshot of the D-Stability model used in the pore water pressure analysis for case study Bergstoep

The results of the D-Stability analysis are displayed in the tables below.

Outer water level [m NAP]	Calculation method	β Reliability index [-]	P_f Probability of failure [-]
0.62	MCIS	4.604	2.07E-06
2.99	MCIS	2.922	1.74E-03
3.63	MCIS	1.548	6.08E-02
4.08	MCIS	0.558	2.88E-01

Table B.9: Results base assessment from D-Stability for case study Bergstoep

Scenario hydraulic head analysis	Outer water level [m NAP]	Calculation method	β Reliability index [-]	P_f Probability of failure [-]
5%	-0.20	MCIS	4.761	9.61E-07
	2.99	MCIS	4.5	3.39E-06
	3.63	MCIS	4.188	1.41E-05
	4.08	MCIS	3.29	5.01E-04
50%	-0.20	MCIS	4.761	9.61E-07
	2.99	MCIS	4.376	6.06E-06
	3.63	MCIS	3.887	5.07E-05
	4.08	MCIS	2.813	2.45E-03
95%	-0.20	MCIS	4.761	9.61E-07
	2.99	MCIS	4.181	1.45E-05
	3.63	MCIS	3.373	3.72E-04
	4.08	MCIS	1.563	5.91E-02

Table B.10: Results Hydraulic head analysis from D-Stability for case study Bergstoep

Scenario intrusion length analysis	Outer water level [m NAP]	Calculation method	β Reliability index [-]	P_f Probability of failure [-]
0.53m intrusion	-0.20	MCIS	3.329	4.35E-04
	2.99	MCIS	3.886	5.10E-05
	3.63	MCIS	3.483	2.48E-04
	4.08	MCIS	3.243	5.91E-04
1.26m intrusion	-0.20	MCIS	4.716	1.20E-06
	2.99	MCIS	3.573	1.76E-04
	3.63	MCIS	3.14	8.44E-04
	4.08	MCIS	2.851	2.18E-03
3.02m intrusion	-0.20	MCIS	3.329	4.35E-04
	2.99	MCIS	2.922	1.74E-03
	3.63	MCIS	2.273	1.15E-02
	4.08	MCIS	2.038	2.08E-02

Table B.11: Results Intrusion length analysis from D-Stability for case study Bergstoep

Scenario phreatic line analysis	**Outer water level [m NAP]**	**Calculation method**	**β Reliability index [-]**	**P_f Probability of failure [-]**
Lower limit	-0.20	MCIS	5.099	1.71E-07
	2.99	MCIS	3.819	6.71E-05
	3.63	MCIS	3.367	3.80E-04
	4.08	MCIS	3.369	3.78E-04
Average	-0.20	MCIS	4.759	9.74E-07
	2.99	MCIS	3.71	1.04E-04
	3.63	MCIS	3.14	8.44E-04
	4.08	MCIS	2.851	2.18E-03
Upper limit	-0.20	MCIS	4.404	5.30E-06
	2.99	MCIS	2.875	2.02E-03
	3.63	MCIS	2.747	3.01E-03
	4.08	MCIS	2.377	8.73E-03

Table B.12: Results Phreatic line analysis from D-Stability for case study Bergstoep

C

Appendix C:Probabilistic ToolKit modeling

Appendix C describes the process of modeling the combined fragility curve for each uncertainty analysis via the Probabilistic ToolKit. Both case studies are discussed separately.

C.1. Case study Kortenhoevendijk

The design points that compose the fragility curves found during the D-Stability analysis are exported via a JSON file. These files are imported into the Probabilistic ToolKit (PTK) to combine the fragility curves. Due to an export issue of the JSON files, these require to be altered manually. The highest water level in the model is assigned to the design point, while the outer water level can be lower than the water level in the dike. The design points assigned in the JSON file are altered manually to the outer water level if necessary.

C.1.1. Subsurface schematization uncertainties

The input for the PTK analysis are the fragility curves describing the design points for each soil scenario. The JSON files for each soil scenario include the reliability index and failure probability for several water levels. The four fragility curves for each soil scenario are combined in the *Combined FC*, visible in figure C.1. The contributions of each soil scenario are defined by assigning the 25% probability of occurrence in the *Composing fragility curve contributions section*. The PTK also displays the fragility curves and the combined curve in the software.

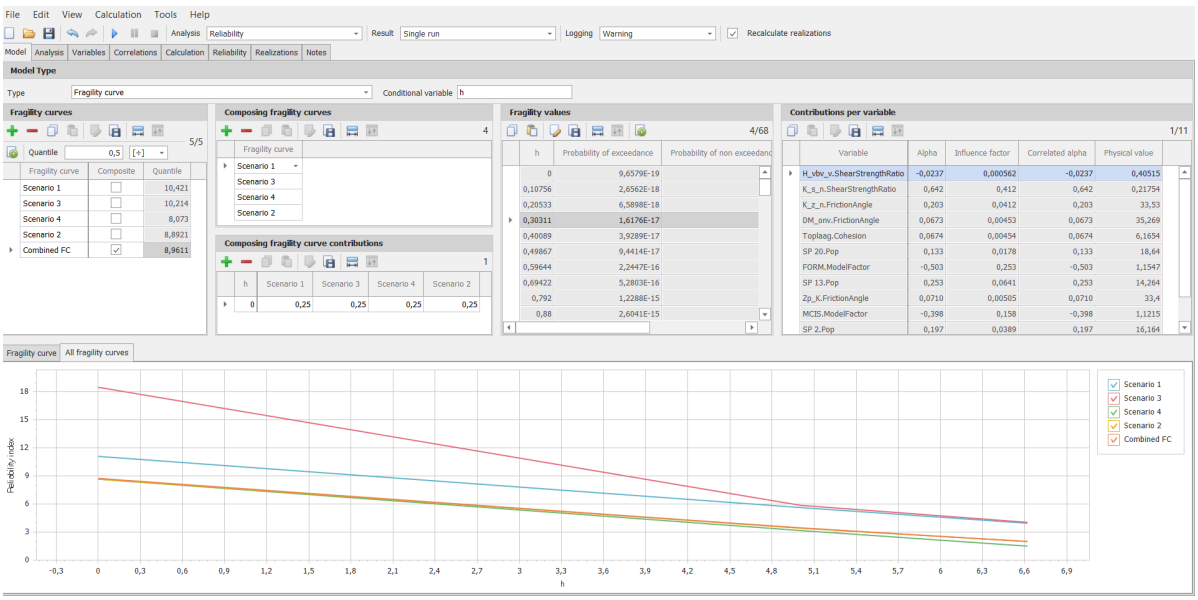

Figure C.1: Model input for combining the fragility curves of the soil scenarios of the Kortenhoevendijk in the PTK

The calculation model that is used is displayed in figure C.2. The analysis that is used is a reliability analysis. Only the reliability analysis can be used in the PTK to combine the fragility curves.

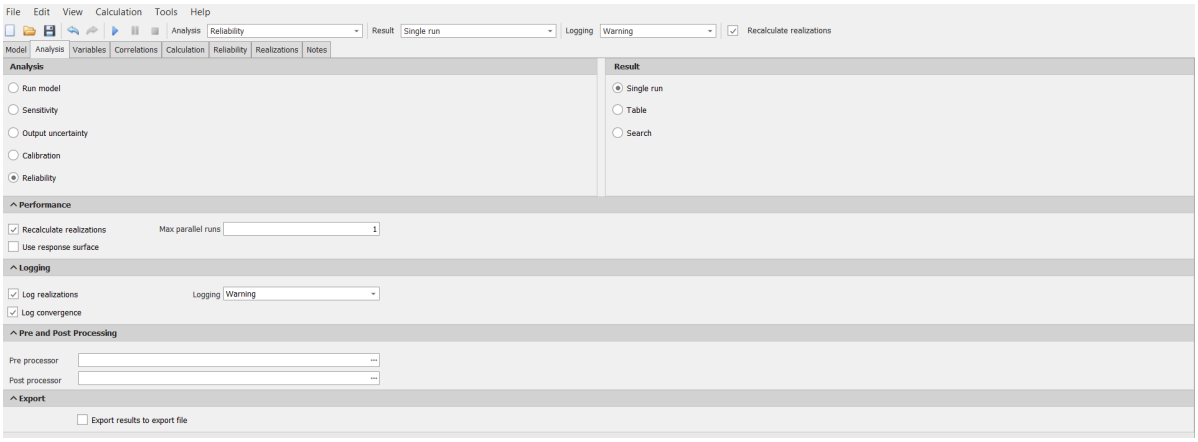

Figure C.2: Reliability analysis settings in the PTK

The next step in the PTK analysis is to define the variables. The outer water level h is defined in the macrostability safety assessment via a Gumbel distribution. However, the PTK has the option to use a CDF curve to include the return periods of the outer water levels provided by Hydra-NL directly. This method therefore prevents the need to fit the CDF values to a Gumbel distribution. This is displayed in figure C.3

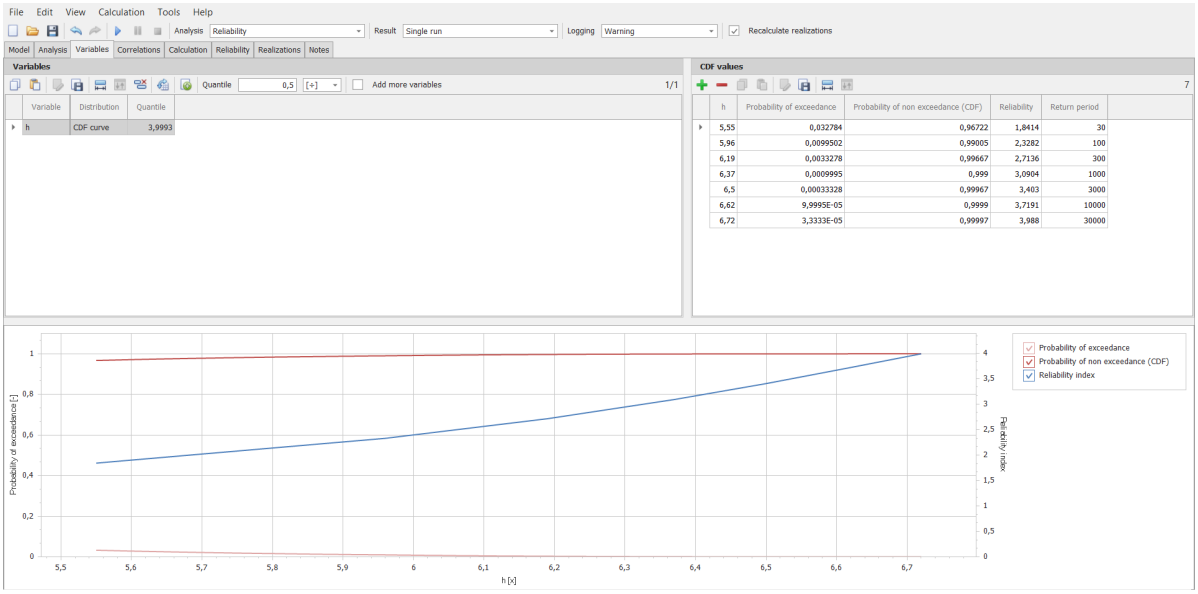

Figure C.3: Input of the CDF values taken from Hydra-NL in the PTK

The correlations that are assigned in the PTK are filled in automatically from data stored in the JSON files. The calculation method as mentioned before is a reliability analysis. The realizations fail if the combined fragility curve is lower than the outer water level h. The calculation method that is used is the fragility curve integration. The results of the analysis in the PTK is shown in figure C.4.

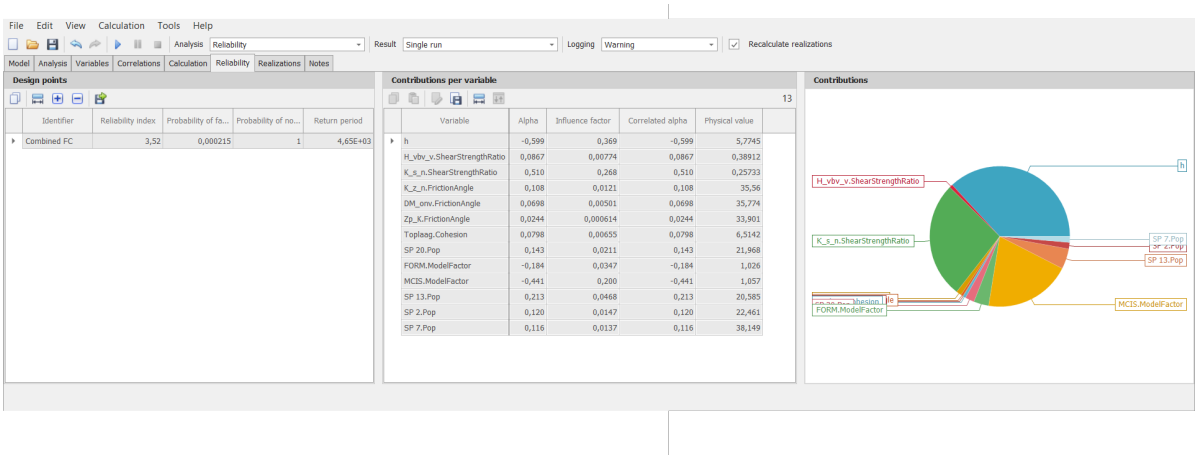

Figure C.4: Results of the PTK analysis for the combined fragility curve of the soil scenarios for the Kortenhoevendijk

The results that are provided by the PTK are the combined reliability index and combined failure probability. The contributions of each variable to the failure probability are provided as well.

C.1.2. Pore water pressure schematization uncertainties

One PTK analysis is set up for each component of the pore water pressure components. The input for the hydraulic head in the aquifer analysis is displayed in figure C.5.

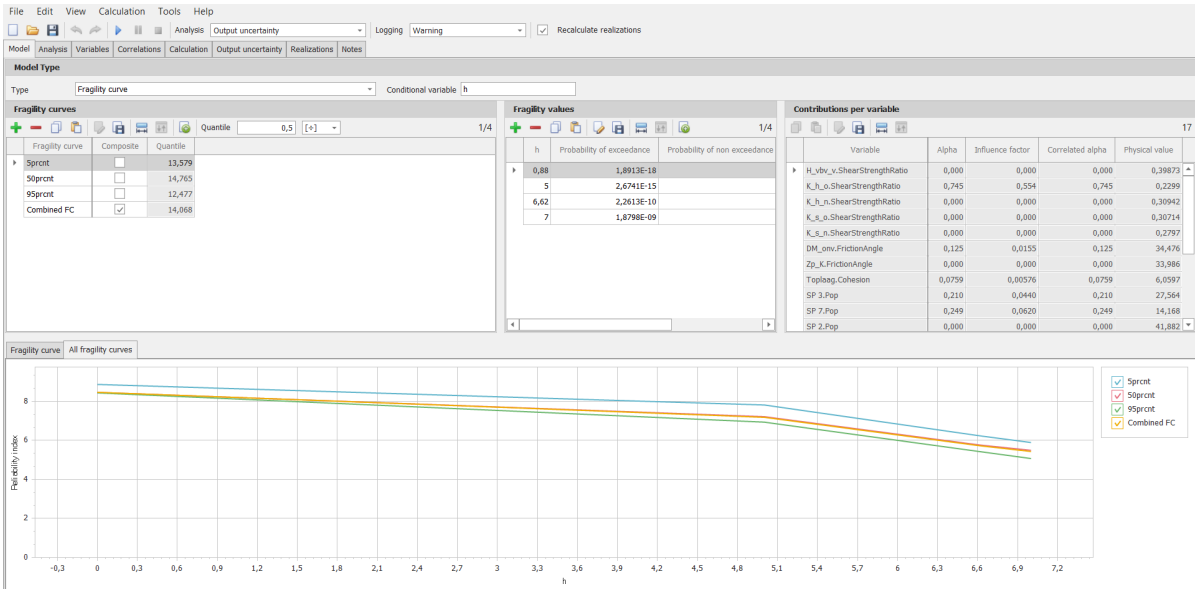

Figure C.5: Results of the PTK analysis for the combined fragility curve of the hydraulic head for the Kortenhoevendijk

The PTK input for the intrusion length analysis is displayed in figure C.6.

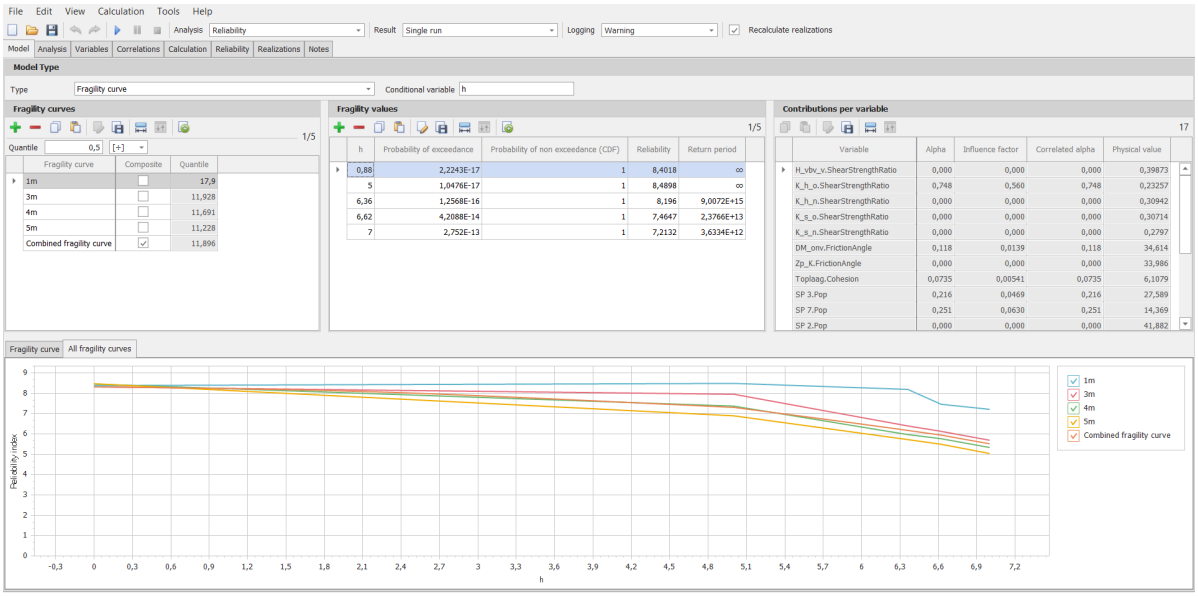

Figure C.6: Results of the PTK analysis for the combined fragility curve of the intrusion length analysis for the Kortenhoevendijk

The PTK input for the phreatic line analysis is displayed in figure C.7.

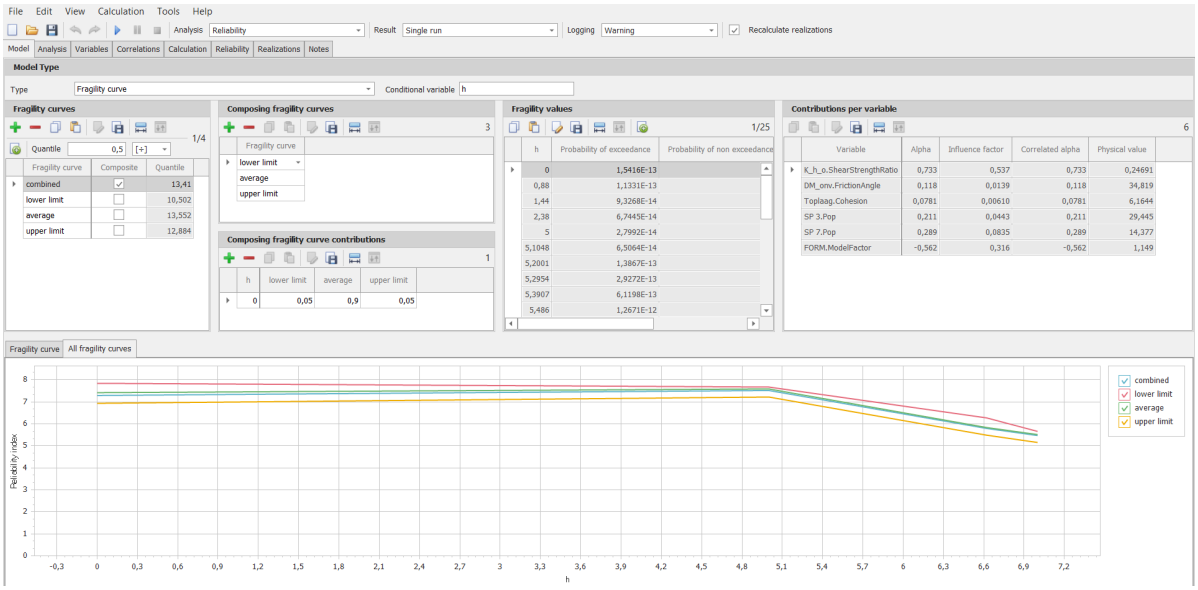

Figure C.7: Results of the PTK analysis for the combined fragility curve of the phreatic line analysis for the Kortenhoevendijk

The reliability analysis is used to integrate the fragility curves. The outer water level h is assigned as the variable by using the CDF values as mentioned before. The reliability realizations are considered to fail if the combined fragility curve is lower than the outer water level. The results from the reliability analysis are the combined reliability index and failure probability.

From each pore water pressure component, the combined fragility curve is extracted and imported into a new PTK file. A screenshot for the PTK file is displayed in figure C.8. The contributions to each pore water pressure component are assigned $1/3$.

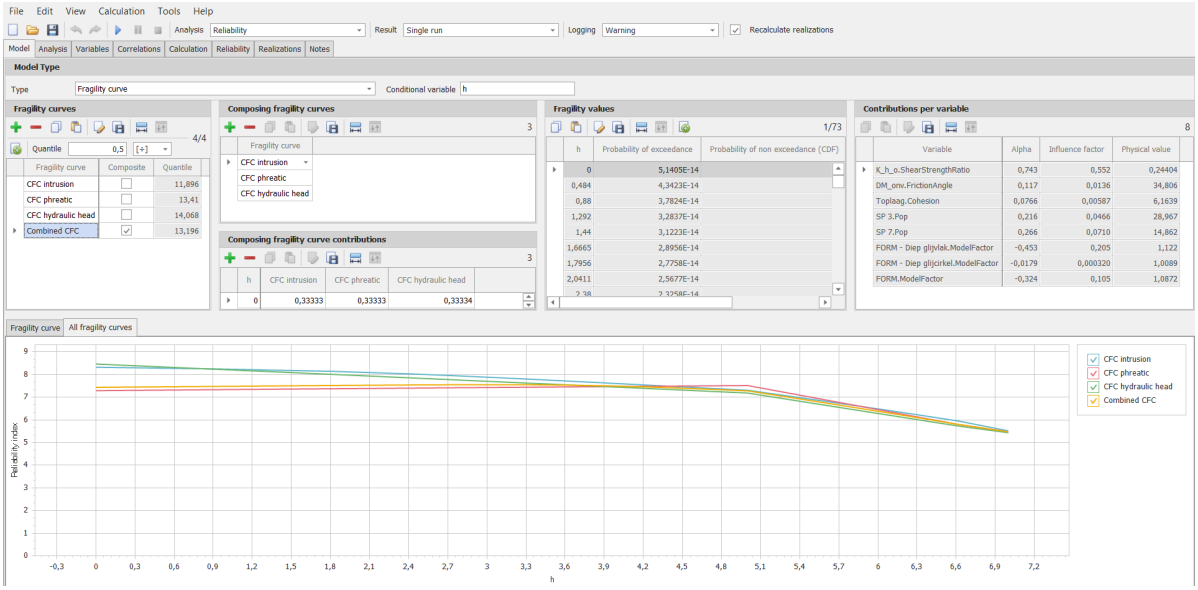

Figure C.8: The PTK analysis for the combined fragility curve of the pore water pressure analysis for the Kortenhoevendijk

The calculation method is the same as for the previously described soil scenario analysis. The reliability analysis is used to integrate the fragility curve to provide a combined failure probability. The results of the combined pore water pressure analysis for the Kortenhoevendijk case study are displayed in figure C.9.

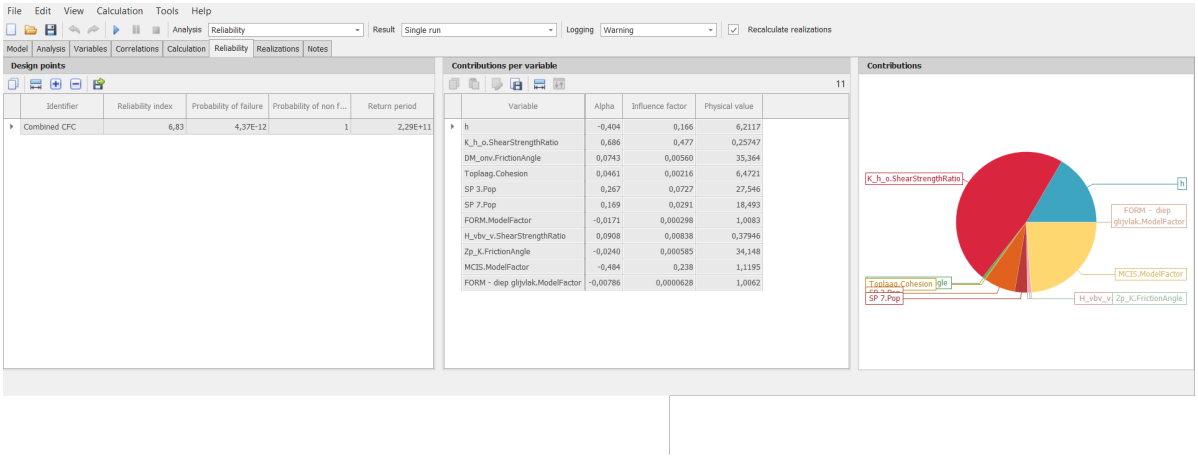

Figure C.9: Results of the PTK analysis for the combined fragility curve of the pore water pressure analysis for the Kortenhoevendijk

C.2. Case study Bergstoep

The pore water pressure uncertainty analysis for the Bergstoep case study in the PTK is discussed in this section. The analysis is similar to the previously described analysis for the Kortenhoevendijk. The hydraulic head component analysis is displayed in figure C.10.

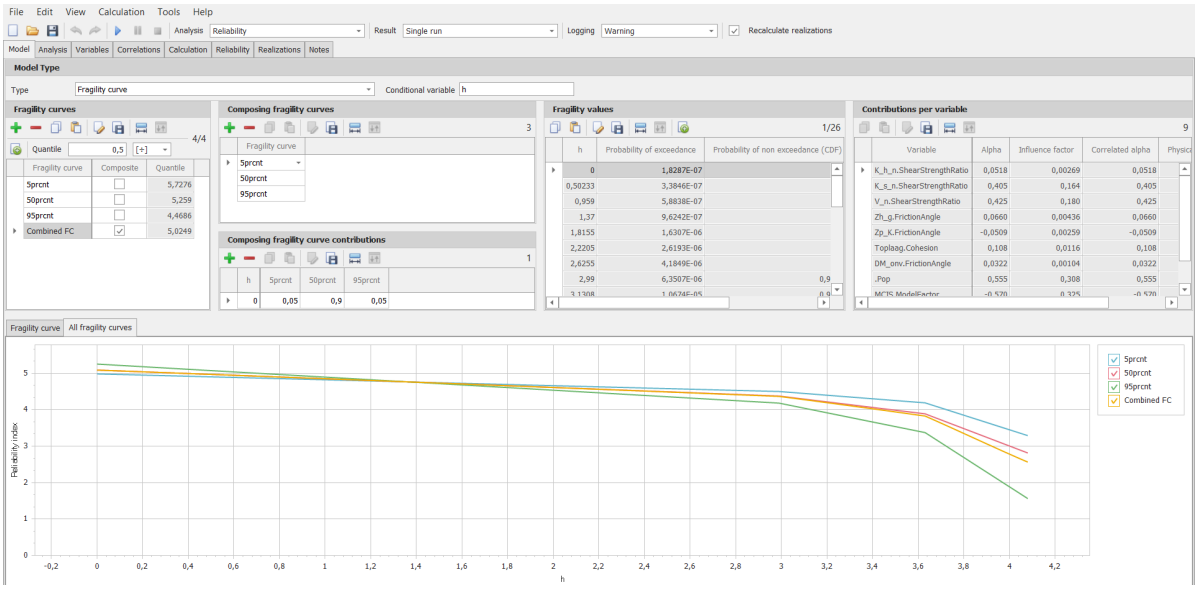

Figure C.10: Screenshot of the PTK for the hydraulic head analysis for case study Bergstoep

The input variable h is assigned by using the CDF curve distribution. The CDF values are taken from Hydra-NL for the location of the case study. This input is provided by figure C.11 and is used throughout the entire pore water pressure analysis for the case study Bergstoep.

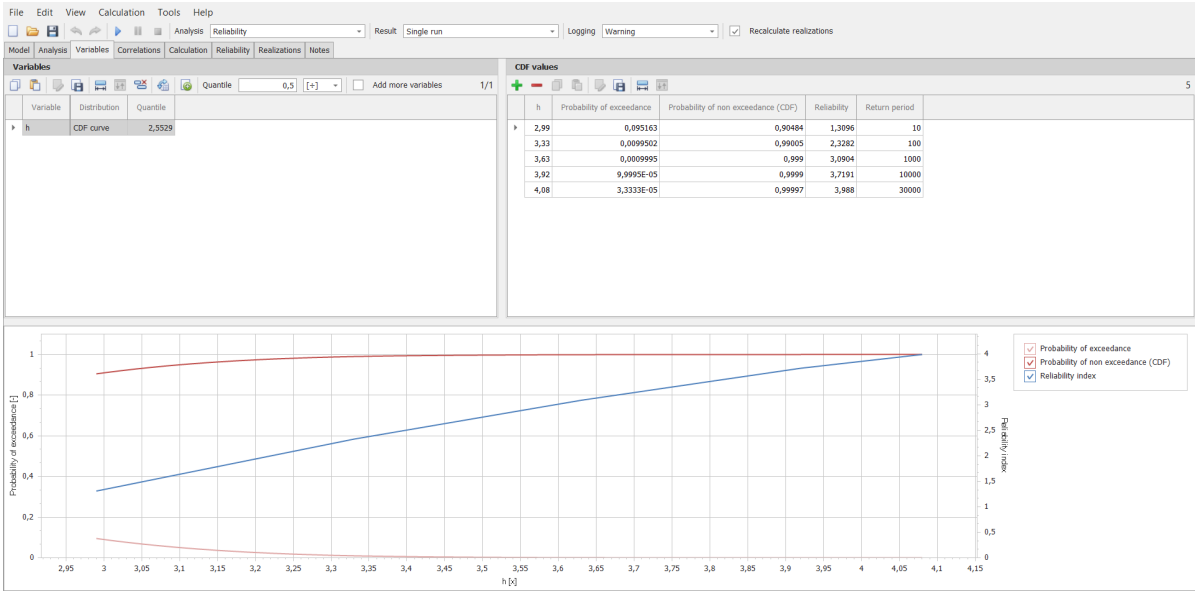

Figure C.11: The CDF values assigned in the PTK for case study Bergstoep

The calculation method used is the fragility curve integration, where the realizations are failing if the combined fragility curve is lower than the outer water level. This process is repeated for the analysis of the intrusion length (figure C.12) and the phreatic line (figure C.13).

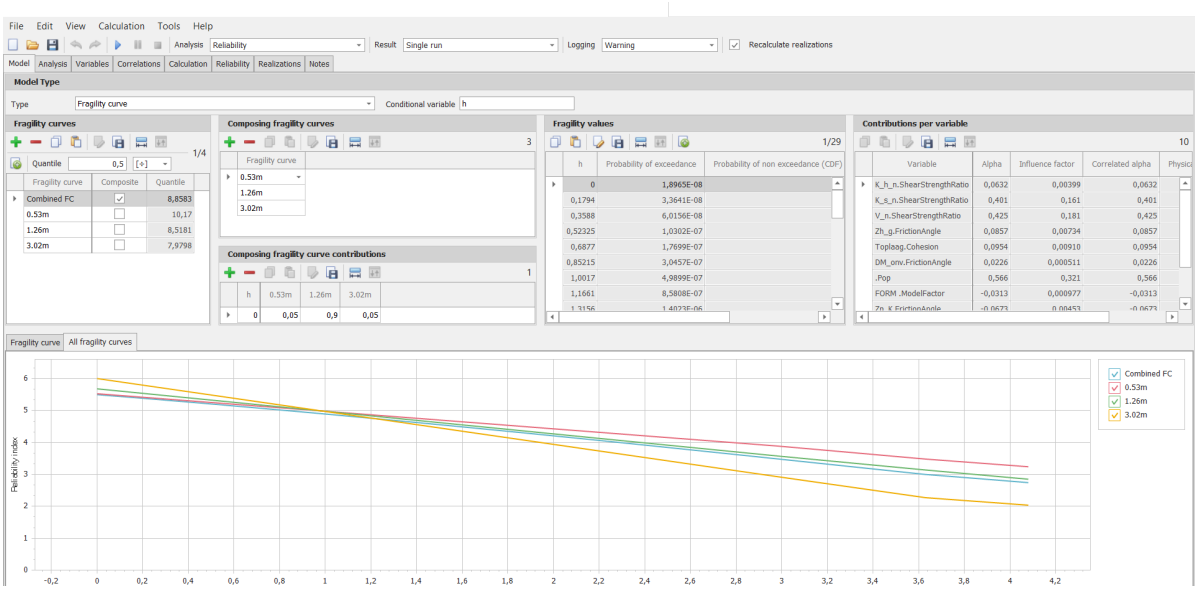

Figure C.12: PTK analysis of the intrusion length for case study Bergstoep

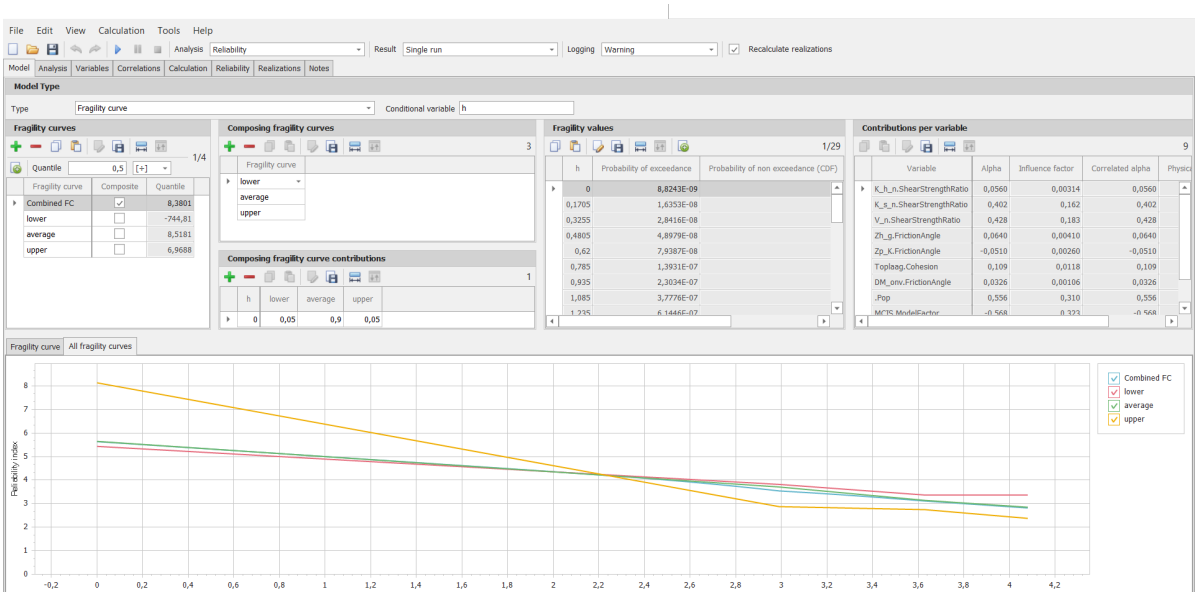

Figure C.13: PTK analysis of the phreatic line for case study Bergstoep

Each of the combined fragility curves is extracted and input for a new PTK file to combine the pore water pressure components. Figure C.14 displays the combining of each pore water pressure component to one fragility curve for the Bergstoep case study. The PTK model provides the combined reliability index and failure probability.

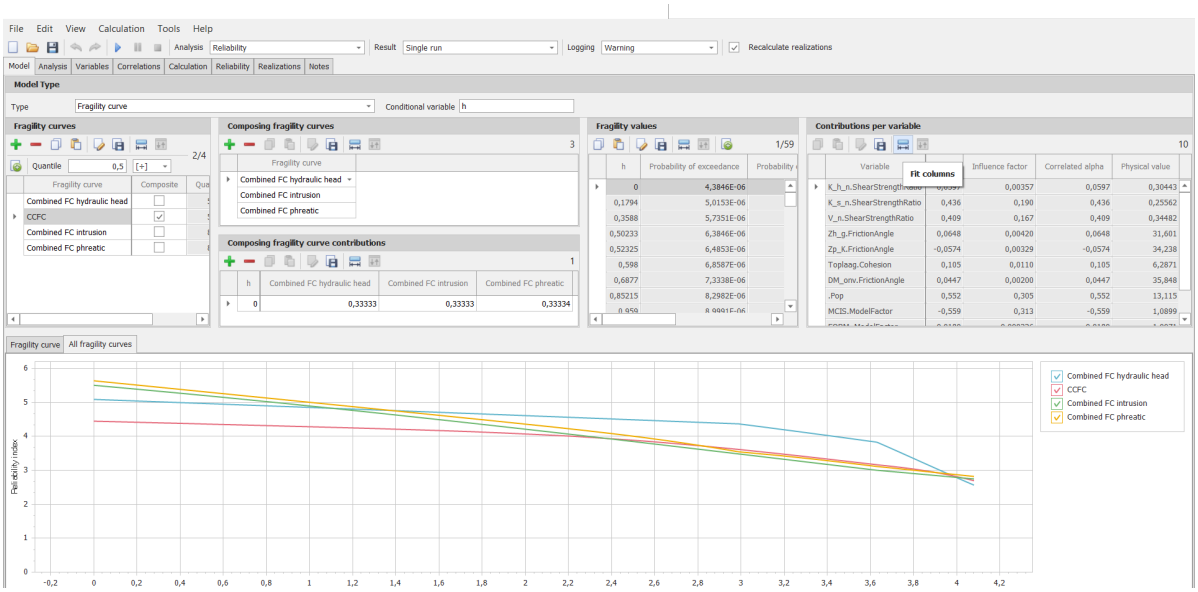

Figure C.14: Results of the PTK analysis of the combined pore water pressure components for case study Bergstoep

D

Appendix D: Python code

D.1. Python code to calculate the uncertainty in the stationary response of the hydraulic head

```
#import modules
import geohydromodels
import openturns as ot
import openturns.viewer as viewer
from matplotlib import pylab as plt
import numpy as np
import pandas as pd
import scipy.stats as sct
import math

#create python function with open turns
def model4a(X):
    k, D, c1, c3, L1, L3, x_but, x_bit, afstand = X
    mdl = geohydromodels.model4a(k, D, c1, c3, L1, L3, x_but, x_bit)
    ans = mdl.respons(afstand)
    return [ans[0]]

#define Openturns model for resistance blanket layer
model4a_OTfunction = ot.PythonFunction(9,1, model4a)

#Deterministic parameters
#usage [L1, L3, x_but, x_bit, afstand]
indices = [4,5,6,7,8]
referencePoint = [0, 5000.0, -28.0, 27.0, 95]
model4a_OTfunction_fixed = ot.ParametricFunction(model4a_OTfunction, indices, referencePoint)

#Input & Output
model4a_OTfunction_fixed.setParameterDescription(['k', 'D', 'c1', 'c3'])

#Stochastic variables
#usage [k, D, c1, c3, L1, L3, x_but, x_bit, afstand]
#lognormal distribution for hydraulic conductivity k
k_param = ot.LogNormalMuSigmaOverMu(54.0, 0.5, 0.0) #Vc= 0.5
k = ot.ParametrizedDistribution(k_param)

#lognormal distribution for aquifer thickness D
D_param = ot.LogNormalMuSigma(50.0, 2.5, 0.0) #sd = 2.5
D = ot.ParametrizedDistribution(D_param)
```

```
#lognormal distribution for c1
c1_param = ot.LogNormalMuSigmaOverMu(325, 0.3, 0.0) #Vc = 0.1
c1 = ot.ParametrizedDistribution(c1_param)

#lognormal distribution for c3
c3_param = ot.LogNormalMuSigmaOverMu(1050, 0.3, 0.0) #Vc = 0.1
c3 = ot.ParametrizedDistribution(c3_param)

#collect distributions
marginals = [k, D, c1, c3]
#correlations between stochastic variables
copula = ot.IndependentCopula(4)

#model input
input_distribution = ot.ComposedDistribution(marginals, copula)
input_random_vector = ot.RandomVector(input_distribution)

#output vector
output_vector = ot.CompositeRandomVector(model4a_OTfunction_fixed, input_random_vector)

#set description
output_vector.setDescription(['respons'])
#monte carlo
montecarlosize = 10000
output_sample_mdl4a = output_vector.getSample(montecarlosize)

#Histogram and lognormal fit
histo_respons = ot.HistogramFactory().build(output_sample_mdl4a).drawPDF()
histo_respons.setTitle("histogram response")
histo_respons.setLegends(["histogram response [-]"])
histo_respons.setAxes(True)
histo_respons.setAutomaticBoundingBox(True)
fit_respons = ot.LogNormalFactory().build(output_sample_mdl4a)
fit_respons_pdf = fit_respons.drawPDF()
fit_respons_pdf.setColors(["blue"])
fit_respons_pdf.setLegends(["lognomal"])
histo_respons.add(fit_respons_pdf)
view = viewer.View(graph=histo_respons)
plt.show()

#Summary
def summary_OT_Fit(fit):
    """print the summary of the OpenTurns distribution
    input   : OpenTurns fit"""
    gem = fit.getMean()[0]
    sd = fit.getStandardDeviation()[0]
    Vc = sd / gem
    ConfidenceInterval = fit.computeBilateralConfidenceInterval(0.90)
    ans = print('Summary fit:\n'
                'Average: ', round(gem, 3), '\n'
                'Standard deviation: ', round(sd, 3), '\n'
                'Coefficient of Variation: ', round(Vc, 3), '\n'
                'Reliability index: ', ConfidenceInterval)
    return ans

summary_OT_Fit(fit_respons)
```

D.2. Python code to calculate the uncertainty in the time-dependent response of the hydraulic head

D.2.1. Analysis measurements

```
import matplotlib.pyplot as plt
import numpy as np
import pandas as pd
from dateutil.parser import parse
from pathlib import Path
import datetime
from skimage import data, util, measure
import math
from scipy.signal import find_peaks
import os

wd = Path('')
#filename
fn1 = "Raai_AW222_055.xlsx" #achterland

df1 = pd.read_excel(Path(wd,fn1), header = 0, index_col = 0, parse_dates=True)

df_ana = df1.resample('s').interpolate().resample('10T').asfreq().dropna()

df_ana.loc['2010-04-02': '2010-04-10', ['Rivierwaterstand', 'Rivierwaterstand_2',
'Rivierwaterstand_3', 'B 83 F2']].plot()

df_ana = df_ana.drop('Rivierwaterstand', axis=1)

df_ana.info()
df_sel = df_ana[['Rivierwaterstand_2', 'B 81 F3', 'B 82 F3', 'B 83 F2']]

df_sel.plot()

#periode van 15 tot 17 mei
df_sel = df_sel.loc['2010-05-15': '2010-05-17']


#pieken vinden op de rivier
df_rivier = df_sel[['Rivierwaterstand_2']]

def analyse_getij_rivier (df, searchperiod, distance_between_peaks):
    '''Functie om uit een pandas serie tijdreeks binnen een opgegeven periode de maxima,
    minima en gemiddelde te bepalen
    df: pandas serie met datetime index
    searchperiod: periode in uren
    distance_between_peaks: minimale afstand tussen de samples'''

    #peak finding
    #convert tot array
    df_arr= df.values
    df_arr = df_arr.ravel()
    #finding peaks
    peaks, properties = find_peaks(df_arr, height=df_arr.mean(),
    distance = distance_between_peaks)
```

```
    #create df with peaks, mins en average
    result = pd.DataFrame(columns=['start_period', 'max_time',
    'max_value', 'min_time', 'min_value', 'average_time', 'average_value', 'amplitude'])

    #looping over peaks
    for i in peaks:
        start_period = df.iloc[i].name
        max_value = df.iloc[i,0]
        end_search_period = df.iloc[i].name + datetime.timedelta(hours= searchperiod - 1.0)
        min_time = df[start_period:end_search_period].idxmin()
        #max_time = dfOW001[start_period:end_search_period].idxmax()
        max_time = start_period
        min_timestamp = min_time[0].timestamp()
        max_timestamp = max_time.timestamp()
        min_value = df.loc[min_time].values[0,0]
        average = (max_value + min_value) / 2.0
        amplitude = max_value - average
        amplitude2 = average - min_value
        average_timestamp = (max_timestamp + min_timestamp) / 2.0
        average_time = pd.Timestamp(average_timestamp, unit='s')
        tmp_dict = {'start_period': start_period,
                    'max_time': max_time,
                    'max_value': max_value,
                    'min_time': min_time[0],
                    'min_value': min_value,
                    'average_time': average_time,
                    'average_value': average,
                    'amplitude': amplitude}
        result.loc[len(result)] = tmp_dict

    return peaks, properties, result

pieken_rivier, properties_rivier, resultRivier = analyse_getij_rivier(df_rivier,
searchperiod= 13.0, distance_between_peaks=50)

#functie om fit met ellips op hysterese te maken
def analyse_hysterese_amplitude(df, field_river, peak_timestamps, search_bounds,
result_analyse_Rivier, Plot_wd, Plot=False):
    '''Functie om per top een ellipse te bepalen en deze terug te geven
    df : dataframe met alle peilbuizen inclusief rivier
    field_river: veldnaam met rivierdata
    peak_timestamps : lijst met timesstamps
    search_bound : zoekperiode in uur'''

    #lijst met kolommen van df
    kolommen = df.columns.to_list()
    #rivierverwijderen
    kolommen.remove(field_river)
    #lege dataframe met resultaat
    result = pd.DataFrame(columns=['Peilbuis', 'peak_time', 'river_center', 'pb_center', 'a',
    'b', 'theta', 'max', 'min', 'average', 'amplitude','max_time rivier', 'max_value rivier',
    'min_time rivier', 'min_value rivier', 'average_time rivier', 'average_value rivier',
    'amplitude rivier', 'amplitude peilbuis'])

    for kolom in kolommen:
```

```
        for peak in peak_timestamps:
            start_selectie = peak - datetime.timedelta(hours=search_bounds)
            einde_selectie = peak + datetime.timedelta(hours=search_bounds)
            #x is rivier
            x = df[field_river].loc[start_selectie: einde_selectie].to_list()
            #y is peilbuis
            y = df[kolom].loc[start_selectie: einde_selectie].to_list()
            #samenvoegen
            xy = np.array(list(zip(x,y)))
            if len(x) > 8:
                model = measure.EllipseModel()
                model.estimate(xy)
                xc, yc, a_origine, b_origine, theta_radian = model.params
            else:
                xc, yc, a_origine, b_origine, theta_radian = [99, 99, 99, 99, 99]

            theta_degrees = math.degrees(theta_radian)
            if theta_degrees>90:
                theta = theta_degrees-90
                a = b_origine
                b = a_origine
            else:
                theta = theta_degrees
                a = a_origine
                b = b_origine

            start_selectie_max = peak - datetime.timedelta(hours=1.0)
            einde_selectie_max = peak + datetime.timedelta(hours=2.0)
            start_selectie_min = peak + datetime.timedelta(hours=2.0)
            einde_selectie_min = peak + datetime.timedelta(hours=12.0)

            #y is peilbuis de max
            y_max = df[kolom].loc[start_selectie_max: einde_selectie_max].max()
            #samenvoegen
            y_min = df[kolom].loc[start_selectie_min: einde_selectie_min].min()
            #average
            av = (y_max+y_min) / 2.0
            #amplitude
            amp = y_max-av

            r = result_analyse_Rivier.loc[result_analyse_Rivier['start_period'] == peak]
            A_peil = r['amplitude'].values[0] * np.tan(math.radians(theta))
#             print (r['start_period'].values())
            tmp_dict = {'Peilbuis': kolom,
                        'peak_time': peak,
                        'river_center': xc,
                        'pb_center': yc,
                        'a': a,
                        'b': b,
                        'theta': theta,
                        'max': y_max,
                        'min': y_min,
                        'average': av,
                        'amplitude': amp,
#                         'start_period rivier': r['start_period'].values[0],
                        'max_time rivier': r['max_time'].values[0],
```

```
                        'max_value rivier': r['max_value'].values[0],
                        'min_time rivier': r['min_time'].values[0],
                        'min_value rivier': r['min_value'].values[0],
                        'average_time rivier': r['average_time'].values[0],
                        'average_value rivier': r['average_value'].values[0],
                        'amplitude rivier': r['amplitude'].values[0],
                        'amplitude peilbuis': A_peil}
            result.loc[len(result)] = tmp_dict

            if Plot:
                xy_predict = measure.EllipseModel().predict_xy(np.linspace(0, 2 * np.pi, 25),
                params=model.params)
                fname = str(kolom) + "_" + peak.strftime('%Y-%m-%d %H.%M.%S') + ".png"
                if os.path.exists(Plot_wd):
                    plt.figure()
                    plt.plot(x,y, "x")
                    plt.plot(xy_predict[:,0], xy_predict[:,1])
                    plt.title("Peilbuis" + str(kolom) + "- top " +
                    peak.strftime('%Y-%m-%d %H:%M:%S'))
                    #plt.savefig(r'Figures\{}.png'.format(fname), dpi=300)
                    plt.savefig(Path(Plot_wd,fname), dpi=300)
                    plt.close()
    return result

#working directory for figures
wd_figures = Path(wd, 'Figures')
result_analyse = analyse_hysterese_amplitude(df_sel, 'Rivierwaterstand_2',
                                             resultRivier['max_time'].to_list(),
                                             3.0,
                                             resultRivier,
                                             wd_figures,
                                             Plot=True)

wd_figures
result_analyse.to_excel(Path(wd,'result_ellips_amplitudes.xlsx'))
resultRivier.to_excel(Path(wd, "Analyse_amplitudes_rivier.xlsx"))

#hystereses plotten

def plot_hysterese(df, field_x, fields_y, start, end):
    '''Functie om een hysterese te plotten'''
    #figuur definitie
    fig, ax = plt.subplots(1, 1, figsize=(5, 5))
    #filter period
    data = df.loc[start:end]
    for field in fields_y:
        ax.plot(data[field_x], data[field], label=field)
    ax.set_xlabel('Rivier')
    ax.set_ylabel('Peilbuis')
    ax.legend()

    return fig

plot_hysterese(df_sel, 'Rivierwaterstand_2', ['B 81 F3','B 82 F3', 'B 83 F2'],
start='2010-05-15', end='2010-05-17')
```

D.2.2. Fit and extrapolation

```
import numpy as np
import scipy.optimize
import matplotlib.pyplot as plt
import math

#data to fit
#afstand peilbuis tot as dijk (in dit geval tot rivier)
xs = np.array([7.2, 40.8, 53 ])
#gemiddelde stijghoogte
ys = np.array([-0.3206, -0.3309, -0.3428])

amp_s = np.array([0.180988371, 0.164092025, 0.159596729])

#onverstoorde stijghoogte in de polder
pp = -1.5 #m

#gemiddeld rivierpeil
r = 0.502628454 #m

#amplitude getij rivier
ar = 0.562571364 #m

#breedte rivier
b = 350.0

#stijghoogte omrekenen naar respons
#Functie voor omrekening van potentiaal naar respons
def calc_respons (phi, h_riv, phi_p): #Van respons naar potentiaal
    return (phi - phi_p) / (h_riv - phi_p)

#Functoe voor omrekening van amplitude naar respons
def calc_respons_amplitude(amp, amp_r):
    return amp / amp_r

#bereken respons van de potentiaal op basis van opgegeven rivierpeil en polderpeil
rs = calc_respons(ys, r, pp)

#Functie voor omrekening van respons naar potentiaal
def calc_respons_to_pot (phi_p, r_exit, h_riv): #Van respons naar potentiaal
    return phi_p + r_exit * (h_riv - phi_p)

plt.plot(xs, rs, '.')
plt.show()

#bepaal functie die het gemiddeld potentiaalverloop beschrijft
def calc_gem_responsverloop (x, W1, W3):
    #Berekening van respons kantelpunt
    rk = 1 / (1 + (W1 / W3))
    #Berekening van respons ter plaatse van uittredeppunt (x positie)
    r_uit = np.exp(-1*(x/W3))
    #Berekening gemiddelde potentiaal bij uittredepunt
    return rk * r_uit

#perform the fit
p0 = (300.0, 1000.0)
```

```
params, cv = scipy.optimize.curve_fit(calc_gem_responsverloop, xs, rs, p0)

W1, W3 = params

print('Stationaire weerstand voorland: ', W1)
print('Stationaire weerstand achterland: ', W3)

#bekijk de invloed van de onverstoorde stijghoogte
onv_pp_list = [-0.5, -1.0, -1.5, -2.0]

for i in range(len(onv_pp_list)):
    rs = calc_respons(ys, r, onv_pp_list[i])
    p0 = (300.0, 1000.0)
    params, cv = scipy.optimize.curve_fit(calc_gem_responsverloop, xs, rs, p0)
    W1, W3 = params
    print('W1: ', W1, 'W3: ', W3)

# determine quality of the fit
squaredDiffs = np.square(rs - calc_gem_responsverloop(xs, W1, W3))
squaredDiffsFromMean = np.square(rs - np.mean(rs))
rSquared = 1 - np.sum(squaredDiffs) / np.sum(squaredDiffsFromMean)
print(f"R² = {rSquared}")

# plot the results
plt.plot(xs, rs, '.', label="data")
plt.plot(xs, calc_gem_responsverloop(xs,W1, W3), '--', label="fitted")
plt.title("Respons gemiddeld potentiaalverloop")

def calc_respons_pot4d(x,H0, lam1, lam3, b): #maximale respons op impuls
    theta = calc_theta(b, lam1)
    m = (lam1 / lam3) * calc_f(b, lam1)
    delta = np.log(np.sqrt(1.0 + m**2.0 + 2.0 * m * np.cos(theta)))
    n = (-1.0 * m * np.sin(theta)) / (1.0 + m * np.cos(theta))
    pot = H0 * np.exp(((-0.924 * x) / lam3) - delta) * 1.0
    return pot


# functie theta (figuur b4.13)
# de functies theta en f zijn gedigitaliseerd en vervolgens benaderd door een 5e graads polynoom
def calc_theta(b, lambda_w_vl):
    x = b / lambda_w_vl
    if x > 2.8:
        return 0.0
    else:
        return 0.0078 * math.pow(x,5.0) - 0.082 * math.pow(x, 4.0) +
        0.3139 * math.pow(x, 3.0) - 0.4683 * math.pow(x, 2.0) + 0.035 * x + 0.392699081698724

def calc_f(b, lambda_w_vl):
    x = b / lambda_w_vl
    return 1.0 + 7.0659 * np.exp(-3.648 * x)

def calc_respons_pot4d_zonder_voorland(x,H0, x_intrede, lam3): #maximale respons
    pot = H0 * np.exp(-0.924 * (x + x_intrede) / lam3) * 1.0
    return pot

#bereken respons van de amplitude
```

```
amp_rs = calc_respons_amplitude(amp_s, ar)

custom_pot_4d = lambda x, lam1, lam3: calc_respons_pot4d(x, ar, lam1, lam3, b)

custom_pot_4d_zonder_voorland = lambda x, x_intrede, lam3:
calc_respons_pot4d_zonder_voorland(x, ar, x_intrede, lam3)

#voer fit uit
p0 = (150.0, 500.0)
params_ampl, cv_ampl = scipy.optimize.curve_fit(custom_pot_4d, xs, amp_s, p0)
W1_cycl, W3_cycl = params_ampl

print('Cyclische weerstand voorland: ', W1_cycl)
print('Cyclische weerstand achterland: ', W3_cycl)

#voer fit uit
p0 = (150.0, 500.0)
params_ampl_v2, cv_ampl = scipy.optimize.curve_fit(custom_pot_4d_zonder_voorland, xs, amp_s, p0)
x_intrede, W3_cycl_v2 = params_ampl_v2

print('Cyclische weerstand voorland: ', x_intrede)
print('Cyclische weerstand achterland: ', W3_cycl_v2)

# plot the results
plt.plot(xs, amp_s, '.', label="data")
plt.plot(xs, calc_respons_pot4d(xs,ar, W1_cycl, W3_cycl, b), '--', label="fitted")
plt.title("Respons op amplitude rivier")
plt.show()
```

D.2.3. Response analysis

```
import numpy as np
import math
import pandas as pd
from pathlib import Path
#import geohydromodels
import matplotlib.pyplot as plt
import scipy as sct

#stijghoogte omrekenen naar respons
#Functie voor omrekening van potentiaal naar respons
def calc_respons (phi, h_riv, phi_p): #Van respons naar potentiaal
    return (phi - phi_p) / (h_riv - phi_p)

#Functoe uppr omrekening van amplitude naar respons
def calc_respons_amplitude(amp, amp_r):
    return amp / amp_r


#Functie voor omrekening van respons naar potentiaal
def calc_respons_to_pot (phi_p, r_exit, h_riv): #Van respons naar potentiaal
    return phi_p + r_exit * (h_riv - phi_p)

#bepaal functie die het gemiddeld potentiaalverloop beschrijft
def calc_gem_responsverloop (x, W1, W3):
    #Berekening van respons kantelpunt
```

```
    rk = 1 / (1 + (W1 / W3))
    #Berekening van respons ter plaatse van uittredeppunt (x positie)
    r_uit = np.exp(-1*(x/W3))
    #Berekening gemiddelde potentiaal bij uittredepunt
    return rk * r_uit

def calc_respons_pot4d(x,H0, lam1, lam3, b): #maximale respons op impuls
    theta = calc_theta(b, lam1)
    m = (lam1 / lam3) * calc_f(b, lam1)
    delta = np.log(np.sqrt(1.0 + m**2.0 + 2.0 * m * np.cos(theta)))
    n = (-1.0 * m * np.sin(theta)) / (1.0 + m * np.cos(theta))
    pot = H0 * np.exp(((-0.924 * x) / lam3) - delta) * 1.0
    return pot


# functie theta (figuur b4.13)
# de functies theta en f zijn gedigitaliseerd en vervolgens benaderd door een 5e graads polynoom
def calc_theta(b, lambda_w_vl):
    x = b / lambda_w_vl
    if x > 2.8:
        return 0.0
    else:
        return 0.0078 * math.pow(x,5.0) - 0.082 * math.pow(x, 4.0) +
        0.3139 * math.pow(x, 3.0) - 0.4683 * math.pow(x, 2.0) + 0.035 * x + 0.392699081698724

def calc_f(b, lambda_w_vl):
    x = b / lambda_w_vl
    return 1.0 + 7.0659 * np.exp(-3.648 * x)

def calc_respons_pot4d_zonder_voorland(x,H0, x_intrede, lam3): #maximale respons
    pot = H0 * np.exp(-0.924 * (x + x_intrede) / lam3) * 1.0
    return pot

#Functie voor berekening cyclische lekfactor bij andere periode
#functie voor omrekening naar andere perioden
#LambdaCycl_1 = cyclische lekfactor die hoort bij periode 1 (T1)
#T2 = periode waarvoor je de cyclische lekfactor wilt omrekenen
def calc_lambda_cycl (LambdaCycl_1, T2, T1):
    return LambdaCycl_1 * math.pow(T2 / T1, 0.25)

#Functie van golflengte naar duur
def calc_P_from_T(T):
    return T / 2.0

#Functie van duur naar golflengte
def calc_T_from_P(P):
    return P * 2.0

#constanten
r_gem = 0.54 #m+NAP
onv_pp = -1.5 #m+NAP


#stationaire factoren
W1 = 1815.0
W3 = 2623.0
```

```
#periodes [s]
#input voor instationair model

T_getij_input = (12.0+25.0/60.0) * 3600.0 #periode getij is 12 uur en 25 min
T_storm_input = 90.0 * 3600.0 #stormduur 45 uur
T_afvoer_input = 800.0* 3600 #afvoergolf 400 uur

print('getijde periode: ', T_getij_input)
print('storm periode: ', T_storm_input)
print('afvoer periode: ', T_afvoer_input)

wd = Path('C:/......')
fn = 'Samples T10.xls'

df = pd.read_excel(Path(wd, fn), header=0)
df['WBN'] = r_gem + df.iloc[:, [6,7,8]].sum(axis=1)

m = df.iloc[:, [3,5,6,7,8]].to_numpy()
m.shape

#nu de superpositie
#gewenste locaties voor de berekening
#x=40 is de binnenkruinlijn
x = np.array([0.0, 20.0, 40.0, 50.0, 60.0, 70.0, 100.0])

stationair_respons = calc_gem_responsverloop(x, W1, W3)
stationair = calc_respons_to_pot(onv_pp, stationair_respons, r_gem)

res_pot = np.empty(len(x))

for row in m:
    #W1_rivier = calc_lambda_cycl(row[0], T_afvoer_input, T_getij_input)
    W3_rivier = calc_lambda_cycl(row[1], T_afvoer_input, T_getij_input)
    #W1_storm = calc_lambda_cycl(row[0], T_storm_input, T_getij_input)
    W3_storm = calc_lambda_cycl(row[1], T_storm_input, T_getij_input)
    getijde = calc_respons_pot4d_zonder_voorland(x, row[4], row[0], row[1])
    storm = calc_respons_pot4d_zonder_voorland(x, row[3], row[0], W3_storm)
    rivier = calc_respons_pot4d_zonder_voorland(x, row[2], row[0], W3_rivier)
    pot = stationair + getijde + storm + rivier
    res_pot = np.vstack((res_pot, pot))


mean =  np.zeros(len(x))
lower = np.zeros(len(x))
upper = np.zeros(len(x))

for i in range(len(x)):
    data_to_fit = res_pot[:,i]
    mean_fit, std_fit= sct.stats.norm.fit(data_to_fit)
    print(f'The average response at x = {x[i]} is {mean_fit:.3f} with sd {std_fit:.3f}')
    rv = sct.stats.norm(loc=mean_fit, scale=std_fit)   ###
    rv_int = np.asarray(rv.interval(0.90))
    #print(rv_int)
    print(f'The interval at x = {x[i]} is {rv.interval(0.90)}')
```

```
    #filling in the data
    mean[i] = mean_fit
    lower[i] = rv_int[0]
    upper[i] = rv_int[1]

    #waarden voor grafiek
    xg = np.linspace(np.min(data_to_fit), np.max(data_to_fit))
    plt.hist(data_to_fit, density=True, bins='auto', histtype='stepfilled', alpha=0.2,)
    plt.plot(xg, sct.stats.norm.pdf(xg, mean_fit, std_fit), 'r', label=f'{x[i]}')
    plt.legend()
    plt.show()

#confidence interval voor verdeling
rv = sct.stats.norm(loc=mean_fit, scale=std_fit)
print(rv.interval(0.90))

#Dike profile
d_x = [0, 10, 15, 18, 26.5, 34, 53, 80]
d_y = [1.357, 5.101, 5.474, 4.668, 4.671, 0.915, -0.598, -1.12]

#plot potentiaal
plt.subplots(figsize=(16, 8))
plt.plot(d_x, d_y, label='Dike profile', color='black')
plt.plot(x, stationair, label='stationair')
plt.plot(x, rivier, label='rivier')
plt.plot(x, storm, label='storm')
plt.plot(x, getijde, label='getijde')
plt.plot(x, rivier + storm + getijde + stationair, label='average total')
plt.xlabel('Dike location [m]')
plt.ylabel('Heigth [m NAP]')
plt.title('Potential at T = 10')
plt.legend()
plt.grid();
```

D.3. Python code fitting the outer water level to the Gumbel distribution

```
import numpy as np
from scipy.stats import gumbel_r
from scipy.optimize import curve_fit
import matplotlib.pyplot as plt
import sympy

### FITTING THE DISTRIBUTION OF THE OUTER WATER LEVEL
#HYDRA NL DATA
T = [30, 100,300, 1000, 3000, 10000, 30000]       #years
h = [5.55, 5.96, 6.19, 6.37, 6.50, 6.62, 6.72]

Pf = np.zeros(len(T))
for i in range(len(T)):
    a = 1 / T[i]
    Pf[i] = a
print(f' The exceendance frequency for each extreme water level is {Pf}')
```

```
### CREATING THE GUMBEL FIT FOR THE OUTER WATER LEVEL + PROVIDE THE MEAN AND SD
## functions that describe the PDF & CDF of the gumbel distribution
def gumbel_pdf(x, mu, beta):
    pdf = (1 / beta) * np.exp(-(x - mu) / beta - np.exp(-(x - mu) / beta))
    return pdf

def gumbel_cdf(x, c, s):
    cdf = np.exp(- np.exp(-(x - c) / s))
    return cdf

param, cov = curve_fit(gumbel_pdf , h, Pf)
mu, beta = param

gamma = sympy.EulerGamma.evalf()
print (f'Mu = {mu:.3f} the location parameter')
print (f'Beta = {beta:.3f} the scale parameter')
print(f'Mean = {mu + beta * gamma:.3f}')
print(f'Standard deviation = {beta * (np.pi / np.sqrt(6)):.3f}')

x = np.linspace(0, 8, 1000)
y1 = gumbel_pdf(x, mu, beta)
y2 = gumbel_cdf(x, mu, beta)
fig, ax = plt.subplots(1, 2, figsize = (10,5))

#Left plot
ax[0].scatter(h, Pf)
ax[0].plot(x, y1, label='Curve fit Gumbel distribution')

#Right plot
ax[1].scatter(h, Pf)
ax[1].plot(x, y1, label='Curve fit Gumbel distribution')

ax[0].set_title('PDF curve fits')
ax[1].set_title('PDF Data fit')
ax[1].set_xlim([5.3,7])
ax[1].set_ylim([-.01, 0.08])
ax[0].set_xlabel('Water level [m]')
ax[1].set_xlabel('Water level [m]')
ax[0].set_ylabel('PDF [-]')
#ax[1].set_ylabel('PDF [-]')
ax[0].legend()
ax[1].legend()
ax[0].grid()
ax[1].grid();
```

E

Appendix E: Additional analysis

E.1. Dupuit formulation

A calculation methodology that can be used to determine the expectation level of the phreatic line for clay dikes is described by a report on the uncertainties of the parameters that determine the pore water pressures within the WBI (Rozing, 2015). The height of the phreatic line in a soil body can be approximated by using the formula of Dupuit, as described by equation E.1.

$$h = \sqrt{-\frac{N}{k}x^2 + (\frac{\phi_2^2 - \phi_1^2}{L} + \frac{NL}{k})x + \phi_1^2} \tag{E.1}$$

where N includes precipitation, k the hydraulic conductivity of the dike, ϕ the boundary conditions on both sides and L the dike width. From the average precipitation in the Netherlands, a value for N can be differentiated where the assumption is made that not all of the precipitation will infiltrate the dike, where $N = 300mm/year$ (Rozing, 2015). The hydraulic conductivity K is valid for the entire dike body and is suggested to be set at 10^-7 for a clay dike core. However, this value is only valid for permanently saturated clay and is not a representative value for clay dike material that is not permanently saturated. The conductivity can increase by 10^-1 due to visible cracks in the clay. From the technical report on clay used in dikes (TAW, 1996), the hydraulic conductivity of clay dikes is measured at several locations to be in the order of 10^-4 to 10^-5. These values are measured between early spring, into fall. The largest uncertainty within the Dupuit formulation is the hydraulic conductivity (k). The phreatic line is approximated by Dupuit's formulation for different values for the hydraulic conductivity in figures E.1 and E.2.

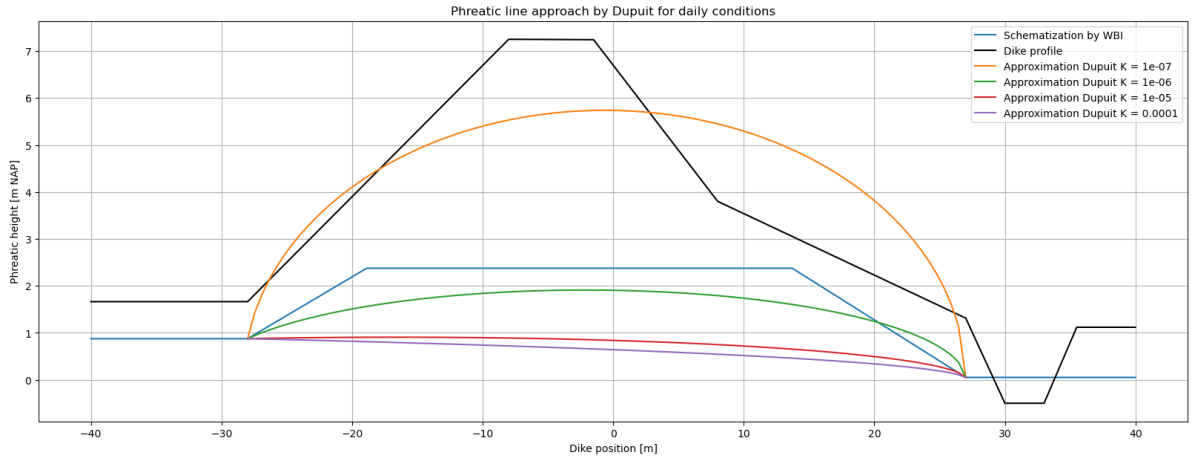

Figure E.1: Phreatic line approximation by Dupuit at daily conditions for different hydraulic conductivity

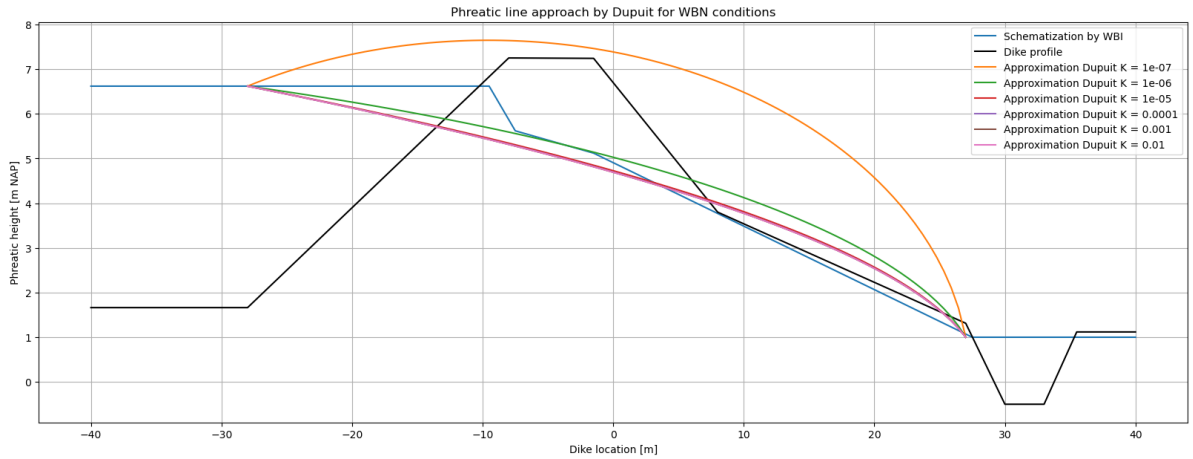

Figure E.2: Phreatic line approximation by Dupuit at WBN conditions for different hydraulic conductivity

It is difficult to predict a realistic value for the hydraulic conductivity of dike material. The soil structure has a major influence on the parameter, which is difficult to simulate in a soil laboratory test. The dike material is affected by weather influences resulting in drying and wetting cycles of the material. This can result in the cracking of clay, influencing the hydraulic conductivity. Since it is also a large assumption that the hydraulic conductivity is constant over the entire dike body, this method is not suitable for the project. By applying the Dupuit formulation to estimate the height of the phreatic line, larger uncertainties will arise which are difficult to include in the analysis process. Both figures additionally display an overestimation of the phreatic line since the method of Dupuit is mostly applied on solid square soil bodies. This method is not suitable for the schematization of the phreatic line in a dike cross-section, so is not included in the uncertainty analysis.

E.2. Case study: subsurface schematization uncertainties Kinderdijk

Another subsurface schematization uncertainties analysis is performed, for a local primary dike cross-section near Kinderdijk in the Alblasserwaard. The location of the dike considered in this analysis is displayed in figure E.3. The most recent macrostability safety assessment for this section was performed for the dike reinforcement project KIS, reinforcing the Lekdijk from Kinderdijk to Streefkerk from 2013 to 2018. During this particular safety assessment, no probabilistic calculations were performed yet.

Figure E.3: Location of the Lekdijk near Kinderdijk concerning the Alblasserwaard

This particular dike location is also investigated during the Additional Graduation Work. This primary dike section is located directly on the river Lek. The subsurface contains thick peat layers that are high

in organic content.

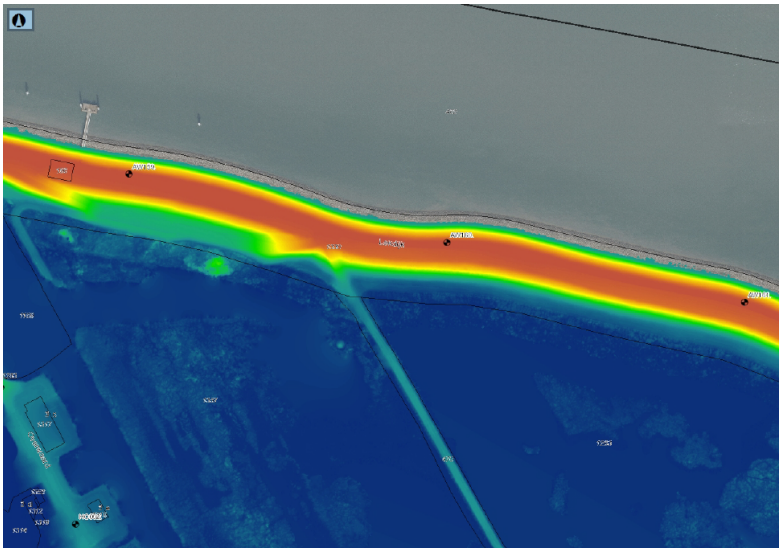

Figure E.4: Lekdijk near Kinderdijk with respect to the Alblasserwaard 1:500

The vertical soil profile underneath the inner dike slope is displayed in figure E.5. The local subsurface is mainly composed of peat interlayered with clay (brown and green on the vertical soil profile). The dike has been reinforced multiple times in the past by adding dike material (yellow and blue), resulting in differential settlements of the blanket layer. The dike material is situated from -3 m NAP to about -5 m NAP. A river sand deposit is visible from -10m to -15m NAP.

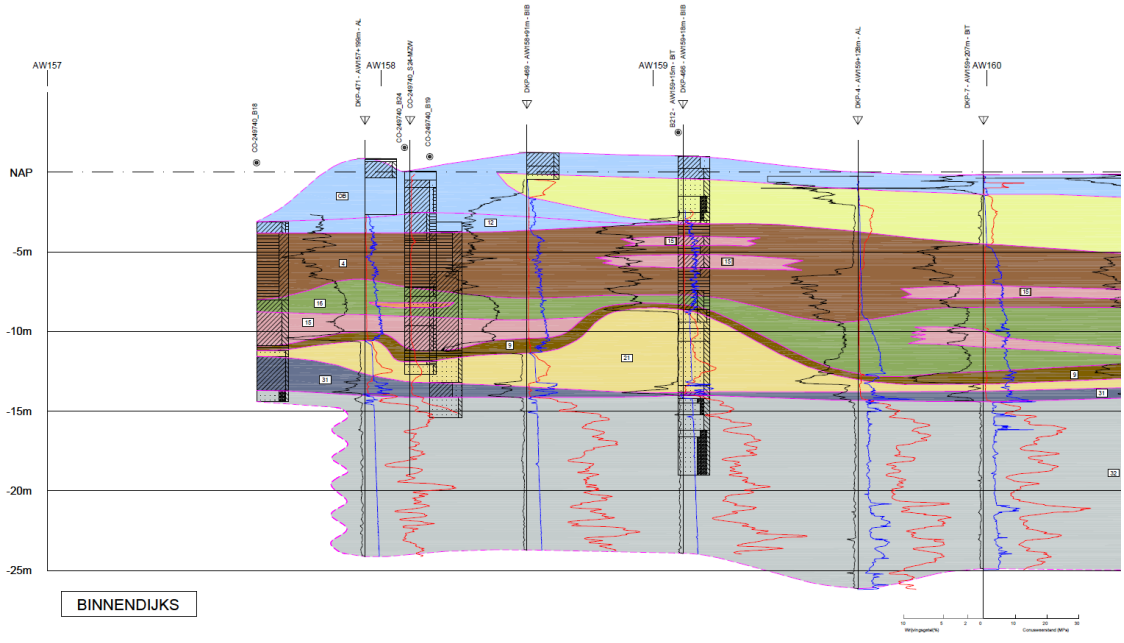

Figure E.5: Vertical soil profile of the inner dike slope of the Lekdijk near Kinderdijk

The stability model used in the previous macrostability safety assessment is displayed in figure E.6. The model for the macrostability safety assessment applies soil types based on the previous test collection set up for this reinforcement project specifically from the WSRL. The model separates the soil layers located underneath the dike and next to the dike. The layers are assigned additional strength

here since the soils have been exposed to higher loads.

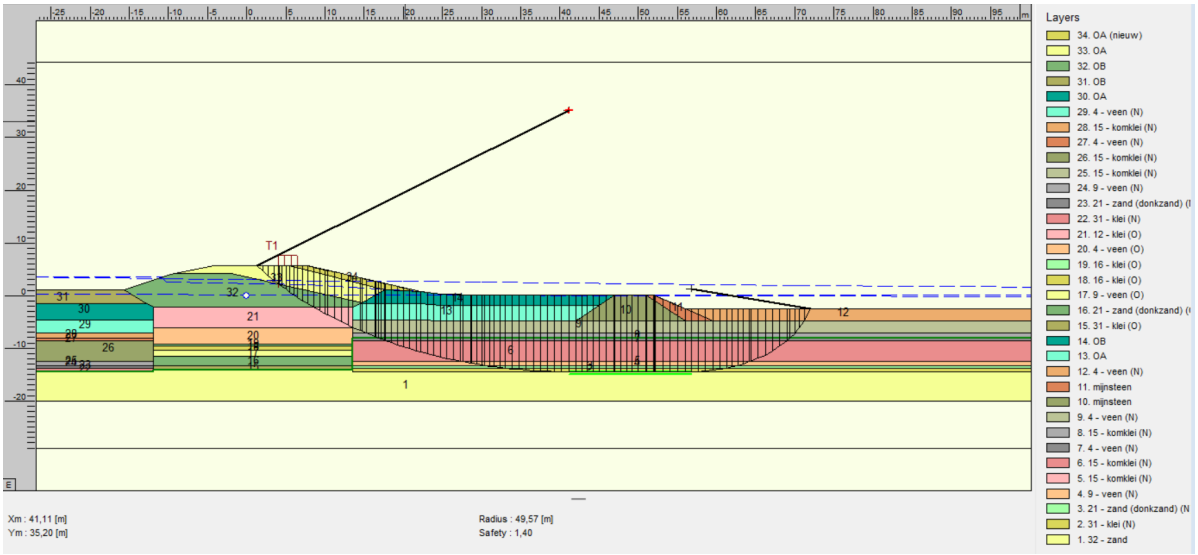

Figure E.6: Most recent macrostability safety assessment

The dike material is separated into sandy dike material, clayey dike material, and the new reinforcement material used to increase the dike stability and widen the dike crest for a bicycle lane. Drainage material is applied at the end of the berm.

The WBI SOS soil scenarios are taken from D-Soil Model for the relevant dike trajectory including the local dike cross-section. A total of nine soil scenarios are set up and are displayed in figure E.7. The same soil notation is applied as for the subsurface schematization of the Kortenhoevendijk case study.

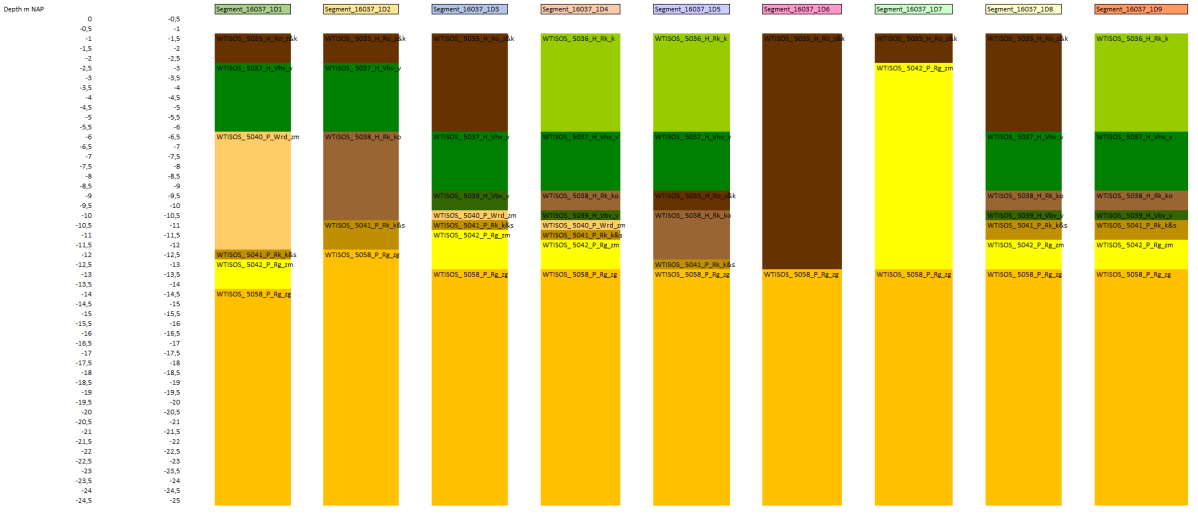

Figure E.7: SOS scenarios for Kinderdijk

The soil scenarios are mainly composed of clay (in brown) and peat material (in green). The scenarios mainly composed of sandy soil have a relatively low probability of occurrence. The probability of occurrence of each soil scenario is given in E.1. The scenario probabilities are divided equally over the different scenarios, where the largest probability is 15%.

Soil scenario	Probability of occurrence %
Segment_16037_1D1	6
Segment_16037_1D2	9
Segment_16037_1D3	15
Segment_16037_1D4	15
Segment_16037_1D5	5
Segment_16037_1D6	15
Segment_16037_1D7	5
Segment_16037_1D8	15
Segment_16037_1D9	15

Table E.1: SOS probabilities for dike section 37

Local soil scenarios

To set up a local soil profile of the subsurface at location Kinderdijk, local CPT and mechanical borings are investigated in more detail. The locations of the CPT tests and borings are displayed in figure E.8.

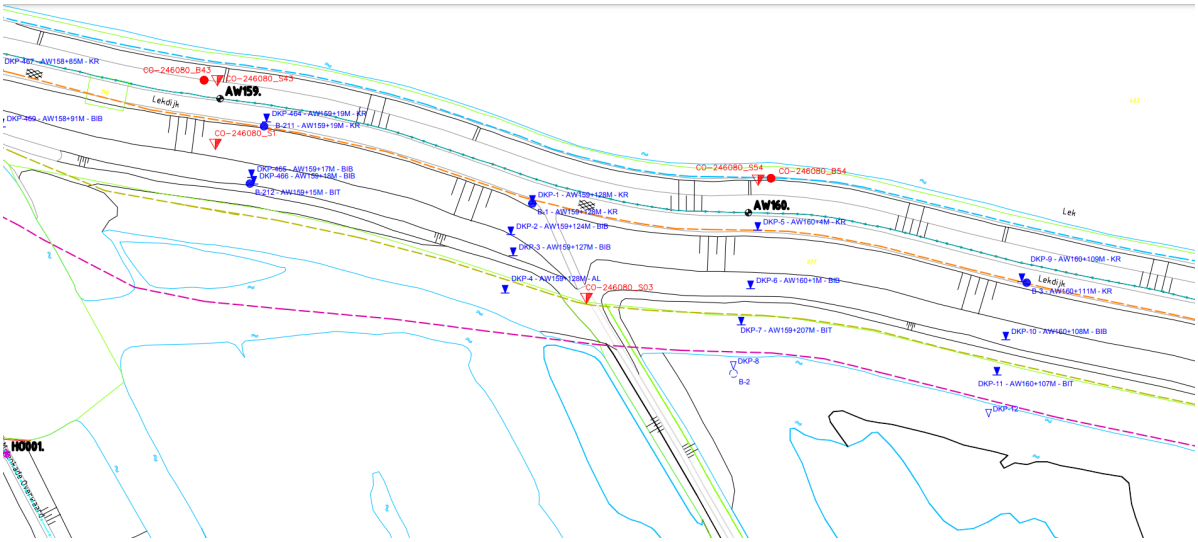

Figure E.8: Locations CPT and boring

Figure E.9 displays the local soil scenarios that can be set up for the Kinderdijk case study. Each scenario is set up by using the local soil investigation data provided at the end of the chapter. Scenarios 1 and 4 are used to simulate the influence of the settled dike reinforcement material. Scenarios 3 and 4 have a more complex soil profile to investigate the influence on the reliability.

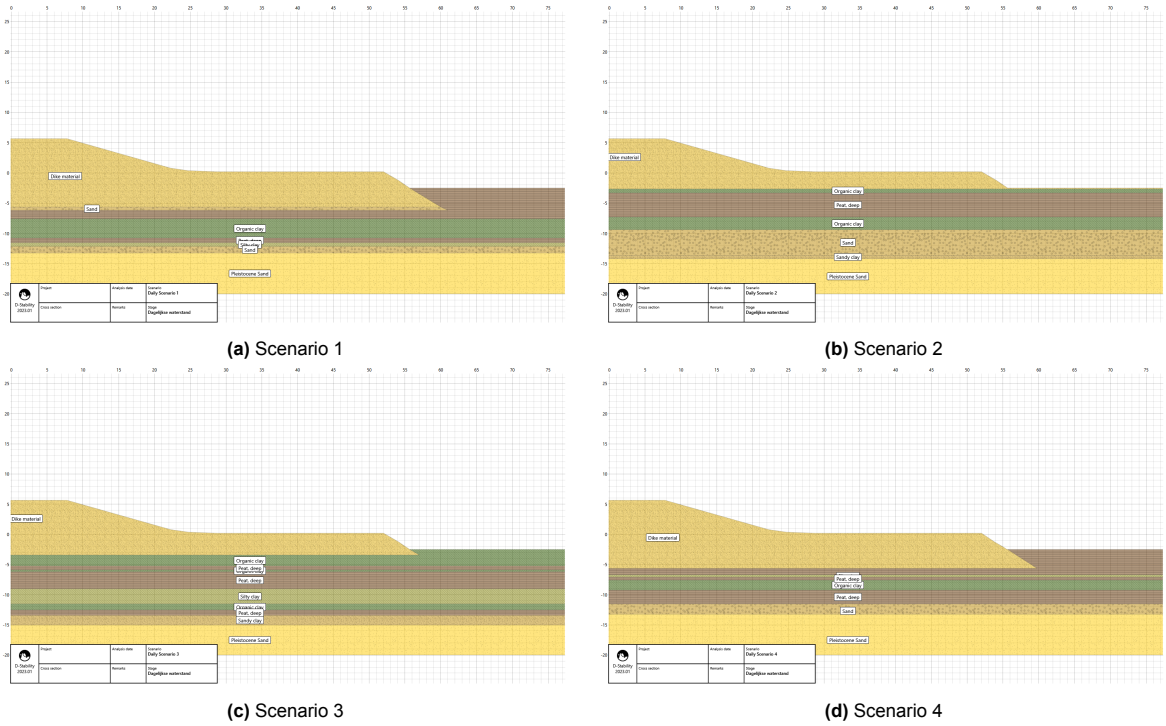

(a) Scenario 1 **(b)** Scenario 2

(c) Scenario 3 **(d)** Scenario 4

Figure E.9: D-Stability models for the local soil scenarios for case study Kinderdijk

Scenario 2 describes the soil profile that includes the old river deposit as shown in the vertical soil profile in figure E.5. An additional soil scenario is set up next to this deposit, so the influence of the river deposit in the subsurface on the macrostability and the reliability index can be investigated directly. This additional scenario is displayed in figure E.10.

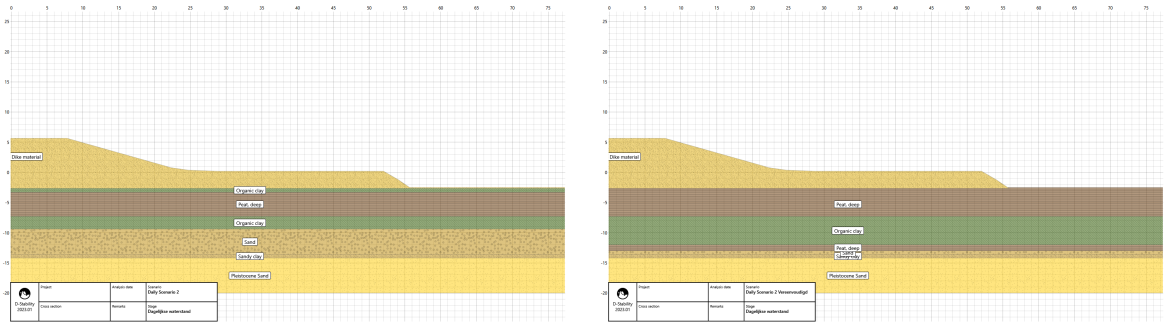

(a) Scenario 2 including the river deposit **(b)** Scenario 2 next to river deposit

Figure E.10: Additional D-Stability models for the investigation into the influence of the local river deposit Kinderdijk

Each of the local soil scenarios is used as input for the D-Stability model. The original soil parameters from the previous safety assessment are used during this analysis. Since the test collection of this dike section only includes deterministic values for the soil strength parameters, the WBI is used to include the parameters as stochastic variables. The deterministic value is set equal to the average value of the stochastic variable. The coefficient of variation is constant for the strength parameter. These are provided in table E.2.

Parameter	Coefficient of variation [-]
S	0.03
ϕ	0.05
POP peat soil	0.45
POP other soils	0.3

Table E.2: Coefficients of variation as described by the WBI (Rijkswaterstaat and Ministerie van Infrastructuur en Waterstaat, 2021)

Table E.3 displays the input parameters that are used in the D-Stability modeling for the soil scenarios of the Lekdijk near Kinderdijk.

Soil type	Notation	Unit weight $[kN/m^3]$	$\phi[^\circ]$	$\phi[^\circ]$ Mean	$\phi[^\circ]$ SD	m [-]	S [-]	S [-] Mean	S [-] SD
OA new		18	24.003	25	1.6	0.8	0.31	0.31	0.03
OA	DK_z	18.56	33.6	36.2	1.6				
OB	DK_k	17.5	22.318	25	1.25	0.8	0.31	0.31	0.03
Peat, shallow		10.5				0.78	0.34	0.34	0.03
Organic clay	K_o	13.9				0.85	0.24	0.26	0.013
Silty clay	K_s	16.86				0.5	0.26	0.28	0.013
Sandy clay	K_z	18.56	33.6	36.2	1.6				
Sand	Z_h	20	32.4	34	0.986				
Peat, deep	V	11				0.8	0.35	0.4	0.032
Pleistocene sand	Z_p	20	35.4	34	0.986				

Table E.3: Input parameters D-Stability model soil scenarios

The parameters assigned to the organic clay soil are also based on the data provided in the WBI. The new version of the test collection could not be used for additional information on the strength parameters since this collection considered the number of observations of this soil layer too low to consider this soil type as a separate category. The organic clays are combined with the humus clay category (Kwakman, 2023).

The values that are used to define the POP of the soil layers are given in table E.4.

Soil type	POP Deterministic	POP Mean	POP SD
Peat	1	11	4.95
Clay	15	25	7.5

Table E.4: Values for POP used in the D-Stability modeling

The water levels for which the macrostability of the local dike section will be calculated are taken from Hydra-NL and shown in table E.5. This includes the return period of the outer water levels.

Return period	Outer water level [m NAP]
Daily conditions	0.33
T = 10 years	2.801
T = 1000 years	3.380
T = 30000 years	3.716

Table E.5: Outer water levels and return periods taken from Hydra-NL

Preliminary results

The results of the soil scenario analysis in D-Stability of the local case study of Kinderdijk are displayed in table E.6.

Scenario	Outer water level [m]	Reliability index β [-]	Probability of failure P_f [-]
Scenario 1	0.33	9.305	6.70E-21
	2.80	8.537	6.90E-18
	3.38	8.221	1.01E-16
	3.72	8.035	4.66E-16
Scenario 2	0.33	6.224	2.423E-10
	2.80	5.838	2.54E-09
	3.38	5.652	7.34E-09
	3.72	5.552	1.41E-08
Scenario 2a	0.33	4.479	3.74E-06
	2.80	5.282	6.40E-08
	3.38	5.137	1.40E-07
	3.72	5.054	2.16E-07
Scenario 3	0.33	10.66	8.22E-27
	2.80	6.663	1.34E-11
	3.38	7.655	9.63E-15
	3.72	7.519	2.76E-14
Scenario 4	0.33	9.578	4.97E-22
	2.80	8.948	1.81E-19
	3.38	8.674	2.09E-18
	3.72	8.502	9.35E-18

Table E.6: Results D-Stability analysis soil scenarios Kinderdijk case study

All calculation results displayed in table E.6 are gained via the FORM analysis. During this analysis, the overall stability of the dike cross-section overall soil scenarios is large. The reliability index, most of the time, is larger than 8. Since this resulted in many non-convergence issues during the stability analysis of the case study Kortenhoevendijk, the analysis of this dike cross-section is not investigated further. Due to time constraints on the project, another dike cross-section with a lower general reliability is chosen in the pore water pressure analysis. Since the impact of the reliability is larger in the pore water pressure uncertainty schematization, the subsurface schematization will not be considered for the case study Bergstoep.

E.3. Local soil investigation case study Kinderdijk

Mechanical borings

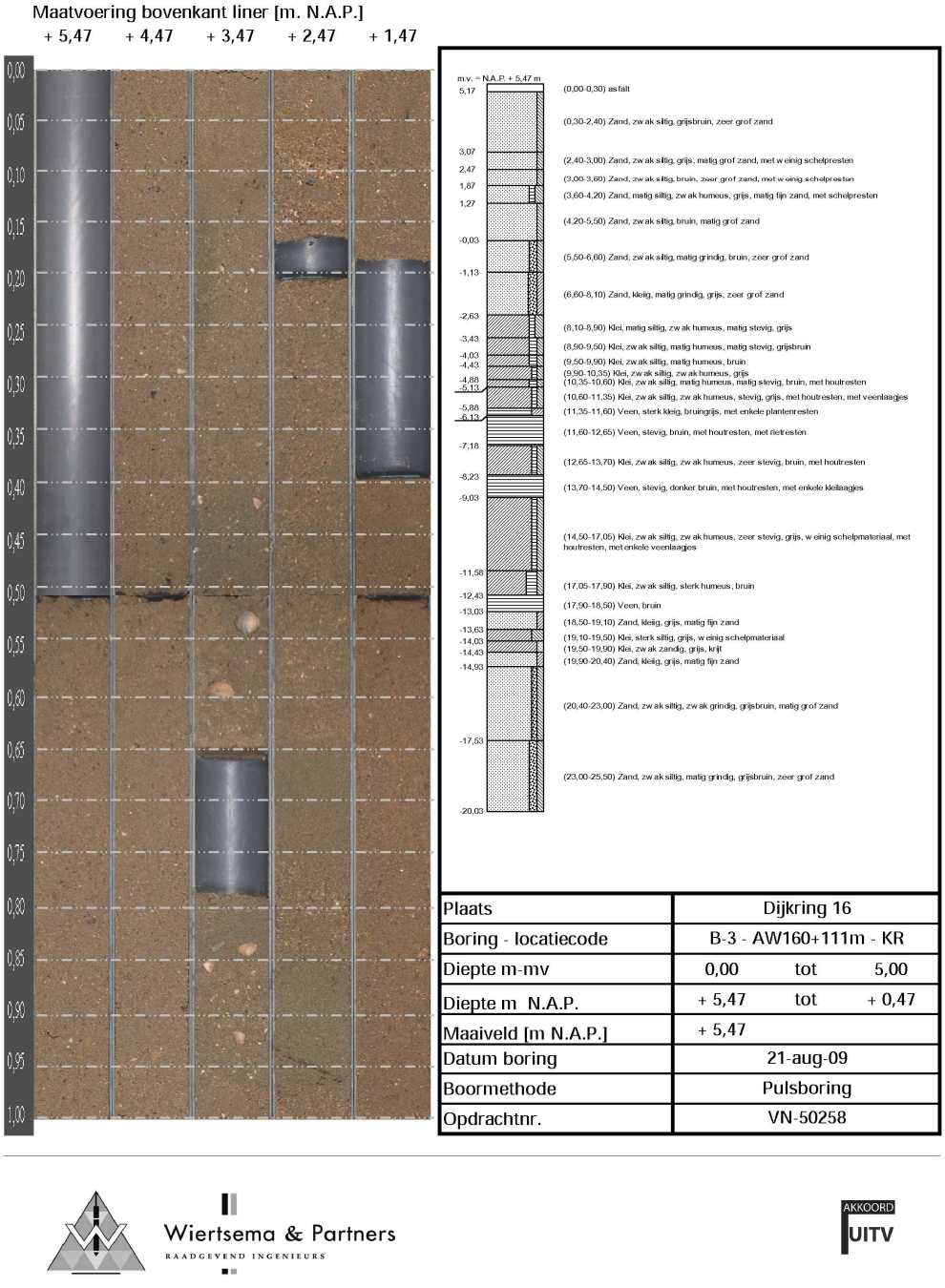

Figure E.11: Mechanical boring crest case study Kinderdijk

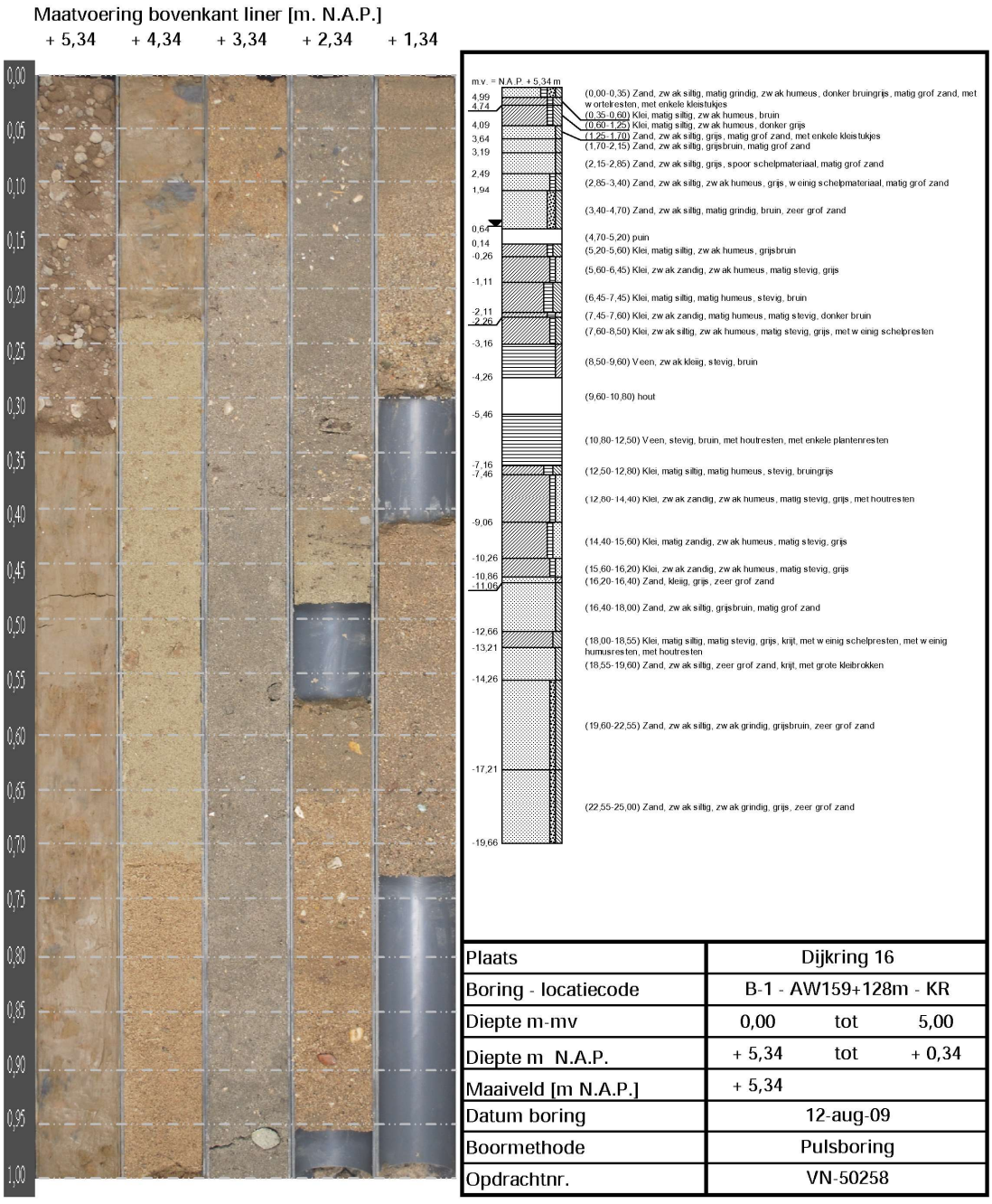

Figure E.12: Mechanical boring crest case study Kinderdijk

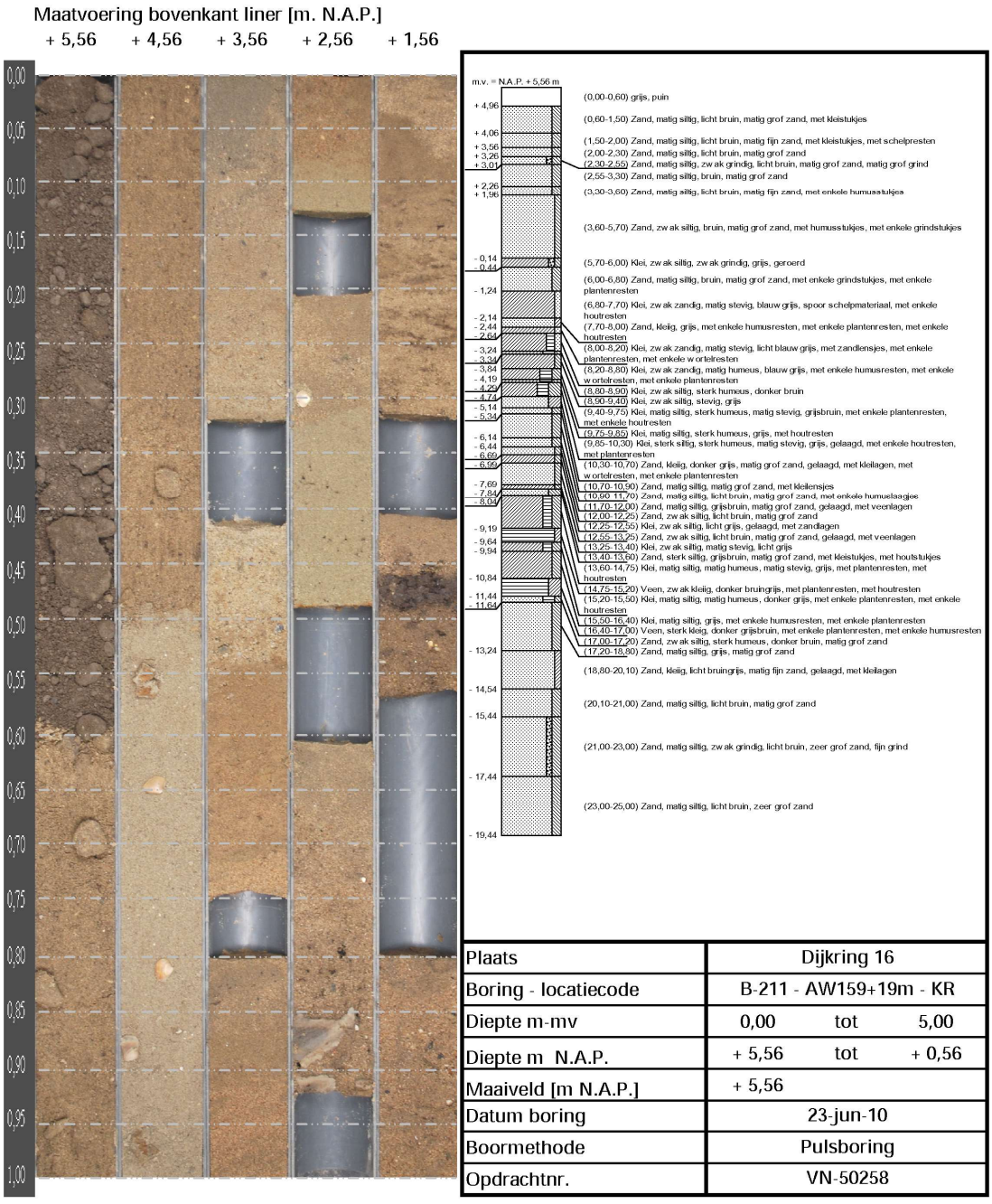

Figure E.13: Mechanical borings crest case study Kinderdijk

CPT's

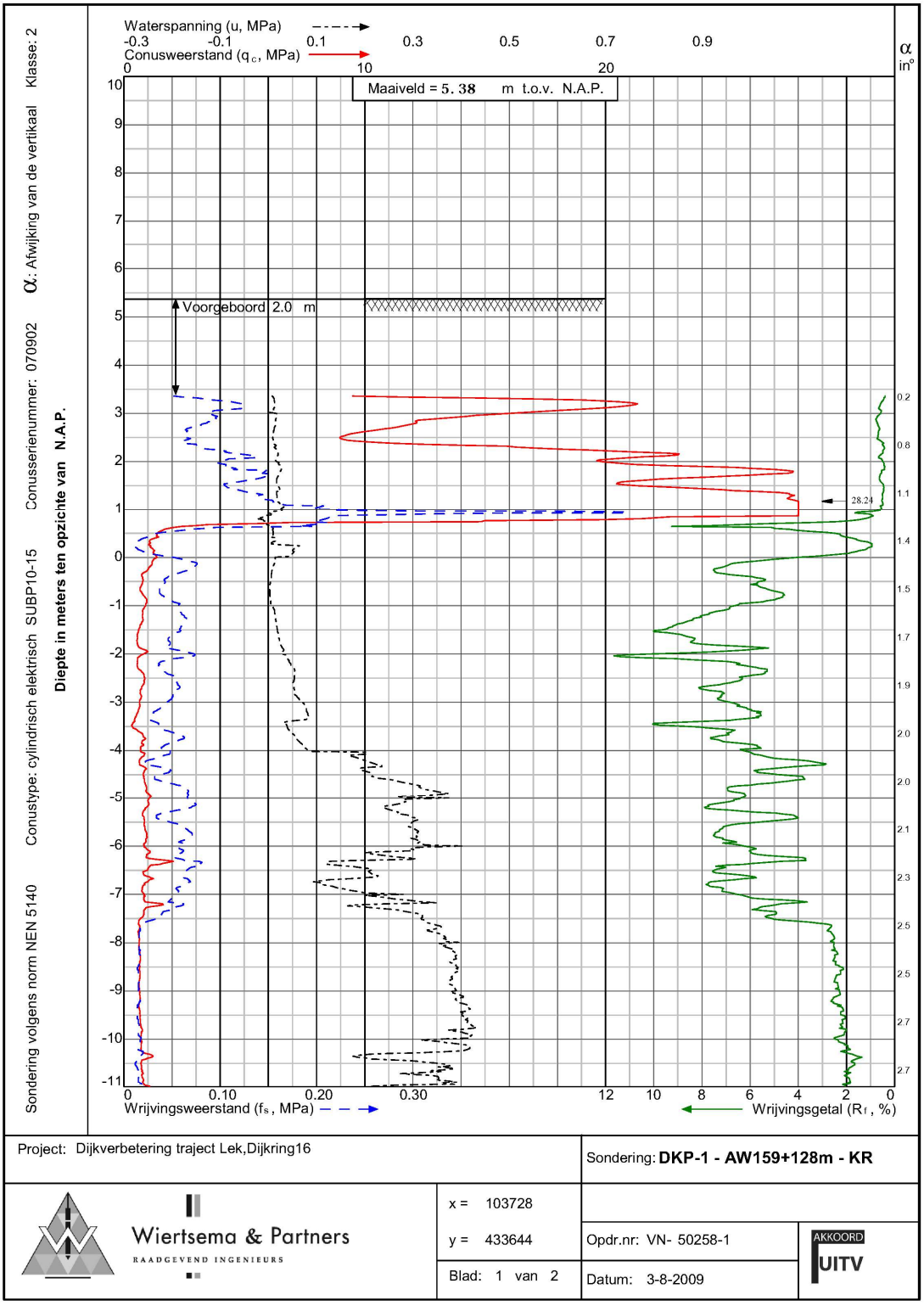

Figure E.14: CPT crest case study Kinderdijk

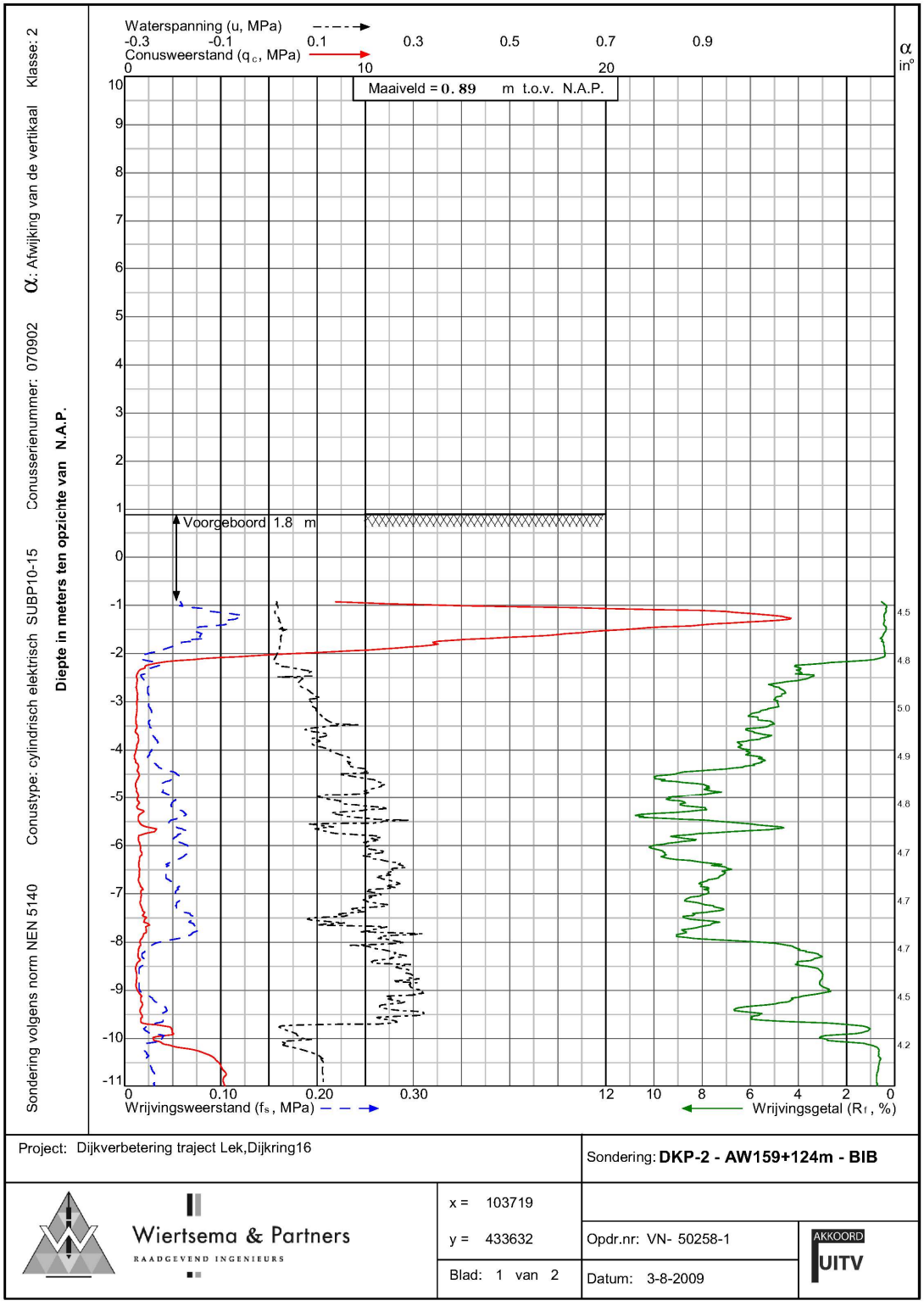

Figure E.15: CPT inner dike slope case study Kinderdijk

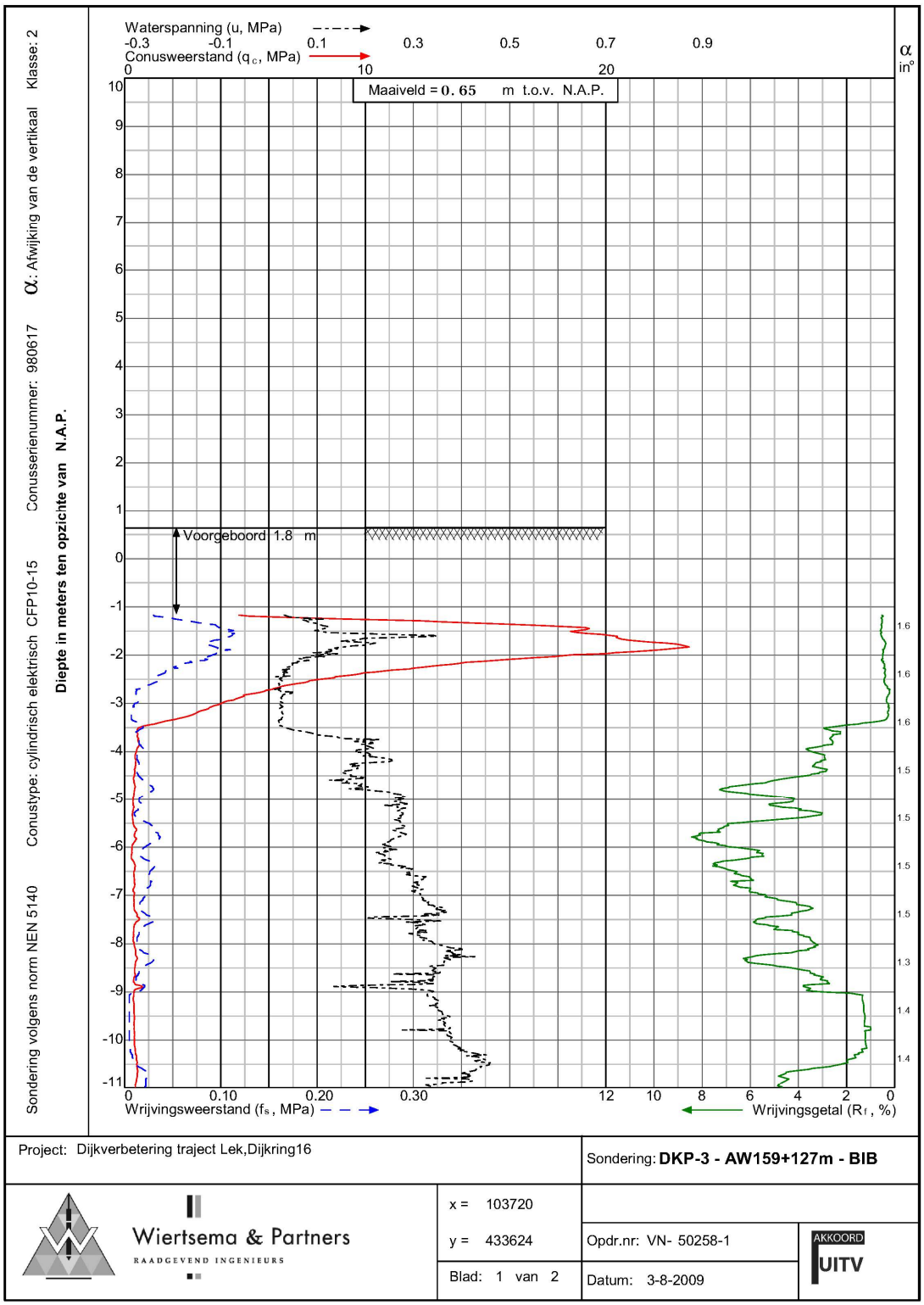

Figure E.16: CPT inner dike slope case study Kinderdijk

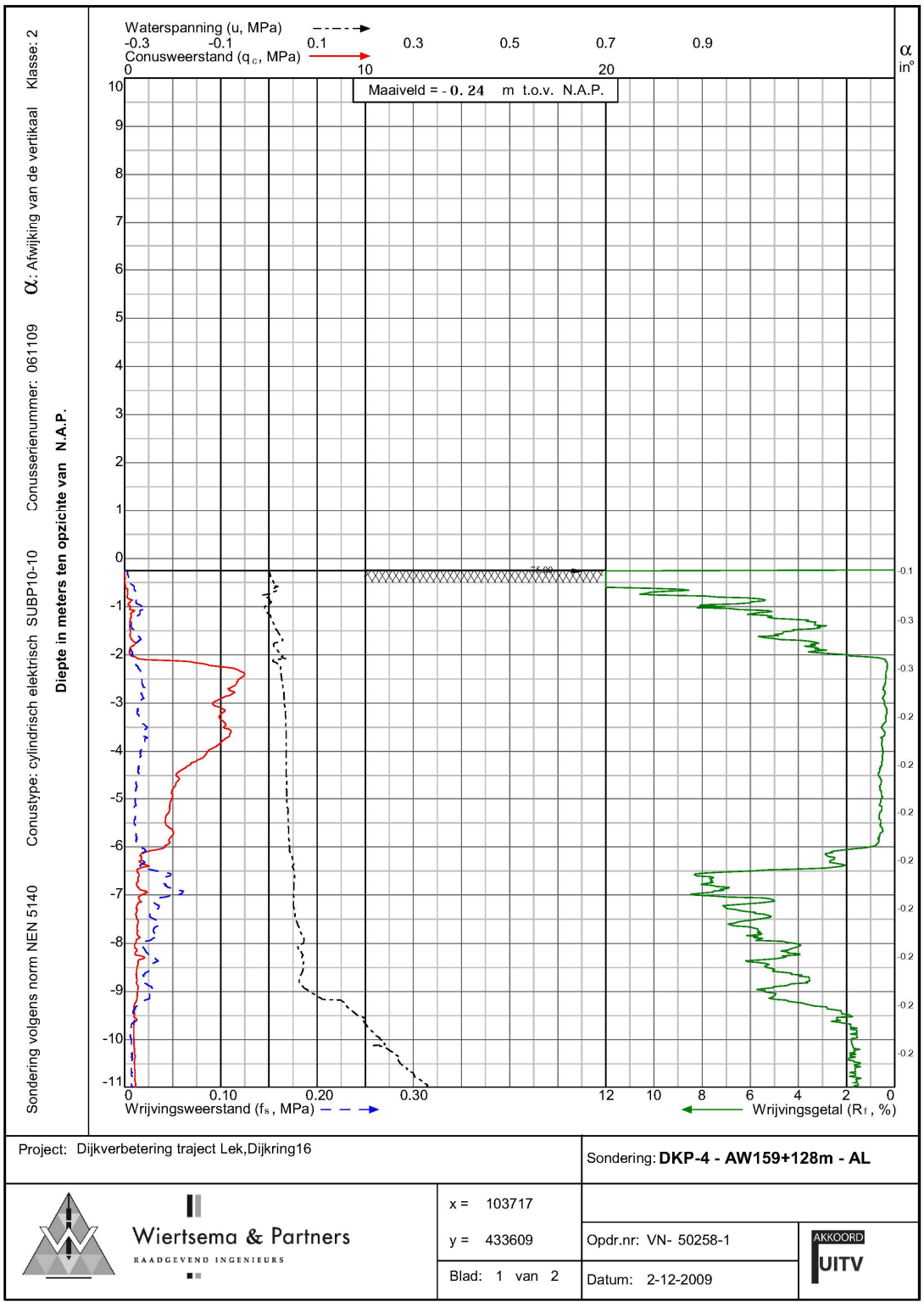

Figure E.17: CPT hinterland case study Kinderdijk